AD-A273 796
I||||||||||

$$S\quad\begin{array}{l}\textbf{DTIC}\\ \text{ELECTE}\\ \text{DEC 16 1993}\\ \textbf{A}\end{array}$$

THE EFFECT OF CUTOUT DIMENSIONALITY
ON THE COLLAPSE CHARACTERISTICS OF CYLINDRICAL
COMPOSITE SHELLS OF VARYING THICKNESS

THESIS

John C. Del Barga, Captain, USAF

AFIT/GAE/ENY/93D-11

93-30413
||||||||||||

93 12 15 033

The views expressed in this thesis are those
of the author and do not reflect the official policy or
position of the Department of Defense or the U. S. Government.

Accesion For		
NTIS CRA&I		V
DTIC TAB		☐
U announced		☐
Justification		
By		
Distribution /		
Availability Codes		
Dist	Avail and/or Special	
A-1		

AFIT/GAE/ENY/93D-11

THE EFFECT OF CUTOUT DIMENSIONALITY ON THE COLLAPSE

CHARACTERISTICS OF CYLINDRICAL COMPOSITE SHELL STRUCTURES

OF VARYING THICKNESS

THESIS

Presented to the Faculty of the Graduate School of Engineering

of the Air Force Institute of Technology

Air University

In Partial Fulfillment of the

Requirements for the Degree of

Master of Science in Aeronautical Engineering

John C. Del Barga

Captain, USAF

December, 1993

Acknowledgements

I express my deepest gratitude to my wife, Kirsten, for her continued suppport and wonderful attitude during this endeavor, and to my son, Christopher, for keeping a smile on my face. In addition, I thank Giovanni and Elaine Del Barga whose encouragement and support sustained me through the most difficult times that I encountered while at AFIT.

I am grateful to all the professional people I had the opportunity to work with at the Flight Dynamics Lab. From the manufacturing to the testing of the panels, the efforts of the people involved were second to none. I am especially indebted to Dr. R. S. Sandhu who coordinated the individual efforts required to complete this project, and Dr. Greg Schoeppner and Forrest Sandow who provided the MacIntosh tutoring I needed to create this document. I acknowledge Lt. Kevin Gibbons, Jack Smith, Charley Hayden, and Odie Blackburn whose efforts were responsible for the composite panels being manufactured and instrumented in a timely manner. I thank Don Cook and Larry Bates whose get it done attitude and professionalism were a testament to having smooth running tests and the capture of good data.

I would also like to thank Captain Scott Schimmels for teaching me the basics of the SHELL program and Captain Rick Tuznik who like me refused to run with the pack. Finally, I thank my thesis advisor, Dr. Anthony Palazotto who motivated me when I needed it the most.

Table of Contents

List of Figures

List of Tables

Abstract

This study involved a numerical and experimental investigation of the geometric instability of graphite/epoxy cylindrical panels with free vertical edges undergoing axial compression. Symmetric quasi-isotropic laminates with five different size centralized cutouts, were investigated for two axial lengths of panels and three thicknesses. The study compared experimental data to results from SHELL, a geometrically nonlinear finite-element program which incorporates a parabolic transverse shear strain distribution through the thickness. The research verified that the SHELL program will provide good predictions of the collapse characteristics of a panel with large cutouts of varying dimensions undergoing large displacements and rotations. The best correlation between the numerical and experimental results occurred for 16 ply panels in comparison to 8 and 24 ply panels. The variation between these results is attributed to panel curvature, material, and geometric imperfections. This study verified that cutout dimensionality effects the panel transverse shear strain, which in turn effects the panel collapse load. In addition, this research conducted parametric studies to determine one dimensional models that could be used in lieu of SHELL to estimate collapse loads from a known solution for a panel with geometric variations from the known panel solution.

THE EFFECT OF CUTOUT DIMENSIONALITY ON THE COLLAPSE CHARACTERISTICS OF CYLINDRICAL COMPOSITE SHELL STRUCTURES OF VARYING THICKNESS

I. Introduction

1.1 Background

Today's aircraft use graphite/epoxy composite shells (panels) in both monocoque and semimonocoque structures. Frequently, aircraft require openings in these composite shell structures. These openings may be necessary for armament installations, windows, landing gear doors, or holes and access doors for inspection and maintenance in service. These openings (rectangular and square) cut in fuselages and wings change the collapse characteristics of the structure. Similarly, the shell structures collapse characteristic is sensitive to cutout dimensionality. Cutout dimensionality is defined for this study as when a centrally located cutout's dimensions are varied. A better understanding of the effects of cutout dimensionality on the collapse characteristics of monocoque composite shells is necessary to properly design these shells for the anticipated loading environment.

The curved nature of a monocoque cylindrical shell in axial compression presents a problem which is inherently nonlinear. This nonlinearity becomes even more prevalent as the thickness of the shell panel and the area of the cutout region increases [1,2]. The study of these structures

1

requires nonlinear analysis whenever compressive loading is applied.

A geometric nonlinear finite element program developed at the Air Force Institute of Technology (AFIT) addresses this nonlinearity. This finite element program, called SHELL, takes into account large displacements and moderately large rotations and incorporates a parabolic distribution of shear through the panel thickness. It is important to retain the effects of transverse shear in an analytical model for thick shells due to the magnitude of transverse shear moduli (G_{12} and G_{13}) being one to two orders of magnitude as compared to the longitudinal modulus (E_1) for a composite material. Since G_{12} and G_{13} are smaller in magnitude to E_1, than for an isotropic material, the effects of transverse shear plays a greater role in the collapse of a composite panel than it does for an isotropic panel [3]. In addition, the effect of transverse shear becomes more prevalent as the thickness of the panel is increased [4].

The SHELL program employs a Modified Newton Raphson (MNR) technique incorporating a displacement control algorithm. The MNR technique traces the equilibrium path up to and through the collapse load. The collapse load is defined as the point where the tangent stiffness matrix slope is zero and the load begins to fall off with increased axial displacement. It should be noted that the MNR technique, using a load control approach, can not accurately predict the nonlinear response beyond the collapse load. The axial load

is obtained by using the MNR iterative technique until there is convergence to the input displacement. The convergence tolerance used for this study is 0.01% or 0.001. The MNR technique does not update the tangent stiffness matrix every iteration, consequently, the MNR technique takes more iterations to converge [5]. However, the MNR technique guarantees convergence. In addition, since the stiffness matrix is not refactored every iteration the amount of CPU time required to converge to the collapse load is reduced.

Previous research done in the area of collapse of composite shell structures with large centrally located cutouts has primarily been done by AFIT and the National Aeronautical and Space Administration (NASA). The majority of published research on geometric instability examines composite shells without cutouts [6-8], and isotropic shells in compression with and without cutouts [9-13]. The majority of work done with composite shells with cutouts has been conducted using small cutouts, or simply supported panels with larger cutouts [2,14,15]. However, work done by Knight and Starnes [16] does examine the collapse characteristics of composite shells with larger circular cutouts .

The primary investigations made in the area of composite shell structures with large cutouts were conducted at AFIT by Scott Schimmels [17] and James Hatfield [18]. Schimmels compared experimental results for composite shell panels with large cutouts using two different nonlinear programs. The two programs Schimmels compared results with were Lockheed's

3

Structural Analysis for General Shells (STAGSC-1) and the
SHELL program developed by Scott Dennis as part of his
doctoral dissertation. Schimmels found that the SHELL
program provided better results for panels with large cutouts
with free edge rotations greater than 17 degrees compared to
the STAGSC-1 results [17]. Similarly, Dennis and Palazotto
concluded that experimental test results for panel surface
rotations around a 101.6 mm x 101.6 mm (4" x 4") cutout,
obtained by Tisler, in comparison with STAGSC-1 results
exceeded the intermediate nonlinear capability of the
STAGSC-1 finite element program [4]. In addition, Knight and
Starnes [16] arrived at the same conclusion in their
comparison of STAGSC-1 and experimental results which
involved axial compression of composite panels with larger
circular cutouts.

Hatfield's research investigated the effects of
thickness, ply lay-up, and panel axial length on the collapse
characteristic of a panel with and without a large cutout
[18]. Specifically, Hatfield performed a collapse analysis
using the SHELL program for a 101.6 mm x 101.6 mm (4" x 4")
cutout using a 304.8 mm x 304.8 mm (12" x 12") and
304.8 mm x 508 mm (12" x 20") panel with free vertical panel
edges. Hatfield investigated both symmetric quasi-isotropic
and symmetric cross-ply lay-ups. Hatfield compared these
analytical results to experimental results he obtained. He
concluded that the greatest radial displacements and
rotations for a panel with a cutout occurred along the free

4

vertical edges of the panel and the corners of the cutout.
The maximum values of radial displacement and rotations
tended to occur along the horizontal centerline of the panel
at the free vertical edge. Hatfield also verified that the
quasi-isotropic lay-ups for similar panel configurations
collapsed at higher loads than the cross-ply lay-ups. In
addition, he verified that increasing the axial length from
304.8 mm (12") to 508 mm (20") causes a reduction in collapse
load for equivalent number of plies.

1.2 Objective

The objective of this research was to study the effects
of cutout dimensionality on the instability of graphite/epoxy
cylindrical shell panels. A collapse analysis was performed
on panels with varying centrally located size cutouts, while
the panels underwent axial compression. Experimental data
was collected to check the accuracy of the SHELL computer
program for a wider range of cutout dimensions.

Previous research prior to Hatfields limited their
studies to relatively thin panels (8 plies). Hatfield
studied the effects of 16 and 24 plies on 101.6 mm x 101.6 mm
(4" x 4") cutouts. This research extended his study by
addressing the effects of 16 and 24 plies on four other size
cutouts. This required that experiments and computer
analyses be conducted on these different configurations.

The boundary conditions assumed experimentally and
analytically for all panel configurations were free vertical
edges with the horizontal bottom edge of the panel fixed.

5

The top horizontal edge of the panel was assumed to only displace in the axial (u) direction. The panel's horizontal edges were assumed to be fixed circumferentially.

Another objective of this research was to correct the problem of circumferential shift of the panel in the test fixture exhibited in previous experimentation done at AFIT, Experiments conducted by Hatfield exhibited experimental data suggesting movement of the panel circumferentially. In particular, Hatfield reported that this phenomenon was quite evident when testing the thicker panels (16 to 24 plies) where the deformations were increasingly dominated by the transverse shear stresses [18]. A modification to the axial compression machine was developed to prevent circumferential movement of the 16 and 24 ply panels. Details of this modification are provided in section 3.2.1.

1.3 Scope

Four panel configurations with five different size cutouts were analyzed and tested. Two panels were fabricated and tested per panel configuration and cutout combination. Therefore, a total of 40 panels were fabricated and tested. All panels had a symmetric quasi-isotropic lay-up of [0/45/-45/90], and were fabricated from a AS4/3501-6 graphite/epoxy material system. Each of the cutouts were centrally located in the panel.

To be consistent throughout this document the following panel and cutout convention is used. The circumferential

6

dimension is always listed first followed by the axial dimension. Each cutout was analyzed for four different panel configurations. These configurations were:

304.8 mm x 304.8 mm (12" x 12") panel with 8 plies

304.8 mm x 508 mm (12" x 20") panel with 8 plies

304.8 mm x 508 mm (12" x 20") panel with 16 plies

304.8 mm x 508 mm (12" x 20") panel with 24 plies

The cutout sizes used to determine the effects of cutout dimensionality on the collapse characteristic of a panel were:

50.8 mm x 50.8 mm (2" x 2"),
101.6 mm x 101.6 mm (4" x 4")
127 mm x 127 mm (5" x 5")
50.8 mm x 203.2 mm (2" x 8")
203.2 mm x 50.8 mm (8" x 2")

2.SHELL Theory

2.1 General

The SHELL program incorporates a geometrically nonlinear static shell theory. This theory accomodates large displacements and rotations. The following is a summary of the assumptions made by Dennis in the development of this geometrically nonlinear static shell theory. First, the shell is assumed to be thin, which allows an approximate state of plane stress to occur ($\sigma_3 = 0$). This reduces a three dimensional shell problem to a two dimensional shell problem. Specifically, this assumption allows the shell behavior to be described by the shell datum surface. Second, the transverse shear distribution is parabolic through the panel thickness with the transverse shear being equal to zero at the top and bottom surface of the panel. Third, the shell consists of linear elastic laminated orthotropic material which implies a small strain assumption (no plasticity).

The static shell theory that SHELL employs is a higher order shell theory. This higher order shell theory is called Simplified Large Rotation (SLR) theory. The SLR theory was developed by Palazotto and Dennis [19]. The application of this theory generates cylindrically shaped finite-elements. These cylindrically shaped finite-elements capture the shell bending-membrane coupling by matching the curvature of the shell surface. This makes it superior to flat finite-

elements used in moderate rotation analytical models in predicting panel responses for shells with large cutouts.

A brief explanation and description of the more important equations used in SLR theory is presented in the following sections. A more detailed description and derivation can be found in Nonlinear Analysis of Shell Structures by Palazotto and Dennis [19]

2.1.1 SHELL's Geometry and Contracted Notation

The curvilinear orthogonal coordinate system used in the SHELL formulation is shown in Figure 1. Figure 1 also depicts the positive ply lay up orientation angle θ. The surface formed by the X and S axes lies in the center of the thickness of the panel. Therefore, the thickness coordinate is negative on the outer surface and positive on the inner surface of the panel. The radius of curvature of the panel is 304.8 mm (12") which is measured to the outside surface of the cylindrical shell. Displacements along the X, S, and Z axes are u, v, and w respectively. Subscripts denoting the stress and strain orientation are summarized in Table 1.

Table 1. SHELL Contracted Notation [17]

Stress	Strain	Cylindrical Coordinates
$\sigma_{11} = \sigma_1$	$\varepsilon_{11} = \varepsilon_1$	X = 1
$\sigma_{22} = \sigma_2$	$\varepsilon_{22} = \varepsilon_2$	S = 2
$\sigma_{33} = \sigma_3$	$\varepsilon_{33} = \varepsilon_3$	Z = 3
$\sigma_{23} = \sigma_4$	$\varepsilon_{23} = \varepsilon_4$	S-Z = 4
$\sigma_{13} = \sigma_5$	$\varepsilon_{13} = \varepsilon_5$	X-Z = 5
$\sigma_{12} = \sigma_6$	$\varepsilon_{12} = \varepsilon_6$	X-S = 6

2.1.2 SHELL's Constitutive Equation

SHELL assumes a modified plane stress condition in its development of the constitutive equations. This allows $\sigma_3 = 0$, in addition, σ_4 and σ_5 are not set equal to zero, so that thru-the-thickness shear stress is incorporated into the finite-element code [1]. A complete derivation can be found in Schimmels master's degree thesis which leads to the reduced stiffness constitutive equation, equation (1) [17].

$$\begin{Bmatrix} \sigma_1 \\ \sigma_2 \\ \sigma_6 \\ \sigma_4 \\ \sigma_5 \end{Bmatrix} = \begin{bmatrix} Q_{11} & Q_{12} & 0 & 0 & 0 \\ Q_{12} & Q_{22} & 0 & 0 & 0 \\ 0 & 0 & Q_{66} & 0 & 0 \\ 0 & 0 & 0 & Q_{44} & 0 \\ 0 & 0 & 0 & 0 & Q_{55} \end{bmatrix} \begin{Bmatrix} \varepsilon_1 \\ \varepsilon_2 \\ \varepsilon_6 \\ \varepsilon_4 \\ \varepsilon_5 \end{Bmatrix} \qquad (1)$$

RADIUS OF CURVATURE
R = 304.8 mm (12")

t = THICKNESS
(VARIES WITH LAY UP)

304.8 mm (12.0")

or

508 mm (20.0")

+θ

X, u

Z, w

S, v

ARC LENGTH = 304.8 mm (12")
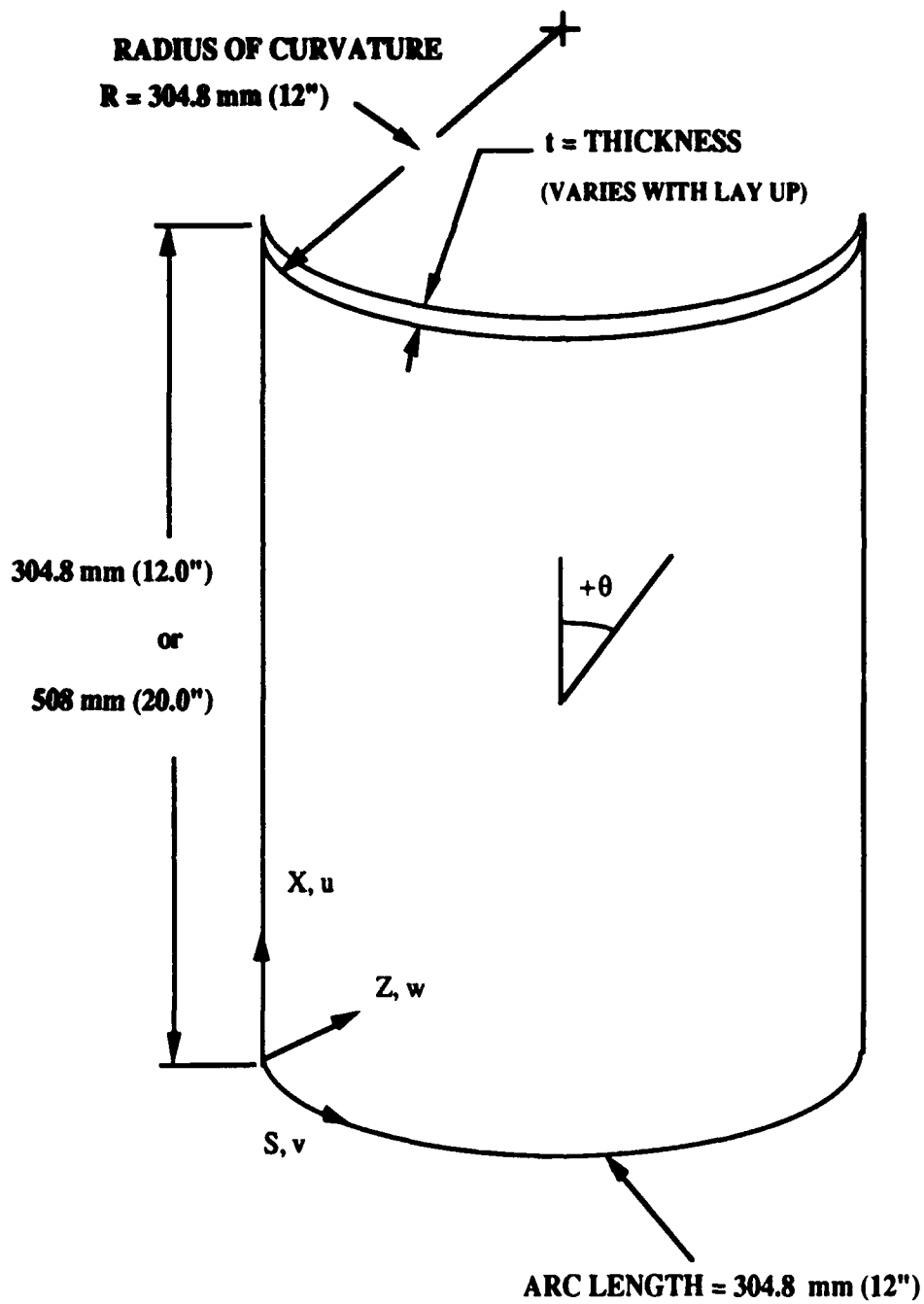
Figure 1. Shell Panel Geometry With Positive Ply Orientation Angle

11

The reduced stiffness coefficients (Q_{ij}) related in terms of engineering constants are [20]:

$$Q_{11} = E_1 / (1 - \nu_{12}\nu_{21})$$

$$Q_{12} = \nu_{12}E_2 / (1 - \nu_{12}\nu_{21}) = \nu_{21}E_1 / (1 - \nu_{12}\nu_{21})$$

$$Q_{22} = E_2 / (1 - \nu_{12}\nu_{21}) \qquad\qquad (2)$$

$$Q_{66} = G_{12}$$

$$Q_{44} = G_{23}$$

$$Q_{55} = G_{13}$$

Equations (1) and (2) apply for an orthotropic material whose stresses and strains are defined with respect to the principal material directions. The following equation is used to analyze a laminate with arbitrary lamina whose fiber directions do not coincide with the global coordinate directions. To analyze a laminate, each ply must be referenced to a global axis system and their effects summed. Therefore, the stress-strain relations with respect to the global X-Y coordinate system is defined by:

$$\{\sigma_i\}_k = [\, T \,][\, Q_{ij}\,]_k \; [T]^T \; \{\varepsilon_i\}_k \qquad\qquad (3)$$

where,

$$[T] = \begin{bmatrix} c^2 & s^2 & -2cs \\ s^2 & c^2 & 2cs \\ cs & -cs & (c^2 - s^2) \end{bmatrix} \quad \text{for} \quad \begin{bmatrix} Q_{11} & Q_{12} & 0 \\ Q_{12} & Q_{22} & 0 \\ 0 & 0 & Q_{66} \end{bmatrix} \qquad (4)$$

and

$$[T] = \begin{bmatrix} c & -s \\ s & c \end{bmatrix} \quad \text{for} \quad \begin{bmatrix} Q_{44} & 0 \\ 0 & Q_{55} \end{bmatrix} \qquad (5)$$

with $c = \cos\theta$ and $s = \sin\theta$. The transformed constitutive relation, equation (3) can be written in the following form.

$$\{\sigma_i\}_k = [\bar{Q}_{ij}]_k \{\varepsilon_i\}_k \qquad (6)$$

Using transformation equation (4), the transformed reduced stiffnesses ($\bar{Q}_{11}$, $\bar{Q}_{12}$, $\bar{Q}_{16}$, $\bar{Q}_{26}$ and $\bar{Q}_{66}$) are as defined in reference [21]. Applying transformation equation (5), yields the following three equations which are added to the transformed constitutive equations.

$$\bar{Q}_{44} = Q_{44}\cos^4\theta + Q_{55}\sin^4\theta$$
$$\bar{Q}_{45} = (Q_{44} - Q_{55})\cos\theta\sin\theta \qquad (7)$$
$$\bar{Q}_{55} = Q_{44}\sin^4\theta + Q_{55}\cos^4\theta$$

The k in equation (6) means each kth ply in the laminate is characterized by this equation. The kth ply is defined by its distance from the midplane of the laminate.

2.1.3 Strain-Displacement Relations

SLR theory includes through the thickness shear distribution and maintains the exact Green's strain-displacement relations for the in-plane strains (ε_1, ε_2, and ε_6). In addition, the transverse shear strain equations

(ϵ_4 and ϵ_5) include only the linear Green's strain-displacement terms. The physical strains (ϵ_{ij}) are defined by:

$$\epsilon_{ij} = \gamma_{ij} / (h_i \, h_j) \quad \text{(no sum)} \qquad (8)$$

where (γ_{ij}) is the Green's strain-displacement relations as shown in Saada [22]. Green strain is defined in terms of the metric tensor of the transformed coordinate system as a result of deformation (G_{ij}) and the metric tensor of the transformed coordinate system prior to deformation (g_{ij}). The metric tensor links the cartesian to the curvilinear coordinate system through the invariant property of length. The Green's strain-displacement relations are a function of the u_1, u_2, and u_3 displacements and the shell shape factors (h_i). The shell shape factors are a function of the coordinate system scale factors (α_i) and radii of curvature of the shell (R_1 and R_2). The coordinate system scale factors and radii of curvature are defined as $\alpha_1 = \alpha_2 = 1$ and $R_1 = \infty$ and $R_2 = R$, respectively. Substitution of the coordinate system scale factors and radii of curvatures into the general shell shape factor equations gives the shell shape factors used in this study.

$$h_1 = 1 \qquad h_2 = 1 - (z/R) \qquad h_3 = 1 \qquad (9)$$

A detailed derivation of the Green's strain displacement equations can be found in Saada [22]. Note the Green's strain displacement equations are valid only for small strain situations (no plasticity).

The shear effects are incorporated by keeping just the linear (first order) displacement terms for Green's strain-displacement relations γ_{23} and γ_{13}. Equation (8) is then used to calculate the transverse shear strains ε_4 and ε_5. Where $\varepsilon_4 = \varepsilon_{23}$ and $\varepsilon_5 = \varepsilon_{13}$.

$$\varepsilon_4 = 1/h_2 \ (u_{3,2} + h_2 u_{2,3} - u_2 h_{2,3}) \tag{10}$$

$$\varepsilon_5 = 1/h_1 \ (u_{3,1} + h_1 u_{1,3} - u_1 h_{1,3})$$

The displacement equations in the thickness variable z, which permit the incorporation of the through-the-thickness feature, are:

$$u_1(x,s,z) = u^0 + z\psi_x + z^2\phi_x + z^3\gamma_x + z^4\theta_x \tag{11}$$

$$u_2(x,s,z) = v^0[1 - z/R] + z\psi_s + z^2\phi_s + z^3\gamma_s + z^4\theta_s$$

$$u_3(x,s,z) = w$$

Where u^0, v^0, w, ψ_i, ϕ_i, γ_i, and θ_i are functions of the coordinates X and S. The displacements u^0 and v^0 are of the shell middle surface; transverse displacement w is the same throughout the thickness since transverse normal strain is assumed neglible ($\varepsilon_3 = 0$). The ψ_i terms are rotations of the surface normals in the X and S planes. The ϕ_i, γ_i, and θ_i are

15

functions to be found so that transverse shear stresses σ_4 and σ_5 are zero on the shell's lateral surfaces.

The functions ϕ_i, γ_i, and θ_i are found by substituting equation (11) and equation (9) into equation (10). Carrying out the differentiation of equation (10) and applying the assumption that the transverse shear and transverse strain are zero on the top and bottom surface of the shell, the ϕ_i, γ_i, and θ_i functions are solved for [19]. Therefore equation (11) can be rewritten as:

$$u_1(x,s,z) = u^o + z\psi_x - (4/3t^2)z^3(\psi_x + w_{,x})$$
$$u_2(x,s,z) = v^o[1 - z/R] + z\psi_s - (4/3t^2)z^3(\psi_s + w_{,s}) \qquad (12)$$
$$u_3(x,s) = w$$

where the thickness of the laminate is defined as t.

Equation (12) and the shell shape factors (h_i), equation (9), are substituted into equation (10) and small order terms are neglected which yields the transverse shear strains.

$$\varepsilon_4 = [1/\{1-(z/R)\}](\psi_s + w_{,s})[1 - (4z^2/t^2)] \qquad (13)$$
$$\varepsilon_5 = (\psi_x + w_{,x})[1 - (4z^2/t^2)]$$

The in-plane strain displacement relations are found by substituting equation (12) and the shell shape factors h_i into equation (8).

$$\varepsilon_1 = \frac{\gamma_{11}}{h_1^2} = \varepsilon_1^0 + z\kappa_1^1 + z^2\kappa_1^2 + z^3\kappa_1^3 + z^4\kappa_1^4 + z^6\kappa_1^6$$

$$\varepsilon_2 = \frac{\gamma_{22}}{h_2^2} = \varepsilon_2^0 + z\kappa_2^1 + z^2\kappa_2^2 + z^3\kappa_2^3 + z^4\kappa_2^4 + z^6\kappa_2^6 \qquad (14)$$

$$\varepsilon_6 = \frac{\gamma_{12}}{h_1 h_2} = \varepsilon_6^0 + z\kappa_6^1 + z^2\kappa_6^2 + z^3\kappa_6^3 + z^4\kappa_6^4 + z^6\kappa_6^6$$

Substituting a binomial series expansion of the general shell shape factor expressions, which are truncated after the first order z terms, into the above equations results in the following equation [19].

$$\varepsilon_i = \varepsilon_i{}^0 + z^p\kappa_{ip}$$

$$i = 1,2,6 \qquad (15)$$

$$p = 1,\ldots,7$$

The strain displacement equation, equation (15), written in matrix format

$$\begin{Bmatrix} \varepsilon_1 \\ \varepsilon_2 \\ \varepsilon_6 \end{Bmatrix} = \begin{Bmatrix} \varepsilon_1^0 \\ \varepsilon_2^0 \\ \varepsilon_6^0 \end{Bmatrix} + \begin{bmatrix} \kappa_{11} & \kappa_{12} & \kappa_{13} & \kappa_{14} & \kappa_{15} & \kappa_{16} & \kappa_{17} \\ \kappa_{21} & \kappa_{22} & \kappa_{23} & \kappa_{24} & \kappa_{25} & \kappa_{26} & \kappa_{27} \\ \kappa_{61} & \kappa_{62} & \kappa_{63} & \kappa_{64} & \kappa_{65} & \kappa_{66} & \kappa_{67} \end{bmatrix} \begin{Bmatrix} z \\ z^2 \\ z^3 \\ z^4 \\ z^5 \\ z^6 \\ z^7 \end{Bmatrix}$$

$$(16)$$

$$\begin{Bmatrix} \varepsilon_4 \\ \varepsilon_5 \end{Bmatrix} = \begin{Bmatrix} \varepsilon_4^0 \\ \varepsilon_5^0 \end{Bmatrix} + \begin{bmatrix} \kappa_{42} \\ \kappa_{52} \end{bmatrix} z^2$$

17

and as a general expression:

$$\{\mathcal{E}\} = \{\mathcal{E}^o\} + [K]\{Z\} \tag{17}$$

The ε_i^o and κ_{ip} are functions of the displacements and the shell shape factors, and can be found in Appendix A of [19].

2.1.4 Equations of Motion

The potential energy equation is defined as the internal strain energy minus the work of the applied forces;

$$\Pi_p = U - W \tag{18}$$

where the internal strain energy is defined as:

$$U = 1/2 \iint \left([\overline{Q}]\{\varepsilon\}\right)^T \{\varepsilon\} d\Omega dt = U_1 + U_2 \tag{19}$$

where the shell middle surface is represented by Ω. The internal strain energy consists of two parts. The first part is composed of in-plane terms, it is called U_1. The second part is made up of the transverse shear terms, and it is called U_2. Inserting equation (15) into equation (19) gives:

$$U_1 = 1/2 \iint \left[\bar{Q}_{11}(\varepsilon_1^0 + z^P \kappa_{1p})^2 + \bar{Q}_{22}(\varepsilon_2^0 + z^P \kappa_{2p})^2 \right.$$

$$+ 2\bar{Q}_{12}(\varepsilon_1^0 + z^P \kappa_{1p})(\varepsilon_2^0 + z^r \kappa_{2r}) + \bar{Q}_{66}(\varepsilon_6^0 + z^P \kappa_{6p})^2$$

$$+ 2\bar{Q}_{16}(\varepsilon_1^0 + z^P \kappa_{1p})(\varepsilon_6^0 + z^r \kappa_{6r})$$

$$\left. + 2\bar{Q}_{26}(\varepsilon_2^0 + z^P \kappa_{2p})(\varepsilon_6^0 + z^r \kappa_{6r}) \right] dz\, d\Omega$$

(20)

$$U_2 = 1/2 \iint \left[\bar{Q}_{44}(\varepsilon_4^0 + z^2 \kappa_{42})^2 + \bar{Q}_{55}(\varepsilon_5^0 + z^2 \kappa_{52})^2 \right.$$

$$\left. + 2\bar{Q}_{45}(\varepsilon_4^0 + z^2 \kappa_{42})(\varepsilon_5^0 + z^2 \kappa_{52}) \right] dz\, d\Omega$$

where p,r = 1,2,....7. Integrating the z over the laminate
thickness (t) gives the strain energy as function of the
shell datum surface. In addition, since the problems to be
investigated deal with symmetric ply lay ups a further
simplification can be made. Symmetric lay ups allow the
cancellation of elasticity arrays which are multiplied by odd
powers of the transverse coordinate z. Further manipulation
yields the final form (see [19]).

$$U_1 = 1/2 \int (\varepsilon^0)^T [A] (\varepsilon^0)\, d\Omega$$

$$+ 1/2 \int 2(\varepsilon^0)^T \Big([B] + [D] + [E] + [F] + [G] + [H] + [I] \Big) (\kappa)\, d\Omega \qquad (21)$$

$$+ 1/2 \int (\kappa) \Big([D] + [E] + [F] + [G] + [H] + [I] + [J] + [K] + [L] + [P] + [R]$$

$$+ [S] + [T] \Big) (\kappa)\, d\Omega$$

$$U_2 = 1/2 \int \Big((\varepsilon^0)^T [A] (\varepsilon^0) + 2(\varepsilon^0)[D](\kappa) \qquad\qquad (22)$$

$$+ (\kappa)^T [F] (\kappa) \Big)\, d\Omega$$

where

$$\{[A, B, D, E, F, G, H, I, J, K, L, P, R, S, T]\}$$
$$= \int [\bar{Q}] \{1, z, z^2, z^3, z^4, z^5, z^6, z^7, z^8, z^9, z^{10}, z^{11},$$
$$z^{12}, z^{13}, z^{14}\} dz \qquad (23)$$

2.1.5 Finite Element Formulation

The equation to be solved is the static equilibrium equation $\Sigma F = 0$. The first variation of the potential energy equation (18), $\delta\Pi_p = 0$, yields the static equilibrium equation which is at a minimum for static equilibrium [22]. The internal strain energy can be represented as:

$$U = 1/2 \ q^T \left[K + N_1(q)/3 + N_2(q^2)/6 \right] q \qquad (24)$$

The column array of nodal displacements is defined as q, and K is an array of constant stiffness terms, N_1 is an array of stiffness terms that are a function of linear displacements, and N_2 is an array of stiffness terms that are a function of quadratic displacements. The external work is represented by:

$$W = q^T R \qquad (25)$$

where R is a column array of nodal loads. Therefore, substituing equation (24) and (25) into equation (18) gives:

20

$$\Pi_p = 1/2 \ q^T \left[K + N_1(q)/3 + N_2(q^2)/6 \right] q \quad - \ q^T R \qquad (26)$$

Taking the first variation of equation (26), using matrix differentiation rules results in:

$$\delta\Pi_p = \delta q^T \left[\left(K + N_1(q)/2 + N_2(q^2)/3 \right) q - R \right] = 0 \qquad (27)$$

Let $F(q) = \left(K + N_1(q)/2 + N_2(q^2)/3 \right) q - R$. Therefore, equation (27) can be written as:

$$\delta q^T F(q) = 0 \qquad (28)$$

Since δq is arbitrary and independent $F(q) = 0$. Writing $F(q + \Delta q)$ using Taylor series expansion and neglecting higher order terms yields:

$$F(q + \Delta q) = F(q) + (\partial F/\partial q)\Delta q = 0 \qquad (29)$$
$$\therefore \ (\partial F/\partial q)\Delta q = - \ F(q)$$

Applying the matrix differentiation of equation (29) to F gives equation (30).

$$\left(K + N_1(q) + N_2(q^2) \right) \Delta q = - \ F(q) \qquad (30)$$

The group of terms inside the bracket in equation (30) are considered together to be the tangent stiffness matrix $[K_T]$.

Therefore, the equation be solved by the Modified Newton Raphson technique using a displacement control algorithm is:

$$[K_T]\Delta q = -\left(K + N_1(q)/2 + N_2(q^2)/3\right)q + R \qquad (31)$$

See reference [17] and [19] for details of the Modified Newton Raphson technique using a displacement control algorithm.

3. Experimental Methods

3.1 Manufacturing

There were eighteen 584.2 mm x 647.7 mm (23" x 25.5") panels layed up in 304.8 mm (12") inside radius of curvature molds. These molds produced panels which had a 304.8 mm radii of curvature measured to the outside convex surface of the panel. These panels were layed up in accordance with the axis system as shown in Figure 1. Lay ups were [0/45/-45/90]$_s$, [0/45/-45/90]$_{2s}$, and [0/45/-45/90]$_{3s}$. These eighteen panels were bagged and then cured in the autoclave. Upon completion of curing, all eighteen panels were sent out to be C-scanned to ensure no delaminations or internal defects were present. All of the panels successfully passed the C-scan inspection. Panel thickness was measured at thirteen locations for each of these panels and the average ply thickness calculated. The average ply thickness data was used in the SHELL input decks. These eighteen large size panels produced the required 40 panels designated for testing by the experimental test plan (see test plan, Appendix A). See Table 2 for a summary of the experimental test panels.

Fabrication of the test panels from the large panels was consistent with previous studies [2, 14, 15, 17, 18]. All vertical edges of the panels were trimmed using the water jet. The horizontal edges of the panels were cut using a radial arm saw with a diamond blade. All test panels were fabricated so that the actual axial length was 2.54 cm longer

23

than the effective axial length. The extra length is required to create a 1.27 cm holding tab at the panel's top and bottom edge, so that it can be clamped into the test fixture. For example, an effective panel dimension of 304.8 mm x 508 mm (12" x 20") has an actual dimension of 304.8 mm x 533.4 mm (12" x 21").

Table 2. Summary of Experimental Test Panels

# of Plies	Effective Panel Dimensions	Cutouts
8, 16, 24	304.8 mm x 304.8 mm (12" x 12")	50.8 mm x 50.8 mm (2" x 2")
	and	
	304.8 mm x 508 mm (12" x 20")	101.6 mm x 101.6 mm (4" x 4")
		127 mm x 127 mm (5" x 5")
		50.8 mm x 203.2 mm (2" x 8")
		203.2 mm x 50.8 mm (8" x 2")

The panel horizontal and vertical edges were checked by the Flight Dynamics Laboratory against the provided tolerances (see test plan, Appendix A). The panel horizontal edges must be parallel to each other, within a specified tolerance, to ensure uniform and symmetric loading through the panel. Likewise, the panel vertical edges must be parallel to each other. It should be noted that a tolerance

of 0.254 mm (0.01") was used for parallelism of the horizontal and vertical edges of the panels. A tolerance of 0.0254 mm (0.001") should be used in future studies. In most cases the panels horizontal edges were within 0.0762 mm (0.003") as recommended by Hatfield's study [18] (see tolerance data in Appendix B). This is discussed futher in the experimental results section.

The router/template cutting technique developed by Tisler [14], was used to machine the centrally located cutouts into the panels. This research project required that four new cutout templates, used for holding secure the composite panel during the cutting process, be manufactured. The template manufacturing process required that the cutout first be machined into a flat quarter inch thick steel plate. This plate was then cold rolled to an inside radius of curvature of 304.8 mm (12"). Templates were manufactured for the 50.8 mm x 50.8 mm (2" x 2") , 127 mm x 127 mm (5" x 5"), 203.2 mm x 50.8 mm (8" x 2"), and 50.8 mm x 203.2 mm (2" x 8") cutouts. Note, that if the goal is to have a panel with a 127 mm x 127 mm (5" x 5") cutout then the template cutout must be 133.35 mm x 133.35 mm (5.25" x 5.25"). The extra 6.35 millimeters (0.25") is required since the router follows the template using a 6.35 millimeter (0.25") diameter bearing.

The lot of material used for this research was not coupon tested to determine the exact material properties. Experimental response of the test panels suggested that the

material properties used by Hatfield were too stiff for this study [23]. A material study was run analytically based on AS4/3501-6 material properties used in previous studies [23,24]. The material properties considered valid for this research are shown in Table 4 of Section 4.

3.2 Axial Compression

The experimental fixture used for the axial compression test was a 133.446 kN (30,000 lb) hydraulic compression machine (see figure 2). This is the same fixture and test setup as used in previous studies [14, 15, 17, 18 ,25, 26]. However, a modification was made to the curved panel clamping device referred to as the panel restraint system in this document. See section 3.2.1 for details of this modification.

All forty of the test panels were each setup in the test fixture, and the following boundary conditions imposed. The panel's vertical edges were unconstrained. The bottom edge of the panel was fixed and fully constrained ($u = v = w = w_{,x} = w_{,s} = 0$). The top edge of the panel was allowed vertical movement only (u = prescribed, $v = w = w_{,x} = w_{,s} = 0$).

A minimum of two test were run per panel configuration and cutout combination. See Appendix C for panel designation number, panel serial number, and experiment number correlation table. The axial load was applied by the hydraulic compression machine. The compression machine incremented the loading by moving the machine's bottom platen
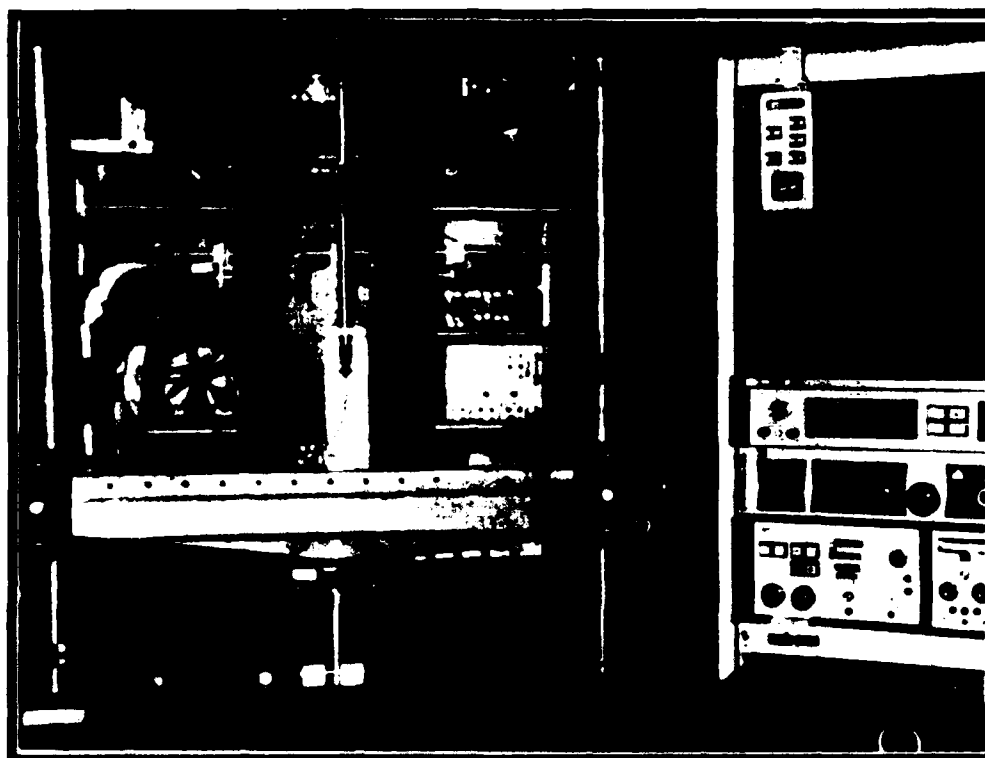
Figure 2. Experimental Setup Showing Axial Compression Fixture

a prescribed uniform displacement toward the machine's fixed top platen. Each test was completed when the collapse load was reached. For most of the tests, when the collapse load was reached, the panel continued to deform smoothly while the loading began to slowly drop off. However, the 24 ply 304.8 mm x 508 mm panel with a 50.8 mm x 50.8 mm cutout experienced sudden an complete failure at the collapse load. This was evident by a loud bang at the collapse load and a dramatic drop off of load. It was visually observed that this panel had experienced instantaneous delamination and material failure at the collapse load.

3.2.1 *Panel Restraint System Modification.* The panel restraint system is made up of a series of restraint blocks which are placed into a 31.75 mm (1.25") channel in the test fixture. The restraint blocks are tighted down against the curved panel by a series of screws. The test fixture's old panel restraint system used Coulumb friction between the restraint blocks and the panel to prevent panel horizontal circumferential movement. However, experimental data obtained by Hatfield [18] indicated movement of the panel circumferentially for the 16 and 24 ply panels. Hatfield concluded that the movement was due to an in-plane shear force brought about by uneven loading. Eight modified restraint blocks were manufactured to alleviate this anomaly. Four modified blocks were manufactured for the 16 ply panels,

28

and four for the 24 ply panels. The existing restraint blocks were used for the 8 ply panels.

The modified restraint blocks were manufactured from 4340 steel. A step was machined into each modified restraint block, so that there was restraint block to fixture contact and restraint block to panel contact at the panel vertical edge (see figure 3). A 1.905 mm (0.075") step was machined into the restraint blocks for the 16 ply panels and a 2.921 mm (0.115") step for the 24 ply panels. The outside radius of curvature of the restraint blocks is 304.8 mm (12") and the inside radius of curvature is 279.4 mm (11").

The modified restraint blocks were used at the four corners of the panel in conjunction with the old restraint blocks to prevent horizontal circumferential movement of the panel. This modification resisted horizontal circumferential movement of the panel since the Coulumb friction between the modified restraint blocks and the test fixture channel was greater than that between the restraint block and the panel. This additional resistance was enough to counter the effects of uneven loading (in-plane shear force) which occurs with the slightest eccentricity of a panel. This provided the necessary physical restraint needed at the four corners of the panel to resist horizontal circumferential movement of the panel.

Unmodified Restraint Block Used for
8 ply panels

Step either 1.905 mm (0.075") for 16 ply
or 2.921 mm (0.115") for 24 Ply

R outer = 304.8 mm (12")

R inner = 279.4 mm (11")

12.7 mm (0.5")
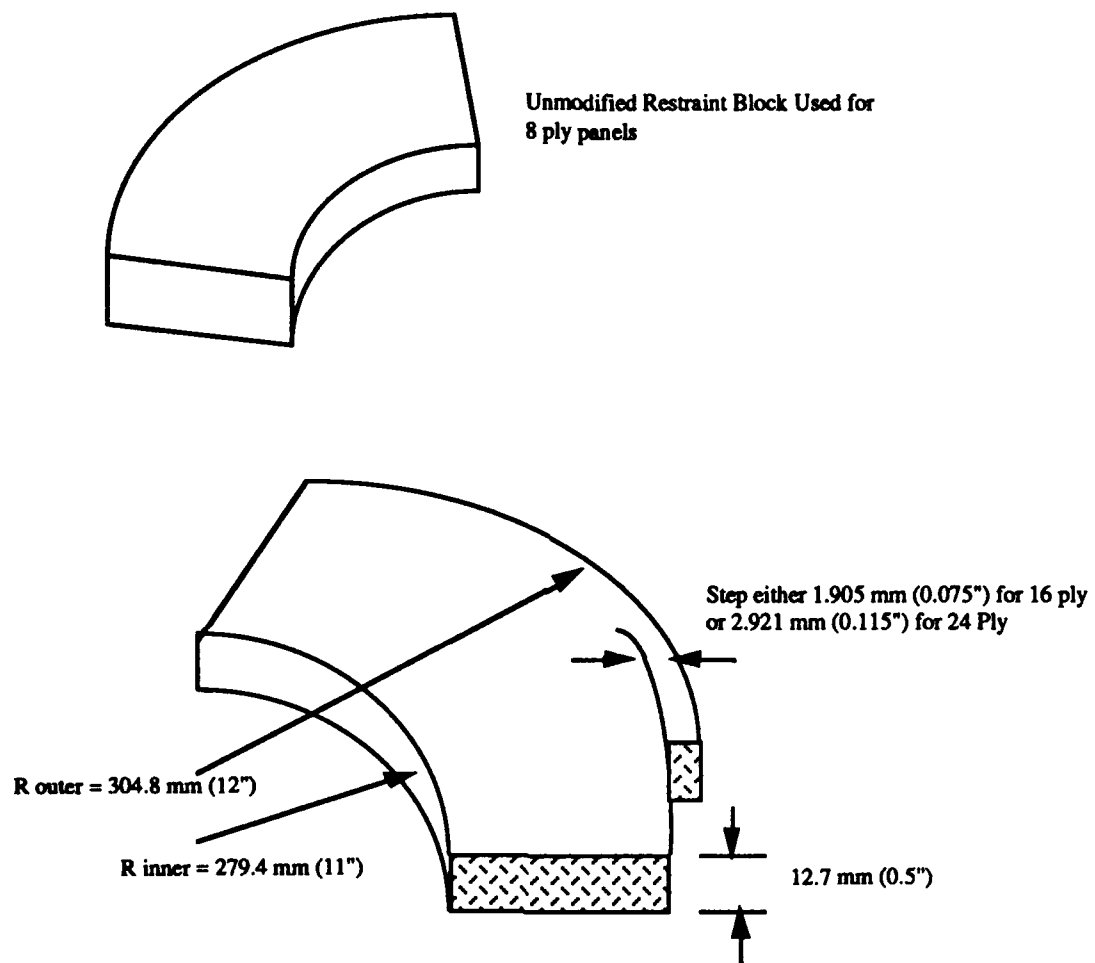
Figure 3. Modification to Restraint Block

3.3 Instrumentation

The axial compression machine had seven linear variable differential transducers (LVDT)s mounted on it. See figure 4 for LVDT locations and identification numbers. The six LVDTs shown in figure 4 were placed along the vertical and horizontal centerlines of the panel. These LVDTs were used to measure panel radial displacements (w) during compression. These LVDTs were positioned 6.35 mm (0.25") in from the panel vertical edges, and 6.35 mm in from the cutout horizontal and vertical edges. The exception being the 50.8 mm x 50.8 mm (2" x 2") and 203.2 mm x 50.8 mm (8" x 2") cutouts. These cutouts required LVDT #23 be positioned 25.4 mm (1") above the top of the cutout. This location was used because there was a mechanical interference between adjacent horizontal LVDT mounting rods. This interference limited how close LVDTs #23 and #35 could be brought together. One LVDT not shown in figure 2 was positioned between the upper and lower axial compression machine platens to measure the prescribed axial displacements at the compression machines upper platen (see test plan, Appendix A, figure A11). The axial compression machine was equipped with a load cell that measured the total applied load. The load data from the load cell and displacement data collected from the LVDTs were used to generate load versus displacement plots. These load versus displacement plots were used to compare to the SHELL numerical results.

31

Figure 4. Linear Variable Displacement Transducer's (LVDT's) Location and Identification Numbers

A total of 320 axial strain gages were required to instrument the 40 test panels. The axial strain gages were manufactured by Micromeasurements and designated by part number CEA-030-250UW-350. Four sets of axial strain gages were mounted back to back per panel. The purpose of these gages was to determine if the axial load and bending through the panels were uniform as well as symmetric. These conditions are necessary to ensure a valid test. In addition, the axial strain gage data plotted against load was used to confirm the panel collapse load. At the collapse load the load versus strain curves dramatically diverge for a set of back to back strain gages (see figure 5). Figure 5 shows divergence of the load versus strain curves immediately upon axial loading between the inside and outside panel curvature strain gages. This divergence indicates that the panel experiences a bending rate which is nonlinear.

Pcr

AXIAL LOAD (N)

● Panel Outside Curvature Strain Gage
● Panel Inside Curvature Strain Gage

0

AXIAL STRAIN (MICRONS)
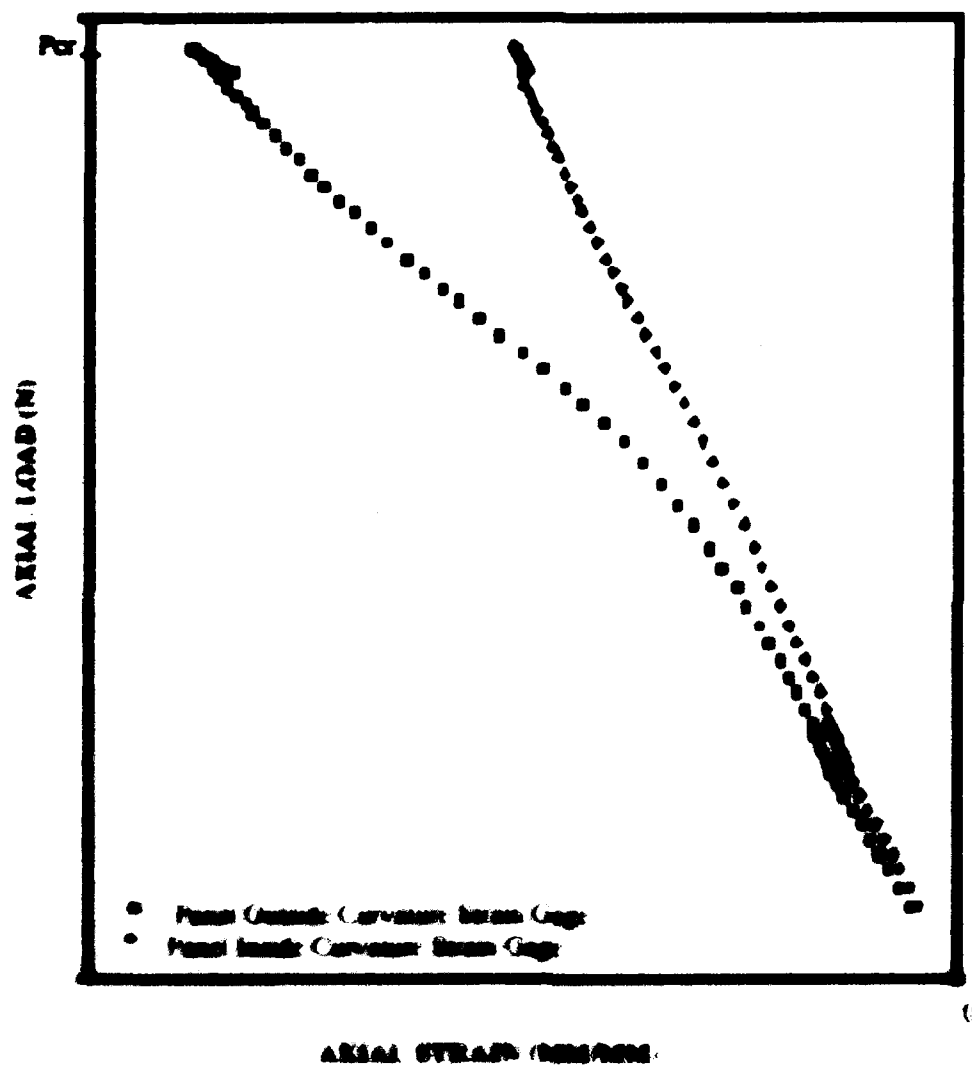
Figure   Examples of Inside vs Outside Strain Gage Divergence at Collapse Load

4. Finite Element Modeling

The first step in the finite element modeling procedure is to generate a mesh. This research required that five meshes be generated to model the two panel sizes and five cutouts. The finite element mesh used for the 304.8 mm x 304.8 mm (12" x 12") panels was the same as that used by Schimmels and Hatfield (see figures 6-10). This mesh had a total of 1825 nodes and 576 elements. The mesh used for the 304.8 mm x 508 mm (12" x 20") panels with a 50.8 mm x 50.8 mm, or 101.6 mm x 101.6 mm (4" x 4") cutout were identical to that used by Hatfield (see figures 11 and 12). This mesh had a total of 1777 nodes and 560 elements. The finite element meshes generated for the 304.8 mm x 508 mm (12" x 20") with a 127 mm x 127 mm (5" x 5"), 50.8 mm x 203.2 mm (2" x 8"), or 203.2 mm x 50.8 mm (8" x 2") cutout, used a mesh arrangement similar to the 101.6 mm x 101.6 mm cutout mesh (see figures 13 thru 15). These meshes used 12.7 mm (0.5") square elements around the cutout, and transitioned to larger elements at a minimum of two inches away from the cutout. Convergence studies conducted by Dennis indicated that the 12.7 mm square element was the optimal size for capturing the panel response around areas of large displacement and rotation while minimizing CPU run times. Therefore, the 12.7 mm element was used around the cutout. The mesh used for the 304.8 mm x 508 mm panels with a
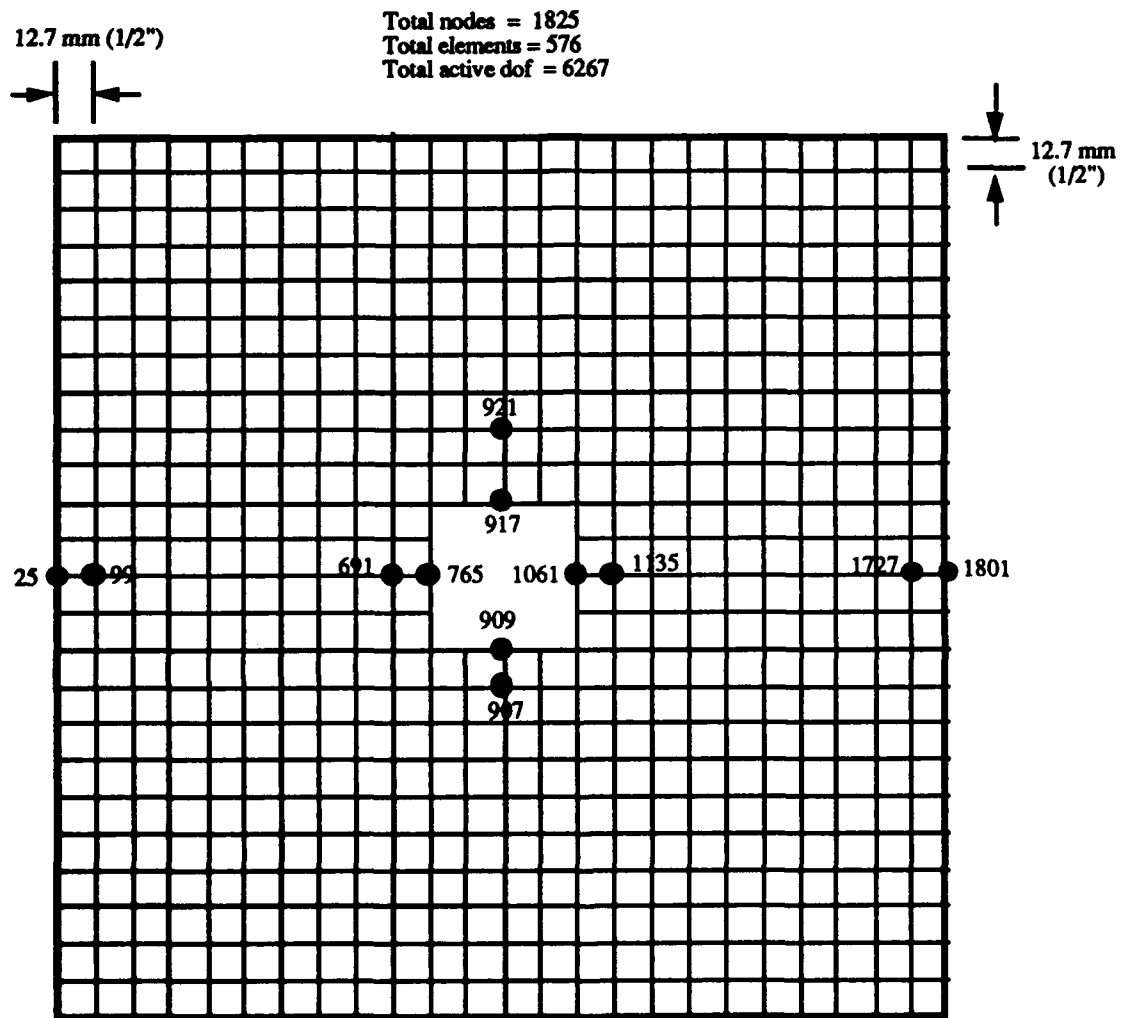
Figure 6. Finite-Element Mesh Used for 304.8 mm x 304.8 mm (12" x 12") Panel
With 50.8 mm x 50.8 mm (2" x 2") Cutout
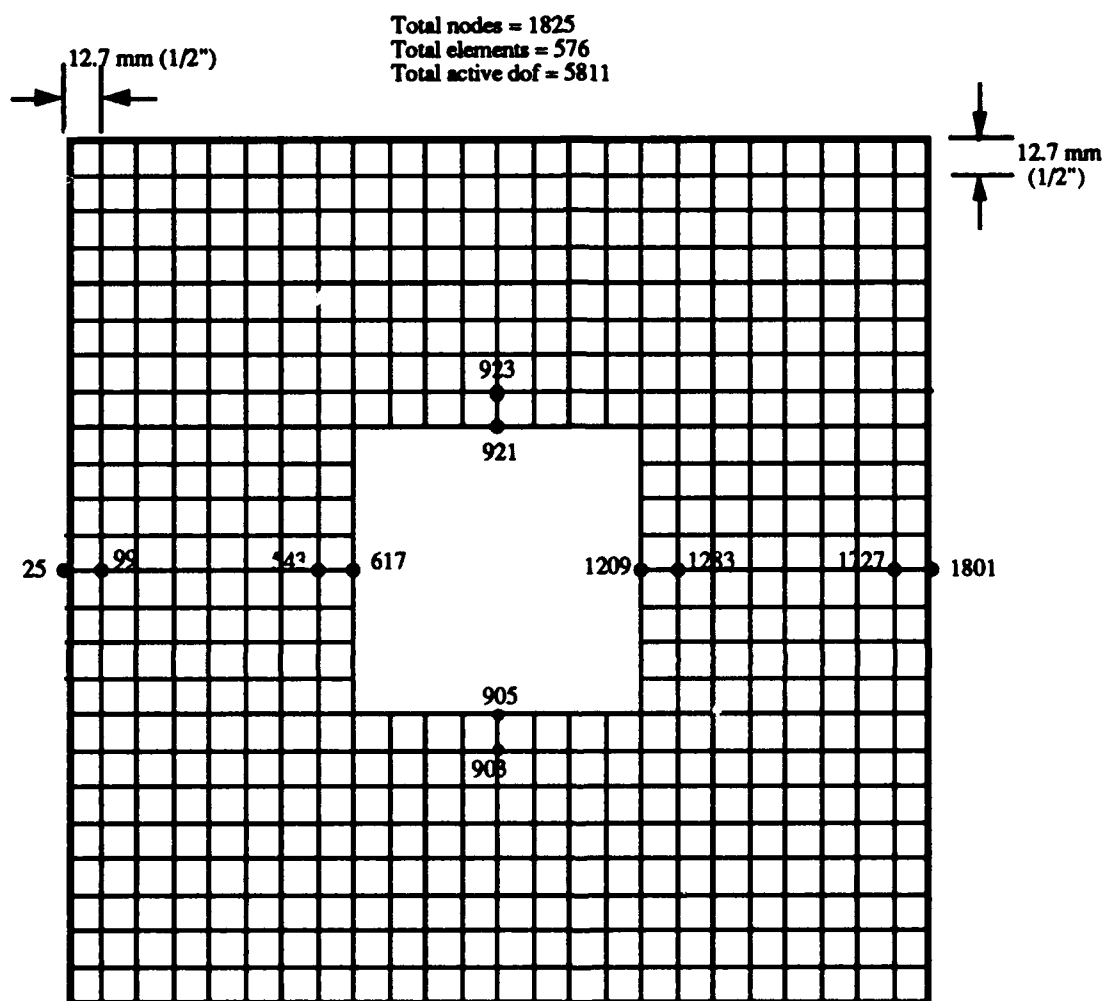
Figure 7. Finite-Element Mesh Used for 304.8 mm x 304.8 mm (12" x 12") Panel
With 101.6 mm x 101.6 mm (4" x 4") Cutout

37
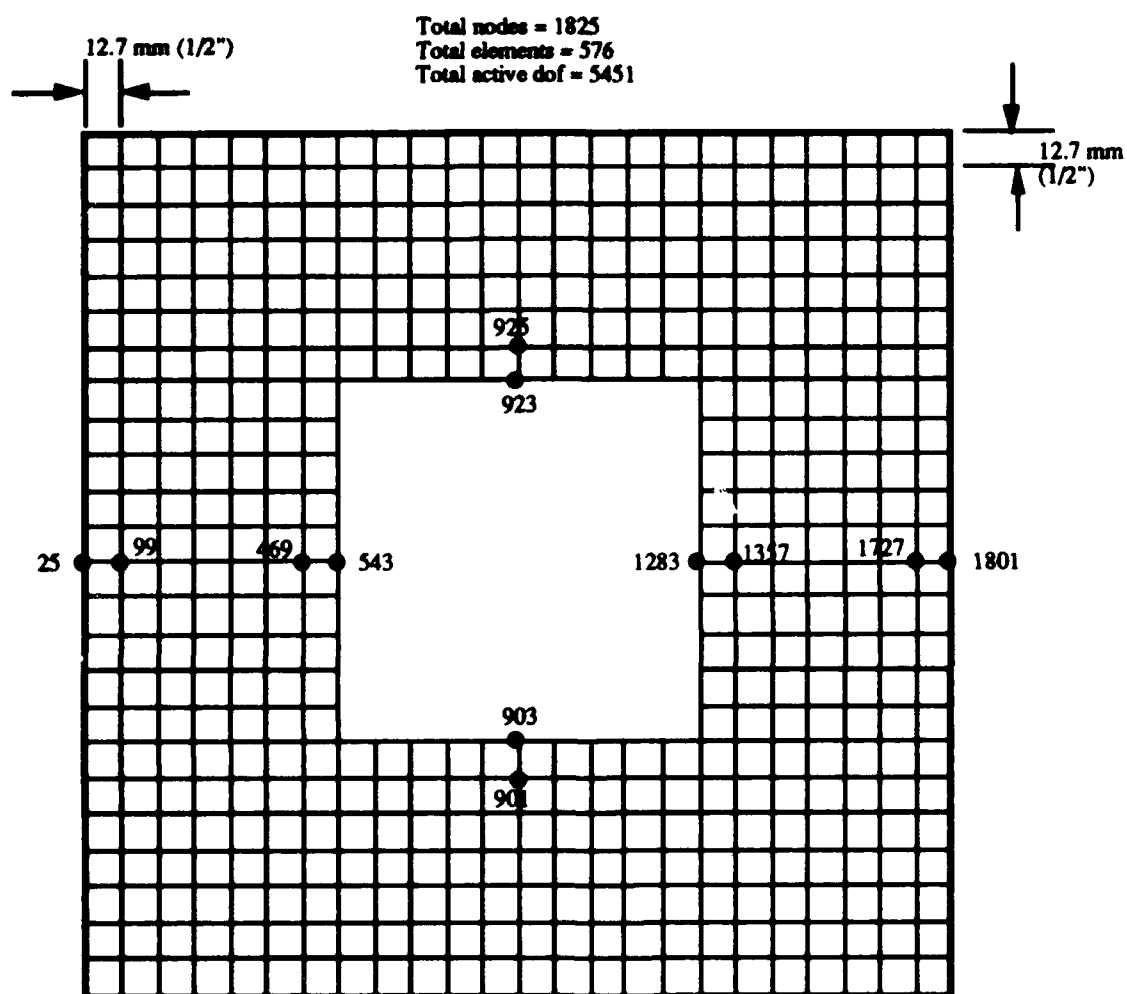
Figure 8. Finite-Element Mesh Used for 304.8 mm x 304.8 mm (12" x 12") Panel With 127 mm x 127 mm (5" x 5") Cutout
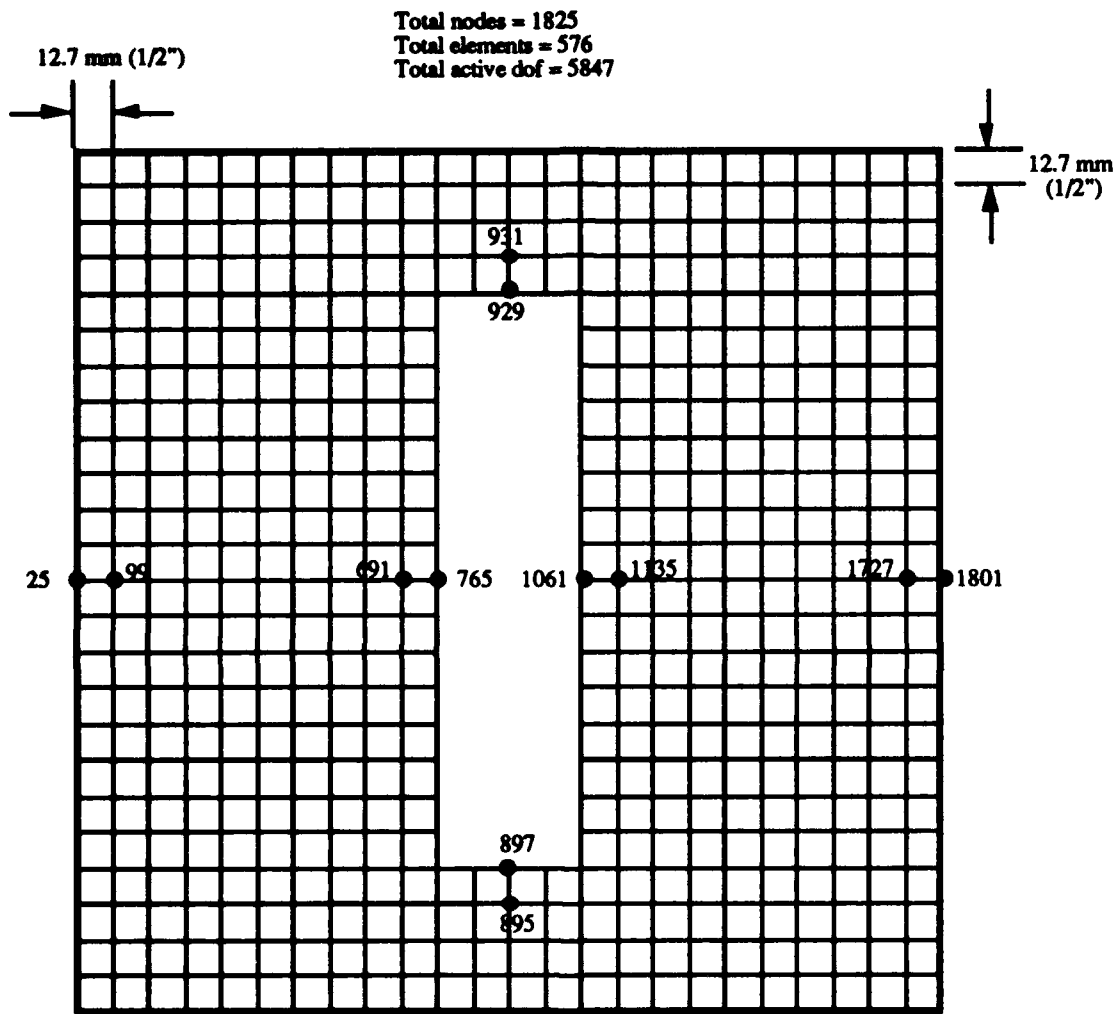
Figure 9. Finite-Element Mesh Used for 304.8 mm x 304.8 mm (12" x 12") Panel
With 50.8 mm x 203.2 mm (2" x 8") Cutout
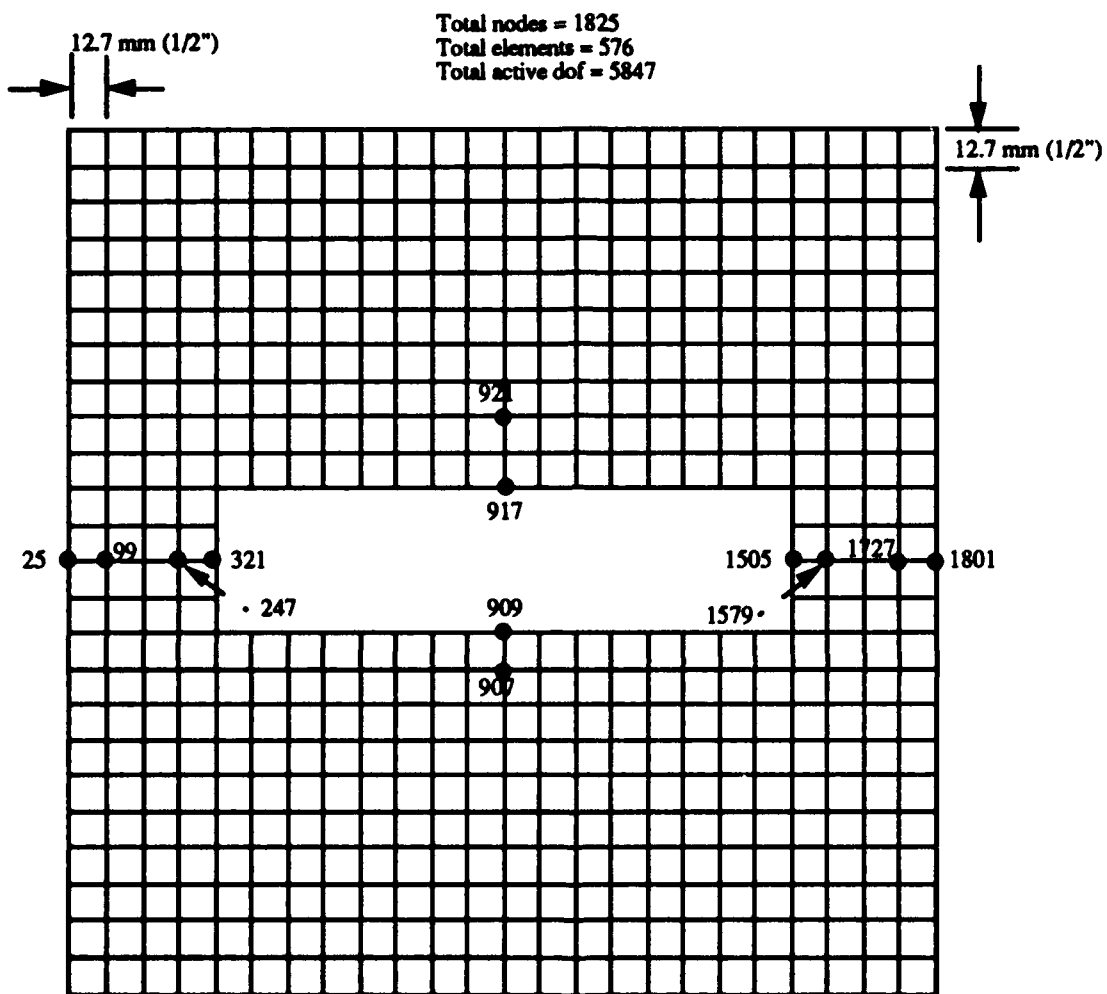
Figure 10. Finite-Element Mesh Used for 304.8 mm x 304.8 mm (12" x 12") Panel
With 203.3 mm x 50.8 mm (8" x 2") Cutout
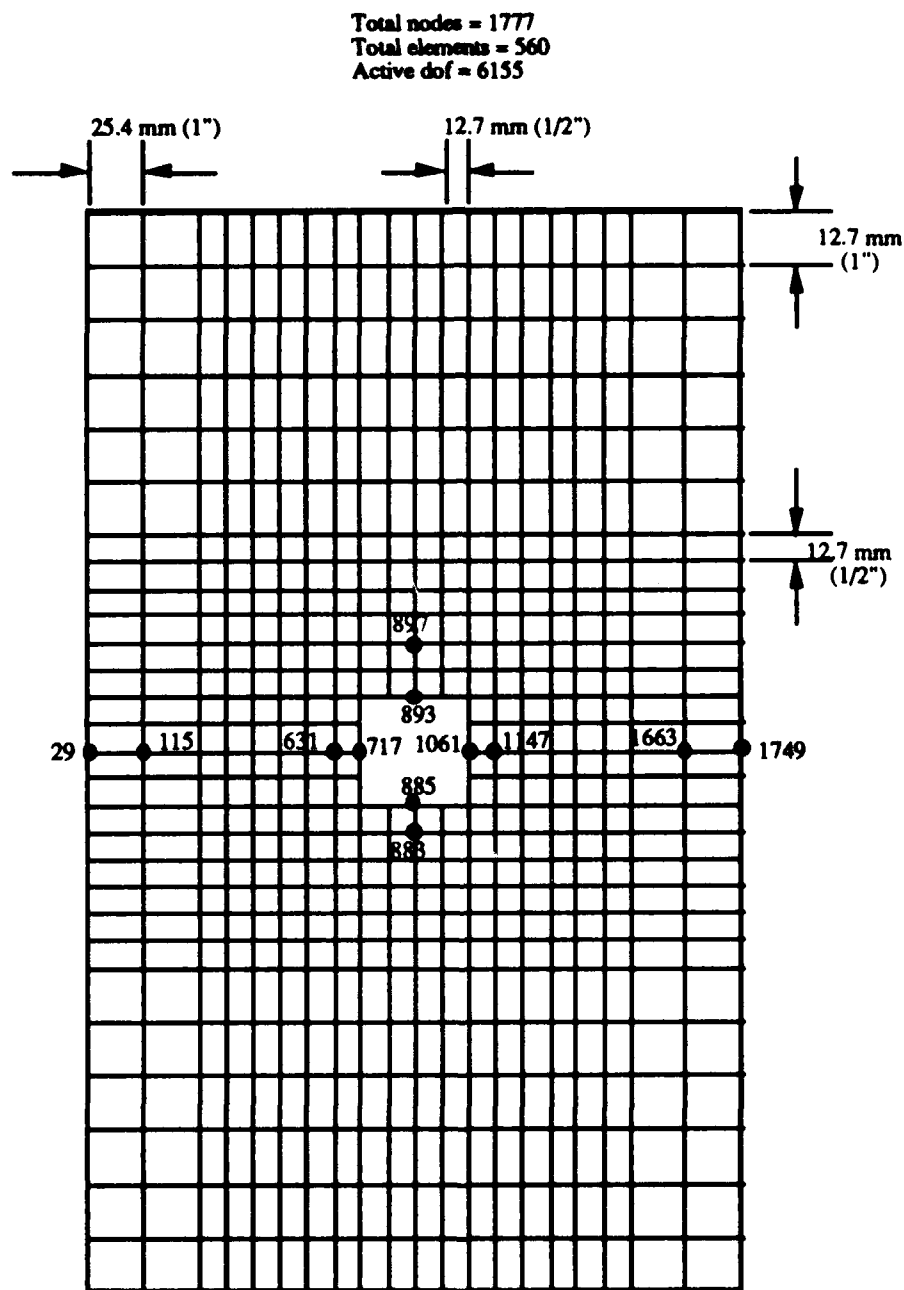
Figure 11. Finite-Element Mesh Used for 304.8 mm x 508 mm (12" x 20") Panel
With 50.8 mm x 50.8 mm (2" x 2") Cutout

41

Total nodes = 1777
Total elements = 560
Total active dof = 5699

25.4 mm (1")   12.7 mm (1/2")

25.4 mm (1")

897

897

29   115   459   545   1233   1319   1663   1749

881

873
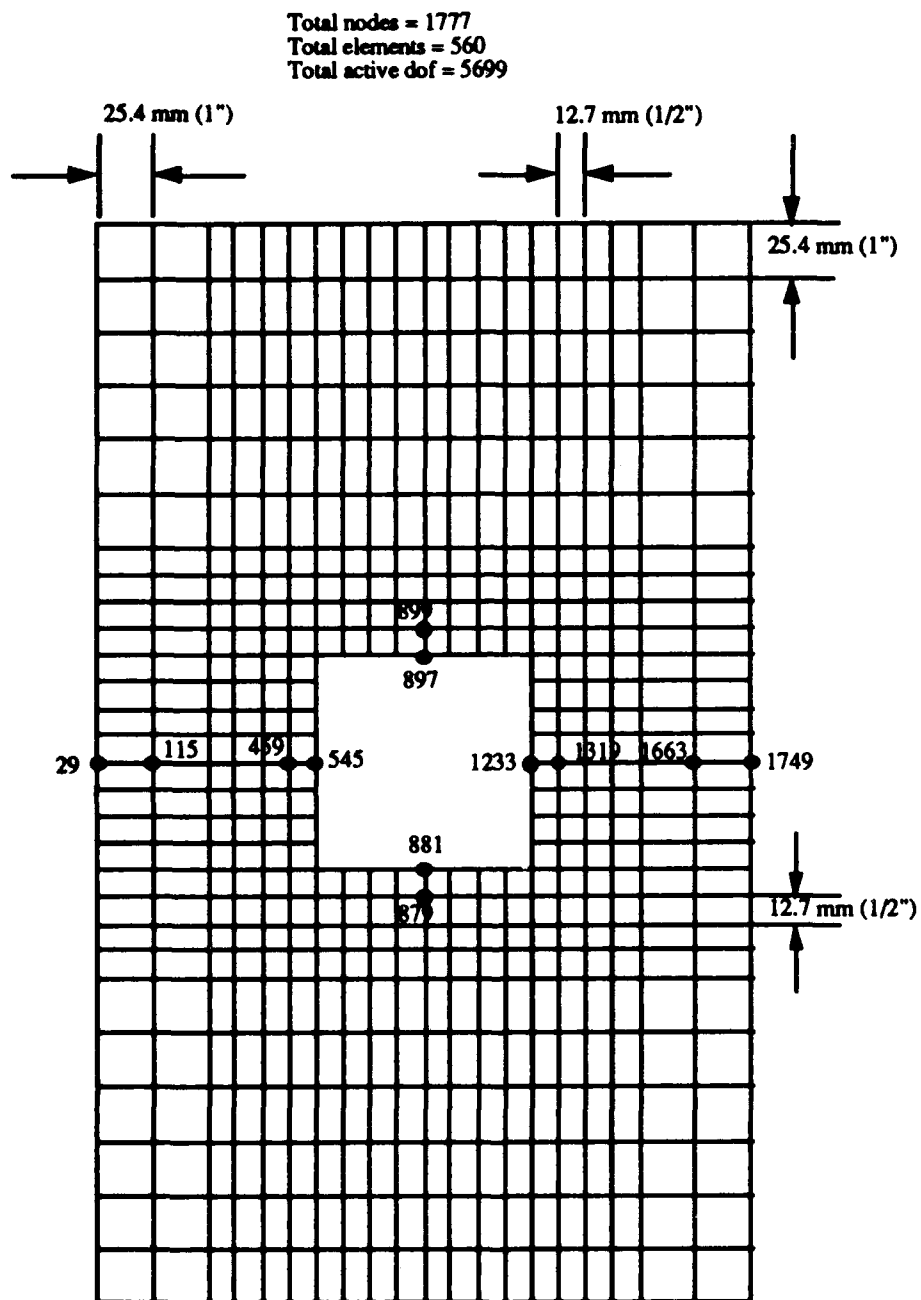
12.7 mm (1/2")

Figure 12. Finite-Element Mesh Used for 304.8 mm x 508 mm (12" x 20") Panel
With 101.6 mm x 101.6 mm (4" x 4") Cutout

42

Total nodes = 2085
Total elements = 660
Total Active dof = 6443
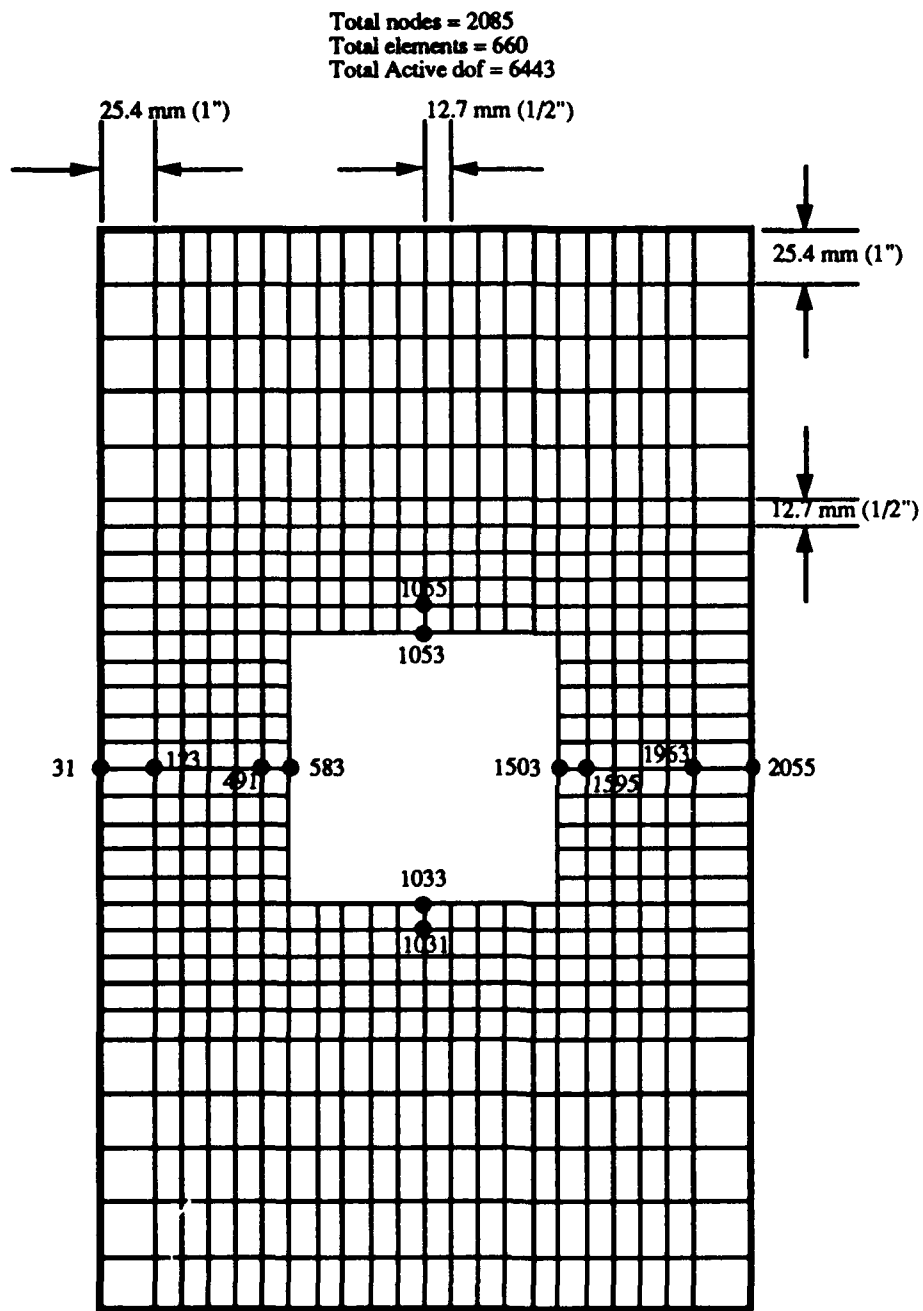
Figure 13. Finite-Element Mesh Used for 304.8 mm x 508 mm (12" x 20") Panel
With 127 mm x 127 mm (5" x 5") Cutout

43

Total nodes = 1829
Total elements = 576
Total active dof = 5961
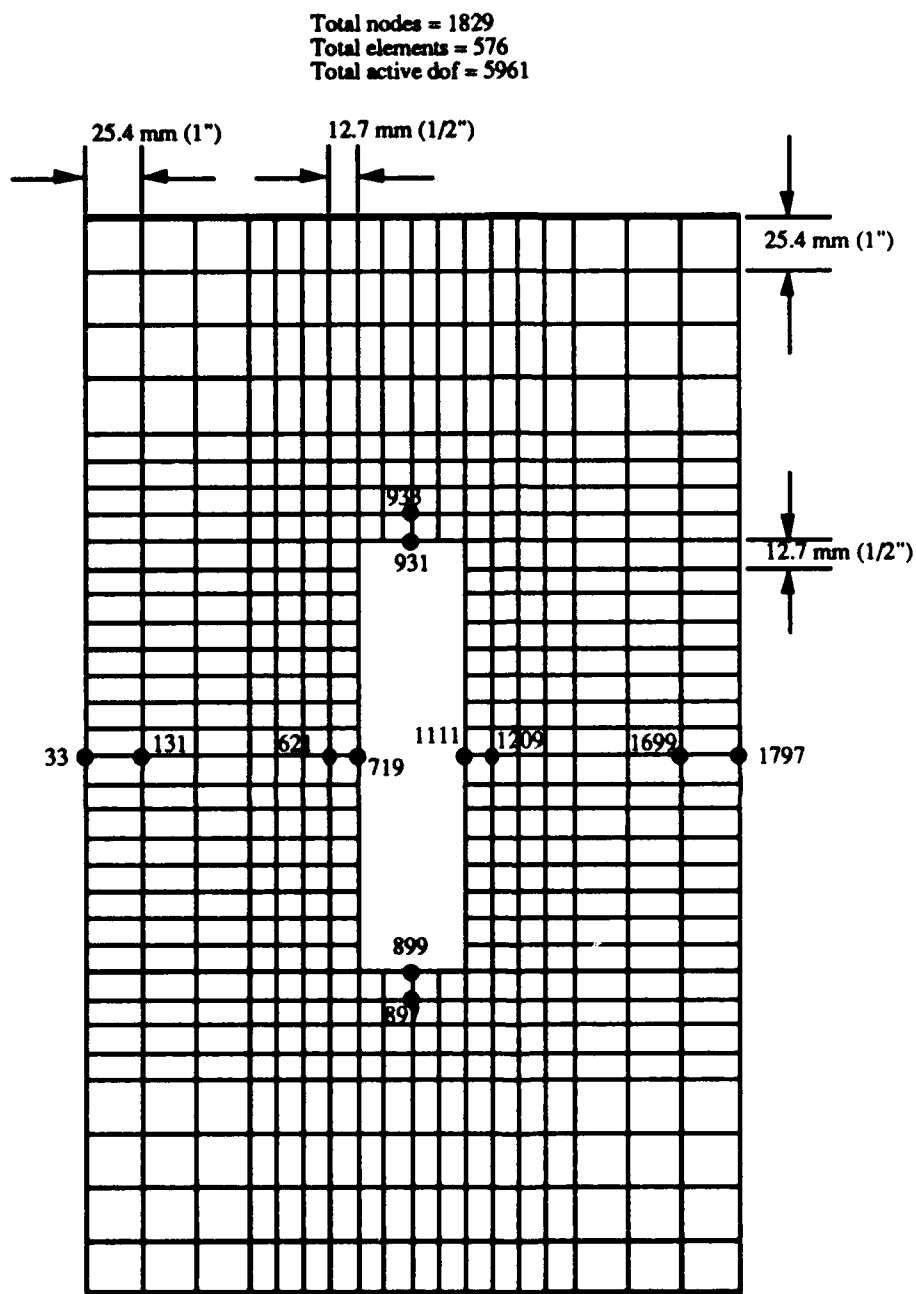
Figure 14. Finite-Element Mesh Used for 304.8 mm x 508 mm (12" x 20") Panel
With 50.8 mm x 203.3 mm (2" x 8") Cutout

Total nodes = 1973
Total elements = 624
Total active dof = 6383

12.7 mm (1/2")

25.4 mm (1")

995

991

27   267   347   1627   707   1867 1947

107

983

981

12.7 mm (1/2")
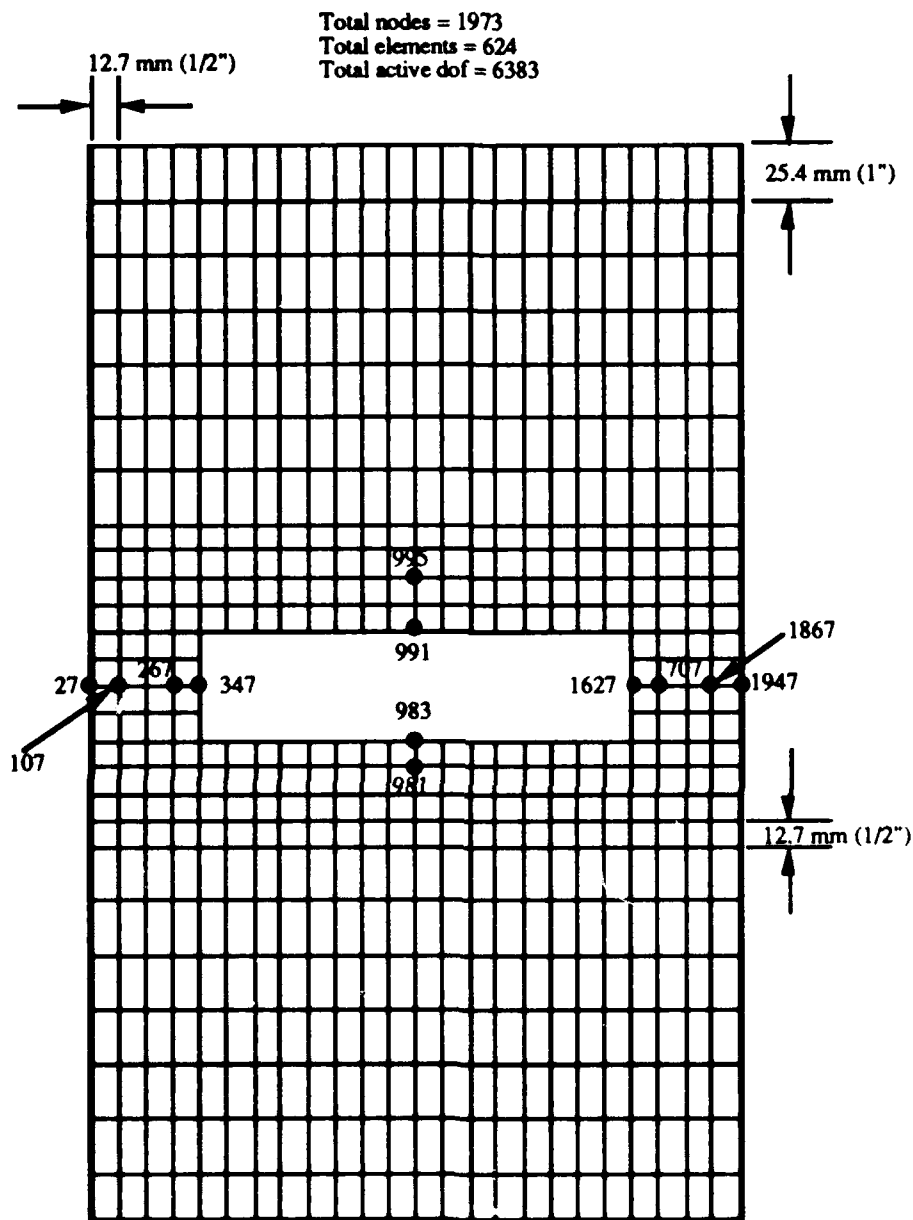
Figure 15. Finite-Element Mesh Used for 304.8 mm x 508 mm (12" x 20") Panel
With 203.2 mm x 50.8 mm (8" x 2") Cutout

45

203.2 mm x 50.8 mm cutout had 1973 nodes and 624 elements. The mesh used for the 304.8 mm x 508 mm panels with a 50.8 mm x 203.2 mm cutout had a total of 1829 nodes and 576 elements. Finally, the mesh used for the 127 mm x 127 mm cutout had 2085 nodes and 660 elements.

The SHELL program uses a two dimensional 36 degrees of freedom rectangular curved finite element where the element shape functions are derived assuming a displacement field. This element incorporates the through-the-thickness parabolic transverse shear distribution. The four corner nodes have seven degrees of freedom (u, v, w, ψ_x, ψ_s, $w_{,s}$, and $w_{,x}$). The mid-side nodes have two degrees of freedom (u and v) (see figure 16). This element was previously used by Schimmels and Hatfield in their collapse analysis of cylindrical panels with large cutouts [17-19].

The material properties used for the SHELL analysis were obtained by Dr. R. S. Sandhu of the Flight Dynamics Laboratory [23]. Table 3 provides a summary of the material properties used analytically. These material properties were later deemed to be too stiff based on experimental results. This lead to the derived set of material properties listed in Table 4 which were based on material properties of AS4/3501-6 used in previous studies. Four analytical problems previously ran with the material properties in Table 3 were ran again using consistent panel boundary conditions and the material properties in Table 4 to determine the linearity in which the collapse load varies given a variation in material

46

properties. This linear variation in collapse load was expressed as a numerical knockdown factor for the set of less stiff material properties. A knockdown factor of 0.9831 was derived based on the average difference of collapse load using Table 3 versus Table 4 material properties. This knockdown factor was applied to all numerical loads obtained.

Table 3. Properties of AS4/3501-6 Used by SHELL

Elastic Modulus Along Fibers in Compression (E_1)	135.8 GPa (19.7 Msi)
Elastic Moduli Transverse to Fibers in Compression ($E_2 = E_3$)	10.9 GPa (1.579 Msi)
Major Poisson's Ratio (V_{12})	0.276
Elastic Moduli in Shear ($G_{12} = G_{13}$)	6.4 GPa (0.925 Msi)
Transverse Elastic Modulus in Shear (G_{23})	3.2 GPa (0.462 Msi)

Table 4. Basic Material Properties of AS4/3501-6 Graphite/Epoxy

Elastic Modulus Along Fibers in Compression (E_1)	135.9 GPa (19.7 Msi)
Elastic Moduli Transverse to Fibers in Compression ($E_2 = E_3$)	10.1 GPa (1.468 Msi)
Major Poisson's Ratio (V_{12})	0.28
Elastic Modulus in Shear (G_{12})	6.09 GPa (0.883 Msi)
Elastic Modulus in Shear (G_{13})	3.04 GPa (0.441 Msi)
Transverse Elastic Modulus in Shear (G_{23})	3.04 GPa (0.441 Msi)
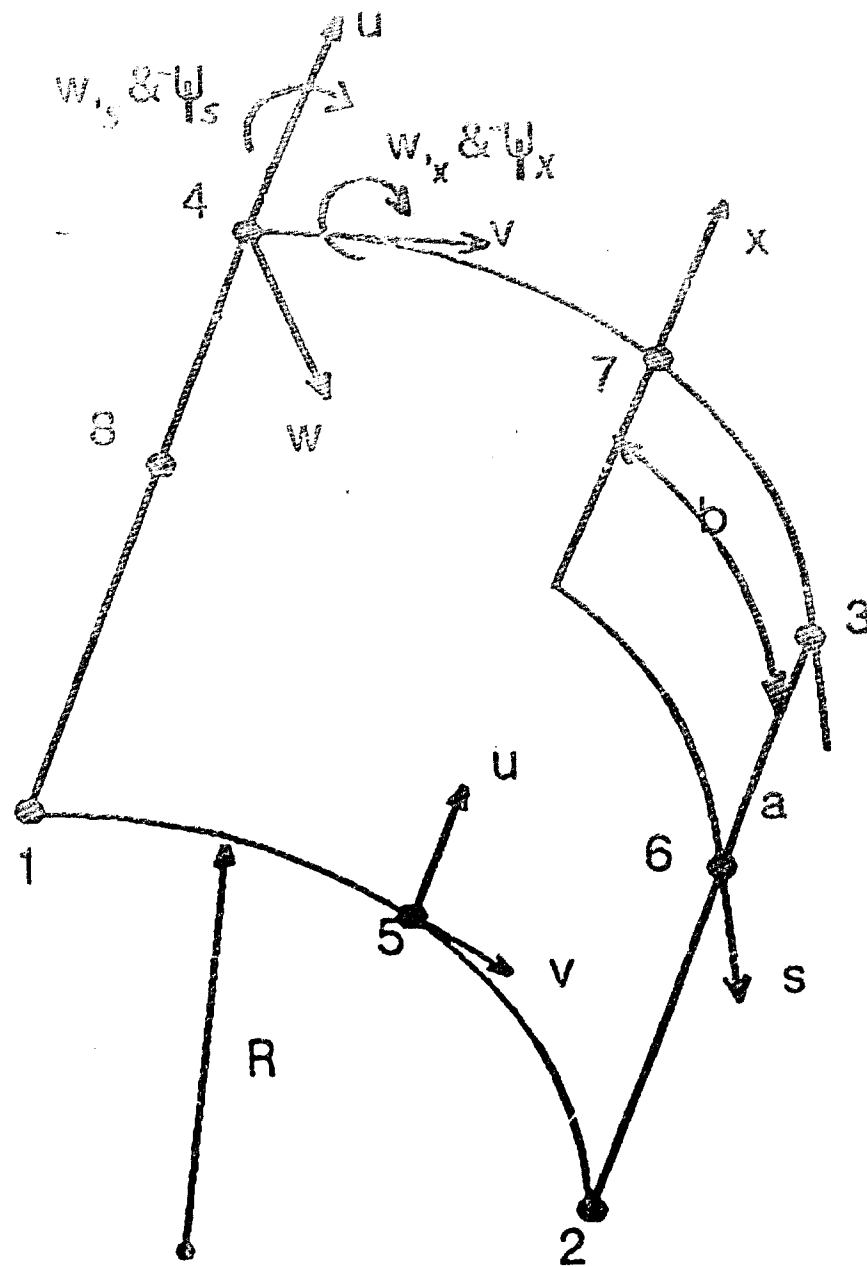
Figure 16: SHELL 36-Degree-of-Freedom Element

Since the SHELL program incorporates a through-the-thickness transverse shear distribution, it is sensitive to the thickness of the panel. Therefore, the average ply thickness of each panel/cutout configuration was taken from the panel thickness measurement data obtained from the Flight Dynamics Laboratory and incorporated into the respective SHELL input deck. The average ply thicknesses used by the SHELL program for each panel configuration and cutout combination are listed in Table 5.

All panels were analyzed for a radius of curvature of 304.8 mm (12"). This dimension is the radius of curvature measured to the convex outside surface of the SHELL. The SHELL program interprets the radius of curvature input to be at the datum surface. An analytical problem was run using the radius of curvature of the concave inside surface of an eight ply panel to determine the effects of varying the radius of curvature. See section 5 for the results of this radius of curvature numerical study.

The ply lay ups studied analytically were all symmetric quasi-isotropic lay ups of [0/45/-45/90]. The panel lay up orientation is consistent with the axes system used by SHELL which is defined in figure 1. A numerical case was run for a symmetric [0/-45/45/90] lay up to investigate the effects of reversing the sequence of the 45 degree plies on the panel collapse load. See section 5 for the results of this study.

Table 5. Average Ply Thickness

Panel Designator	No. of Plies	Average Ply Thickness (mm)
A8-13-22	8	0.134620 (0.0053000")*
A8-13-44	8	0.135255 (0.0053250")
A8-13-55	8	0.136144 (0.0053600")*
A8-13-28	8	0.134620 (0.0053000")*
A8-13-82	8	0.134620 (0.0053000")*
A8-21-22	8	0.138938 (0.0054700")*
A8-21-44	8	0.137109 (0.0053980")
A8-21-55	8	0.140294 (0.0055234")
A8-21-28	8	0.139192 (0.0054800")
A8-21-82	8	0.139497 (0.0054920")
B16-21-22	16	0.129540 (0.0051000")*
B16-21-44	16	0.137160 (0.0054000")*
B16-21-55	16	0.136906 (0.0053900")
B16-21-28	16	0.138013 (0.0054336")
B16-21-82	16	0.132080 (0.0052000")*
C24-21-22	24	0.139954 (0.0055100")*
C24-21-44	24	0.139954 (0.0055100")*
C24-21-55	24	0.139446 (0.0054900")*
C24-21-28	24	0.139954 (0.0055100")*
C24-21-82	24	0.137668 (0.0054200")*

* These thicknesses were later corrected to more exact values obtained
from experimental panel thickness measurements. A ply thickness
interpolating technique was used to adjust the analytical loads
obtained. This ply thickness interpolating technique was verified
analytically. See section 5 for a description of this technique.

All panel configurations and cutout combinations were analyzed using the following boundary conditions. The panel vertical edges were free, therefore all seven degrees of freedom at the element corner nodes and the two degrees of freedom at the element mid-side nodes were unconstrained along the free vertical edges. The bottom horizontal edge of the panel was fully constrained ($u = v = w = \psi_x = \psi_s = w_{,s} = w_{,x} = 0$). Therefore, all seven degrees of freedom at the element corner nodes and the two degrees of freedom at the element mid-side nodes were constrained along the horizontal bottom edge of the panel. The panel top horizontal edge was allowed to displace axially a precribed incremental amount (u), but all other degrees of freedom were constrained ($u = $ prescribed $v = w = \psi_x = \psi_s = w_{,s} = w_{,x} = 0$). Therefore, six of the degrees of freedom at the element corner nodes and one degree of freedom at the element mid-side nodes were constrained along the horizontal top edge of the panel.

Even though not shown in figures 6-15, there are finite elements within the cutout region, this occurs when the automatic mesh generator is used. The SHELL program models the cutout by not calculating the stiffness for the elements within the cutout area [4]. In addition, all nodes of these elements within the cutout region are constrained ($u = v = w = \psi_x = \psi_s = w_{,s} = w_{,x} = 0$).

The SHELL program applies a uniform axial compressive displacement which is prescribed at each of the top edge nodes. The number of top edge nodes ranged from 37 for the

304.8 mm x 508 mm panel with a 50.8 mm x 203.2 mm cutout, to 49 for the 304.8 mm x 508 mm panel with a 203.2 mm x 50.8 mm cutout. The SHELL program calculates the load required at each top edge node in order to displace the prescribed amount. Next, the total compressive load is calculated using the top edge nodal loads. A nonuniform displacement along the top edge of the panel would result if a uniform load was prescribed at each of the top edge nodes. This nonuniform displacement is due to the presence of the cutout [27]. This study used prescribed increments of displacement of 0.0005", 0.001", and 0.002" for the 8, 16, and 24 ply panels, respectively. Some of the 16 and 24 ply panels were ran a second time to refine the panel collapse load. This refinement was obtained by transitioning to a 0.0005" increment near the panel collapse load defined in the previous run.

Figures 6-15 show the numerical nodes used for comparison against the experimental LVDT radial displacement data. The LVDT locations fall between pairs of numerical nodes. Therefore, a linear interpolation of the numerical radial displacement data was used to determine the numerical radial displacements at the LVDT locations. These interpolated numerical values for the radial displacements (w) were then compared to the experimental LVDT radial displacements.

All numerical analyses were done on SUN SPARCstation 2 computers. A sample input deck used for this research is included in Appendix D.

5. Results and Discussion

5.1 Introduction

This chapter is broken into three distinct parts. The first section dicusses other numerical studies conducted as part of this research and the results. This section is first, because some of the techniques discussed were used in adjusting the numerical results obtained by SHELL. The second section discusses the significant numerical results obtained using SHELL. The final section compares the numerical data to the experimental data obtained for this research.

5.2 Other Numerical Studies

The use of refined meshes, coupled with the dimensionality of the panel specimens used in this study, required large amounts of computer time (on the average of 200,000 CPU seconds) using SHELL. Therefore, the goal of the parametric studies described in this section was to determine practical one dimensional methods which can be used in lieu of SHELL (a two dimensional model) to estimate collapse loads for variations in ply thickness, radius of curvature, cutout size, and ply layup from a known SHELL solution. In addition, these same methods could serve as a practical tool for the designer to estimate collapse loads for panel variations from a standardized panel numerical solution.

These numerical studies were conducted using SHELL to determine the effects of ply thickness, cutout size, radius of curvature, and ply lay up; on the instability of a panel with a centrally located cutout undergoing axial compression. All

studies conducted assumed the panel's lower horizontal edge was fully constrained while the panel's top horizontal edge was allowed to only displace axially. The panel vertical edges were unsupported. In addition, the studies used material properties of AS4/3501-6 graphite epoxy shown in Table 3.

The ply lay up study investigated the effects of reversing the sequence of 45 degree plies in a symmetric quasi-isotropic panel with free vertical edges. Two numerical cases were run using equivalent panels. One case used a $[0/45/-45/90]_s$ lay up and the other used a $[0/-45/45/90]_s$ lay up. Results obtained using SHELL showed no affect on the panel collapse load. Both panels had equivalent load versus displacement curves. Therefore, it is concluded that any $[0/45/-45/90]$ symmetric lay up will collapse at the same load as a symmetric $[0/-45/45/90]$ lay up. This conclusion is valid only for a panel with unsupported vertical edges [14].

The results of changing the radius of curvature numerically in SHELL indicated that as the radius of curvature decreases the collapse load increases. A decrease of 1.02 mm (0.04") in radius of curvature for a 304.8 mm (12") radius of curvature eight ply panel with average ply thickness of 0.127 mm (0.005") showed a 8.9 N (2 lb) increase in collapse load. In terms of percent, a 1.0% decrease from a 304.8 mm (12") radius of curvature results in a 0.48% increase in collapse load. The effect on the panel collapse load would be fairly significant for a larger reduction in radius of curvature. For instance, an increase of radius of curvature of 10%, which correlates to a increased radius of curvature of 335.28

mm (13.2") from a 304.8 mm (12") radius of curvature, results in a 4.8% reduction in collapse load.

The next numerical study was based on the one dimensional Euler buckling equation for a beam with fixed ends and free vertical edges. The Euler buckling equation is introduced merely to identify the geometric parameters which are significant in a plate. The author's intent is not to suggest that the Euler buckling equation is valid for calculating a collapse load for a plate. The Euler buckling equation is defined as [28]:

$$P_{cr} = 4\pi^2 EI / L^2 \tag{1}$$

where the moment of inertia $I = bt^3/12$, and E is the Young's modulus for an isotropic material. This one dimensional equation identifies the parameters which are used to approximate the two dimensional SHELL problem. Although this equation is for a one dimensional problem, it displays some of the features found in a two dimensional plate problem. These features are the thickness cubed in the equation numerator, the length squared in the denominator, and the extensional width in the numerator. Extensional width is defined as the circumferental distance between the cutout and panel vertical edges (see figure 4). The geometric features this one dimensional equation incorporates makes it a simplified base for deriving a one dimensional model which can be used as a practical tool for estimating collapse loads for most panels.

Equation (1) along with the constitutive equation for classical laminated plate theory (CLPT) was used to arrive at a practical collapse load estimating technique. This technique is applied to a known numerical solution to estimate collapse loads for panels of varying average ply thickness, cutout size, and axial length. A major characteristic of this technique is that it is bending stiffness orientated. The flexural rigidity term (EI) in equation (1) is equivalent to the D_{11} term in classical laminated plate theory for a symmetric laminate. This is arrived at by starting with the moment equation for a beam,

$$M_x = EIw_{,xx} \tag{2}$$

and the CLPT constitutive equation:

$$N = [A]\varepsilon^o + [B]\kappa \tag{3}$$

$$M = [B]\varepsilon^o + [D]\kappa$$

where $[B] = 0$ for a symmetric laminate, and $\kappa_x = -w_{,xx}$, $\kappa_y = -w_{,yy}$, $\kappa_{xy} = -2w_{,xy}$. Therefore, M_x for a plate is:

$$M_x = D_{11}w_{,xx} + D_{12}w_{,yy} + D_{16}w_{,xy} \tag{4}$$

Neglecting the effects of $w_{,yy}$ and $w_{,xy}$ in equation (4) yields:

$$M_x = D_{11}w_{,xx} \tag{5}$$

If equation (2) is set equal to equation (5), one obtains D_{11} = EI. This result signifies that the model is bending stiffness orientated. Therefore, collapse load estimates made using this model will yield more accurate estimates for panels that have a propensity for larger magnitudes and distributions of bending rotations.

Equation (1) is applied to a composite shell with a cutout by assuming that the area between the cutout vertical edge and the panel vertical edge behave similar to a beam with free vertical edges. Therefore, in the case of a panel with a cutout there are two beam-like areas, one on each side of the cutout. The model derived from the Euler buckling equation assumes that the area between the cutout vertical edges, above and below the cutout, are not major players in the collapse of the panel. Therefore, the panel is being modeled by two fixed beams with free vertical edges. For a panel to be representative of the model, the stress field above the cutout must be channeled into the column-like areas as soon as possible. This channeling of the stress field is dependent on the extensional length and width of the panel. Extensional length is defined as the axial distance from the horizontal edge of the panel to the horizontal edge of the cutout. This extensional length is not accounted for in the estimating model. However, the smaller the extensional length the sooner the the stress field is channeled to these column-like areas.

The three variables which collapse load estimates require are the panel thickness (t), panel axial length (L), and extensional width (b). The goal is to develop a technique that allows the

57

designer an opportunity to vary one of the three variables and estimate the collapse load for the new panel configuration. This is done by assuming that a factor Y exists such that:

$$P_{cr}' = Y\, P_{cr} \qquad Y = P_{cr}'/P_{cr} \qquad (6)$$

where P_{cr}' is the unknown collapse load, and P_{cr} is the collapse load from the known solution. Equation (6) is applied as an estimating technique for a composite panel with a centrally located cutout by substituting equation (1) into equation (6) for P_{cr} and P_{cr}'. The factor Y is determined by assuming panel material properties, panel number of plies, and two of the three variables (t, b, and L) held constant. In the case of varying thickness:

$$Y = (t_{ave}')^3/(t_{ave})^3 \qquad (7)$$

where t_{ave}' is the panel average ply thickness for the unknown solution, and tave is the average ply thickness for the known solution. Again, the thickness cubed term, the length squared term, and the extensional width term are key features in the one dimensional model since they are terms which are found in most plate equations. In the case of varying length:

$$Y = (L)^2/(L')^2 \qquad (8)$$

where L' is the panel axial length for the unknown solution, and L is the axial length for the known solution. The factor used for varying extensional width is:

$$Y = b'/b \qquad (9)$$

where b' and b are the panel extensional widths for the unknown and known solution, respectively.

The results of varying the average ply thickness using SHELL verified the use of equation (6) with Y as defined in equation (7). Table 6 shows the panel configurations and cutout combinations ran to verify the above equation. See Appendix A for instructions on how to interpret panel designator number. Table 6 should be interpreted as follows. The second and third column of Table 6 show numerical collapse loads obtained using SHELL. The collapse loads in the second column are defined as the known solution. The numerical collapse loads in the third column were obtained to verify the estimated collapse loads using equation (6) and (7). In addition, these two columns show adjacent to the collapse load the respective average ply thickness used by SHELL. The fourth column of Table 6 documents the estimated collapse load (P_{cr}') using equations (6) and (7). The values (P_{cr}') in the fourth column are calculated using the numerical collapse load (P_{cr}) and thickness (t_{ave}) in the second column as the known numerical solution, and the thickness (t_{ave}') in the third column is the panel thickness which a collapse load estimate is sought for. The fifth column is the percent difference between the

estimated collapse load (P_{cr}') and the verification numerical collapse load in the third column.

Table 6 shows P_{cr}' correlation to actual numerical results within 4.6%. The exception is for the short panel with a 50.8 mm x 50.8 mm (2" x 2") cutout. This panel behaves more like a panel without a cutout, therefore a different approach was used to adjust the collapse load for this panel configuration. The other short panel cases showed closer correlation to the values obtained by SHELL and the estimated values. This is due to the bending stresses brought about by the presence of a large cutout having a greater influence on the collapse load of the panel. Since the Euler model is bending stiffness oriented with EI = D_{11}, estimates of the collapse load for panels that have a propensity for larger magnitudes and distributions of bending rotations will yield more accurate estimates of the collapse load.

When comparing the four panel configurations, the greatest deviation between the estimated and SHELL numerical results for the collapse load was experienced for the shorter eight ply panels with an axial length of 304.8 mm. This result is expected because the magnitude and distribution of bending motion occurring in a shorter panel is less than what would be present in a longer thicker panel. Table 6 reflects this since the percent difference between the SHELL estimate and the estimate using equation (6) and (7) decreases with increasing thickness and panel length.

This estimating technique was used to adjust the collapse loads obtained by SHELL for those panels indicated in Table 5 in section 4. The SHELL collapse loads were adjusted for these cases

since they were obtained using approximate values of the panel thickness. The estimated values (P_{cr}') reflect the collapse load for the exact test panel thicknesses (t_{ave}'). Table 7 provides the thicknesses of these panels and the adjusted collapse loads using equation (6) and (7).

Table 6.   SHELL Verification of Equation (6) and (7)

Panel Designator	P_{cr}/t_{ave} (lbs)/(in)	P_{cr}/t_{ave}' (lbs)/(in)	P_{cr}' (lbs)	%
A8-13-22	2339/0.005	2598/0.0053	2786	+6.7
A8-13-22	2598/0.0053	2608/0.005365385	2695	+3.2
A8-13-22	2339/0.005	2608/0.005365385	2890	+9.8
A8-13-44	1228/0.005	1435/0.005325	1483	+3.2
A8-13-44	1418/0.0053	1435/0.005325	1438	+0.2
A8-13-44	1228/0.005	1418/0.0053	1463	+3.1
A8-13-55	1081/0.005	1291/0.00536	1332	+3.1
A8-13-28	1476/0.005	1678/0.0053	1758	+4.6
A8-13-82	622/0.005	709/0.0053	741	+4.5
A8-21-44	1154/0.00533	1186/0.005398	1199	+1.1
A8-21-44	*1100/0.00521	1154/0.00533	1178	+2.0
A8-21-44	*1100/0.00521	1186/0.005398	1223	+3.8
A8-21-55	769/0.00546	789/0.0055234	796	+0.9
A8-21-82	698/0.00548	701/0.005492	703	+0.3
B16-21-44	*5131/0.00532	5309/0.0054	5366	+1.1
B16-21-55	3396/0.00535	3455/0.00539	3473	+0.5
B16-21-28	6296/0.0054	6386/0.0054336	6414	+0.4
C24-21-44	*12959/0.00542	13410/0.00551	13615	+1.5

*Note: Numerical data obtained from reference [18].

Table 7: Adjusted Collapse Load Data

Panel Designator	Average Ply Thickness (t_{ave}')	Adjusted Collapse Load (P_{cr}')
A8-13-22	0.1361 mm (0.005359375")	11.949 kN (2686 lbs)*
A8-13-55	0.1363 mm (0.005365385")	5.761 kN (1295 lbs)
A8-13-28	0.1357 mm (0.00534375")	7.651 kN (1720 lbs)
A8-13-82	0.1337 mm (0.005265625")	3.092 kN (695 lbs)
A8-21-22	0.1390 mm (0.005471154")	7.971 kN (1792 lbs)
B16-21-22	0.1307 mm (0.005144231")	30.651 kN (6891 lbs)
B16-21-44	0.1375 mm (0.005413462")	23.795 kN (5349 lbs)
B16-21-82	0.1321 mm (0.005201923")	12.527 kN (2816 lbs)
C24-21-22	0.1400 mm (0.005512821")	99.617 kN (22395 lbs)
C24-21-44	0.1402 mm (0.005519231")	59.950 kN (13477 lbs)
C24-21-55	0.1396 mm (0.005496795")	40.572 kN (9121 lbs
C24-21-28	0.1399 mm (0.005509615")	53.585 kN (12046 lbs)
C24-21-82	0.1378 mm (0.005426282")	35.679 kN (8021 lbs)

*   In the case of the 50.8 mm x 50.8 mm (2" x 2") cutout for the short panel (L = 304.8 mm) a knockdown ratio was applied. This knockdown ratio was obtained by using a linear interpolation between the thickness and the collapse load data shown in Table 6. This was done for the three short panel cases with a 50.8 mm x 50.8 mm (2" x 2") cutout shown in table 6 and the knockdown ratios averaged. The average knockdown ratio applied was 1.002996.

The buckling extensional width ratio was found to be fairly accurate in estimating collapse loads for varying cutout dimensions for 304.8 mm x 304.8 mm (12" x 12") panels. However, this technique was not as accurate when estimating collapse loads for the 304.8 mm x 508 mm (12" x 20") panels, or panels with a 50.8 mm x 50.8 mm cutout. This is due to the fact that the collapse load is influenced by the extensional width as well as the extensional length. Again, this technique does not account for extensional length. This is a major shortcoming of this estimating technique. By not including the extensional length, this model insinuates that cutouts with equivalent extensional widths yield equivalent collapse loads regardless of the cutout area. This is clearly not the case, see Table 8 for the collapse load results for a 50.8 mm x 50.8 mm cutout and a 50.8 mm x 203.2 mm cutout. However, this technique still is practical for small panel extensional lengths. When the extensional length is reduced, the panel loading becomes more representative of the one dimensional beam model. Specifically, the 304.8 mm x 304.8 mm panels have a range of extensional lengths (2"-5") which are less than the range of extensional lengths for the 304.8 mm x 508 mm panels (6"-9"). Therefore, the collapse load estimates for the 304.8 mm x 304.8 mm panels are better than those for the 304.8 mm x 508 mm panels. The average differences between the estimated collapse loads and the loads obtained using SHELL for the 304.8 mm x 304.8 mm and 304.8 mm x 508 mm panel were 10.8% and 19.0%, respectively. The comparison of numerical collapse load versus

estimated collapse load using the extensional ratio is shown in Table 8.

Table 8 is interpreted as follows. Table 8 uses known solutions for the 304.8 mm x 304.8 mm panel and the 304.8 mm x 508 mm panels. All known panel configurations have a 101.6 mm x 101.6 mm cutout. This size cutout has an extensional width of 101.6 mm (4") for all panel configurations. The average ply thickness and panel length used to obtain the numerical collapse load were consistent within panel configuration groups. In other words, the panel thickness and the panel length are held constant and the effects of varying extensional width are investigated. The known numerical collapse load solution for the 304.8 mm x 304.8 mm panel configuation was P_{cr} = 5.462 kN (1228 lbs). The eight ply 304.8 mm x 508 mm panel known numerical collapse load was P_{cr} = 5.581 kN (1255 lbs). The 16 ply 304.8 mm x 508 mm panel known solution was 23.618 kN (5309 lbs). The 24 ply 304.8 mm x 508 mm panel known solution was 59.649 kN (13410 lbs). The second column in Table 8 expresses the estimated collapse load (P_{cr}') using equations (6) and (9), where the value for the known solution (P_{cr}) is defined for the known panel configurations above. The third column in Table 8 contains the numerical load obtained using SHELL which is used to compare to the estimated load in column two. The fourth column of Table 8 contains the percent difference between the estimated collapse load (column 2) and the numerical collapse load (column 3). As an example, given an eight ply 304.8 mm x 304.8 mm (12" x 12") panel with a 101.6 mm x 101.6 mm (4" x 4") cutout collapses at

Pcr = 5.462 kN (1228 lbs), estimate the collapse load for an identical panel with a 50.8 mm x 203.2 mm (2" x 8") cutout. First, the extensional width for the known solution is b = 101.6 mm (4") and the extensional width for the 50.8 mm x 203.2 mm cutout is b'= 127 mm (5") . Therefore, applying equation (6) and (9) gives:

$$P_{cr}' = 5"/4" \ (1228 \ lbs) = 1534 \ lbs$$

The length ratio technique was not investigated numerically using SHELL. However, it was used as a cursory check to see the effects of panel axial length variations on the experimental collapse loads. This was done for only one test panel. This test panel had an effective axial length of 508.127 mm (20.005"). This panel was chosen since it exceeded the numerical axial length (508 mm). In addition, the 0.127 mm (0.005") axial length variation was the maximum found out of the 40 test panels. This panel had a 203.2 mm x 50.8 mm (8" x 2") cutout and an experimental collapse load of 1.050 kN (236.1 lbs). Using the length ratio technique, equation (6) and (8), a collapse load was estimated for an axial length of 508 mm. The collapse load increased to 1.051 kN (236.3 lbs). Therefore, it was concluded that the slight variations in axial length for the test panels did not significantly effect their collapse loads.

Table 8.   Comparison of Numerical Collapse Load to Estimated Collapse Load Using Extensional Ratio

Shell Designator	(b'/b)Pcr (lbs)	Collapse Load Numerical(lbs)	%
A8-13-22	1534	2339	-34.4
A8-13-55	1043	1081	-3.5
A8-13-82	614	622	-1.3
A8-13-28	1534	1476	+3.8
A8-21-22	1568	1791	-12.4
A8-21-55	1098	778	+29.2
A8-21-28	1568	1269	+19.1
A8-21-82	627	698	-10.1
B16-21-22	6637	7970	-16.7
B16-21-28	6637	6296	+5.1
B16-21-55	4646	3492	+24.8
B16-21-82	2655	3150	-15.7
C24-21-22	16762	22361	-25.0
C24-21-55	11734	9187	+21.7
C24-21-28	16762	12049	+28.1
C24-21-82	6705	8398	-20.2

5.3 Numerical Results and Discussion

A numerical instability study using SHELL was conducted for each of the panel configuration and cutout combinations (20 total). All the studies used the following boundary conditions; the panels had free vertical edges, with the bottom horizontal edge fully constrained and the top horizontal edge allowed only to displace in the axial direction (u). The panels were loaded through a prescribed displacement and the applied total load along the panel top edge was solved for. The applied total load was output by the SHELL program for each increment. In addition, for each increment, the SHELL program output displacements and rotations for all element corner nodes. This data was analyzed and the significant results presented in this section.

Table 9 presents the numerically derived global collapse load and top edge displacements (u). Global is defined as pertaining to the entire panel continuum. Table 9 documents the maximum load analytically applied to the panels just before the panels collapsed (global collapse load). The global collapse loads in Table 9 were adjusted using the material knockdown factor and the thickness estimating technique discussed in sections 4 and 5.1, respectively. In addition, Table 9 presents the panel top edge displacement (u) that is associated with the global collapse load. As expected, Table 9 indicates that the collapse load decreases with increased cutout area and decreased panel thickness. Figures 17-21 illustrate the effects of panel thickness on the collapse loads by cutout size for the 304.8 mm x 508 mm
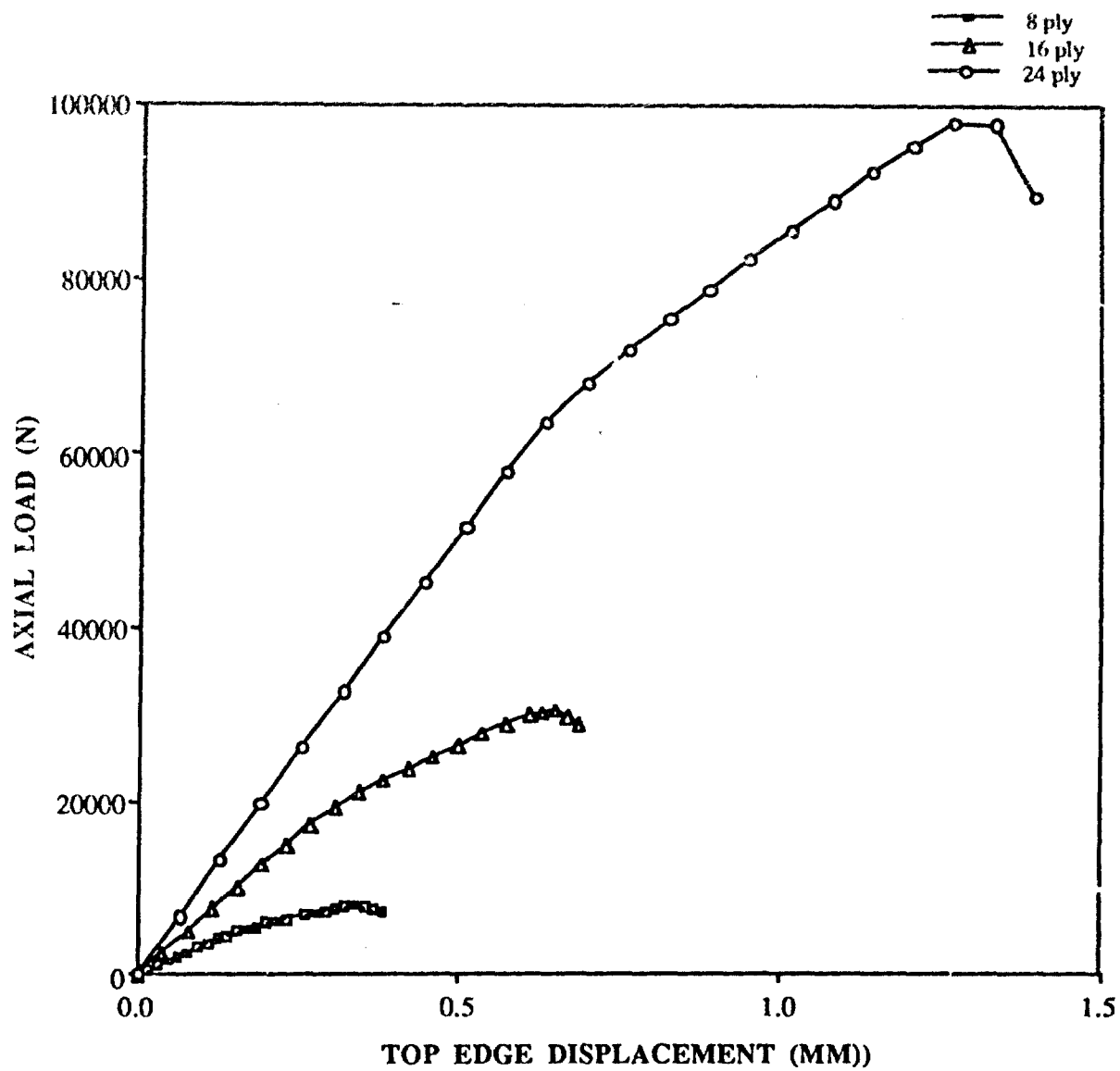
Fig. 17: Effects of Thickness on a
50.8 mm x 50.8 mm (2" x 2") Cutout in a
304.8 mm x 508 mm (12" x 20") Panel
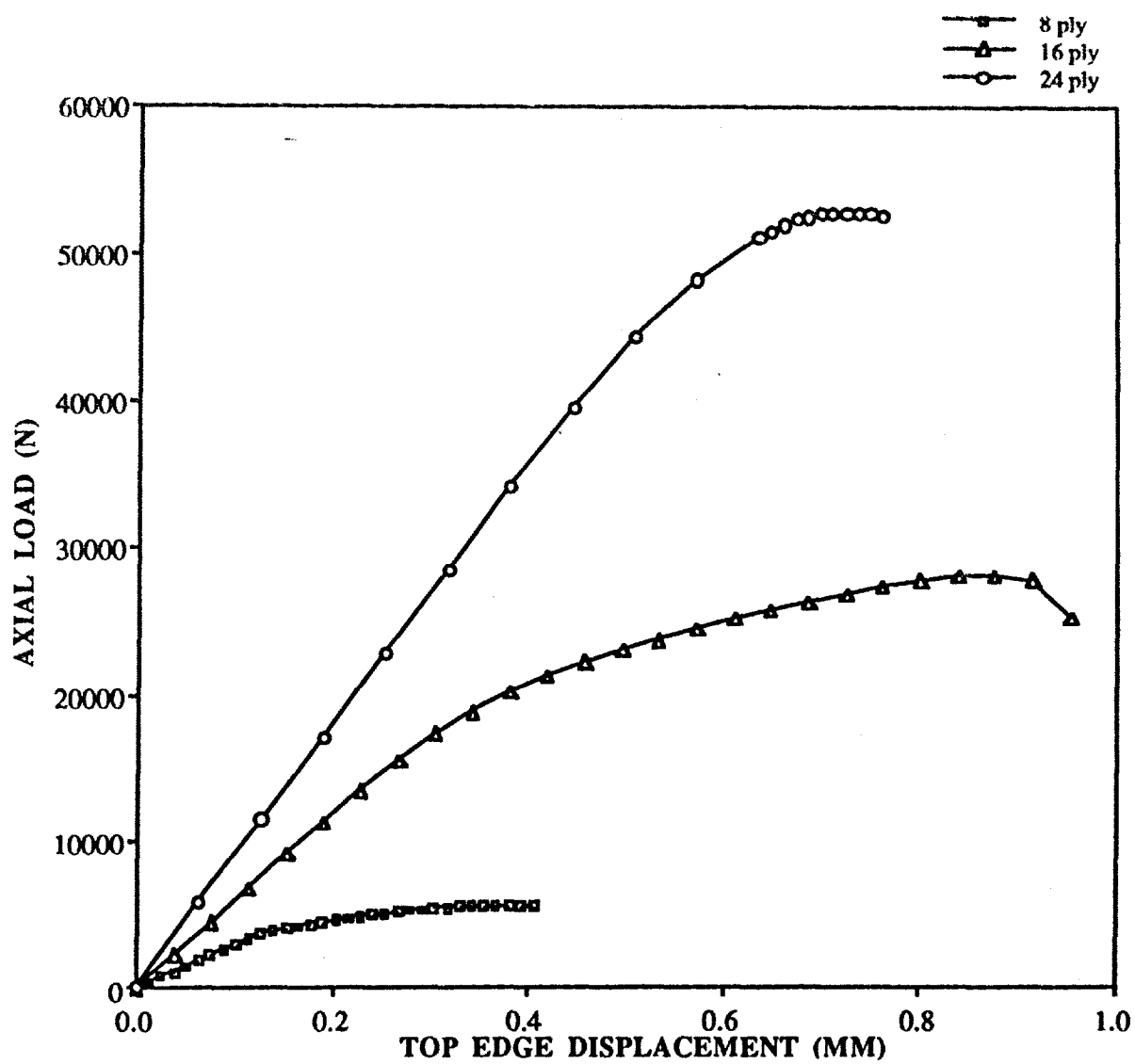
Fig. 18: Effects of Thickness on a
50.8 mm x 203.2 mm (2" x 8") Cutout in a
304.8 mm x 508 mm (12" x 20") Panel
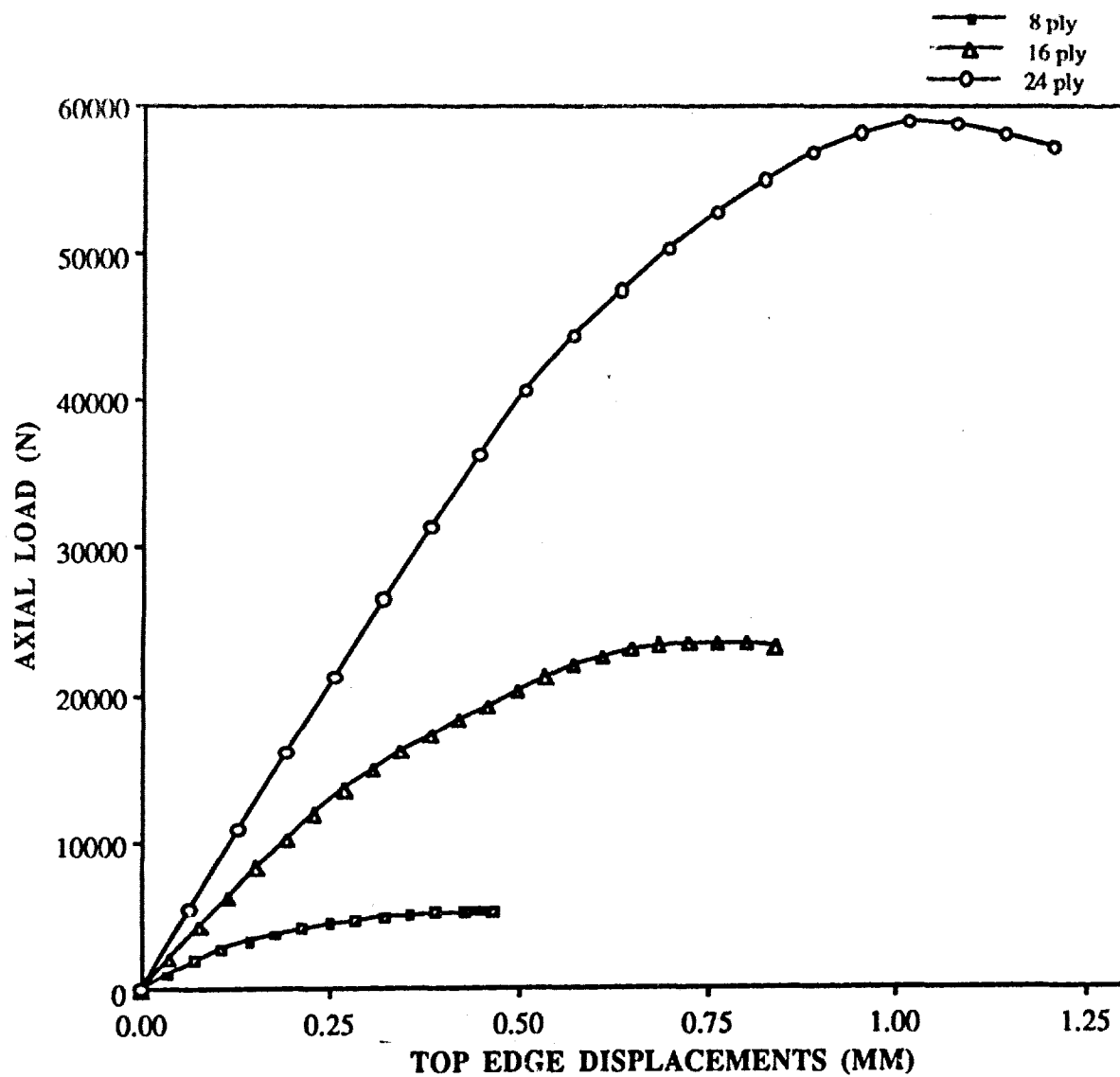
Fig. 19: Effects of Thickness on a
101.6 mm x 101.6 mm (4" x 4") Cutout in a
304.8 mm x 508 mm (12" x 20") Panel
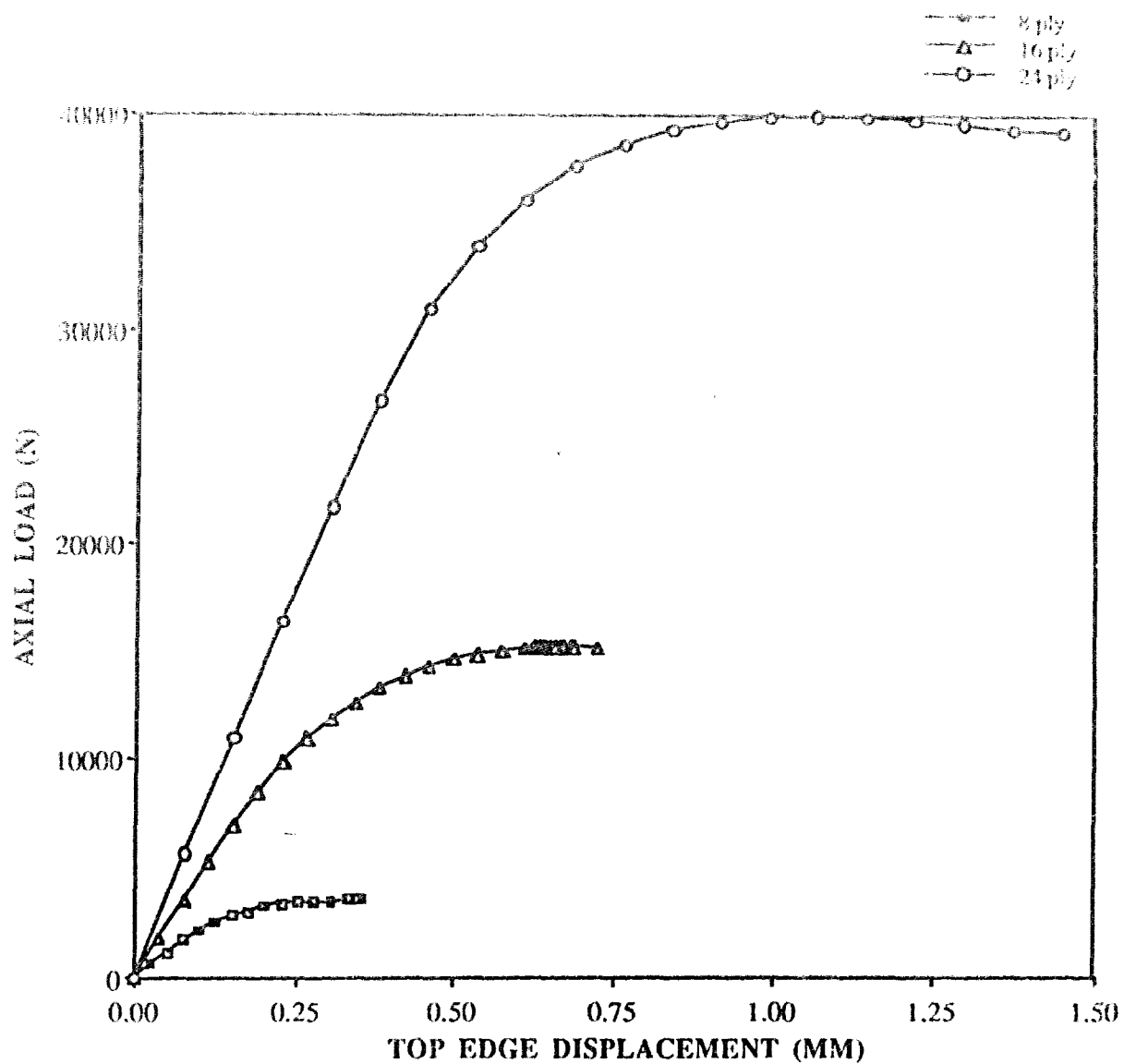
Fig. 20: Effects of Thickness on a
127 mm x 127 mm (5" x 5") Cutout in a
304.8 mm x 508 mm (12" x 20") Panel
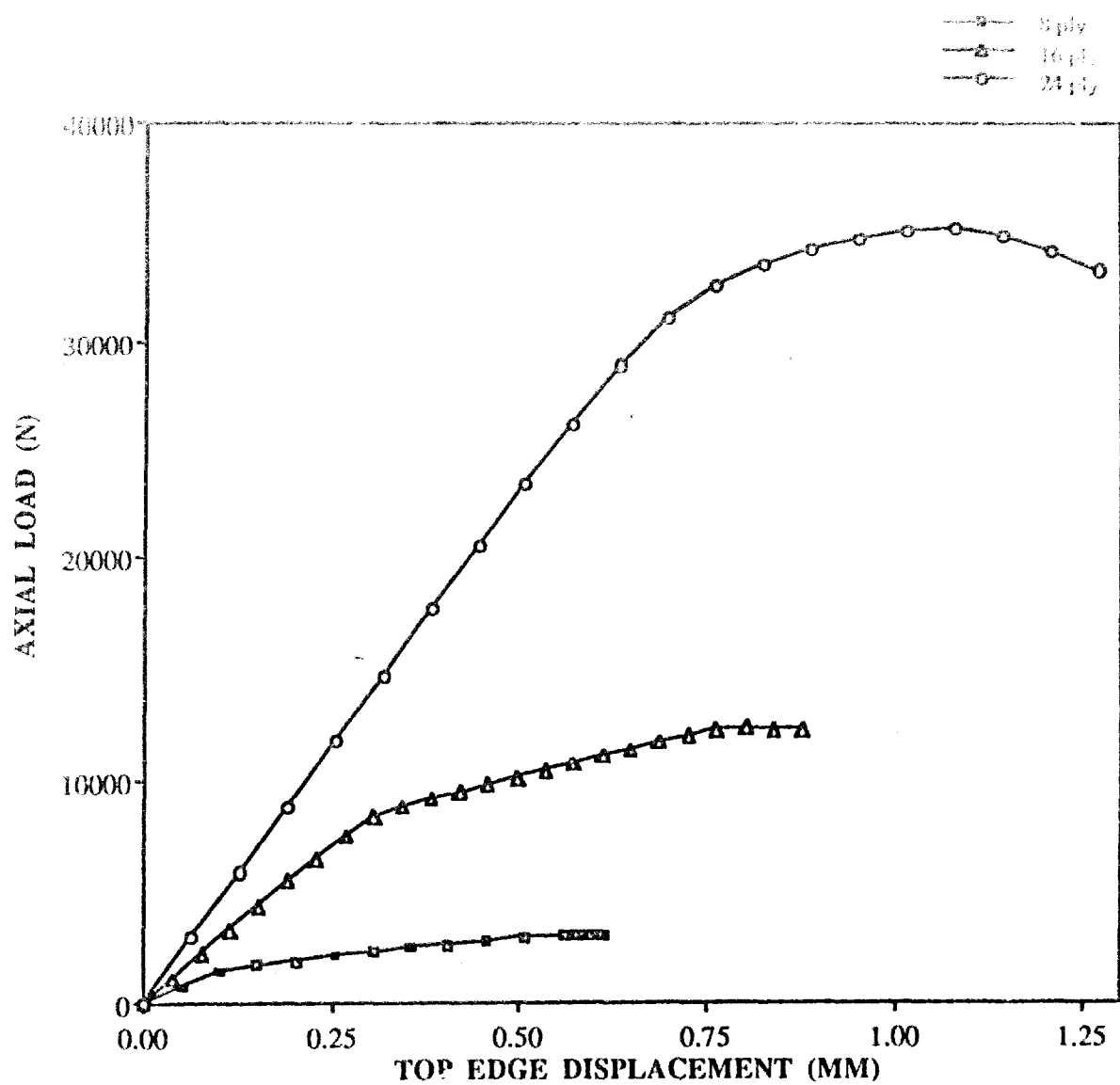
Fig. 21: Effects of Thickness on a
203.2 mm x 50.8 mm (8" x 2") Cutout in a
304.8 mm x 508 mm (12" x 20") Panel

(12" x 20") panels. These figures show the stiffness of the panels increased for increasing panel thickness. In addition, these figures illustrate that the collapse load increases for increasing panel thickness.

Figures 22-25 exemplify the effects of cutout size on collapse load, panel stiffness, and non-linear response of the panel.

First, Figures 22-25 show that for all cases (except one) the collapse load decreases with decreasing extensional width and increasing cutout area. The effects of extensional width becomes more visible when comparing collapse loads of panels with equivalent cutout area. Figures 22-25 reflect that collapse loads decline with decreasing extensional width for panels with equivalent cutout area. The exception is for the 24 ply panel configuration with a 50.8 mm x 203.2 mm cutout which collapsed at a lower load than the 101.6 mm x 101.6 mm cutout (see Figure 23). This can be attributed to the amount of transverse shear and bending motion each of these 24 ply panels experience. This particular case is discussed in detail later in this section when the shear strain results are presented. Note, that the 8 and 24 ply 50.8 mm x 203.2 mm cutout panel configurations indicate signs of instability at lower values of axial displacements than those panels with equivalent cutout area (see Figures 22-23 and 25). The exception to this is the 16 ply panel with a 50.8 mm x 203.2 mm cutout. This configuration is undergoing a large amount of bending, subsequently its load displacement curve becomes increasingly non-linear as the panel collapse load is approached.

Second, Figures 22-25 reveal that the load versus displacement curves become more non-linear as the cutout area increases and the extensional width decreases. This indicates that a greater distribution of bending is occurring for the larger cutouts and cutouts with small extensional widths.

Third, Figures 22-25 indicate that the slopes of the load versus displacement curves (panel stiffness) increase for increasing extensional width and decreasing cutout area.

The effects of increasing the axial length of the eight ply panel from 304.8 mm (12") to 508 mm (20") are concluded from Table 9 and Figure 26. Table 9 and Figure 26 demonstrate that increasing the axial length of the panel decreases the collapse load for equivalent number of plies. In addition, the panel becomes less stiff as the axial length is increased.

The difference in panel axial length appeared to significantly affect the variance in collapse load for panels with large cutout areas and/or large extensional widths. Specifically, the 127 mm x 127 mm (5" x 5") cutout experienced a 39.0% decrease in collapse load going from the shorter to longer axial panel length. The 50.8 mm x 50.8 mm (2" x 2") cutout experienced a 31.2% decrease in collapse load. The 50.8 mm x 203.2 mm (2" x 8") cutout experienced a 26.2% decrease in collapse load, and the 101.6 mm x 101.6 mm (4" x 4") cutout experienced a 17.4% decrease in collapse load. The 304.8 mm x 304.8 mm panel with a 203.2 mm x 50.8 mm (8" x 2") cutout collapse load was not significantly affected by increasing the panel length. This panel

74
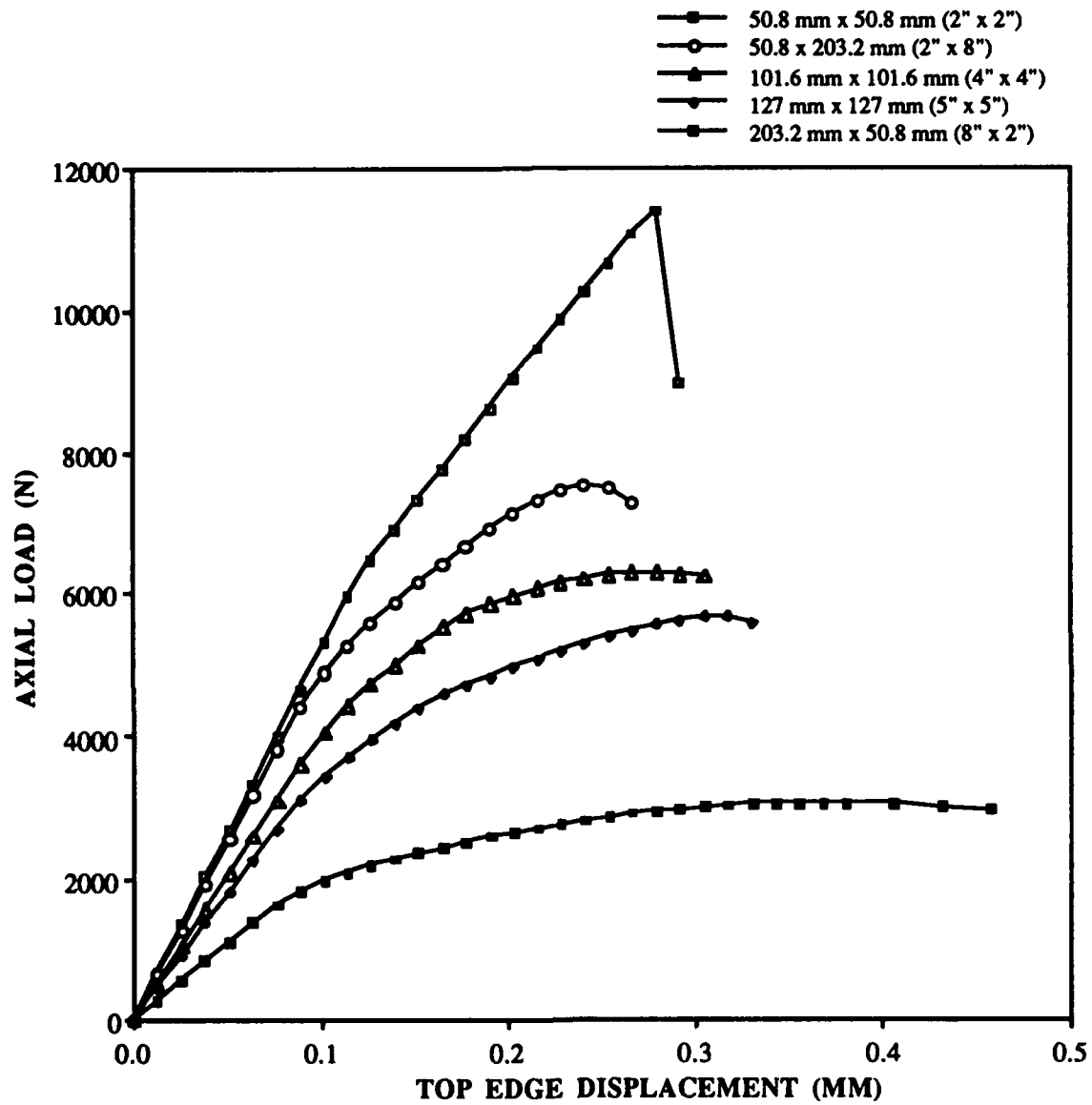
Fig. 22: The Effect of Varying Cutout Size
On the Load vs. Displacement Curve for a
304.8 mm x 304.8 mm (12" x 12") Panel
[0/45/-45/90]s

75
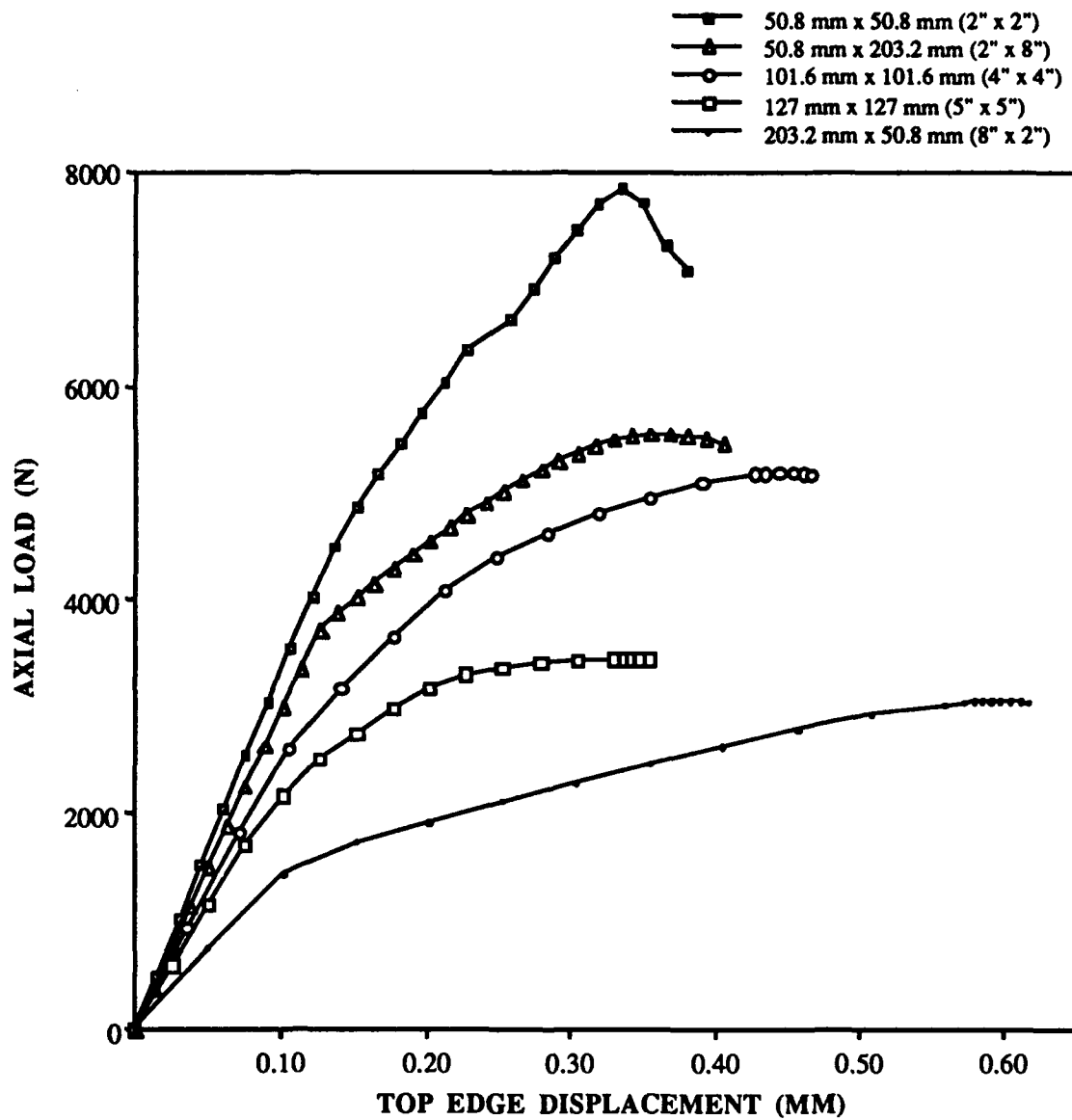
Fig. 23: The Effect of Varying Cutout Size
on the Load vs. Displacement Curve for a
304.8 mm x 508 mm (12" x 20") Panel
[0/45/-45/90]s
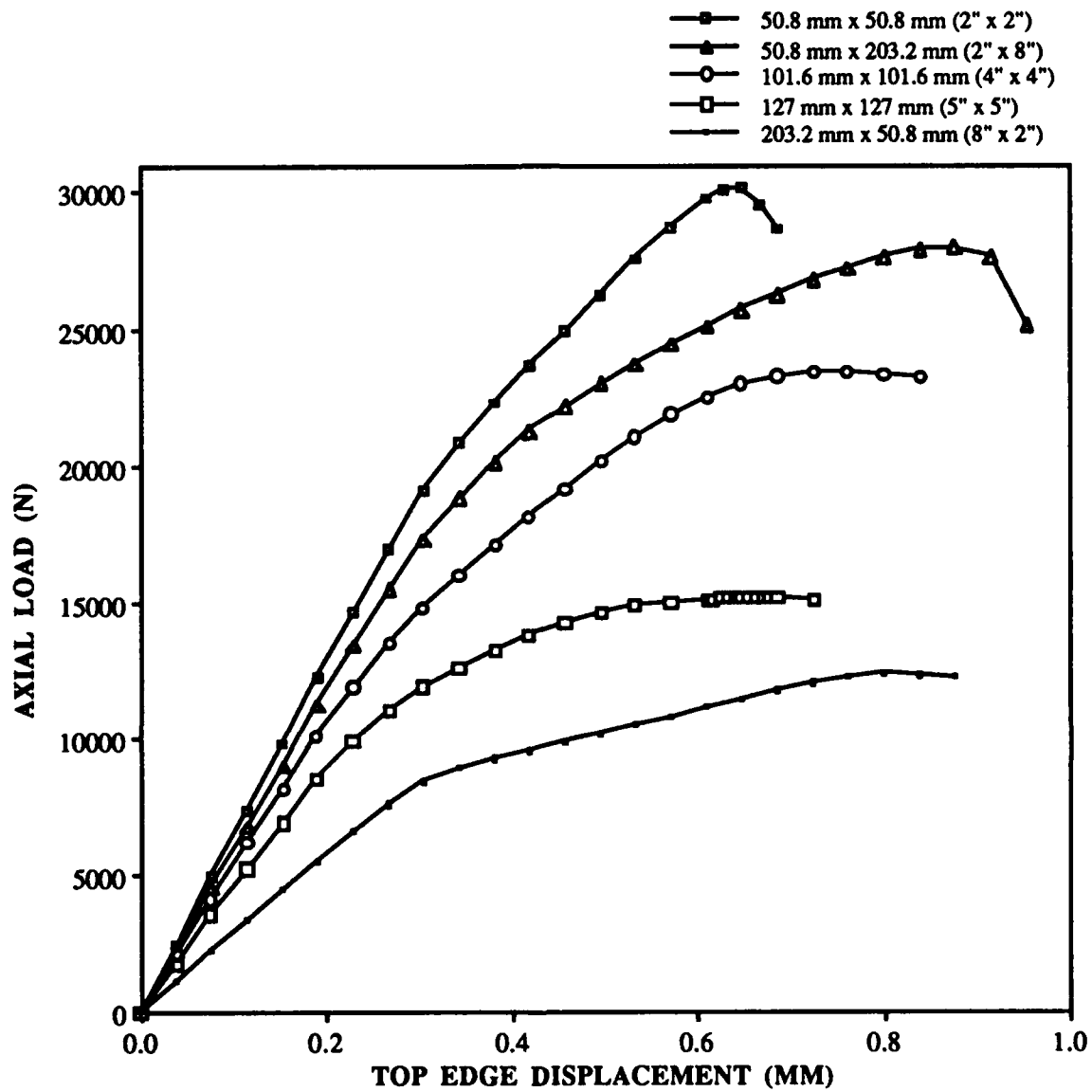
Fig. 24: The Effect of Varying Cutout Size on the Load vs. Displacement Curve for a 304.8 mm x 304.8 mm (12" x 20") Panel [0/45/-45/90]2s
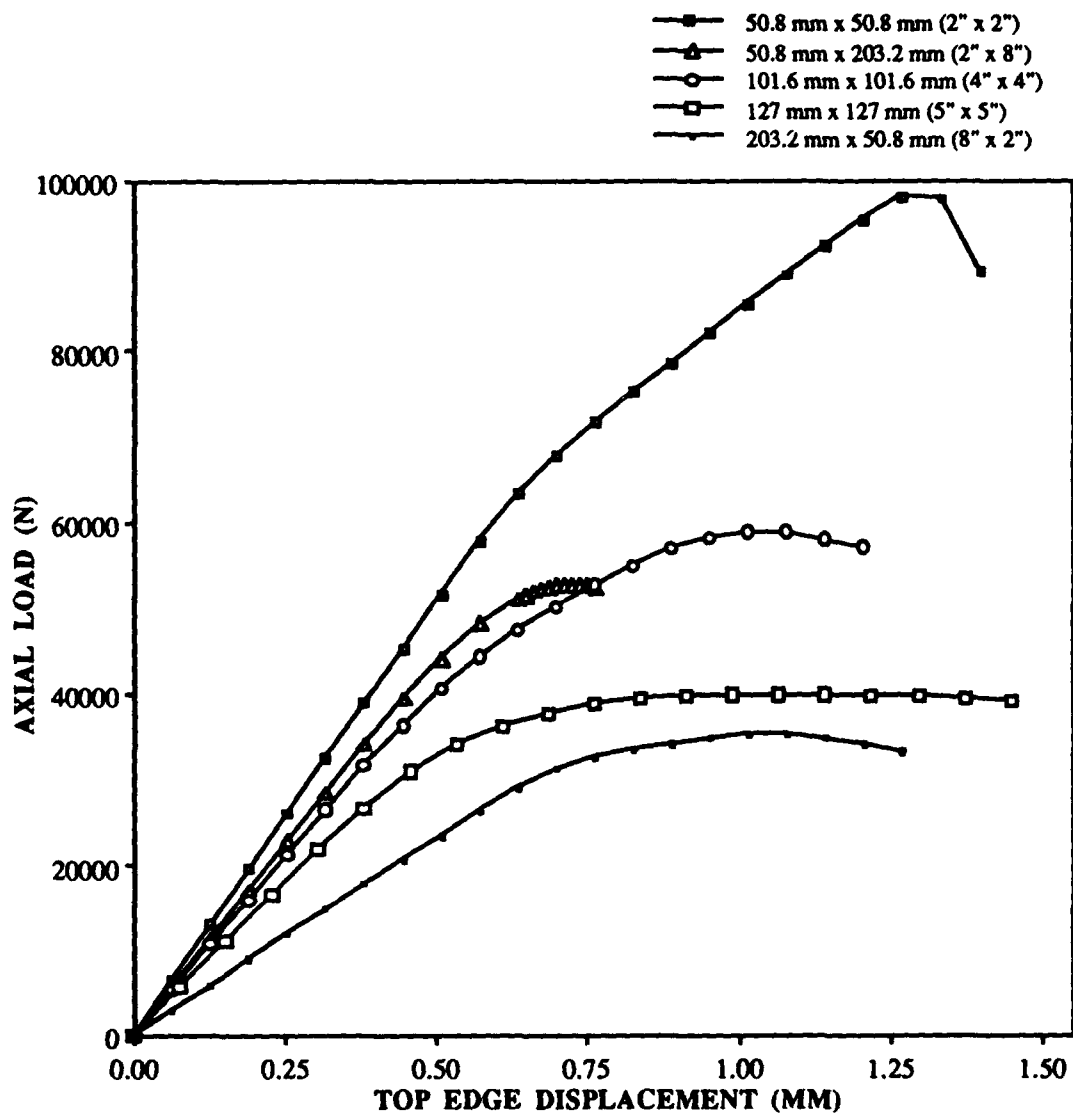
Fig. 25: The Effect of Varying Cutout Size
on the Load vs. Displacement Curve for a
304.8 mm x 508 mm (12" x 20") Panel
[0/45/-45/90]3s

configuration cutout combination experienced a 0.9% decrease in collapse load for an increase in panel axial length.

Focusing attention strictly to the panels with equivalent cutout area, it is concluded that the affects of increasing panel axial length on the panel collapse load becomes more significant as the extensional width is increased (see Figure 26). In particular, the 50.8 mm x ^03.2 mm (2" x 8") cutout has an extensional width of 127 mm (5") and experienced a 26.2% decrease in collapse load; as the axial length increased from 304.8 mm to 508 mm, the 101.6 mm x 101.6 mm (4" x 4") cutout has an extensional width of 101.6 mm (4") and experienced a 17.4% decrease in collapse load; and finally the 203.2 mm x 50.8 mm (8" x 2") cutout has an extensional width of 50.8 mm (2") and experienced a decrease in collapse load of 0.9%.

Table 10 documents the magnitudes of the maximum radial displacements (w) observed in each panel configuration, at the onset of local collapse or global collapse which ever occurred first. Local collapse was assumed to occur when the radial displacements along the panel's horizontal and vertical centerlines at the cutout edge reached a maximum value prior to approaching the global collapse load. The percentage of the global collapse load where the onset of local collapse occurred is documented in Table 10. Table 10 verifies that a nonlinear theory is required for panels with large cutouts undergoing axial compression. Note that the radial displacements for the 8 ply 304.8 mm x 304.8 mm panels range from 4-7 times the panel thickness. The axial longer panels (508 mm) radial displacements
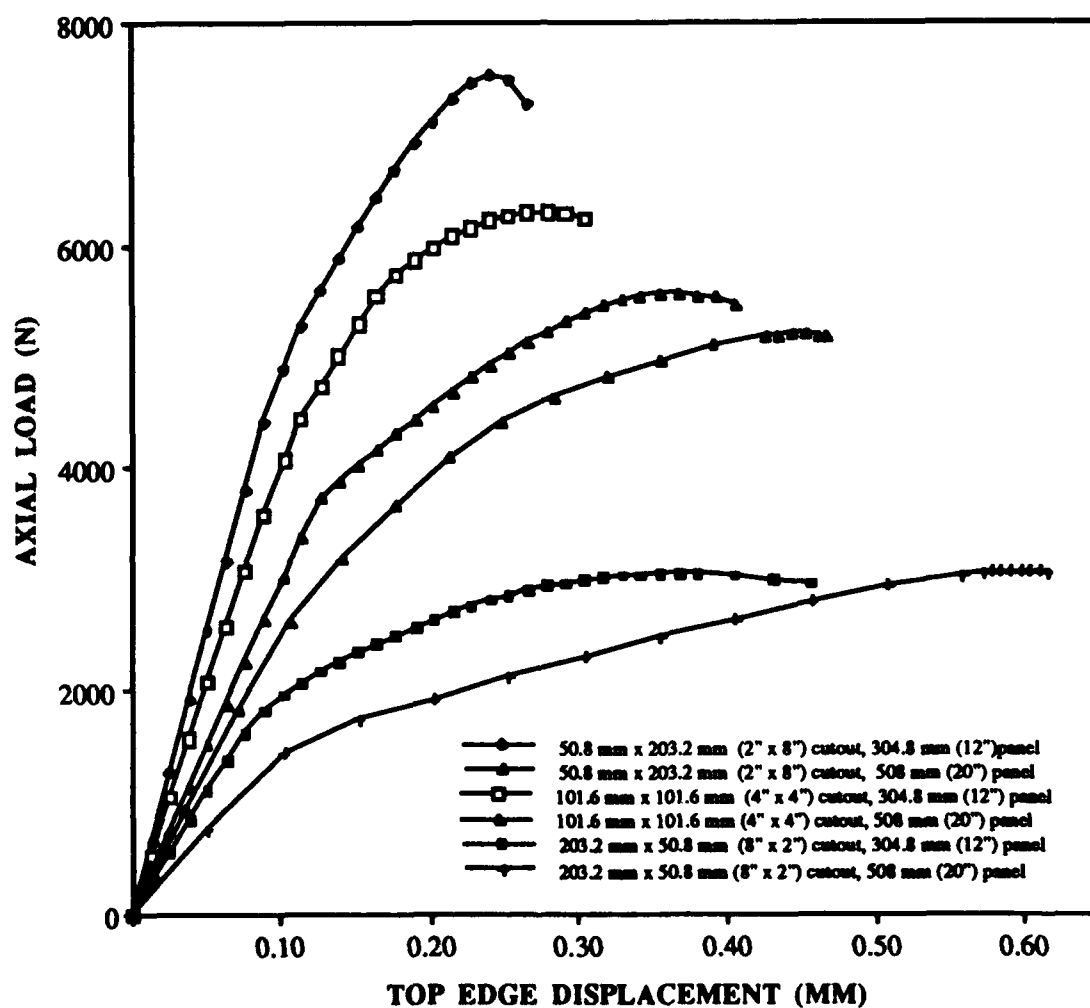
Fig. 26: The Effects of Increased Panel
Axial Length on Equivalent Cutout Areas
for [0/45/-45/90]s Lay Ups

80

range from 3-4 times the panel thickness in the 24-ply cases, 5-7 times the panel thickness in the 16 ply cases, and 8-12 times the panel thickness in the 8 ply cases.

Each panel configuration experienced the maximum radial displacement along the free vertical edge of the panel. This maximum occurred on or near the horizontal centerline of the panel. The distribution of the radial displacements tended to increase in magnitude as the horizontal centerline of the panel was approached. Furthermore, the radial displacements decreased in magnitude along the horizontal centerline as the vertical edge of the cutout was approached. All the panels exhibited exact symmetry of radial displacements along the horizontal and vertical centerlines of the panel. Even though the panels deformed fairly symmetric, the panels exhibited some small signs of panel asymmetry about the horizontal and vertical centerlines of the panel. Equivalent values (magnitude and direction) for radial displacements were at diagonals to each other. This behaviour is brought about by the presence of the +45 and -45 degree plies which affect the the bending stiffness terms D_{16} and D_{26}. The stiffness terms D_{16} and D_{26} in turn affect the in plane twisting moment (M_{xy}). This effect is so small it does not show up in the three dimensional orthotropic plots of the panels (see figures 79-83).

Table 11 represents the numerically derived maximum local radial displacements. Local is defined as those points that fall along the cutout edge. Table 11 displays the magnitudes of the

largest radial displacement (w) observed along the cutout edge for each panel/cutout combination at the onset of local collapse or global collapse which ever occurred first. Table 11 in conjunction with Table 12, which documents the global and local maximum bending rotations (ψ_s), are discussed next.

It was found that the maximum global bending rotation (ψ_s) occurred at or near the same location as the global maximum radial displacement for most of the panels. The location of maximum global radial displacement was at or near the horizontal centerline of the panel along the panel free vertical edge. There were four cases where the maximum global bending rotation did not coincide with the maximum global radial displacement. Instead, for these four cases, the maximum global rotation coincided with, or was near the maximum local radial displacement. The four cases in which this occurred were the eight ply axial short panel (304.8 mm) with a 101.6 mm x 101.6 cutout, the eight ply short panel with a 50.8 mm x 203.2 mm cutout, the 16 ply axial long panel (508mm) with a 50.8 mm x 203.2 mm cutout, and the 24 ply long panel with a 203.2 mm x 50.8 mm cutout.

The radial displacements along the panels free vertical edges, for all the panels, increased as the horizontal centerline of the panel was approached. Similarly, the bending rotations increased as the horizontal centerline of the panel was approached along the panel free vertical edge. Furthermore, the bending rotations were symmetric along the panels horizontal and vertical centerlines. Even though the bending rotations magnitudes were fairly symmetric about the horizontal and vertical centerline of

Table 9. *Numerical Global Collapse Load and Top Edge Displacement*

Panel Designator	Collapse Load		u	
A8-13-22	11.395 kN	(2562 lbs)	0.2794 mm	(0.0110")
A8-13-44	6.277 kN	(1411 lbs)	0.2667 mm	(0.0105")
A8-13-55	5.664 kN	(1273 lbs)	0.3175 mm	(0.0125")
A8-13-28	7.552 kN	(1691 lbs)	0.2413 mm	(0.0095")
A8-13-82	3.039 kN	(683 lbs)	0.3683 mm	(0.0145")
A8-21-22	7.836 kN	(1762 lbs)	0.3200 mm	(0.0126")
A8-21-44	5.185 kN	(1166 lbs)	0.4445 mm	(0.0175")
A8-21-55	3.450 kN	(776 lbs)	0.3493 mm	(0.01375")
A8-21-28	5.551 kN	(1248 lbs)	0.3683 mm	(0.0145")
A8-21-82	3.067 kN	(689 lbs)	0.5969 mm	(0.0235")
B16-21-22	30.133 kN	(6774 lbs)	0.6477 mm	(0.0255")
B16-21-44	23.392 kN	(5259 lbs)	0.7620 mm	(0.0300")
B16-21-55	15.107 kN	(3396 lbs)	0.6629 mm	(0.0261")
B16-21-28	27.927 kN	(6278 lbs)	0.8763 mm	(0.0345")
B16-21-82	12.320 kN	(2769 lbs)	0.8001 mm	(0.0315")
C24-21-22	97.934 kN	(22016 lbs)	1.2700 mm	(0.0500")
C24-21-44	58.936 kN	(13250 lbs)	1.0160 mm	(0.0400")
C24-21-55	39.886 kN	(8967 lbs)	1.0668 mm	(0.0420")
C24-21-28	52.680 kN	(11843 lbs)	0.7239 mm	(0.0285")
C24-21-82	35.076 kN	(7886 lbs)	1.0795 mm	(0.0425")

Table 10. Global Numerical Radial Displacements (w)

Panel Designator	Collapse Load (%)	Maximum |w|
A8-13-22	86.6	5.5253 mm (0.21753")
A8-13-44	91.2	4.4607 mm (0.17562")
A8-13-55	83.2	4.5255 mm (0.17817")
A8-13-28	98.9	4.7795 mm (0.18817")
A8-13-82	100.0	7.6992 mm (0.30312")
A8-21-22	100.0	8.8461 mm (0.34827")
A8-21-44	99.8	11.2248 mm (0.44192")
A8-21-55	100.0	9.7310 mm (0.38311")
A8-21-28	100.0	10.3325 mm (0.40679")
A8-21-82	100.0	12.7942 mm (0.50371")
B16-21-22	100.0	11.8633 mm (0.46706")
B16-21-44	99.3	11.9972 mm (0.47233")
B16-21-55	100.0	11.8407 mm (0.46617")
B16-21-28	100.0	15.1183 mm (0.59521")
B16-21-82	100.0	12.4333 mm (0.48950")
C24-21-22	100.0	14.9992 mm (0.59052")
C24-21-44	98.7	11.7201 mm (0.46142")
C24-21-55	99.9	12.7533 mm (0.50210")
C24-21-28	100.0	9.0427 mm (0.35601")
C24-21-82	100.0	9.5915 mm (0.37762")

Table 11. Maximum Local Radial Displacements

Panel Designator	Collapse Load (%)	Maximum |w|
A8-13-22	86.7	0.6670 mm (0.026258")
A8-13-44	91.2	1.1029 mm (0.043423")
A8-13-55	83.2	1.6500 mm (0.064964")
A8-13-28	98.9	4.4582 mm (0.175520")
A8-13-82	100.0	2.9332 mm (0.115480")
A8-21-22	100.0	2.2740 mm (0.089529")
A8-21-44	99.8	2.8933 mm (0.113910")
A8-21-55	100.0	3.4061 mm (0.134100")
A8-21-28	100.0	6.6304 mm (0.261040")
A8-21-82	100.0	5.5926 mm (0.220180")
B16-21-22	100.0	3.8405 mm (0.151200")
B16-21-44	99.3	2.7643 mm (0.108830")
B16-21-55	100.0	4.0437 mm (0.159200")
B16-21-28	100.0	10.8682 mm (0.427880")
B16-21-82	100.0	5.3457 mm (0.210460")
C24-21-22	100.0	3.5651 mm (0.140360")
C24-21-44	98.7	2.3489 mm (0.092477")
C24-21-55	99.9	4.6464 mm (0.182930")
C24-21-28	100.0	1.8911 mm (0.074452")
C24-21-82	100.0	6.4681 mm (0.254650")

Table 12. *Global and Local Maximum Bending Rotations*

Panel Designator	Collapse Load (%)	Global Ψ_s (deg.)	Local Ψ_s (deg.)
A8-13-22	86.7	6.3	1.1
A8-13-44	91.2	4.7	4.7
A8-13-55	83.2	4.7	3.8
A8-13-28	98.9	5.3	4.4
A8-13-82	100.0	7.7	5.1
A8-21-22	100.0	7.5	3.5
A8-21-44	99.8	9.2	4.0
A8-21-55	100.0	7.8	3.8
A8-21-28	100.0	9.8	5.0
A8-21-82	100.0	10.2	8.5
B16-21-22	100.0	8.1	6.4
B16-21-44	99.3	8.2	5.3
B16-21-55	100.0	7.6	5.1
B16-21-28	100.0	13.0	10.4
B16-21-82	100.0	8.9	8.3
C24-21-22	100.0	9.6	7.0
C24-21-44	98.7	7.3	5.1
C24-21-55	99.9	7.2	5.2
C24-21-28	100.0	4.9	2.6
C24-21-82	100.0	5.3	5.3

the panel they were not exactly symmetric. Instead equivalent magnitudes of bending rotations occurred at diagonals to each other.

Unlike the maximum global bending rotation, the local maximum bending rotation did not coincide with the local maximum radial displacement. Again, local pertains to points around the cutout edge while global pertains to the entire panel continuum. The location of the local maximum bending rotations in relation to the location of the local maximum radial displacement was a function of the cutouts dimension, panel axial length, and thickness of the panel.

The local maximum radial displacements tended to occur along the vertical edge of the cutout on or near the horizontal centerline of the panel. The exceptions to this were the 50.8 mm x 50.8 mm cutout for all panel configurations, and the 101.6 mm x 101.6 mm cutout for the 16 ply and 24 ply axial longer panels (508 mm). These cases experienced maximum local radial displacements along the horizontal edge of the cutout on or near the panel vertical centerline.

The local maximum bending rotations tended to occur at the cutout corners, or near the cutout corners along the cutout vertical edge. This occurrence would be expected since areas of large shear strain occur at the cutout corners. The exceptions to the expected location were:

item a). the 50.8 mm x 50.8 mm cutout for the 8, 16 and 24 ply axial long panels (508 mm)

item b). the axial short panels (304.8 mm) with either a:

- 101.6 mm x 101.6 mm cutout

- 127 mm x 127 mm cutout
                    - or 50.8 mm x 203.2 mm cutout

   item c). and the 50.8 mm x 203.2 mm cutout for the 8 and
              16 ply long panels.

These panels experienced maximum bending rotations along the

vertical edge of the cutout at or near the horizontal centerline

of the panel. This type of behaviour is indicative of what would

be found for a panel with no cutout. Hatfield found that the

maximum shear strains for exact panel configurations without a

cutout occurred along the horizontal centerline of the panel

toward the center of the panel [18]. Since, the shear strain is a

function of the difference of the bending rotations and the

elastic slopes; areas of large bending rotations should correspond

to areas of large strain. This explains the location of the

maximum local bending rotations for the 50.8 mm x 50.8 mm cutout

(item a.). This cutout's area is rather small in comparison to

the overall panel area (1.7%). Therefore, these panel

configurations behave similar to a solid panel. However, this

explanation is not considered valid for the remaining exceptions.

     The exception shown as item b. are eight ply axial short

panel (304.8 mm) configurations. These panels exhibit less

effects due to transverse shear than its 8 ply axial longer panel

(508 mm) counterparts. Therefore, the longer panels are more

susceptible to bending and the presence of transverse shear strain

increases. The effect of increasing the panel axial length shifts

the maximum bending rotations to the corners of the cutout for

these panel. The exception to this was the 50.8 mm x 203.2 mm

cutout which showed no change in location of the maximum local

bending rotation. The maximum local bending rotation for this panel maintained a location along the cutout vertical edge near the horizontal centerline of the panel (item c).

One of the key features of the SHELL algorithm is that it incorporates a parabolic transverse shear strain distribution through the thickness of the panel. The presence of transverse shear decreases the stiffness of the panel. This reduced stiffness enhances the bending that occurs in the shell as it nears the collapse load. Therefore, when the panel thickness for item c. is increased to 24 plies the effect of this increased presence of bending shifts the local maximum bending rotation to the cutout corner location.

Table 13 documents the global and local maximum transverse shear strains. The transverse shear strains are defined as:

$$\varepsilon_4 = |\psi_s| - |w_{,s}|$$ (10)
$$\varepsilon_5 = |\psi_x| - |w_{,x}|$$

Again, global is defined as pertaining to the entire panel continuum and local pertains to the points along the cutout edge. In general, the maximum global transverse shear strains occurred at the cutout corners. Therefore, the terms global and local transverse shear strains are synonymous for most of the panels. Equivalent magnitudes of transverse shear strains occurred at diagonals to each other.

The magnitudes of local maximum transverse shear strain, ε_4 and or ε_5, increase in magnitude going from the eight ply short axial

89

panels (304.8 mm) to the longer axial eight ply panels (508 mm).
This increase in transverse shear strain magnitude is a result of
the increased bending brought about by elongating the axial length
of the panel. This increased bending causes the stiffness of the
eight ply 304.8 mm x 508 mm panels to be reduced (see Figure 26).
Therefore, these panels will collapse at a lower load than the
eight ply 304.8 mm x 304.8 mm panels.

The global maximum ε_4 shear strains for the 8 ply axial longer
panels (508 mm) tended to occur along the cutout edges or the free
vertical edges of the panel. When comparing the magnitudes of the
two locations of concentrated shear strains no appreciable
difference was found in terms of magnitude. This was not the case
for the thicker 16 and 24 ply panels.

The global maximum ε_4 shear strain for the 16 and 24 ply panels
occurred exclusively at the cutout corners, or near the cutout
corners on the horizontal edge of the cutout. There were two
locations where the ε_4 shear strain tended to concentrate for the
16 and 24 ply panels. The primary location was along the
horizontal edge of the cutout. The secondary location was along
the panel free vertical edge near the panel corner. The ε_4
transverse shear strain magnitude at the panel corner was on the
order of two to ten times less than what was experienced at the
cutouts horizontal edge.

The global maximum ε_5 shear strains for the 8 ply 304.8 mm x
508 mm panels tended to occur either on or near the vertical
cutout edge; or along the free vertical edge of the panel near the
panel horizontal centerline.

The global maximum ε_5 shear strain for the 16 and 24 ply panels occurred at the cutout corners or near the cutout corners along the vertical edge of the cutout. One case, involving a 16 ply panel with a 203.2 mm x 50.8 mm cutout, experienced a global maximum ε_5 strain along the free vertical edge of the panel.

There were two locations for the 8, 16 and 24 ply 508 mm axial panels where the ε_5 transverse shear strains tended to congregate. The first location was along the vertical edges of the cutout. The second location was along the free vertical edge of the panel close to the horizontal centerline of the panel. Unlike the two locations of the ε_4 transverse shear strains, the ε_5 shear strain locations exhibited equivalent orders of magnitude at both locations.

Another observation made for the eight ply panels, for both the long and short panels, was that the transverse shear strain was greater for a rectangular cutout versus a square cutout with equivalent cutout area. The opposite observation was made as the panel thickness increased. For instance, the 24 ply panels had larger transverse shear strains with a square cutout than a rectangular cutout with the same cutout area. In addition, this occurrence explains the case mentioned earlier in this section, where the collapse load of the 24 ply panel with a 101.6 mm x 101.6 mm cutout exceeded the collapse load of the 24 ply panel with a 50.8 mm x 203.2 mm cutout (see figure 25). This case is explained by considering the transverse shear strain (ε_5) along the vertical cutout edges of these equivalent area cutouts. For example, if the magnitudes of transverse shear strain (ε_5)

along the cutout vertical edges were equivalent for the 101.6 mm x 101.6 mm and 50.8 mm x 203.2 mm cutout, the panel with the 50.8 mm x 203.2 mm cutout would collapse at a higher load in comparison to the 101.6 mm x 101.6 mm cutout. This would transpire due to the 50.8 mm x 203.2 mm cutout's larger vertical length in comparison to the 101.6 mm x 101.6 mm cutout's vertical length. This increased cutout vertical length results in a larger distribution of shear (ε_5) occurring along the 50.8 mm x 203.2 mm vertical cutout edge, than the 101.6 mm x 101.6 mm vertical cutout edge. The effect of the larger distribution of shear causes the flexural rigidity of the 24 ply panel with a 50.8 mm x 203.2 mm cutout to increase which results in a higher collapse load. On the other hand, when the flexural rigidity decreases the panel collapses at a lower load.

Now, the explanation above is applied to the case shown in figure 25. The magnitudes of transverse shear strain (ε_5) along the cutout vertical edge for this case were greater for the 24 ply panel with a 101.6 mm x 101.6 mm cutout, than 24 ply panel with a 50.8 mm x 203.2 mm cutout (see Table 13). Therefore, the 24 ply panel with a 101.6 mm x 101.6 mm cutout is absorbing the majority of the axial compressive energy through transverse shear strain which means bending decreases and the panel acts less flexibly (flexural rigidity increases). On the other hand, the 24 ply panel with a 50.8 mm x 203.2 mm cutout undergoes a reduction in shear strain (ε_5) in comparison to the 101.6 mm x 101.6 mm cutout, therefore it absorbs the majority of the axial compressive energy through bending. Consequently, this increased bending causes the

24 ply panel with a 50.8 mm x 203.2 mm cutout to respond more flexibly (flexural rigidity decreases) collapsing at a lower load than the 24 ply panel with a 50.8 mm x 203.2 mm cutout.

Table 13. Global and Local Maximum Transverse Strain

Panel Designator	Collapse Load (%)	Global $|\varepsilon_4|$	Local $|\varepsilon_4|$	Global $|\varepsilon_5|$	Local $|\varepsilon_5|$
A8-13-22	86.7	0.000790	0.000247	0.000677	0.000677
A8-13-44	91.2	0.000503	0.000438	0.000386	0.000277
A8-13-55	83.2	0.000494	0.000494	0.000416	0.000416
A8-13-28	98.9	0.000748	0.000748	0.000778	0.000778
A8-13-82	100.0	0.001735	0.001735	0.001072	0.001072
A8-21-22	100.0	0.001190	0.001190	0.001313	0.001313
A8-21-44	99.8	0.000503	0.000366	0.001303	0.000895
A8-21-55	100.0	0.001347	0.001347	0.000964	0.000601
A8-21-28	100.0	0.000824	0.000751	0.000869	0.000869
A8-21-82	100.0	0.002230	0.002230	0.001146	0.001037
B16-21-22	100.0	0.001130	0.001130	0.002322	0.002322
B16-21-44	99.3	0.002333	0.002333	0.001558	0.001558
B16-21-55	100.0	0.002357	0.002357	0.001565	0.001565
B16-21-28	100.0	0.001324	0.001324	0.003420	0.003420
B16-21-82	100.0	0.001970	0.001970	0.001707	0.001496
C24-21-22	100.0	0.002383	0.002383	0.004926	0.004926
C24-21-44	98.7	0.003994	0.003994	0.001944	0.001944
C24-21-55	99.9	0.005185	0.005185	0.002826	0.002826
C24-21-28	100.0	0.002014	0.002014	0.001231	0.001231
C24-21-82	100.0	0.001601	0.001601	0.002393	0.002393

5.4 Experimental Results

The test plan (see Appendix A) was executed, and all forty panels that were manufactured for this research effort were tested. A minimum of two tests were run for each panel cutout combination and in most cases the collapse load presented in Table 14 is an average value (see Appendix C). Appendix C provides a means to track experimental panel response for specific panel serial numbers. Appendix A provides an interpretation of the panel designator number.

For most of the tests, when the collapse load was reached, the panel continued to deform smoothly while the load began to slowly drop off. However, the 24 ply 304.8 mm x 508 mm panel with a 50.8 mm x 50.8 mm cutout experienced sudden and complete failure at the collapse load (see figure 27). This was evident by a loud bang at the collapse load and a dramatic drop off of load. This panel had experienced instantaneous delamination and material failure at the collapse. Delamination occurred along the vertical panel edge and near the cutout corners. Other 16 and 24 ply panels experienced delamination at similar locations, but it was not instantaneous as it was for this case.

Table 14 provides a comparison between experimental and numerical results for the global collapse load. As expected, the experimental panels responded more flexibly than predicted by the stiffer analytical model, SHELL. There are numerous reasons why this is the case.
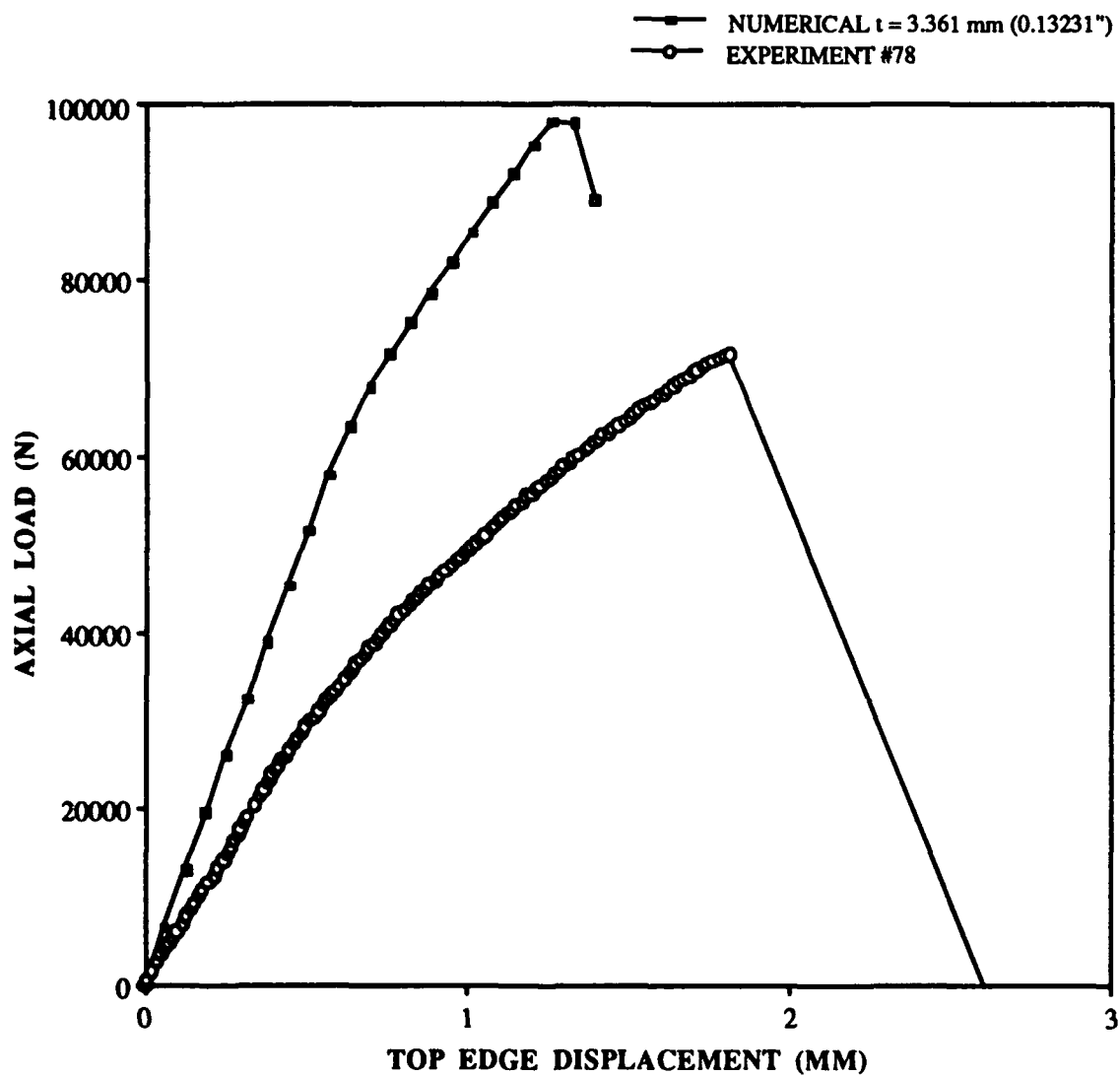
Fig. 27: Load vs. Top Edge Displacement,
Numerical Compared to Experiment #78,
50.8 mm x 50.8 mm (2" x 2") Cuout,
304.8 mm x 508 mm (12" x 20") Panel,
[0/45/-45/90]3s

Table 14. *Comparison Between Experimental and Numerical Collapse Loads*

Panel Designator	Experimental Load (N)	Numerical Load (N)	Difference (%)
A8-13-22	6206	11395	45.5
A8-13-44	4449	6277	29.1
A8-13-55	3207	5644	43.4
A8-13-28	4972	7522	33.9
A8-13-82	2511	3039	17.4
A8-21-22	5525	7836	29.5
A8-21-44	3473	5185	33.0
A8-21-55	3073	3450	10.9
A8-21-28	3938	5551	29.1
A8-21-82	1050	3067	65.8
B16-21-22	28257	30133	6.2
B16-21-44	21979	23392	6.0
B16-21-55	14545	15107	3.7
B16-21-28	27028	27927	3.2
B16-21-82	7846	12315	36.3
C24-21-22	71603	97934	26.9
C24-21-44	48186	58936	18.2
C24-21-55	35925	39886	9.9
C24-21-28	45944	52680	12.8
C24-21-82	22896	35076	34.7

All composite materials, from a micromechanics viewpoint, experience some level of fiber/matrix material property imperfections, as well as interlaminar slipping between lamina.The SHELL program assumes the material properties are constant through each ply, and that the lamina are perfectly bonded. In reality, these two factors vary between lamina. In addition, the fiber/matrix properties could vary within each ply. Furthermore, the SHELL program assumes there is no variation in ply thickness between lamina. Again, actual ply thickness does vary between lamina, and along each ply. Consequently, a variation in ply thickness promotes off-axis loading, with respect to the fibers, which could produce additional shear stress. This additional shear stress is not accounted for by the SHELL program. Therefore, these shear stresses reduce the stiffness of the panels resulting in lower panel collapse loads.

The effects on panel collapse load due to panel curvature imperfections is a primary reason for the reduction of collapse load in some of the experimental panels. This effect is a function of the geometric imperfection of curvature of the panel in its relaxed state and the cutout area. Specifically, the eight ply panels, upon curing, tended to curl up slightly decreasing the radius of curvature of the panel in its relaxed state. The effect of uncurling this panel when clamping it into the 304.8 mm radius of curvature loading fixture causes the center of the panel to slightly flatten out. A large cutout in a thin panel tends to flatten out the radius of curvature in the middle of the panel around the cutout edge. This effect was visually noticeable when

the eight ply panels with large cutout areas were setup in the test fixture and an initial load applied. In addition, visual inspection of all panel configurations (8, 16, or 24 ply) revealed slight radius of curvature imperfections along the curvature of the panel. These imperfections could be responsible for some of the panel responses obtained for the thicker panels with large circumferential horizontal dimensions. Recall a parametric study was run to determine the effects of radius of curvature variations. This study confirmed that a moderate variation in radius of curvature significantly effects the panel collapse load. The effects of curvature imperfections are discussed in more detail in subsequent paragraphs.

Furthermore, the degree to which the experiment is incapable of enforcing the boundary conditions is the degree to which the numerical analysis will be stiffer than the experiment. The modified panel restraint system was not used for the eight ply panels, therefore the variation between numerical and experimental collapse loads for these panels could be partly attributed to this.

In addition to Table 14, experimental versus numerical panel response is graphically displayed throughtout this section and in Appendix E in the form of load versus top edge displacement curves and load versus radial displacement curves. Appendix E contains some eight ply 304.8 mm x 304.8 mm panel response data (figures 84-93) and the majority of the 8 and 24 ply 304.8 mm x 508 mm panel response data (figures 94 - 140). The experimental and numerical radial displacement curves compare data obtained at

discrete LVDT locations shown in Figure 4, and linear
interpolations of numerical data obtained at nodes shown in
Figures 6-15. The 16 ply panels numerical response at collapse,
are also graphically displayed in the form of three dimensional
orthotropic surface plots for visual comparison to photographs of
these experimental panels at collapse (see figures 79-83). These
three dimensional plots when compared to the experimental
photographs indicate that the SHELL program accurately captures
the shape of deformation of the panel at collapse.

Some general observations are made in the comparison of the
numerical and experimental collapse loads, and are discussed in
more detail in subsequent paragraphs. Table 14 illustrates the
best correlation between the experimental and numerical collapse
loads occurred for the 16 ply 304.8 mm x 508 mm panels. Likewise,
the best correlation between the numerical and experimental panel
response data occurred for the 16 ply panels (see figures 50-78).
On the other hand, the largest deviations between experimental and
numerical collapse loads occurred for the eight ply panels which
were most affected by panel curvature imperfections. In addition,
to these observations the SHELL program was successful in
predicting experimental trends. Specifically, SHELL predicted
that the collapse load decreases with increasing cutout area, and
decreasing extensional width and panel thickness. Furthermore, it
predicted that the collapse load for the 304.8 mm x 508 mm panel
with a 101.6 mm x 101.6 mm cutout would exceed the collapse load
of a 203.2 mm x 50.8 mm cutout when a 24 ply panel was used (see
Table 14 and 15). Recall this was found numerically to be a

function of transverse shear strain along the cutout's vertical edge.

The short panels showed no real trend of numerical to experimental collapse load variation when exclusively examining the results in Table 14. However, analysis of the numerical and experimental radial displacement data lead to the following conclusion. The effects of imperfections of panel curvature were the main contributer to the large variation between the numerical and experimental collapse load for the axial short panels (see figures 28-33). As stated earlier, this effect is a function of the geometric imperfection of curvature of the panel in its relaxed state and the cutout area. The eight ply panels, upon curing, tended to curl up slightly decreasing the radius of curvature of the panel in its relaxed state. The effect of uncurling this panel when clamping it into the 304.8 mm radius of curvature loading fixture causes the center of the panel to slightly flatten out. Therefore, the radius of curvature at the center of the panel was greater than 304.8 mm (12"). Recollect that the radius of curvature parametric study confirmed that an increase in radius of curvature results in a decrease in panel collapse load. The following paragraphs discuss additional findings which support the conclusion that panel curvature imperfections were a primary instigator in the large variations between the experimental and numerical collapse load as well as the panel response for the 8 ply panels.

Figures 28 and 29 show the radial displacement data for an axial short panel (304.8 mm) with a 50.8 mm x 50.8 mm cutout.

100

Figure 28 illustrates, both numerically and experimentally, the panel response near the vertical edge of the panel displaced radially away from the panel center of curvature (negative displacement). Figure 29 indicates the numerical and experimental panel response near the vertical edge of the cutout displaced radially inward toward the panel center of curvature (positive displacement). Figure 30 and 31 show the radial displacement data for an axial short panel (304.8 mm) with a 101.6 mm x 101.6 mm cutout and are compared to figures 28 and 29. Figure 30 illustrates, both numerically and experimentally, the panel response near the vertical edge of the panel displaced radially away from the panel center of curvature (negative displacement). Figure 31 indicates the numerical panel response near the vertical edge of the cutout displaced radially toward the panel center of curvature (positive displacement). However, Figure 31 shows that the experimental panel response near the vertical edge of the cutout experienced a negative radial displacement. Therefore, both the vertical edge of the panel and vertical edge of the cutout displaced in the same direction radially. This is contrary to what occurred for the panel with the 50.8 mm x 50.8 mm cutout. A flat plate with a large cutout undergoing axial compression would deform such that the vertical edges of the plate and the vertical edges of the cutout displace in the same radial direction. Therefore, the panel with a 101.6 mm x 101.6 mm cutout can be thought of as behaving similar to a plate. Consequently, the panel with a 101.6 mm x 101.6 mm cutout is behaving more like a flatter panel with a larger radius of curvature. Likewise, the

Fig. 28: Load vs. Radial Displacement,
Numerical Compared to Experiment #64,
50.8 mm x 50.8 mm (2" x 2") Cutout,
304.8 mm x 304.8 mm (12" x 12") Panel,
[0/45/-45/90]s
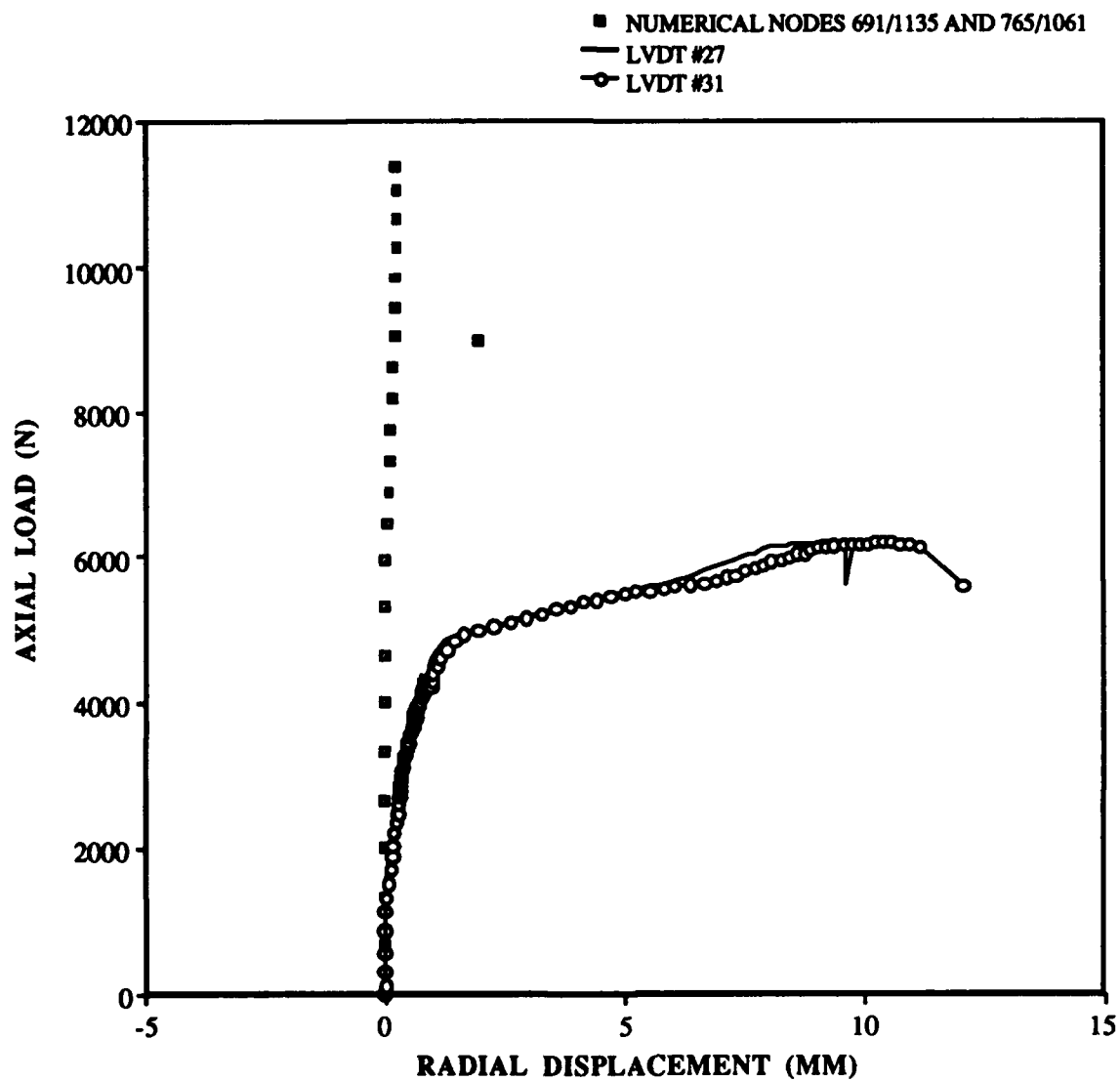
Fig. 29: Load vs. Radial Displacement,
Numerical Compared to Experiment #64,
50.8 mm x 50.8 mm (2" x 2") Cutout,
304.8 mm x 304.8 mm (12" x 12") Panel,
[0/45/-45/90]s
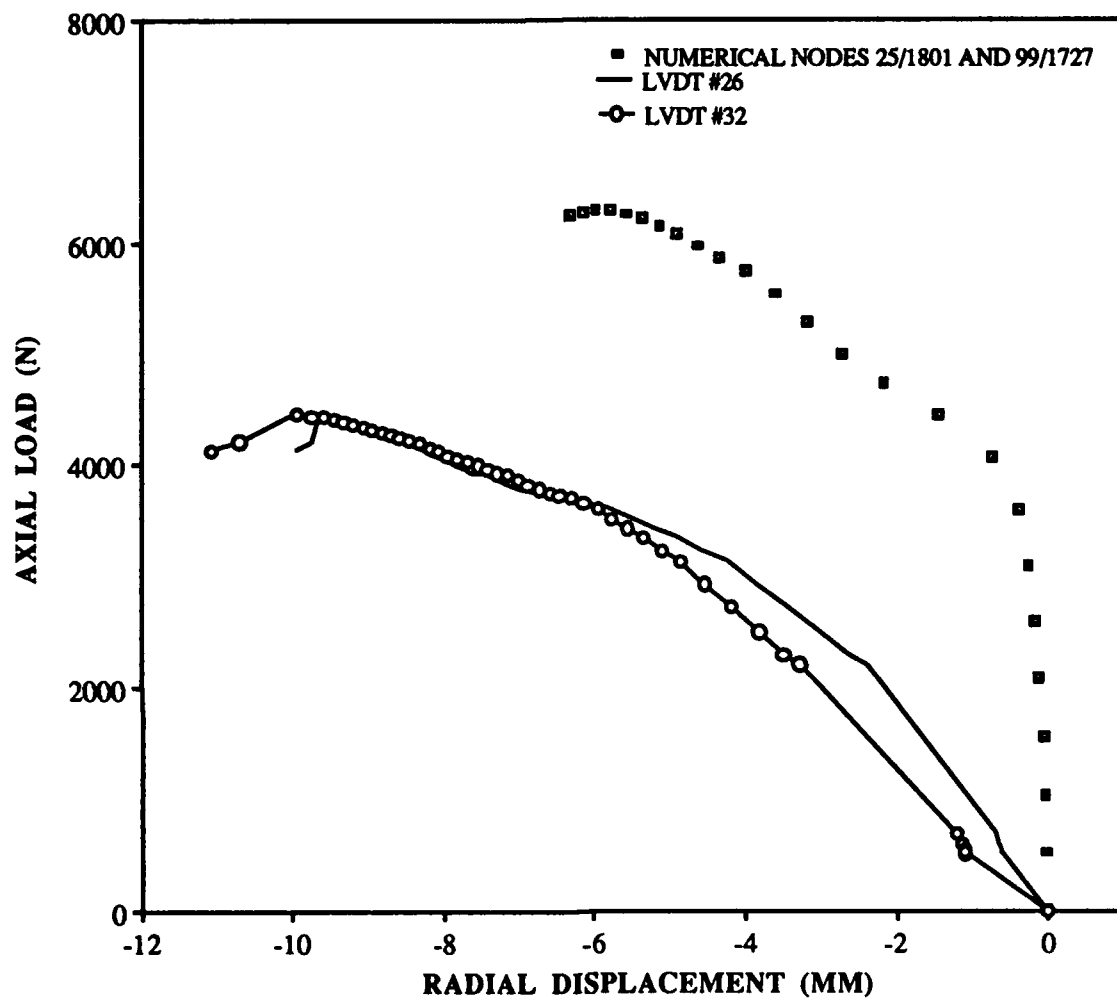
Fig. 30: Load vs. Radial Displacement,
Numerical Compared to Experiment #67,
101.6 mm x 101.6 mm (4" x 4") Cutout,
304.8 mm x 304.8 mm (12" x 12") Panel,
[0/45/-45/90]s

Fig. 31: Load vs. Radial Displacement
Numerical Compared to Experiment #67,
101.6 mm x 101.6 mm (4" x 4") Cutout,
304.8 mm x 304.8 mm (12" x 12") Panel,
[0/45/-45/90]s

Fig. 32: Load vs. Radial Displacement,
Numerical Compared to Experiment #68,
127 mm x 127 mm (5" x 5") Cutout,
304.8 mm x 304.8 mm (12" x 12") Panel,
[0/45/-45/90]s
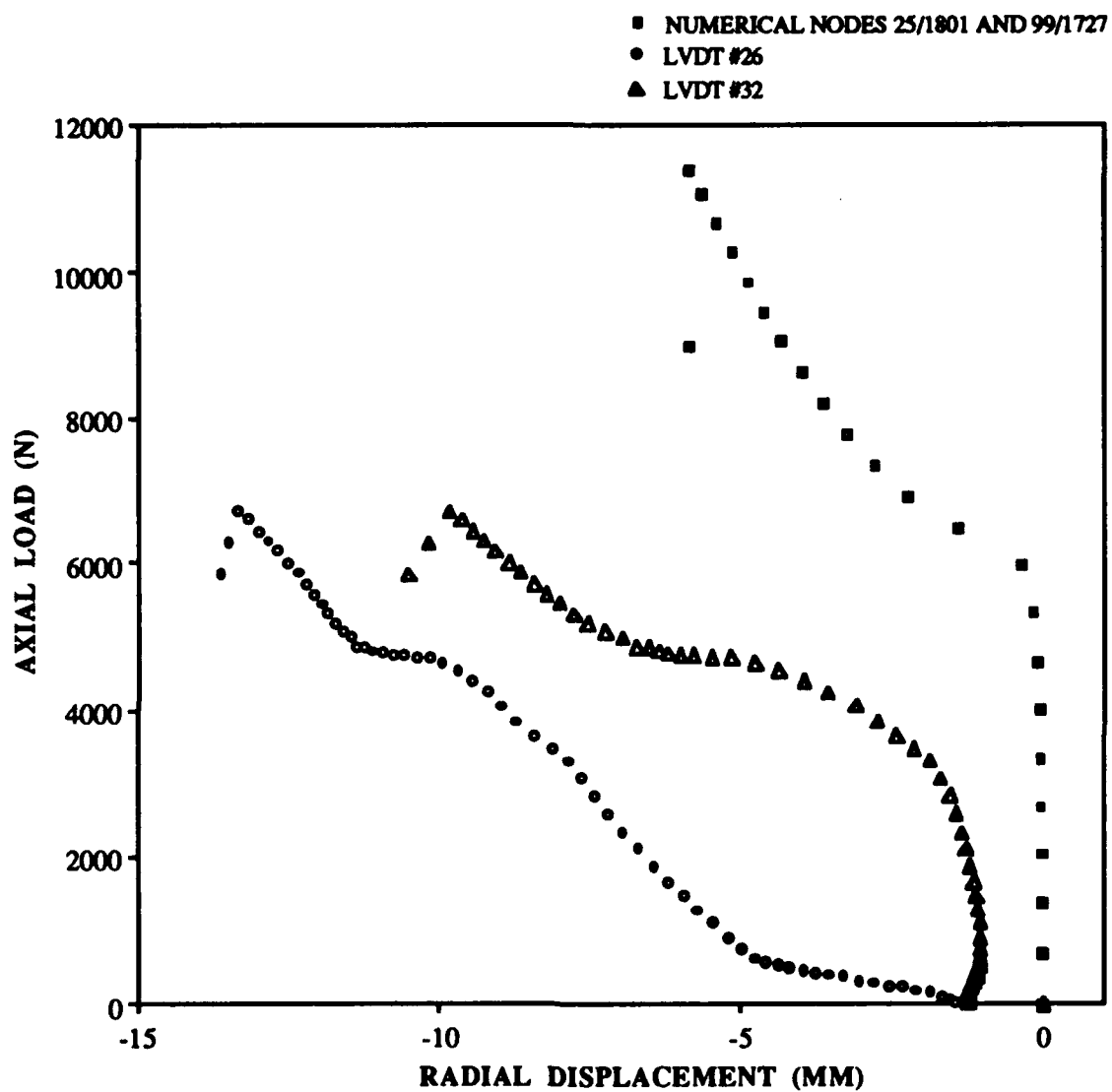
Fig. 33: Load vs. Radial Displacement,
Numerical Compared to Experiment #68,
127 mm x 127 mm (5" x 5") Cutout,
304.8 mm x 304.8 mm (12" x 12") Panel,
[0/45/-45/90]s

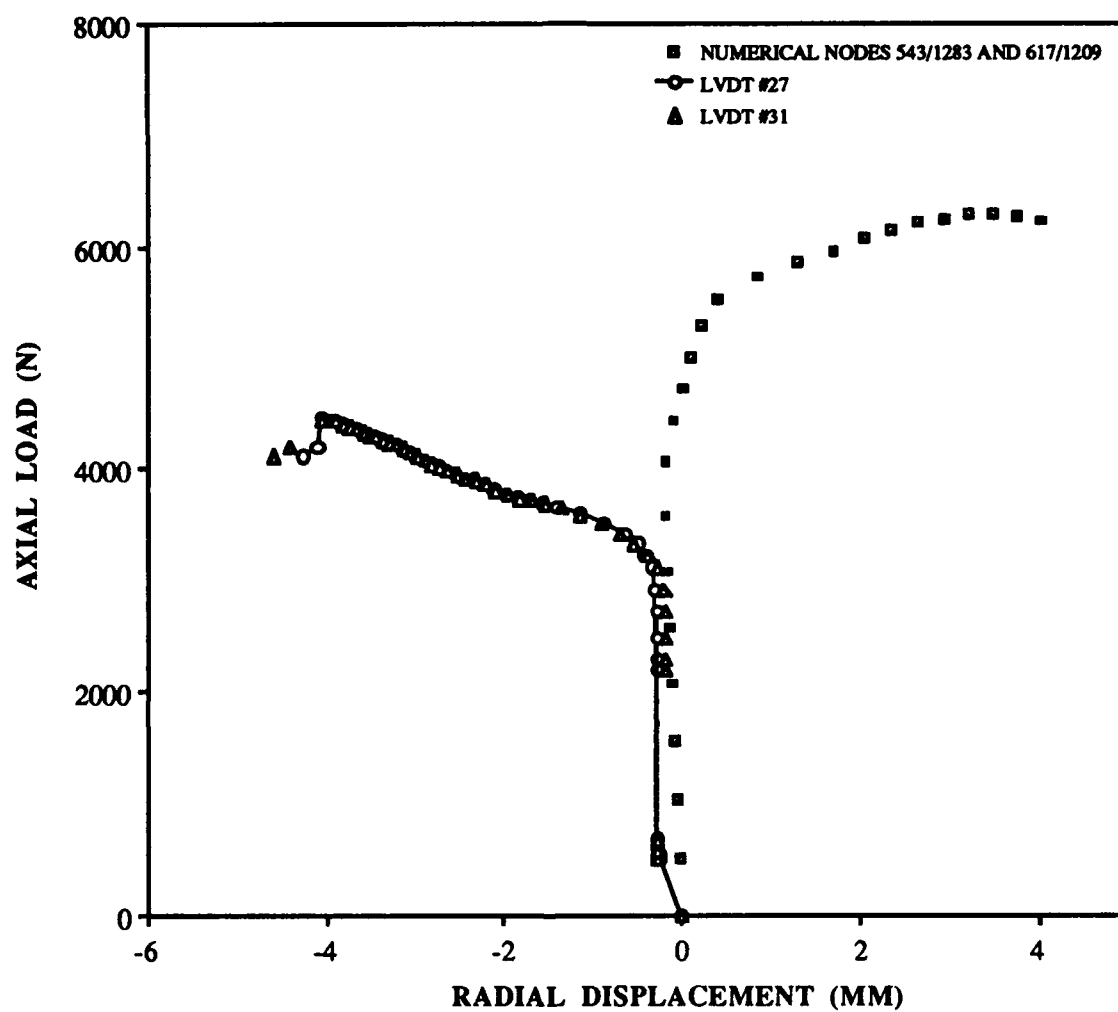short panel with a 127 mm x 127 mm cutout exhibited a similar panel response (see figures 32 and 33). Recall enlarging the cutout area increases the distribution of flatness in the panel, which results in an elongated radius of curvature near the center of the panel. It has been confirmed numerically that increasing the panel radius of curvature results in a decrease in panel collapse load. It is concluded that the decrease in experimental panel collapse as compared to the numerical collapse load is largely caused by the panel flattness effect brought about by the the uncurling of the panel when clamping them into the test fixture.

In comparison the panel with a 50.8 mm x 50.8 mm cutout did not experience the magnitude of flattening around the cutout as the panel with 101.6 mm x 101.6 mm cutout, so it behaved more like a panel with a 304.8 mm radius of curvature. Although, there are still effects due to curvature imperfections for this panel it was not of the same magnitude as for the panels with larger cutouts. The large descrepancy between the numerical and experimental collapse load was probably also a result of panel material imperfections discussed earlier. This panel has only a small portion of its surface area removed by the cutout, therefore it is more susceptible to material imperfections than those panels with larger surface areas removed.

The short axial panel which showed the best correlation between the numerical and experimental collapse load was the panel with a 203.2 mm x 50.8 mm cutout. In addition, among all the other short panel cutout combinations, this panel showed the best

correlation between the numerical and experimental panel response (see figures 34-37). This panel exhibited the largest magnitude of transverse shear and bending rotation out of the short axial panels (see Tables 12 and 13). The load versus top edge displacement curve (figure 34) is reflective of a panel experiencing a large amount of transverse shear strain brought about by bending. This is concluded since the load displacement curve becomes increasingly nonlinear as the collapse load is approached. The panel response for the duplicate test panel confirms these findings (see figures 38-41).

Comparing the effects of cutout dimension on the effects of experimental and numerical collapse load differences, indicates a general trend in the axial longer panels (508 mm). These panels exhibited smaller variations between the experimental and numerical collapse loads for the 127 mm x 127 mm cutout. Moreover, this trend for the axial longer panels was consistent regardless of panel thickness. This trend is attributed to the large cutout area which dominates the panel collapse. The probability of effects of material imperfections and panel geometric imperfections on the panel collapse load decrease as the cutout area increases. In addition, these longer panels experienced increased variations between the experimental and numerical collapse loads when the cutout area remained constant and extensional width of the panel decreased. Likewise, this trend was consistent regardless of panel thickness.

Fig. 34: Load vs. Top Edge Displacement,
Numerical Compared to Experiment #73,
203.2 mm x 50.8 mm (8" x 2") Cutout,
304.8 mm x 304.8 mm (12" x 12") Panel,
[0/45/-45/90]s

Fig. 35: Load vs. Radial Displacement,
Numerical Compared to Experiment #73,
203.2 mm x 50.8 mm (8" x 2") Cutout,
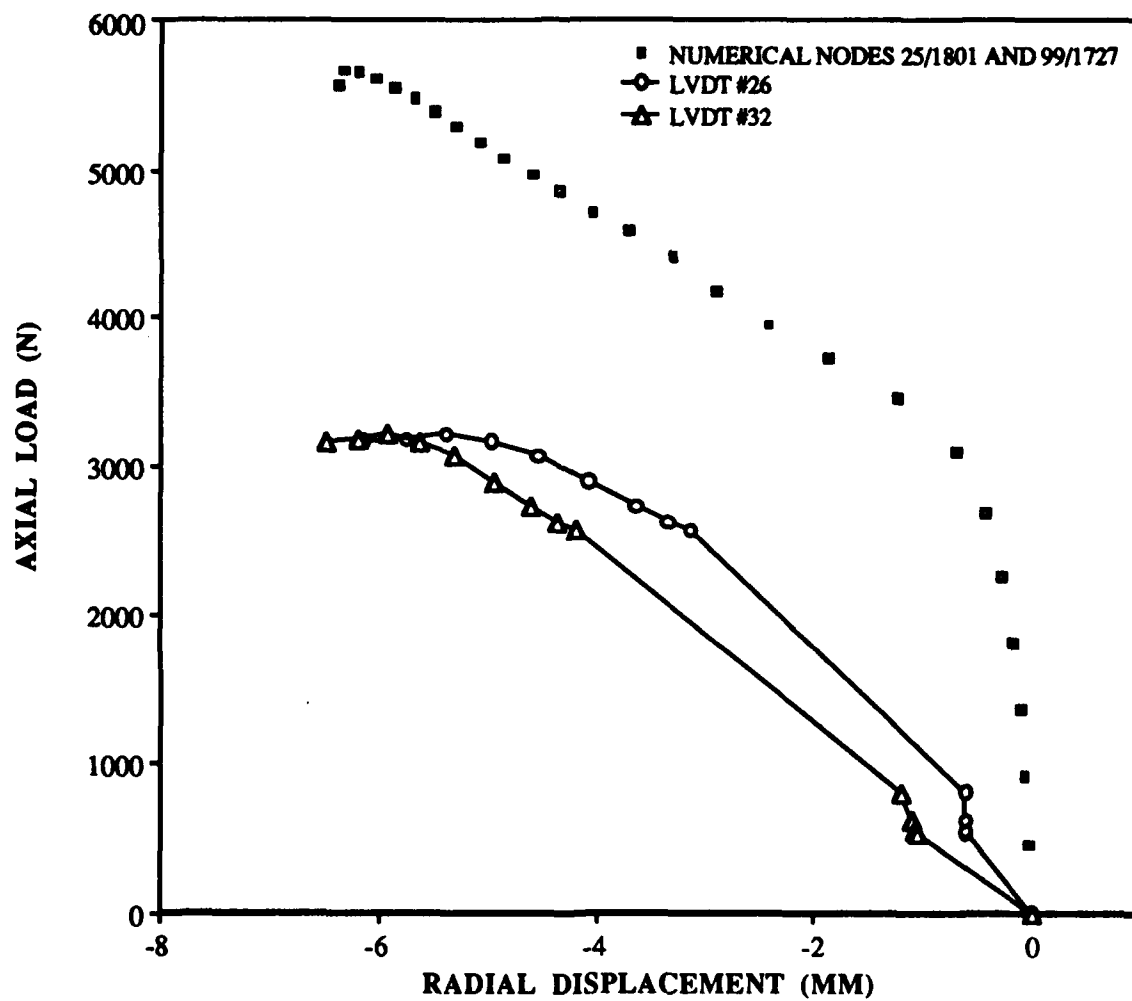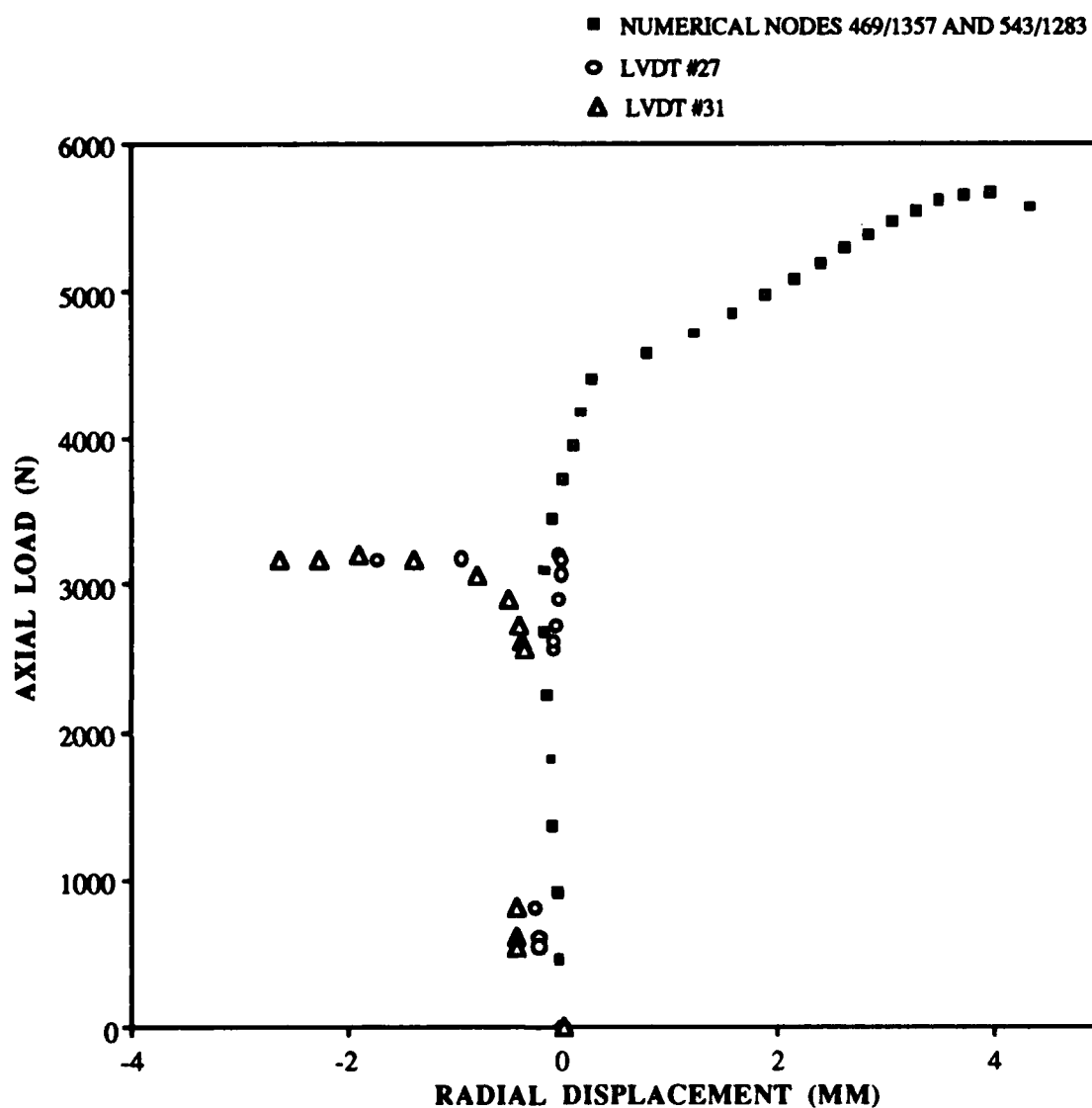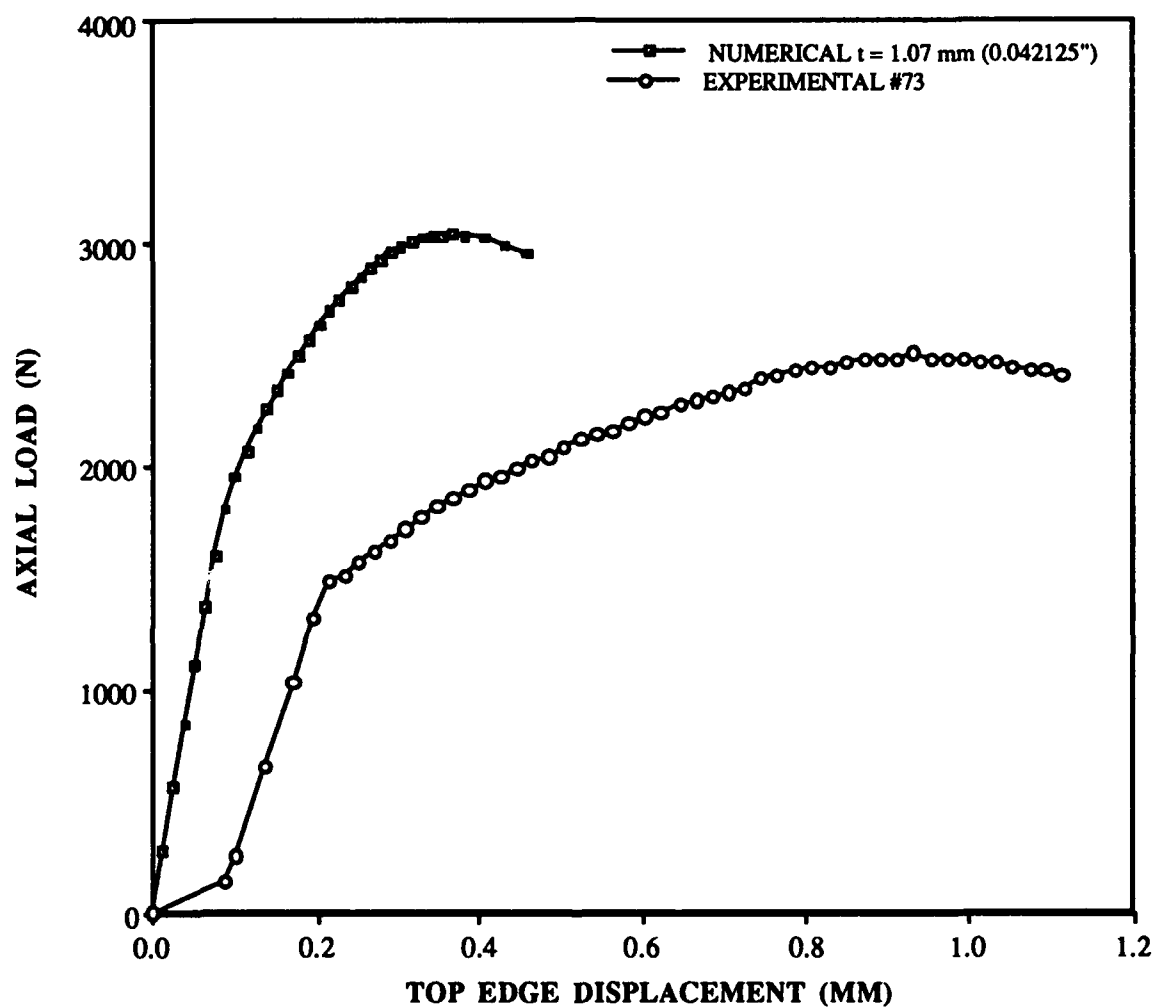304.8 mm x 304.8 mm (12" x 12") Panel,
[0/45/-45/90]s

111
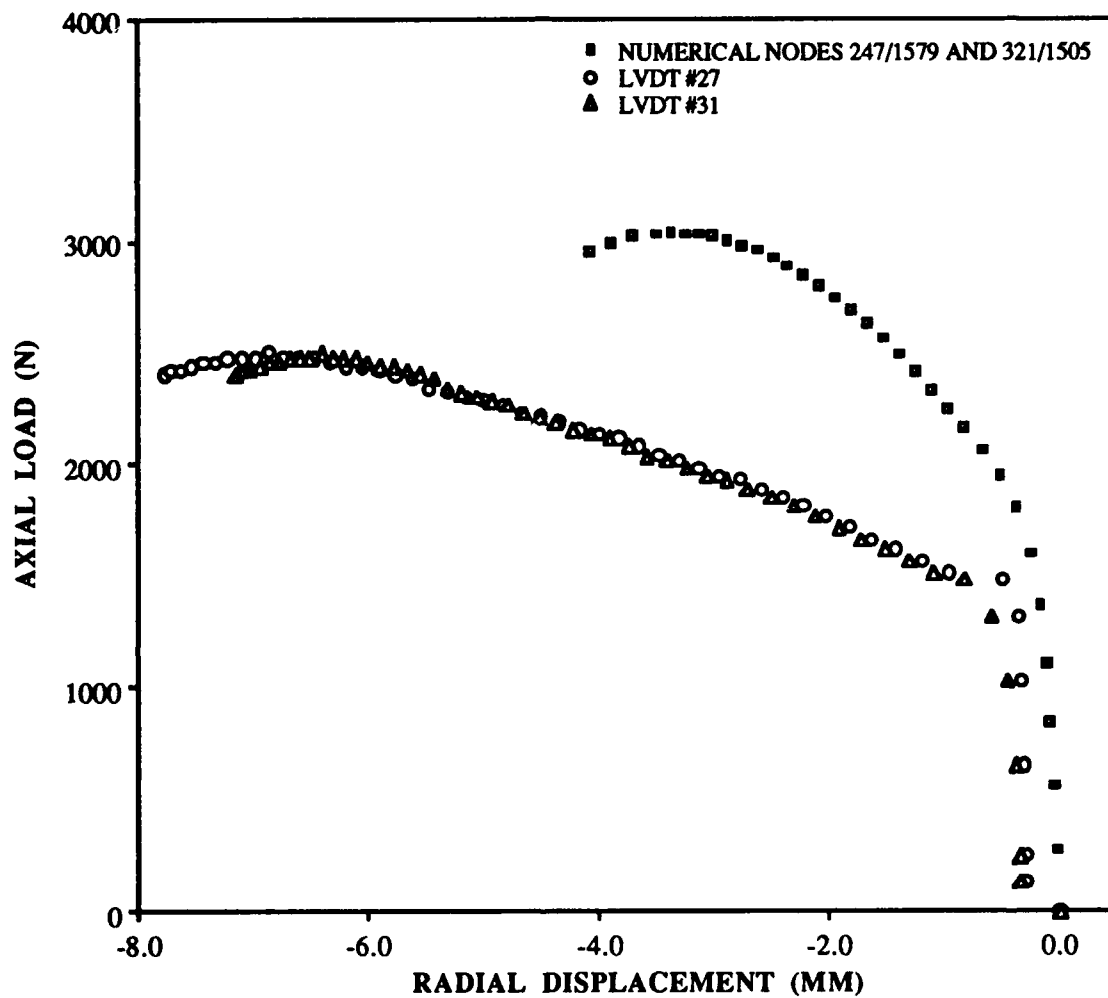
Fig. 36: Load vs. Radial Displacement,
Numerical Compared to Experiment #73,
203.2 mm x 50.8 mm (8" x 2") Cutout,
304.8 mm x 304.8 mm (12" x 12") Panel,
[0/45/-45/90]s
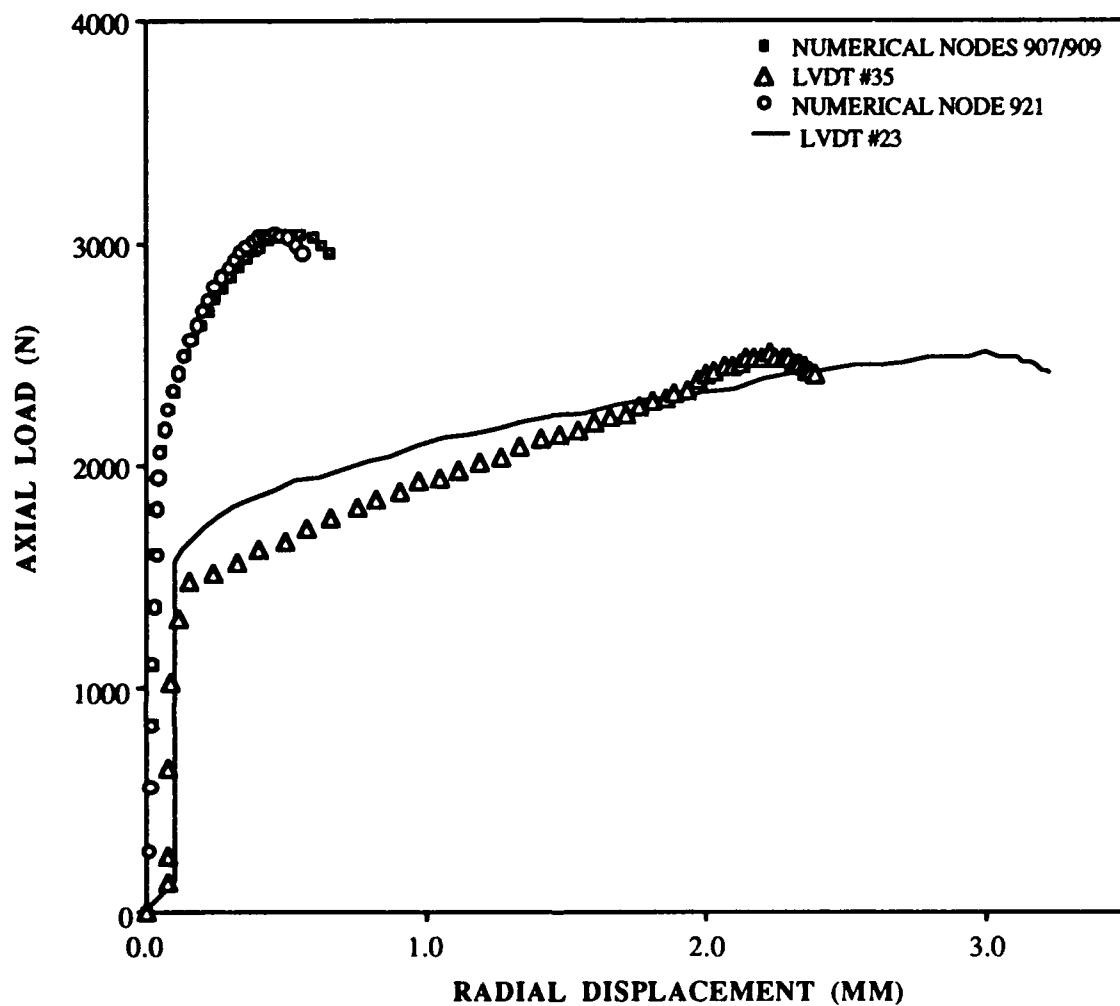
Fig. 37: Load vs. Radial Displacement,
Numerical Compared to Experiment #73,
203.2 mm x 50.8 mm (8" x 2") Cutout,
304.8 mm x 304.8 mm (12" x 12") Panel,
[0/45/-45/90]s

Fig. 36: Load vs. Top Edge Displacement,
Numerical Compared to Experiment #76,
203.2 mm x 50.8 mm (8" x 2") Cutout,
304.8 mm x 304.8 mm (12" x 12") Panel,
[0/45/-45/90]s

114
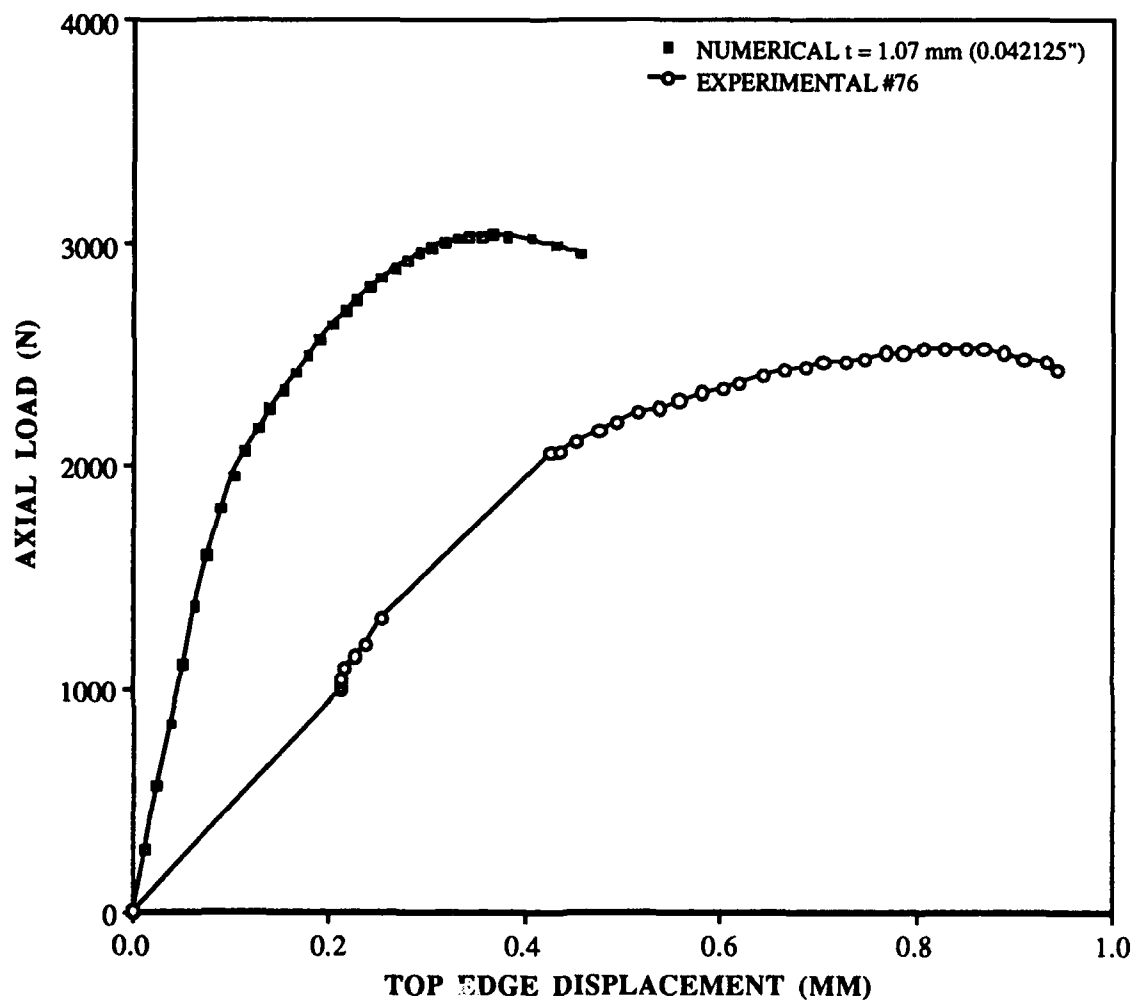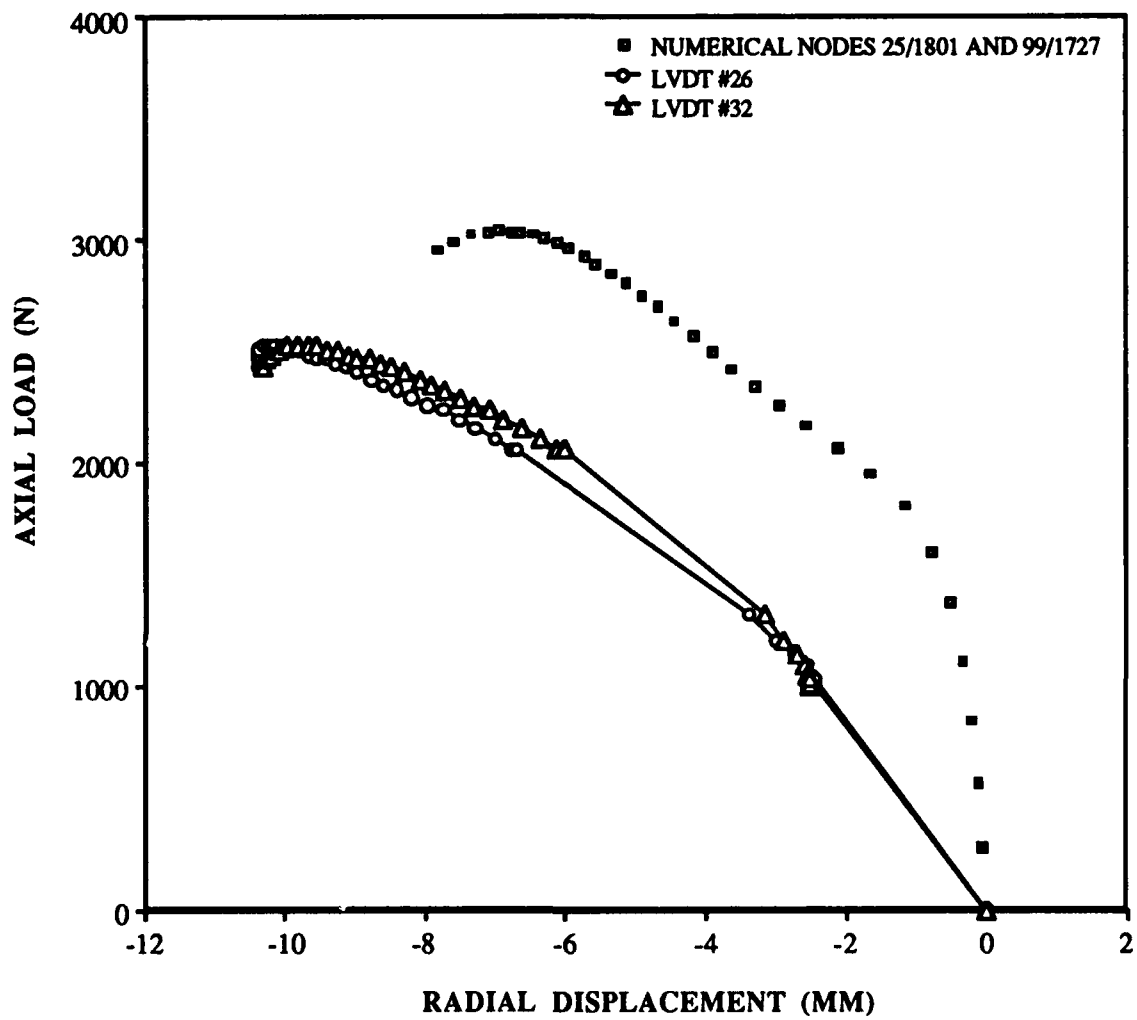
Fig. 39: Load vs. Radial Displacement,
Numerical Compared to Experiment #76,
203.2 mm x 50.8 mm (8" x 2") Cutout,
304.8 mm x 304.8 mm (12" x 12") Panel,
[0/45/-45/90]s
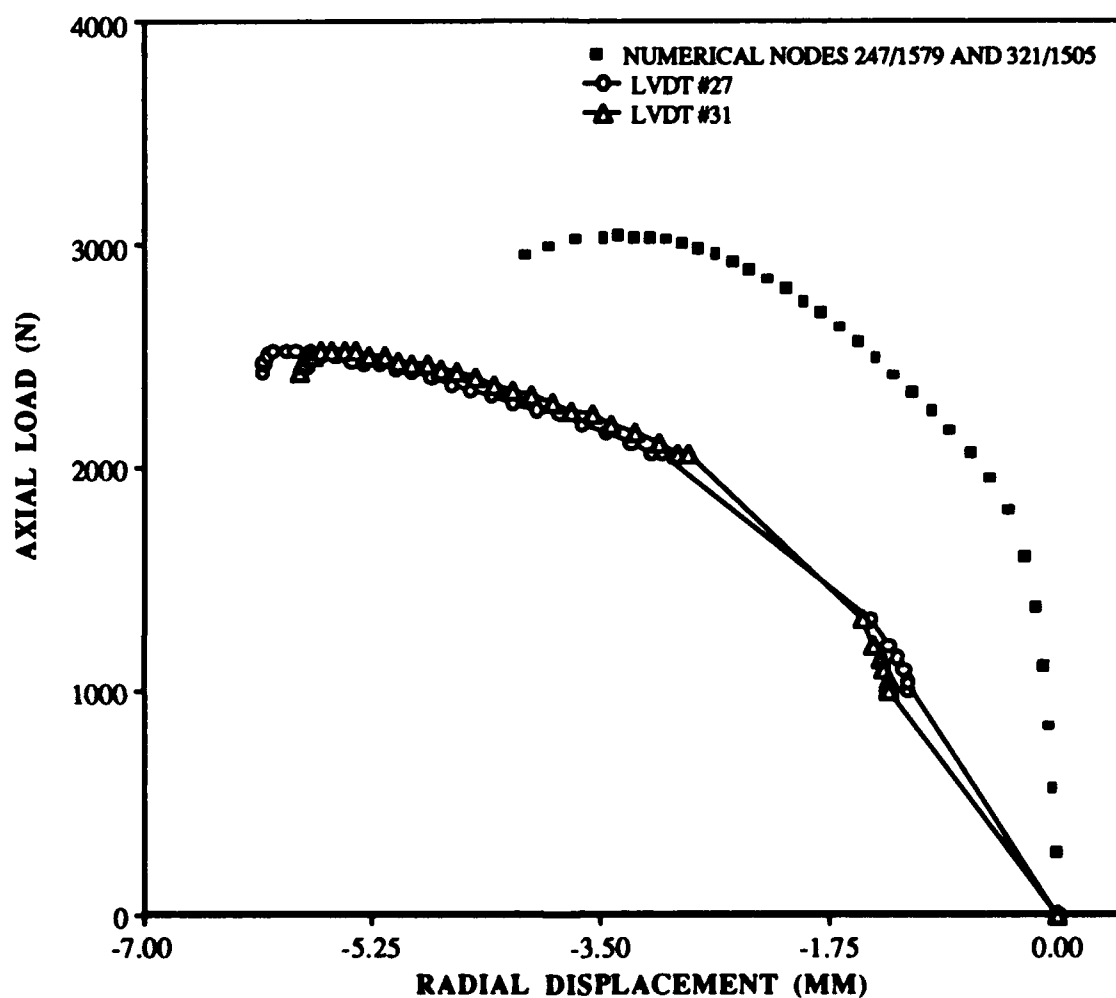
Fig. 40: Load vs. Radial Displacement,
Numerical Compared to Experiment #76,
203.2 mm x 50.8 mm (8" x 2") Cutout,
304.8 mm x 304.8 mm (12" x 12") Panel,
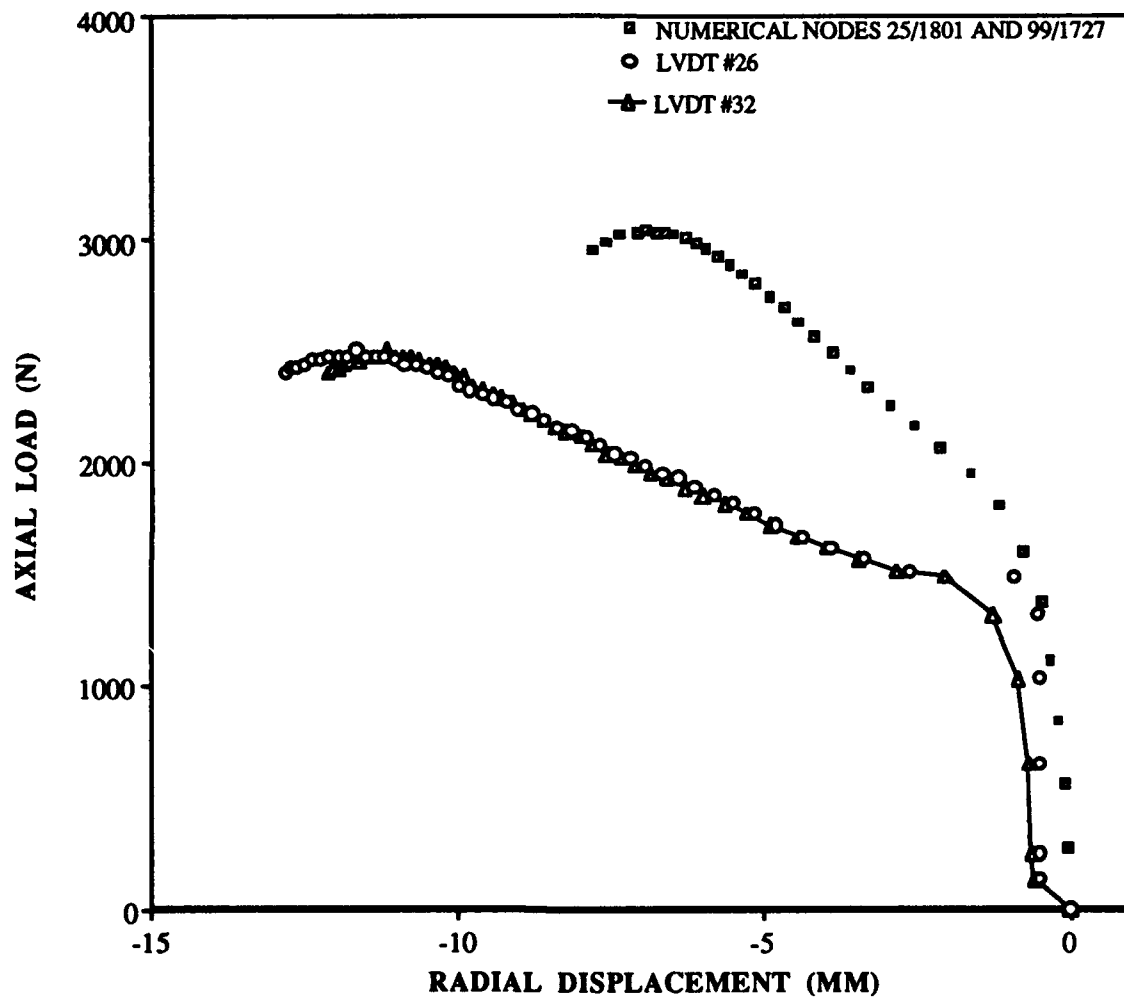[0/45/-45/90]s

116
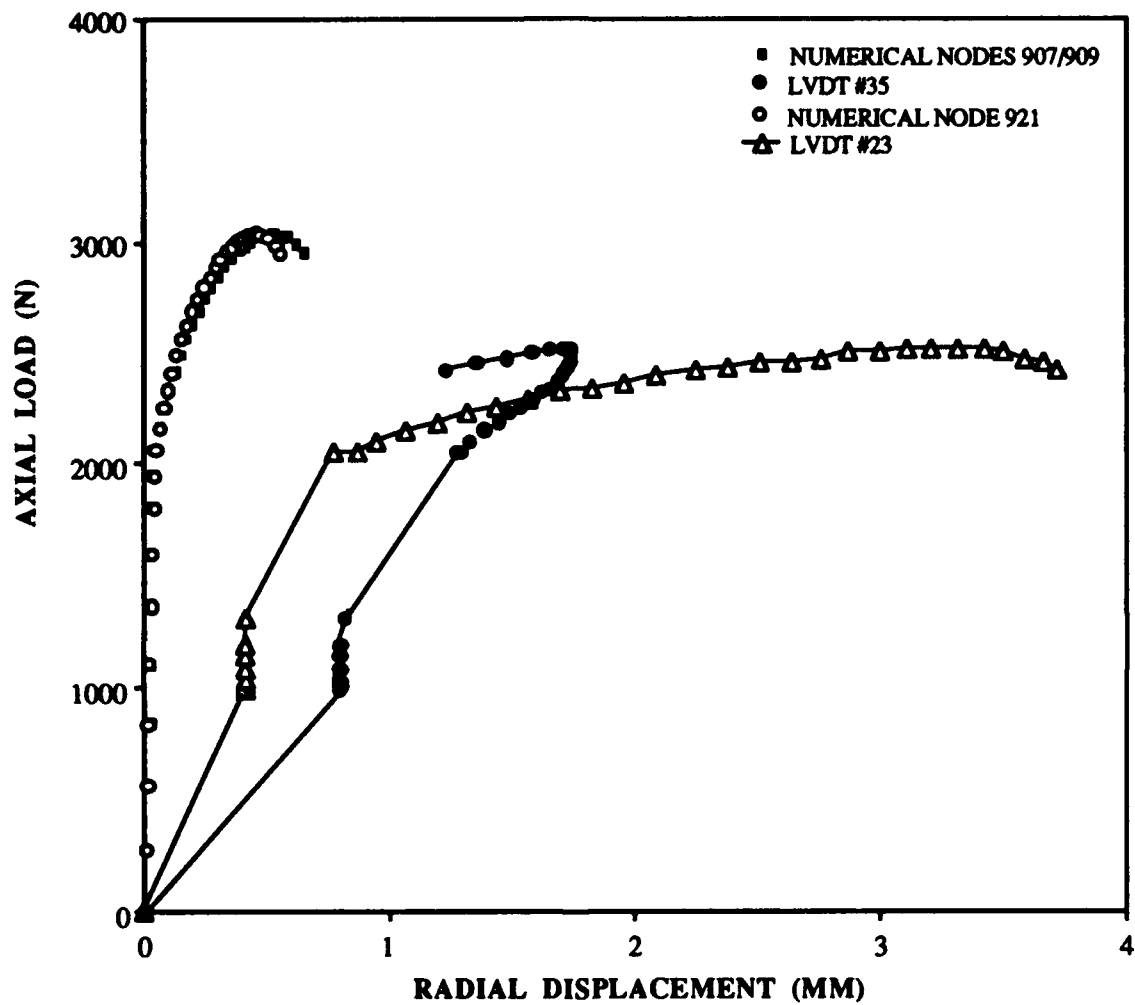
Fig. 41: Load vs. Radial Displacement,
Numerical Compared to Experiment #76,
203.2 mm x 50.8 mm (8" x 2") Cutout,
304.8 mm x 304.8 mm (12" x 12") Panel,
[0/45/-45/90]s

117

All test cases involving the longer panels with a 203.2 mm x 50.8 mm cutout (b = 50.8mm) resulted in an asymmetrical panel response (see figures 76-77, 87-88, 124-125, 143-144, and 147-148). In some cases panels were very close to zero tolerance and still experienced an asymmetrical response (see figures 124-125 and 147-148). Again this could be due to slight curvature imperfections of the panel. The long circumferential length of these cutouts combined with the small panel extensional widths could make this case more susceptible to curvature imperfections when compared to other cutout dimensions. Any variation in radius of curvature near the cutout in the area between the vertical cutout edge and the panel vertical edge could predetermine the collapse of the panel. If one of these areas is flatter than the other, the panel response could be a response of least resistance resulting in a asymmetric panel pattern.

Focusing the comparison of experimental to numerical collapse load variations to the square cutouts for the axial longer panels, it is revealed that the variation of numerical to experimental collapse load increases for decreasing cutout area. This trend is primarily attributed to the effects due to material and geometric imperfections discussed earlier. As the cutout area decreases the effects due to material imperfections increase.

All panels were preloaded to ~1100 N (~250 lbs) to seat the panels in the test fixture. However, the 16 and 24 ply longer panels load versus top edge displacement curves reflected panel seating difficulties in the test fixture. The load displacement curves were corrected to reflect the true experimental axial

displacement of the panel. Figure 62 is an example of data which exhibits a seating problem in the fixture. Figure 63 shows figure 62 data corrected for this problem.

In spite of the differences in panel stiffness, the SHELL algorithm was able to predict reasonably accurate local panel responses. Although the increased flexibility of the experimental panels resulted in larger magnitudes of displacements, the experimental curves followed closely the general movement of the numerical curves in terms of direction and slope. Again, the numerical and experimental panel responses showed the best correlation for the 16 ply panels. Although the 24 ply panel experimental and numerical response data was good, it was fair in comparison to the 16 ply panel data. The greater thickness of the 24 ply panels may have contributed to more imperfections resulting from the curing process. In particular, greater residual stesses and greater thickness variation within and between laminae may be more prevalent in the 24 ply cases than in the 8 and 16 ply cases.

The modification to the loading fixture panel restraint system was believed to have corrected the uneven loading anamoly experienced in Hatfield's research [18]. The majority of data collected during this research did not show signs of uneven loading. In addition, results obtained by Hatfield for the 16 and 24 ply 101.6 mm x 101.6 mm cutout panels were compared to the results obtained in this study. This study obtained smaller variations between numerical and experimental collapse loads than Hatfield for the 16 and 24 ply panel with a 101.6 mm x 101.6 mm cutout. This variation between numerical and experimental

119

collapse loads showed a ten and four percent improvement for the 16 and 24 ply panel, respectively, compared to Hatfield's results.

Hatfield recommended that the tolerance between the panel upper and lower horizontal edge, for a quasi-isotropic panel, be within 0.0762 mm (0.003") [18]. This tolerance was recommended to ensure no effects due to uneven loading were brought about. In some cases, this tolerance was exceeded (see Appendix B). Specifically, the 24 ply panel with a 127 mm x 127 mm cutout experienced a variation of axial length between the panel horizontal edges of 0.178 mm. Comparing the panel response of this panel (figures 51-53) to a similar panel which was within the 0.0762 mm tolerance (figures 47-49) revealed both panels had a symmetrical response. The response of the panel within the tolerance was more symmetrical, but also the fact that the panel that was out of tolerance did not behave asymmetrically indicates that the restraint block modification worked.

Fig. 42: Load vs. Top Edge Displacement,
Numerical Compared to Experiment #92,
127 mm x 127 mm (5" x 5") Cutout,
304.8 mm x 508 mm (12" x 20") Panel,
[0/45/-45/90]3s

Fig. 43: Load vs. Radial Displacement,
Numerical Compared to Experiment #92,
127 mm x 127 mm (5" x 5") Cutout,
304.8 mm x 508 mm (12" x 20") Panel,
[0/45/-45/90]3s

122

Fig. 44: Load vs. Radial Displacement,
Numerical Compared to Experiment #92,
127 mm x 127 mm (5" x 5") Cutout,
304.8 mm x 508 mm (12" x 20") Panel,
[0/45/-45/90]3s

Fig. 45: Load vs. Radial Displacement,
Numerical Compared to Experiment #92,
127 mm x 127 mm (5" x 5") Cutout,
304.8 mm x 508 mm (12" x 20") Panel,
[0/45/-45/90]3s

Fig. 46: Load vs. Top Edge Displacement,
Numerical Compared to Experiment #93,
127 mm x 127 mm (5" x 5") Cutout,
304.8 mm x 508 mm (12" x 20") Panel,
[0/45/-45/90]3s

Fig. 47: Load vs. Radial Displacement,
Numerical Compared to Experiment #93,
127 mm x 127 mm (5" x 5") Cutout,
304.8 mm x 508 mm (12" x 20") Panel,
[0/45/-45/90]3s

126

Fig. 48: Load vs. Radial Displacement,
Numerical Compared to Experiment #93,
127 mm x 127 mm (5" x 5") Cutout,
304.8 mm x 508 mm (12" x 20") Panel,
[0/45/-45/90]3s

127

Fig. 49: Load vs. Radial Displacement,
Numerical Compared to Experiment #93,
127 mm x 127 mm (5" x 5") Cutout,
304.8 mm x 508 mm (12" x 20") Panel,
[0/45/-45/90]3s

Fig. 50: Load vs. Top Edge Displacement,
Numerical Compared to Experiment #80,
50.8 mm x 50.8 mm (2" x 2") Cutout,
304.8 mm x 508 mm (12" x 20") Panel,
[0/45/-45/90]2s

Fig. 51: Load vs. Radial Displacement,
Numerical Compared to Experiment #80,
50.8 mm x 50.8 mm (2" x 2") Cutout,
304.8 mm x 508 mm (12" x 20") Panel,
[0/45/-45/90]2s

Fig. 52: Load vs. Radial Displacement,
Numerical Compared to Experiment #80,
50.8 mm x 50.8 mm (2" x 2") Cutout,
304.8 mm x 508 mm (12" x 20") Panel,
[0/45/-45/90]2s

131

Fig. 53: Load vs. Radial Displacement,
Numerical Compared to Experiment #80,
50.8 mm x 50.8 mm (2" x 2") Cutout,
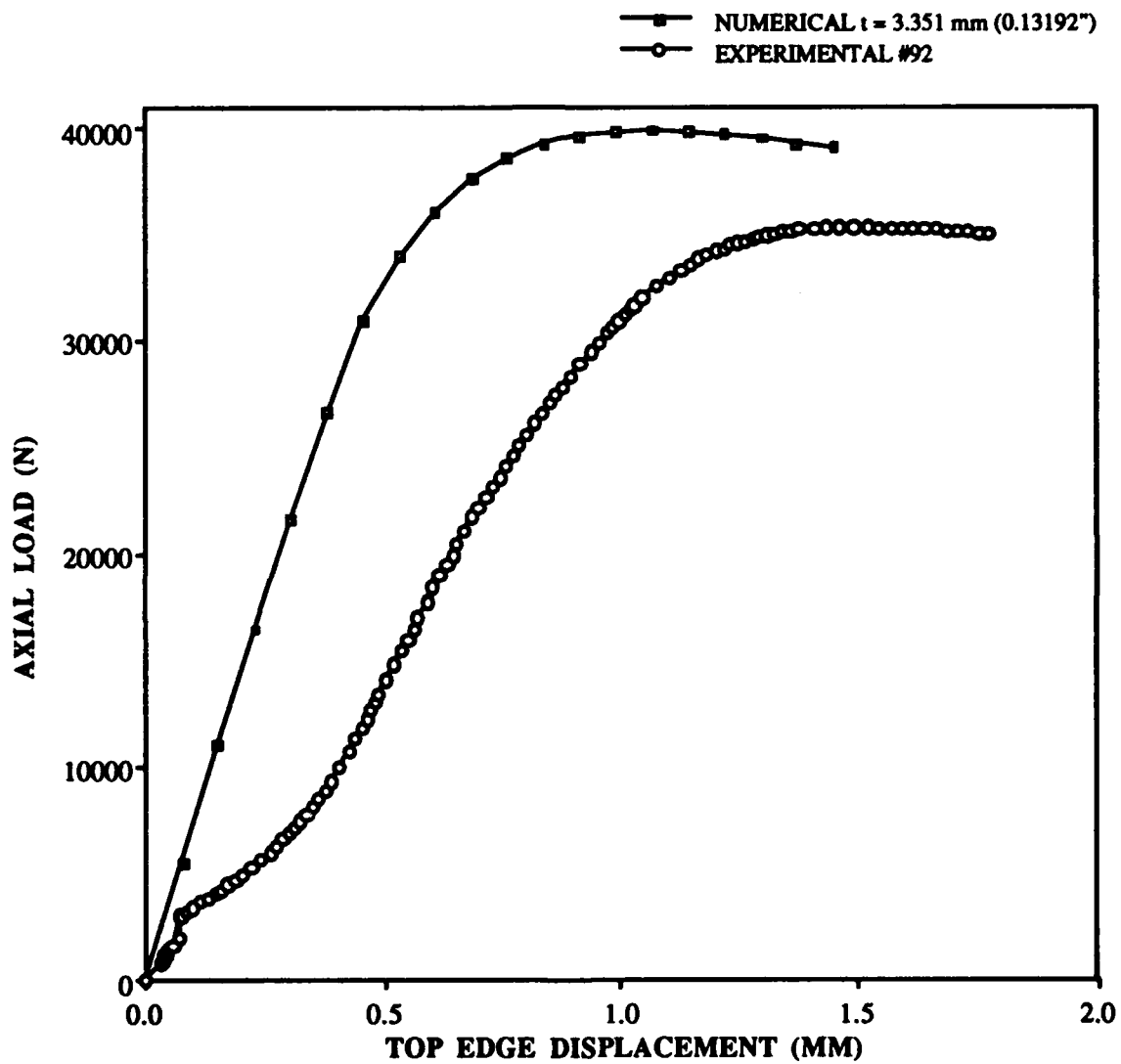304.8 mm x 508 mm (12" x 20") Panel,
[0/45/-45/90]2s

Fig. 54: Load vs. Top Edge Displacement,
Numerical Compared to Experiment #81,
50.8 mm x 50.8 mm (2" x 2") Cutout,
304.8 mm x 508 mm (12" x 20") Panel,
[0/45/-45/90]2s

Fig. 55: Load vs. Radial Displacement,
Numerical Compared to Experiment #81,
50.8 mm x 50.8 mm (2" x 2") Cutout,
304.8 mm x 508 mm (12" x 20") Panel,
[0/45/-45/90]2s

Fig. 56: Load vs. Radial Displacement, Numerical Compared to Experiment #81, 50.8 mm x 50.8 mm (2" x 2") Cutout, 304.8 mm x 508 mm (12" x 20") Panel, [0/45/-45/90]2s

135

Fig. 57: Load vs. Radial Displacement,
Numerical Compared to Experiment #81,
50.8 mm x 50.8 mm (2" x 2") Cutout,
304.8 mm x 508 mm (12" x 20") Panel,
[0/45/-45/90]2s

136

Fig. 58: Load vs. Top Edge Displacement,
Numerical Compared to Experiment #98,
50.8 mm x 203.2 mm (2" x 8") Cutout,
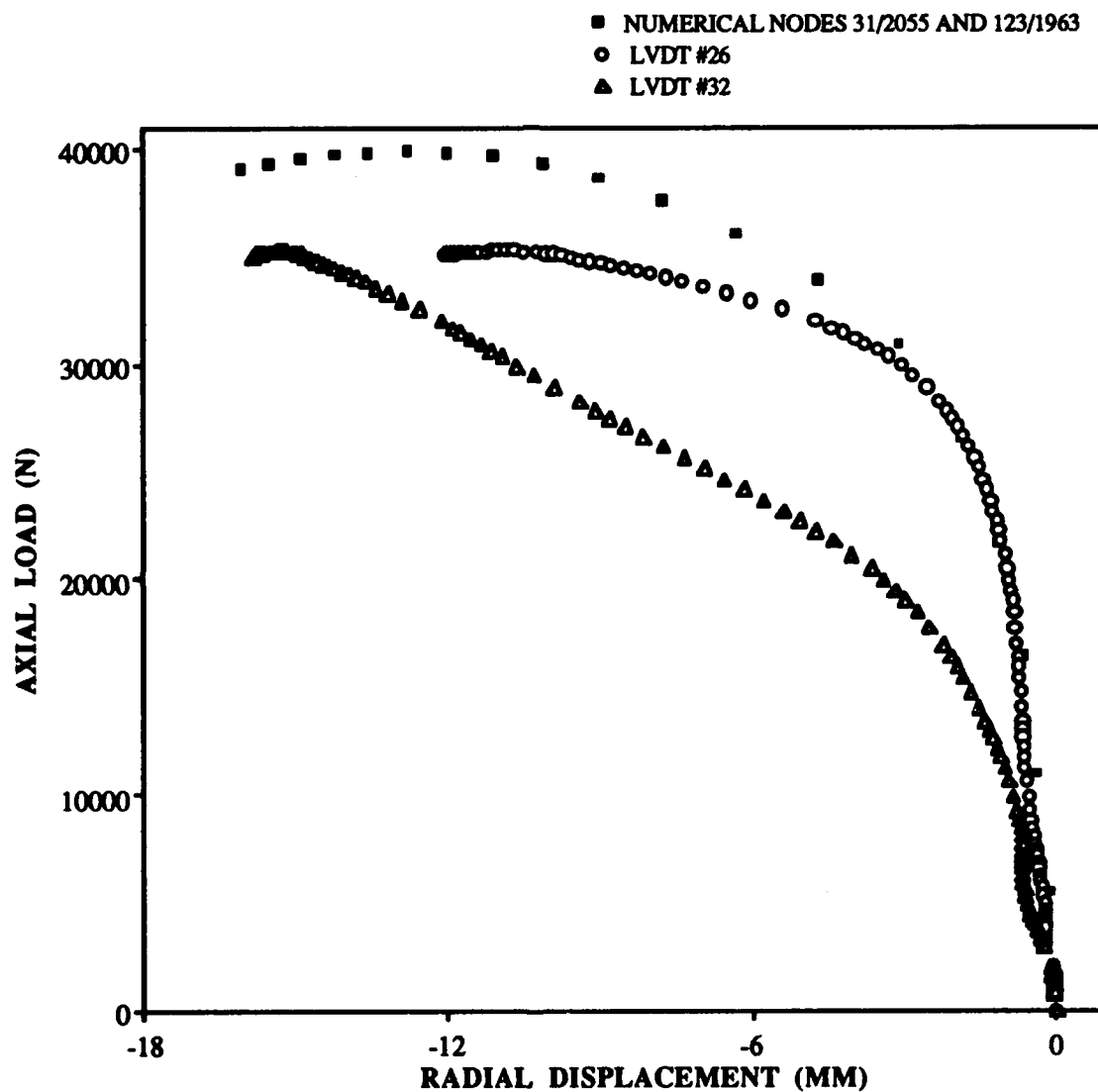304.8 mm x 508 mm (12" x 20") Panel,
[0/45/-45/90]2s

137
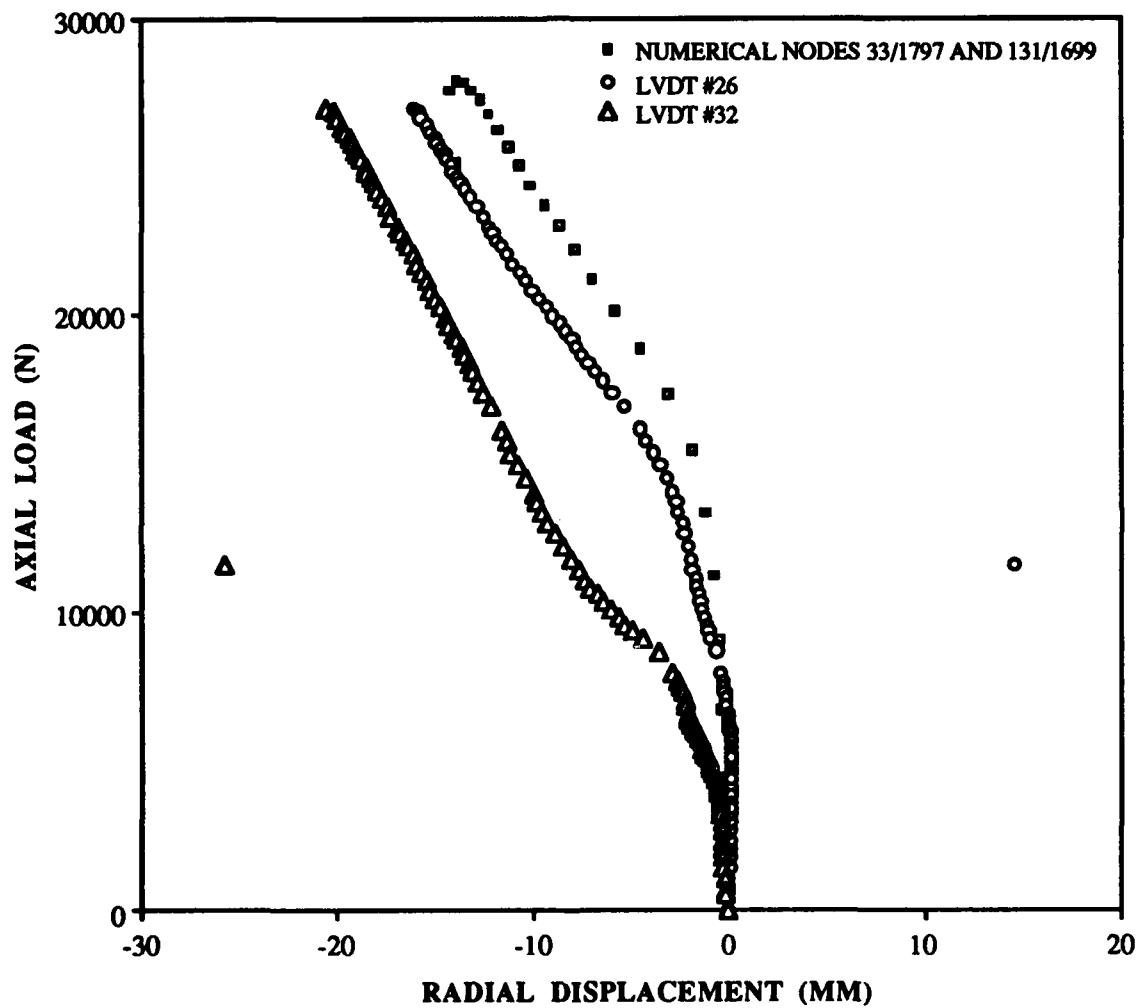
Fig. 59: Load vs. Radial Displacement,
Numerical Compared to Experiment #98,
50.8 mm x 203.2 mm (2" x 8") Cutout,
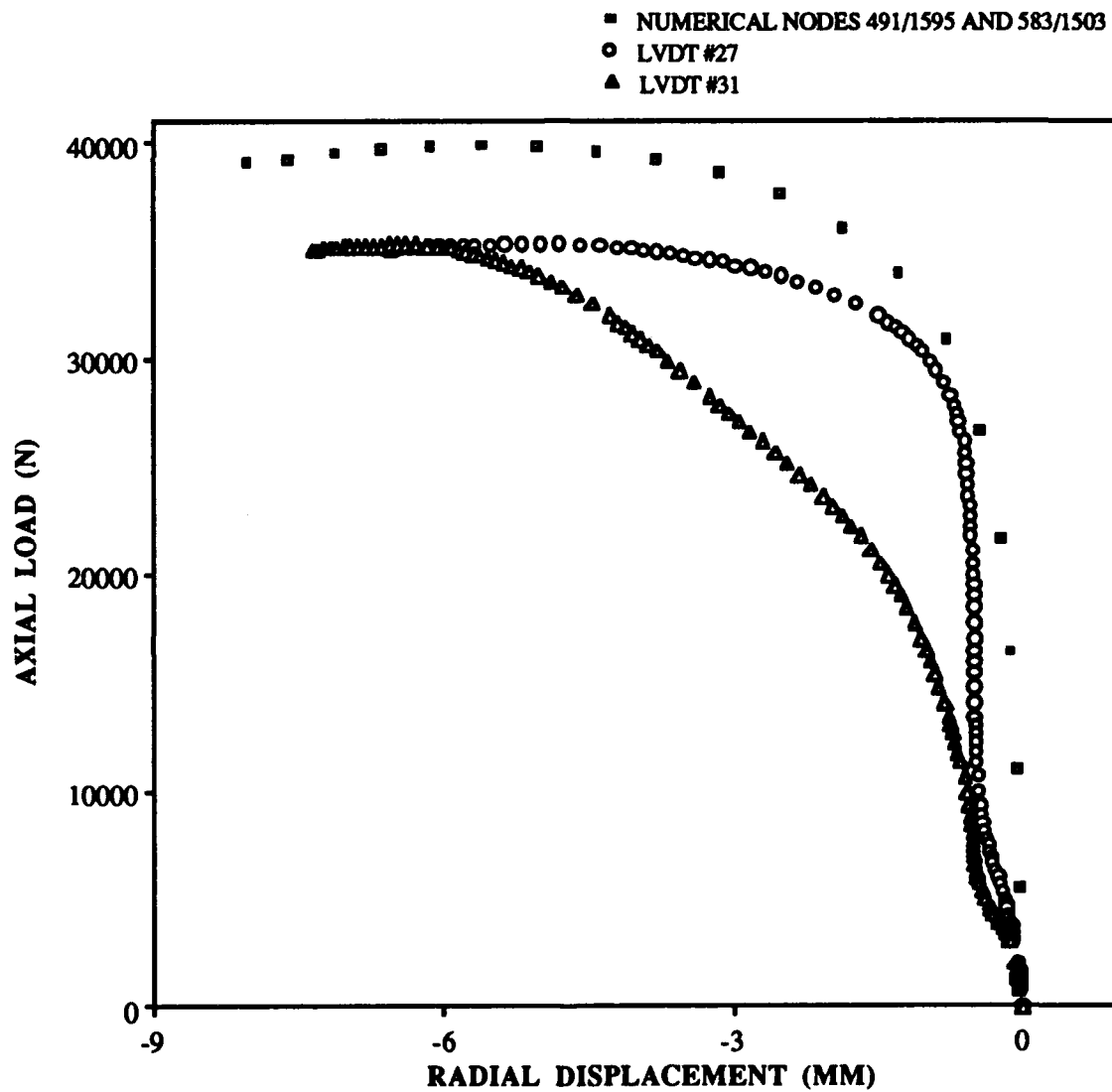304.8 mm x 508 mm (12" x 20") Panel,
[0/45/-45/90]2s
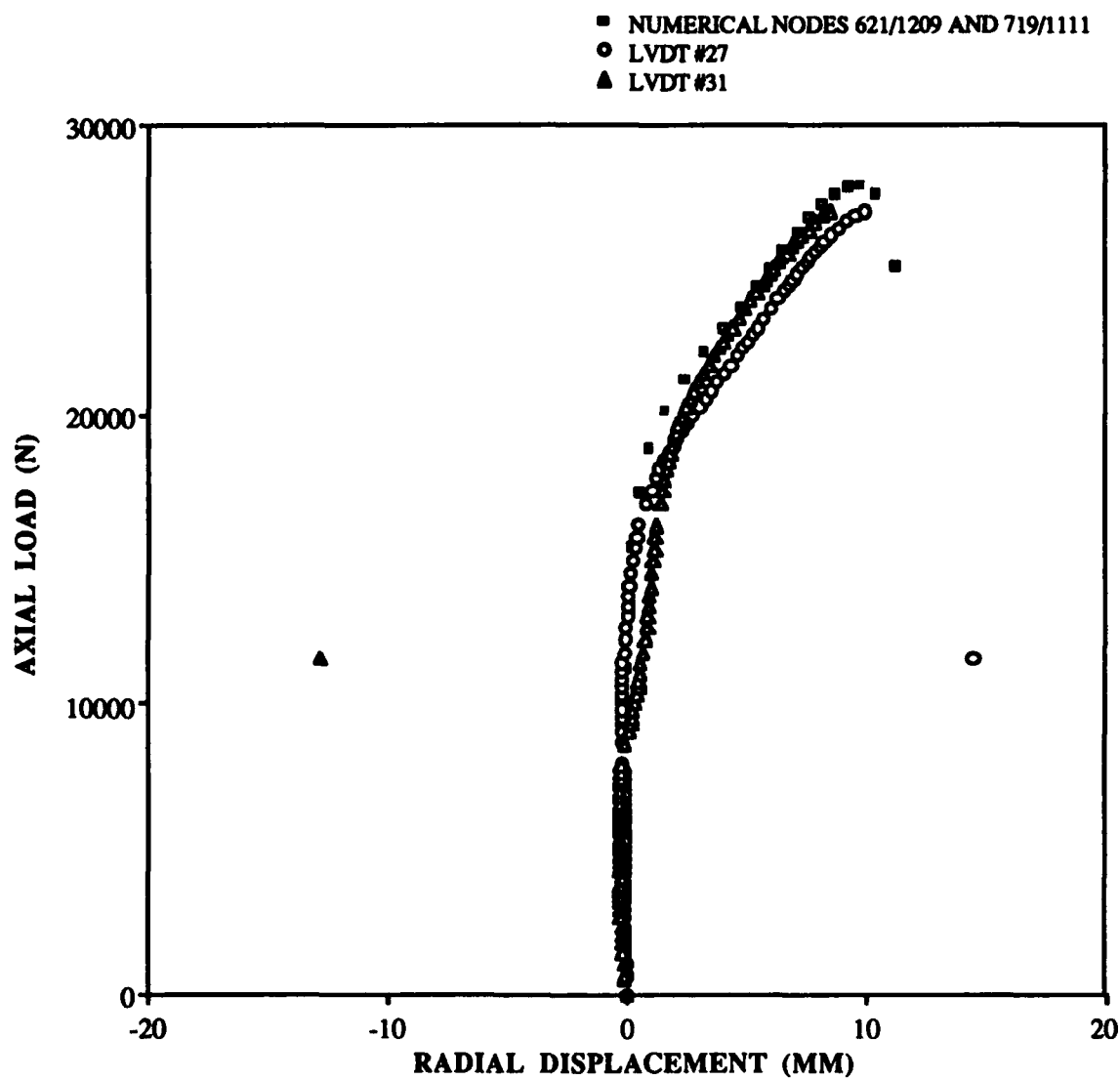
Fig. 60: Load vs. Radial Displacement,
Numerical Compared to Experiment #98,
50.8 mm x 203.2 mm (2" x 8") Cutout,
304.8 mm x 508 mm (12" x 20") Panel,
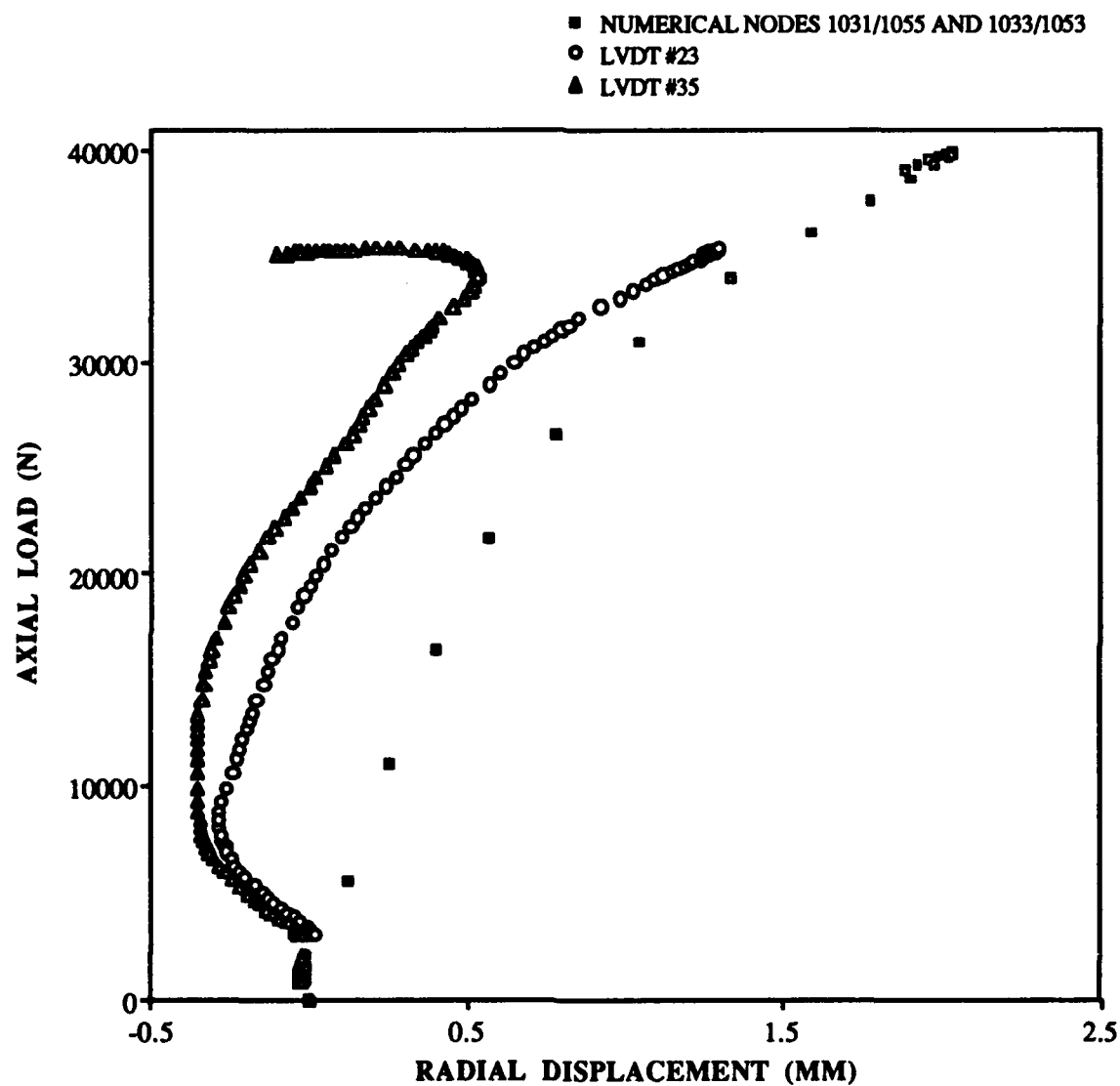[0/45/-45/90]2s
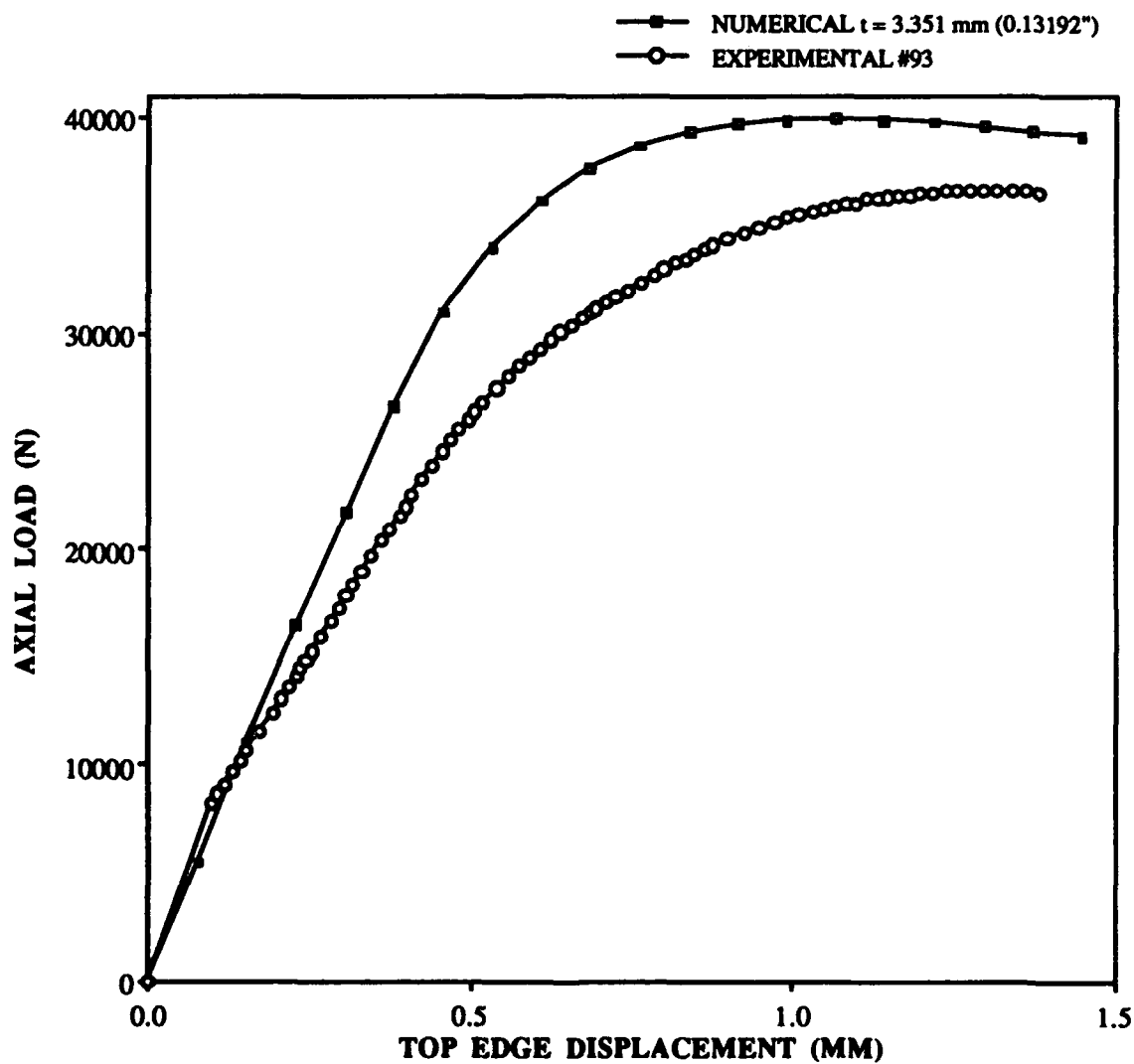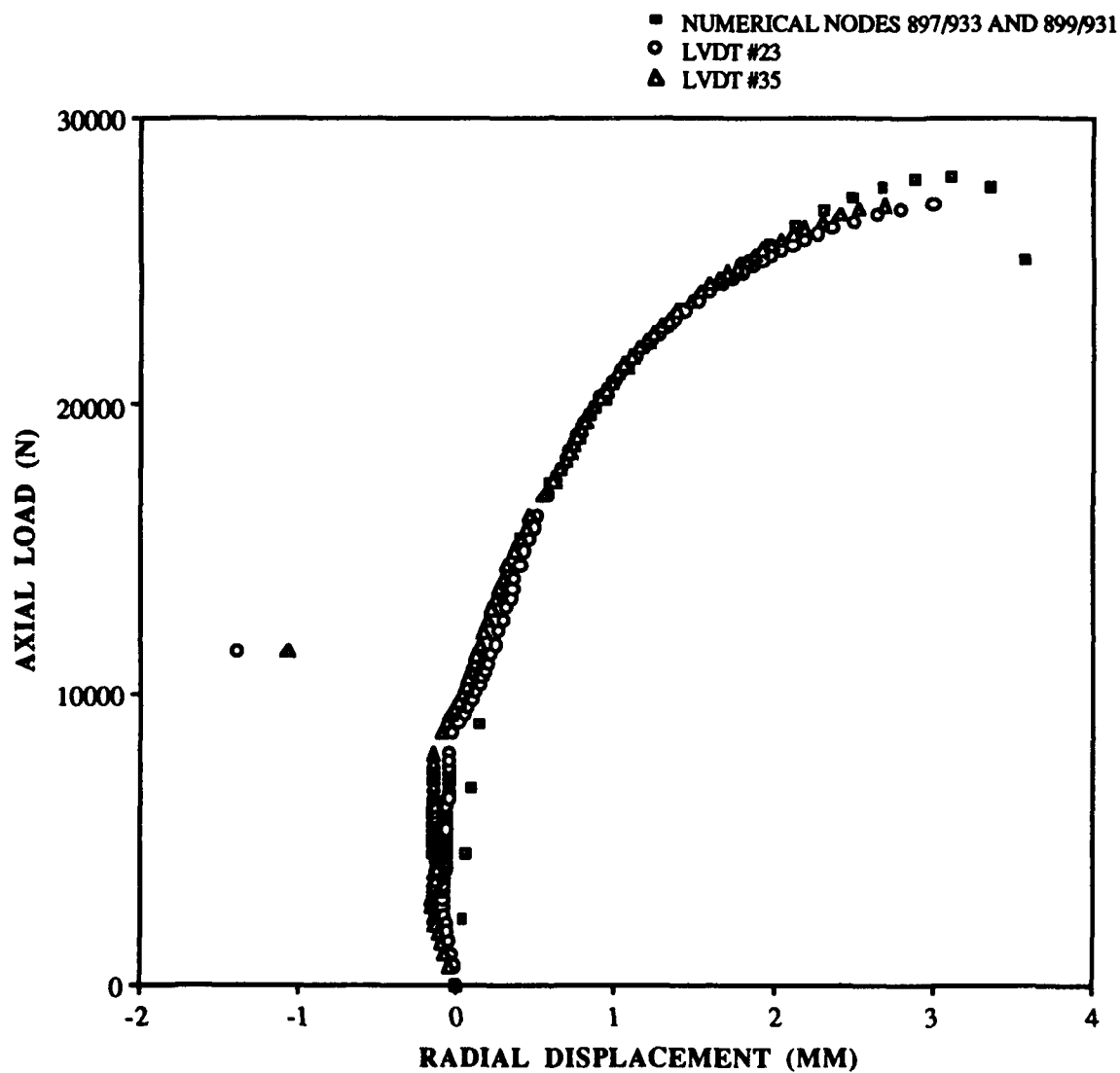
Fig. 61: Load vs. Radial Displacement,
Numerical Compared to Experiment #98,
50.8 mm x 203.2 mm (2" x 8") Cutout,
304.8 mm x 508 mm (12" x 20") Panel,
[0/45/-45/90]2s
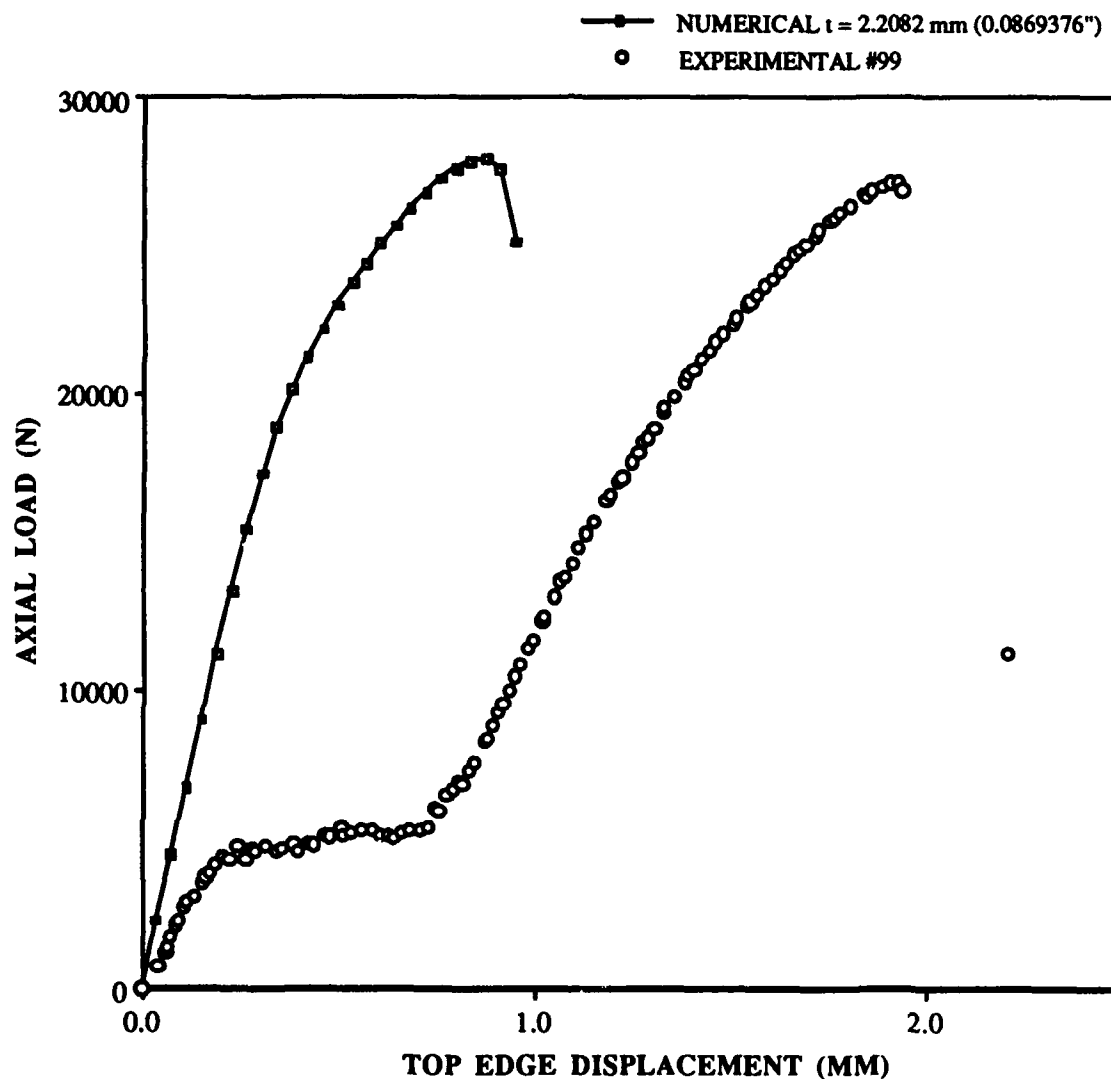
Fig. 62: Load vs. Top Edge Displacement,
Example of Panel Shift in Test Fixture,
50.8 mm x 203.2 mm (2" x 8") Cutout,
304.8 mm x 508 mm (12" x 20") Panel,
[0/45/-45/90]2s
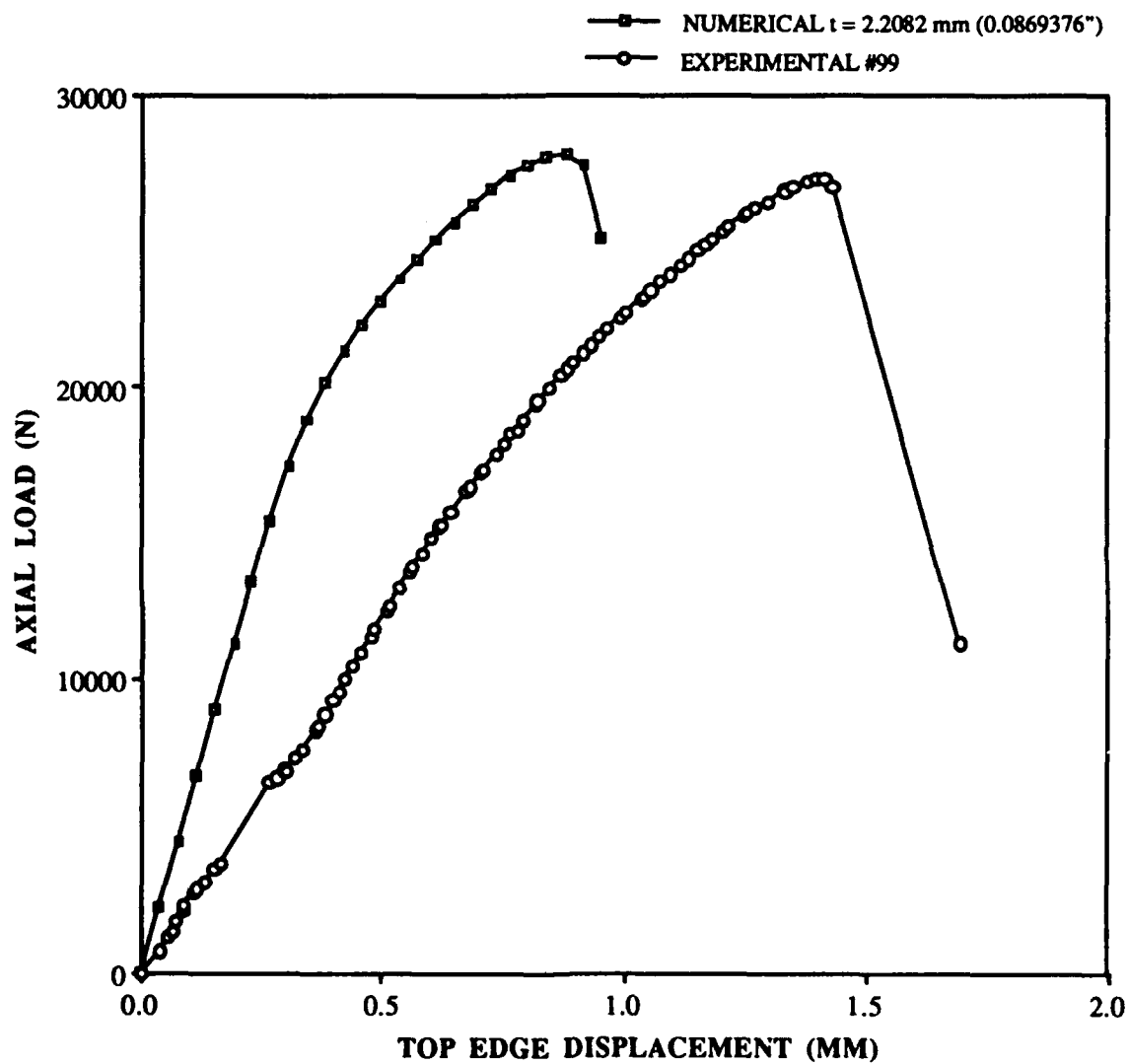
Fig. 63: Load vs. Top Edge Displacement,
Numerical Compared to Experiment #99,
50.8 mm x 203.2 mm (2" x 8") Cutout,
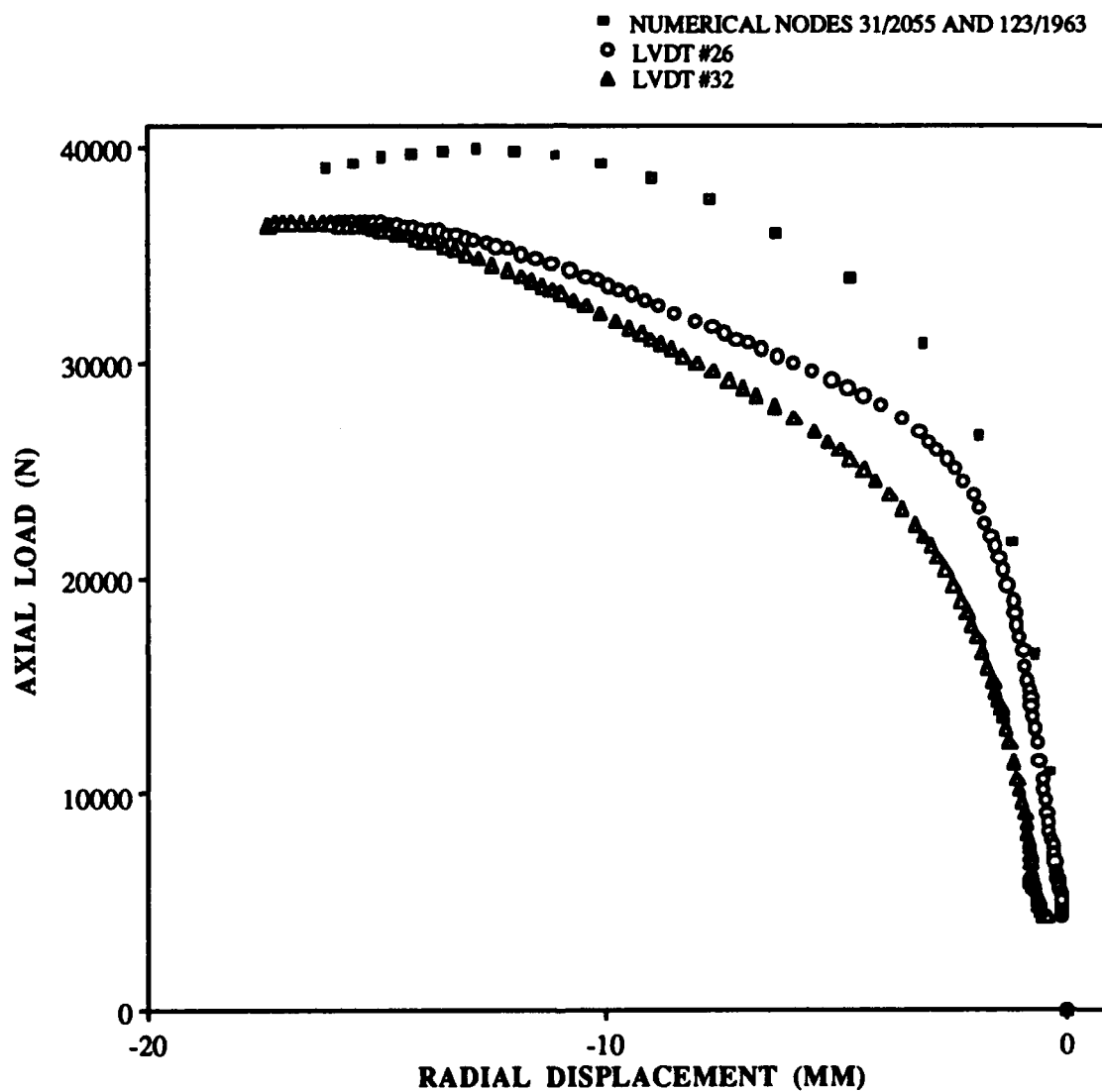304.8 mm x 508 mm (12" x 20") Panel,
[0/45/-45/90]2s

142
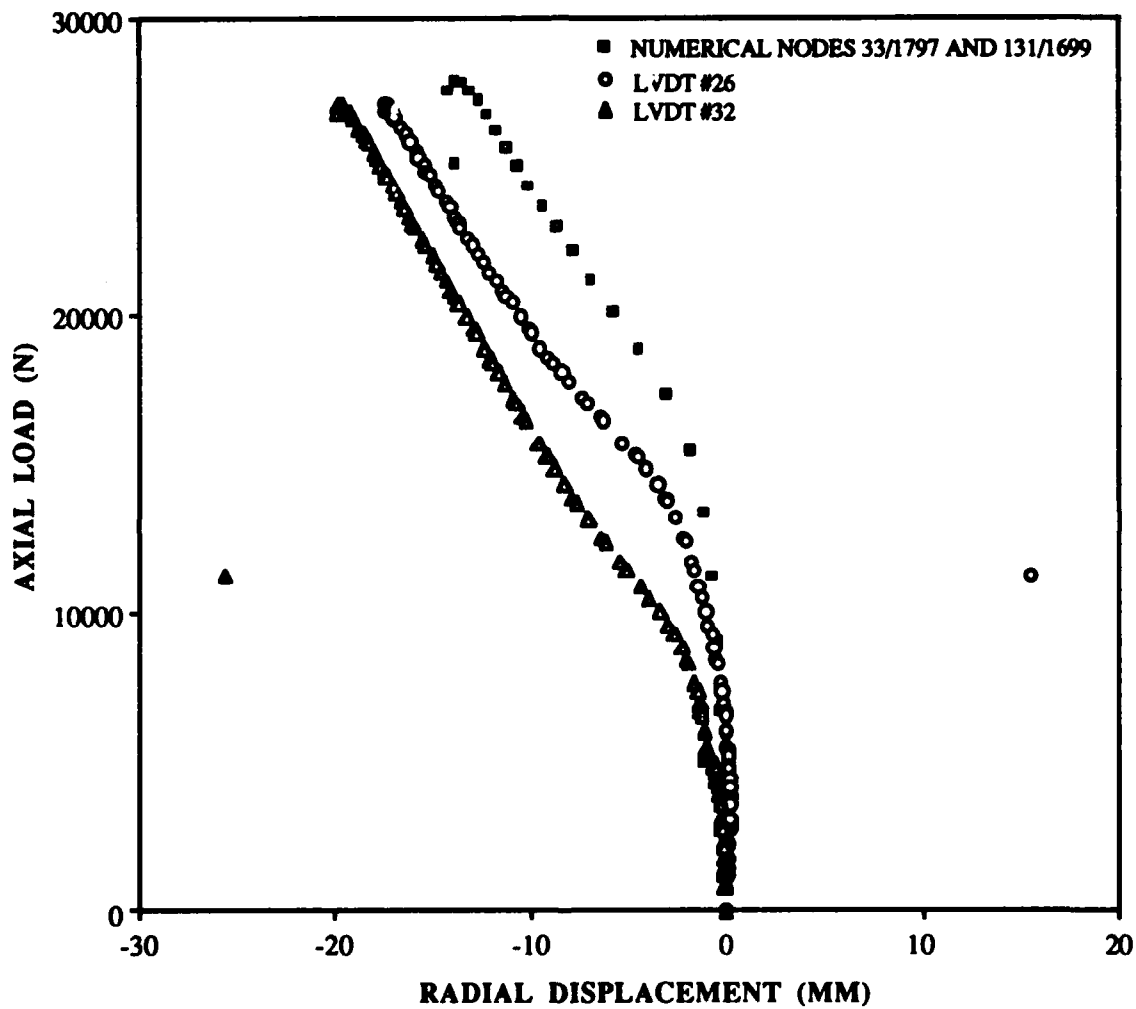
Fig. 64: Load vs. Radial Displacement,
Numerical Compared to Experiment #99,
50.8 mm x 203.2 mm (2" x 8") Cutout,
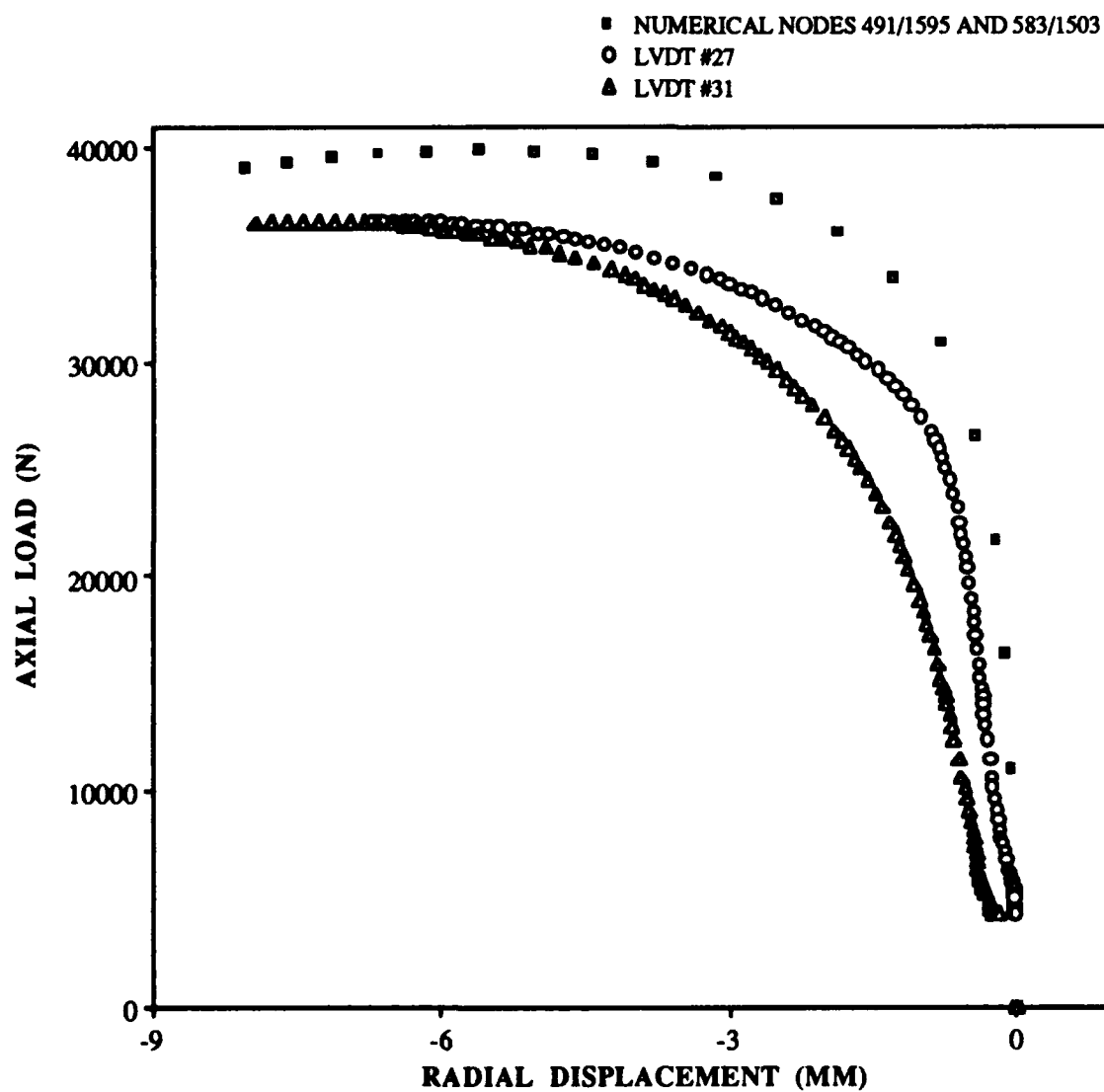304.8 mm x 508 mm (12" x 20") Panel,
[0/45/-45/90]2s

143
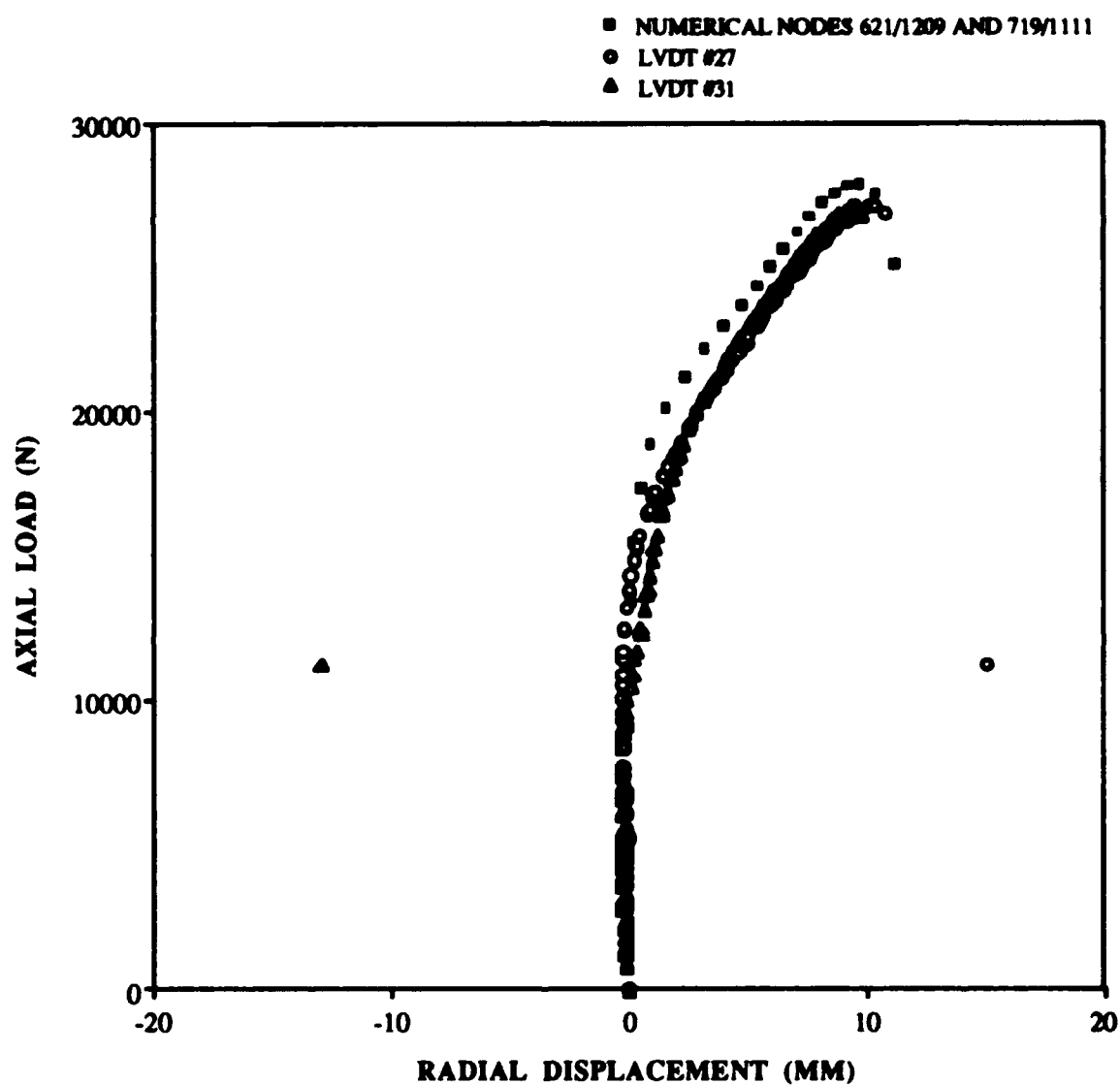
Fig. 65: Load vs. Radial Displacement,
Numerical Compared to Experiment #99,
50.8 mm x 203.2 mm (2" x 8") Cutout,
304.8 mm x 508 mm (12" x 20") Panel,
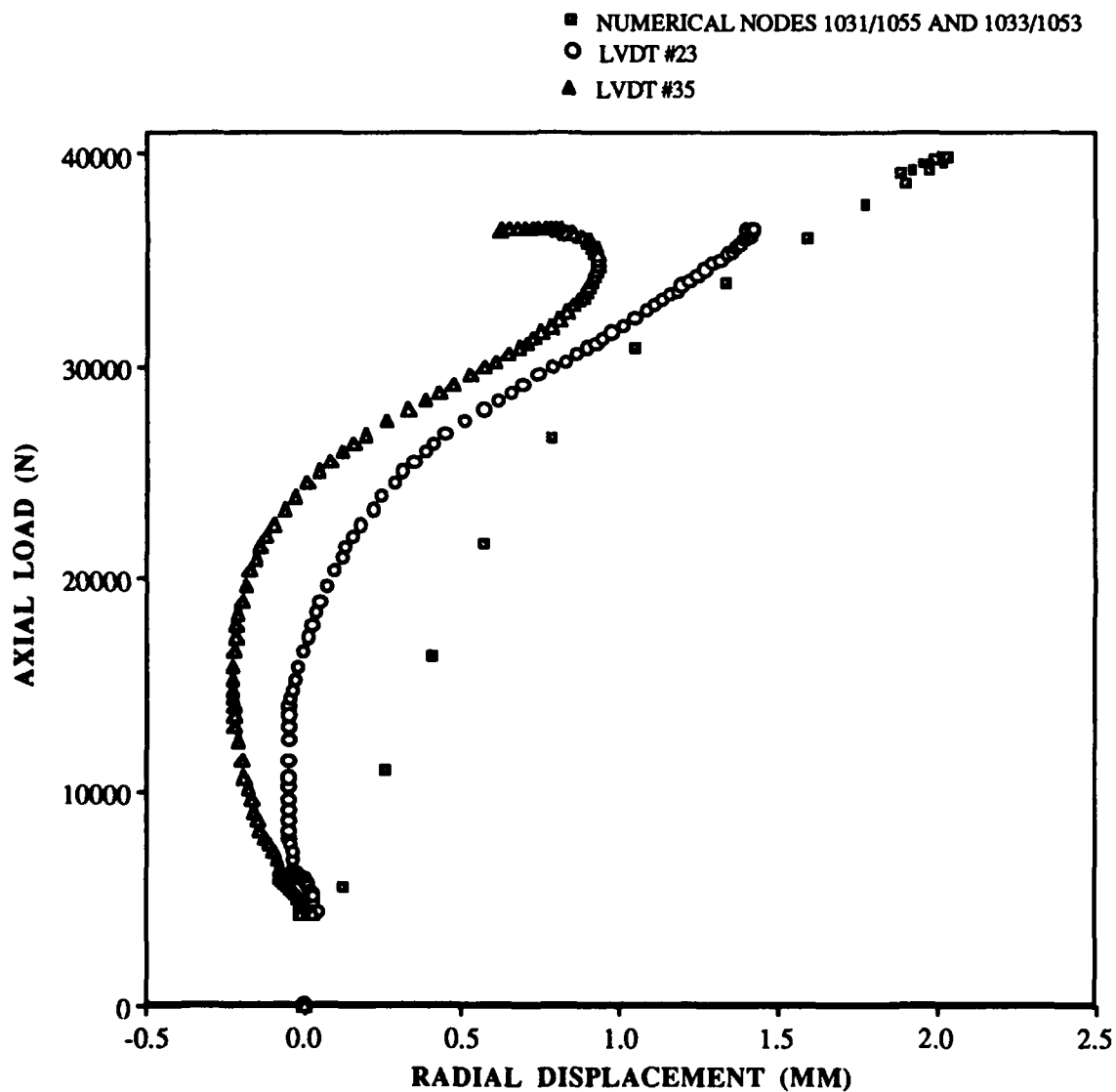[0/45/-45/90]2s
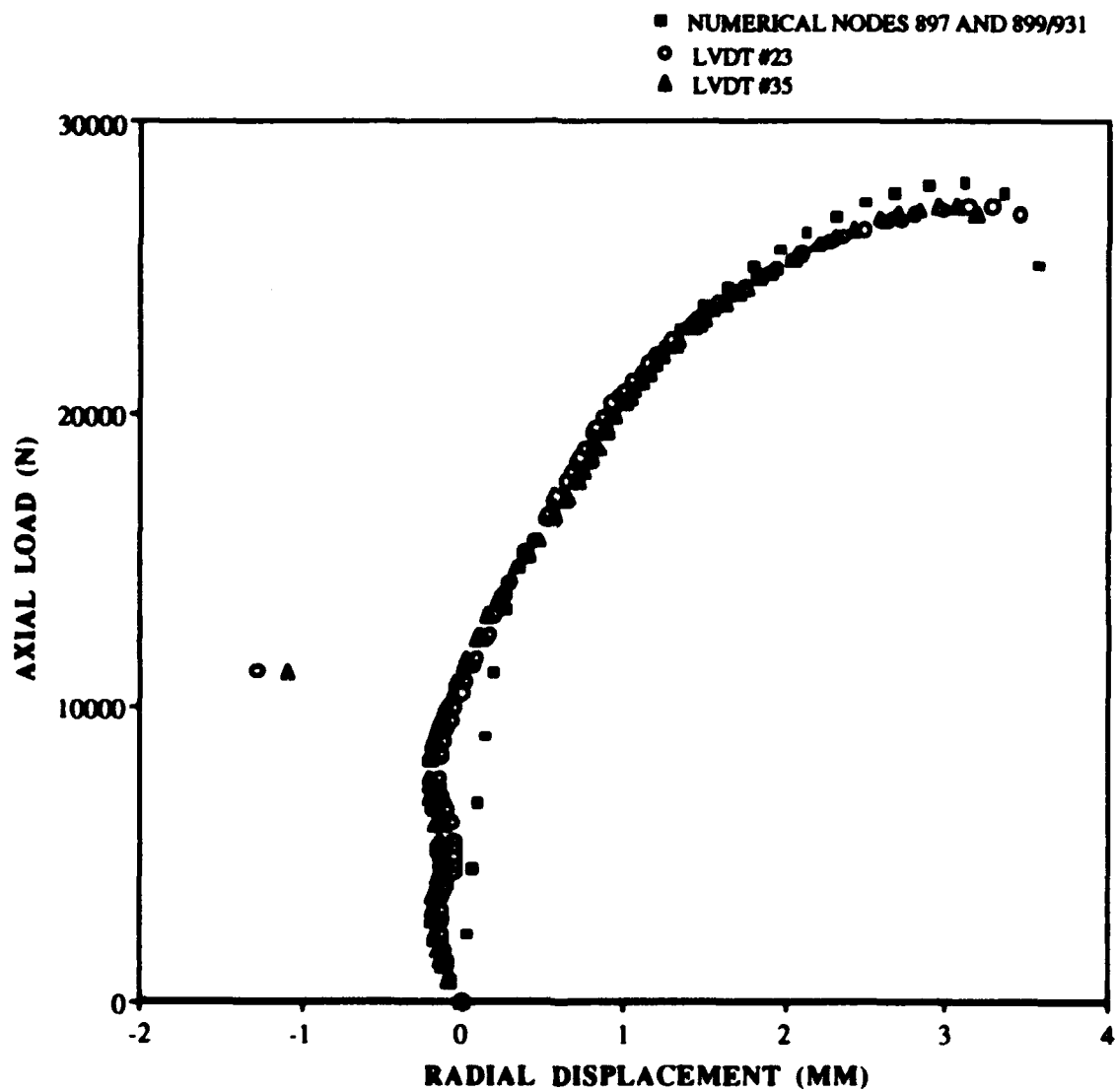
Fig. 66: Load vs. Radial Displacement.
Numerical Compared to Experiment #99,
50.8 mm x 203.2 mm (2" x 8") Cutout,
304.8 mm x 508 mm (12" x 20") Panel,
[0/45/-45/90]2s
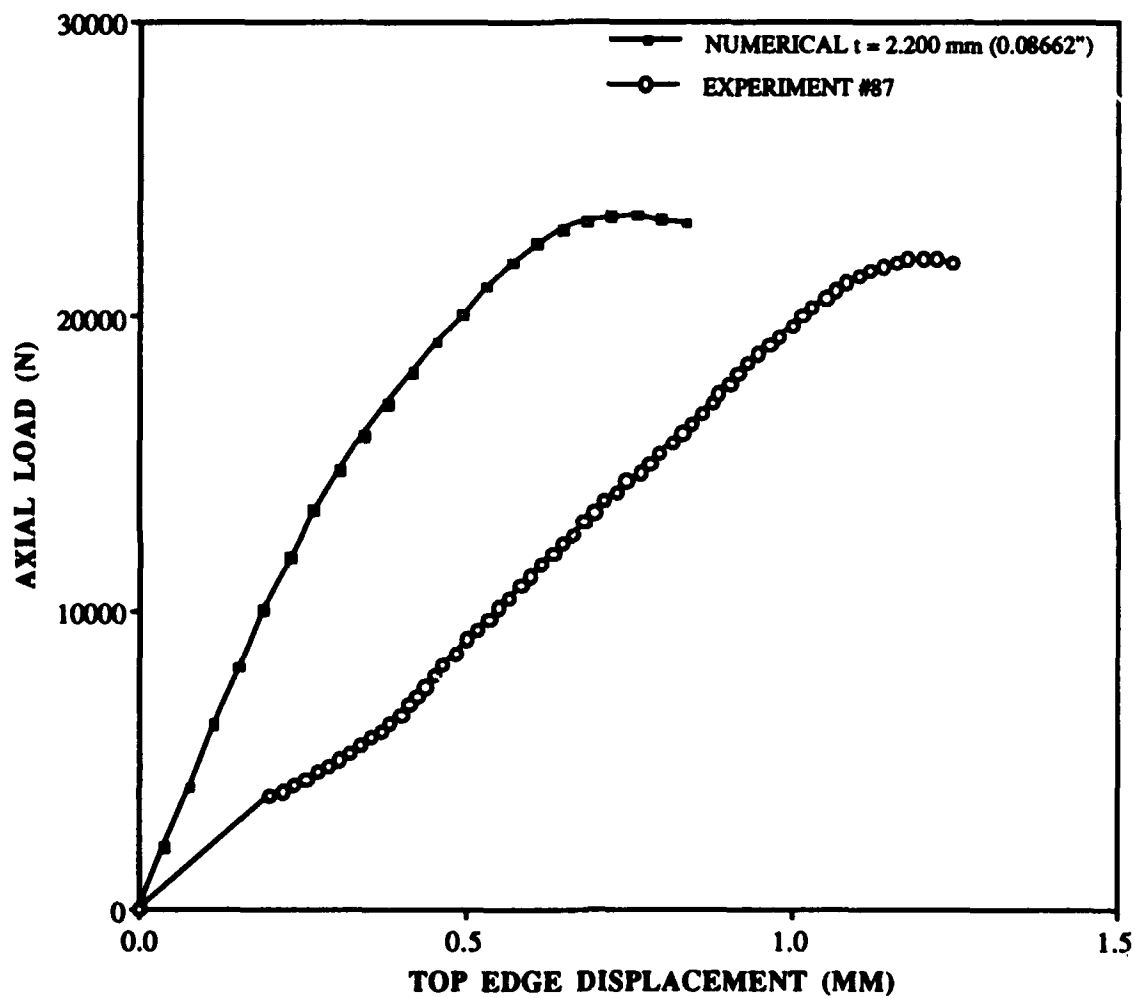
Fig. 67: Load vs. Top Edge Displacement, Numerical Compared to Experiment #87, 101.6 mm x 101.6 mm (4" x 4") Cutout, 304.8 mm x 508 mm (12" x 20") Panel, [0/45/-45/90]2s
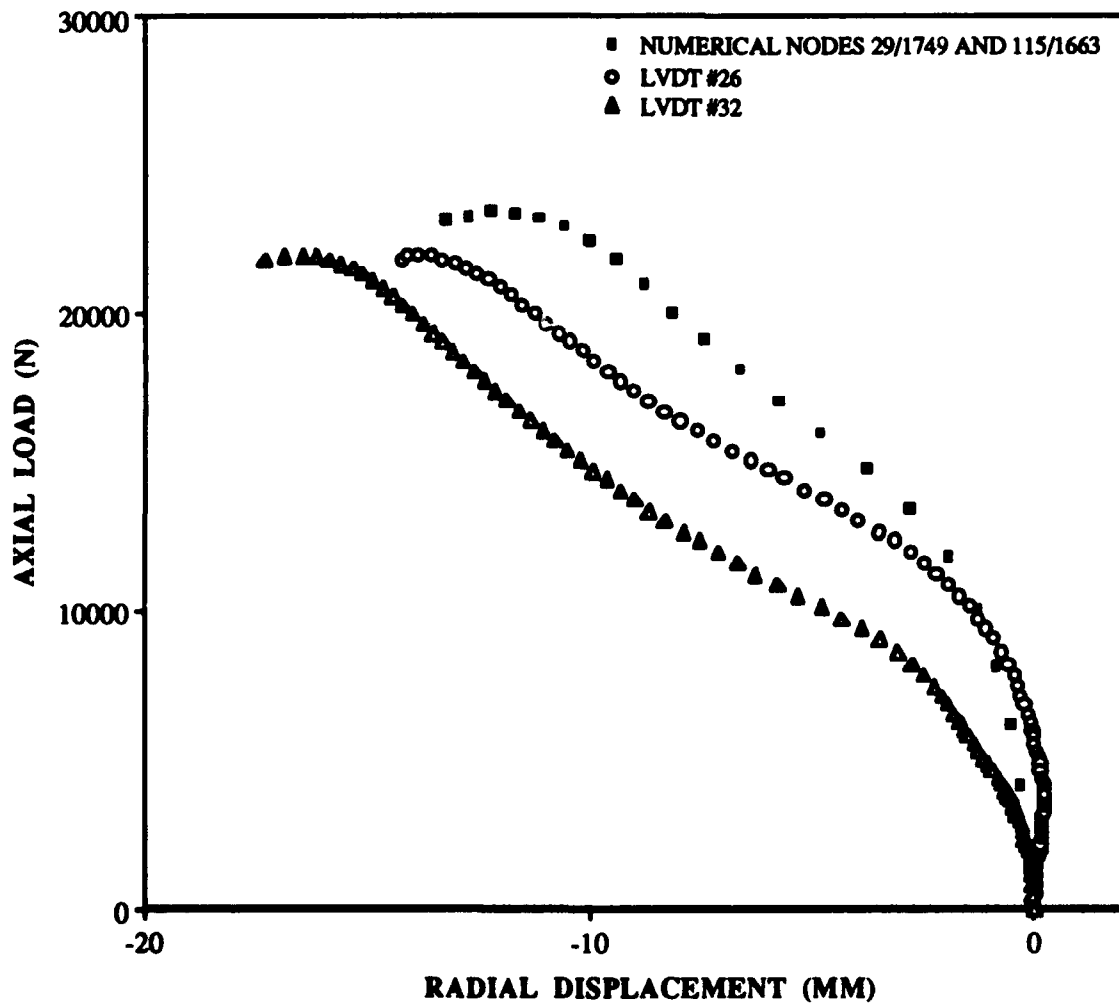
Fig. 68: Load vs. Radial Displacement,
Numerical Compared to Experiment #87,
101.6 mm x 101.6 mm (4" x 4") Cutout,
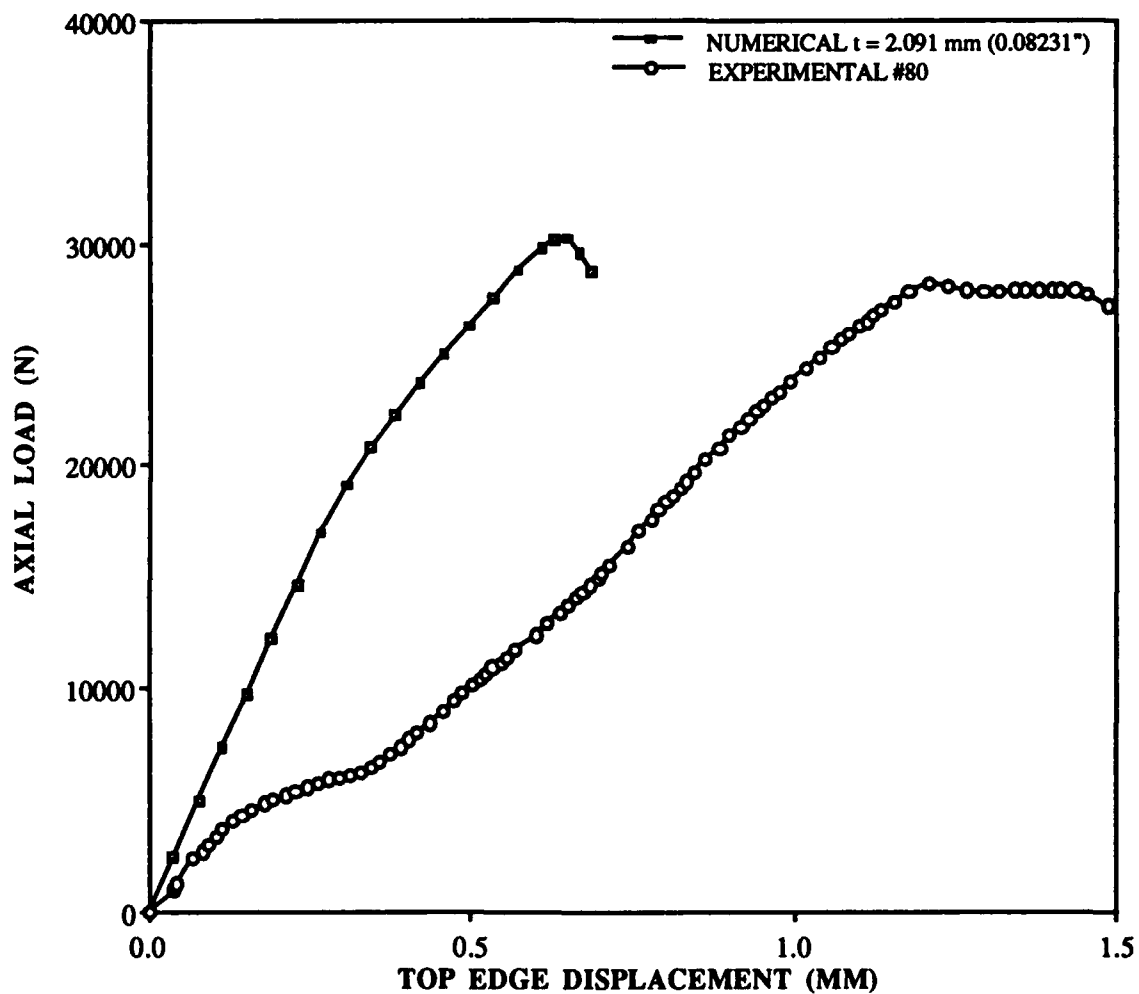304.8 mm x 508 mm (12" x 20") Panel,
[0/45/-45/90]2s
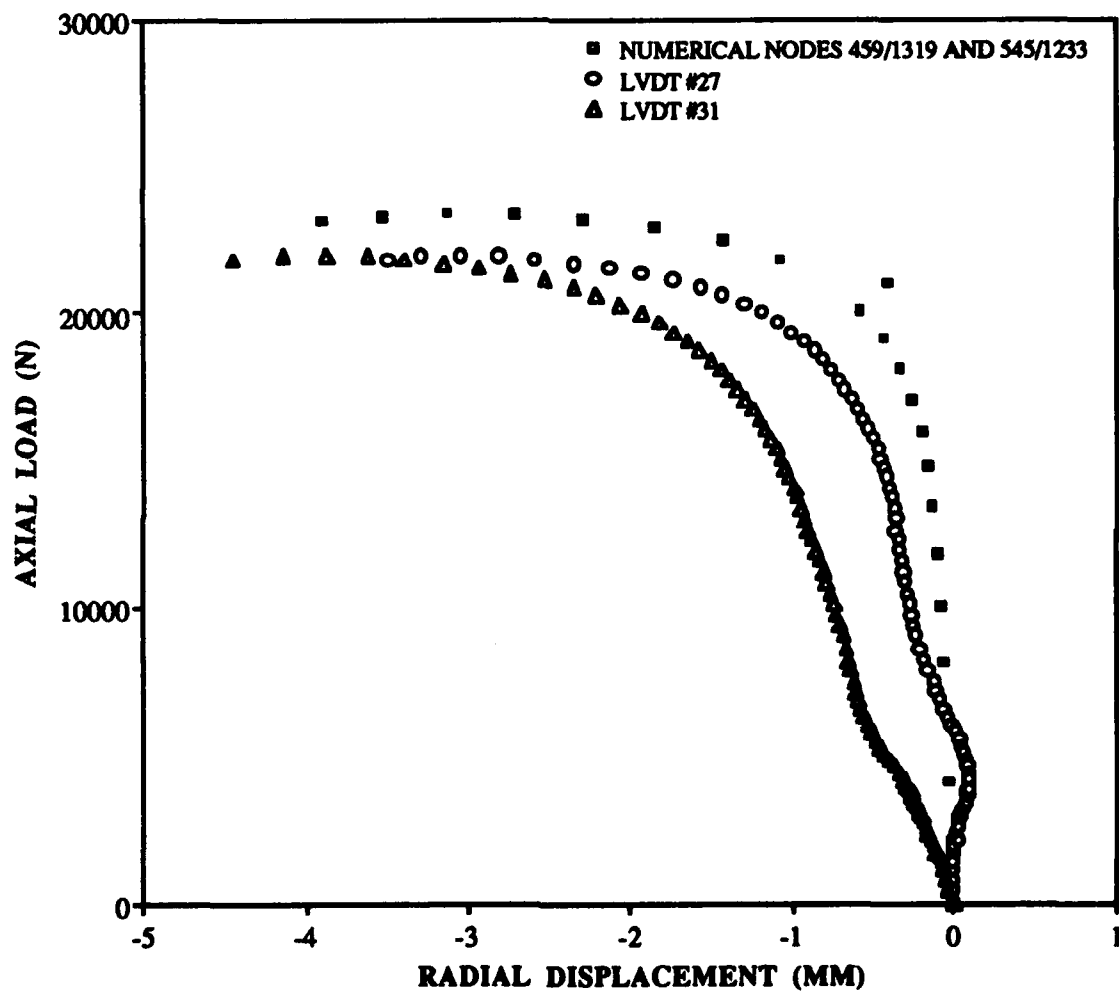
Fig. 69: Load vs. Radial Displacement,
Numerical Compared to Experiment #87,
101.6 mm x 101.6 mm (4" x 4") Cutout,
304.8 mm x 508 mm (12" x 20") Panel,
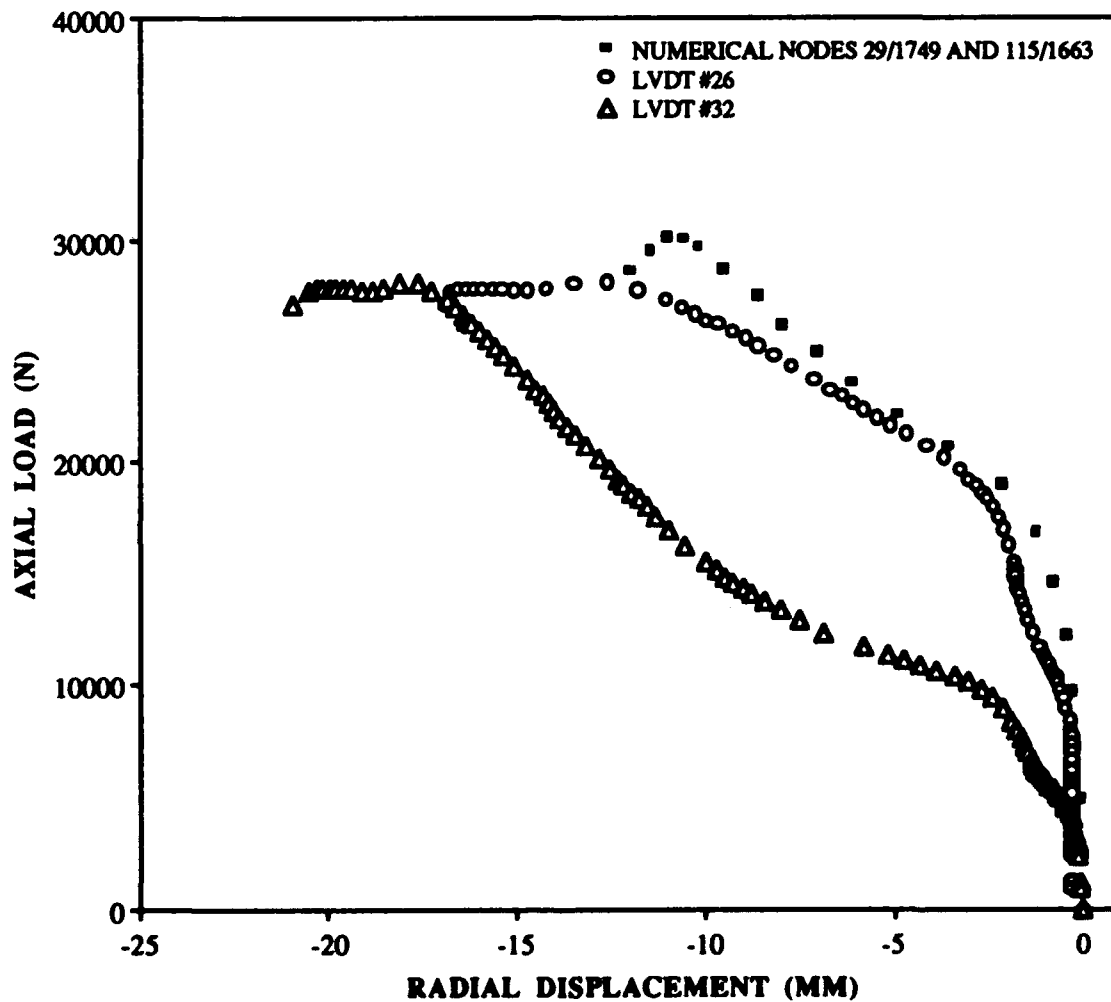[0/45/-45/90]2s
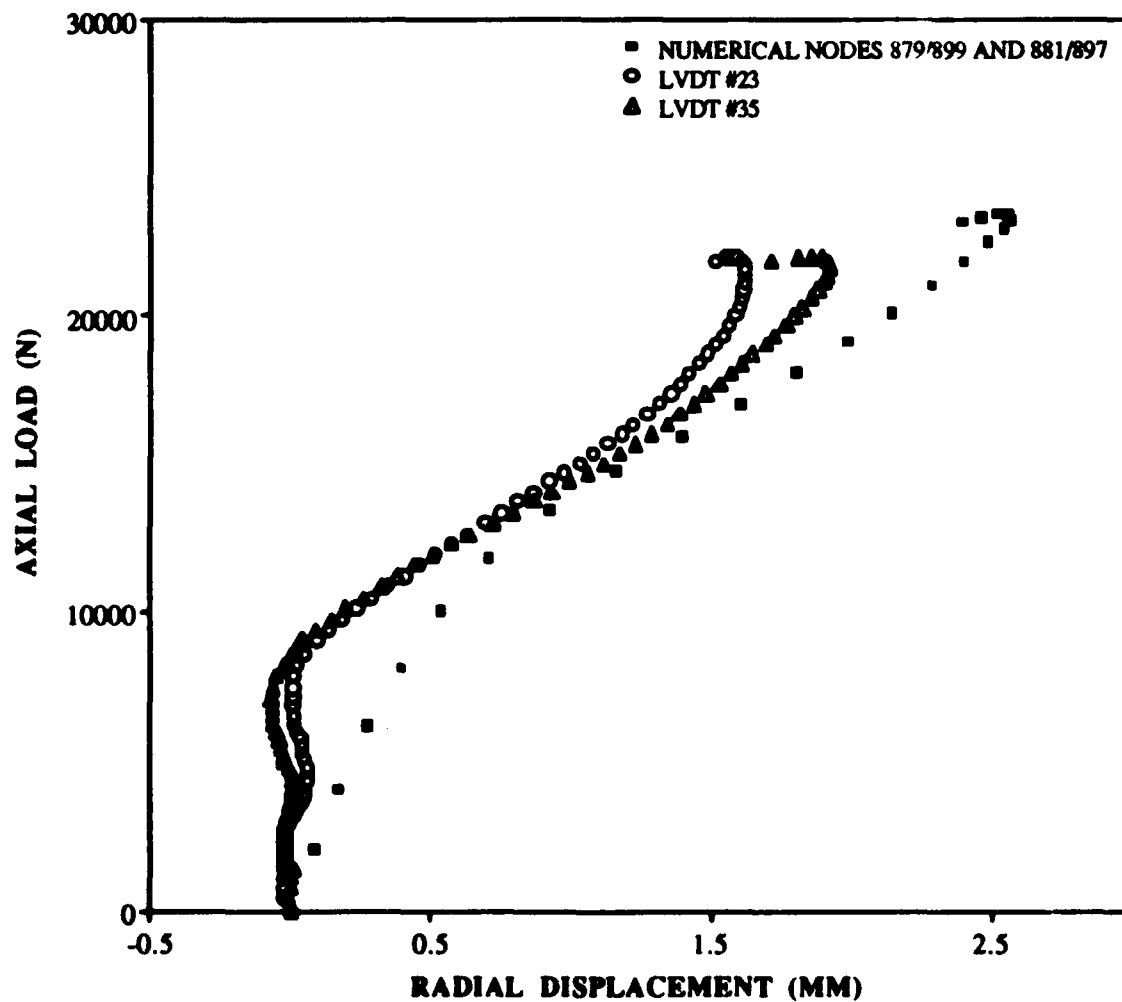
Fig. 70: Load vs. Radial Displacement,
Numerical Compared to Experiment #87,
101.6 mm x 101.6 mm (4" x 4") Cutout,
304.8 mm x 508 mm (12" x 20") Panel,
[0/45/-45/90]2s

149
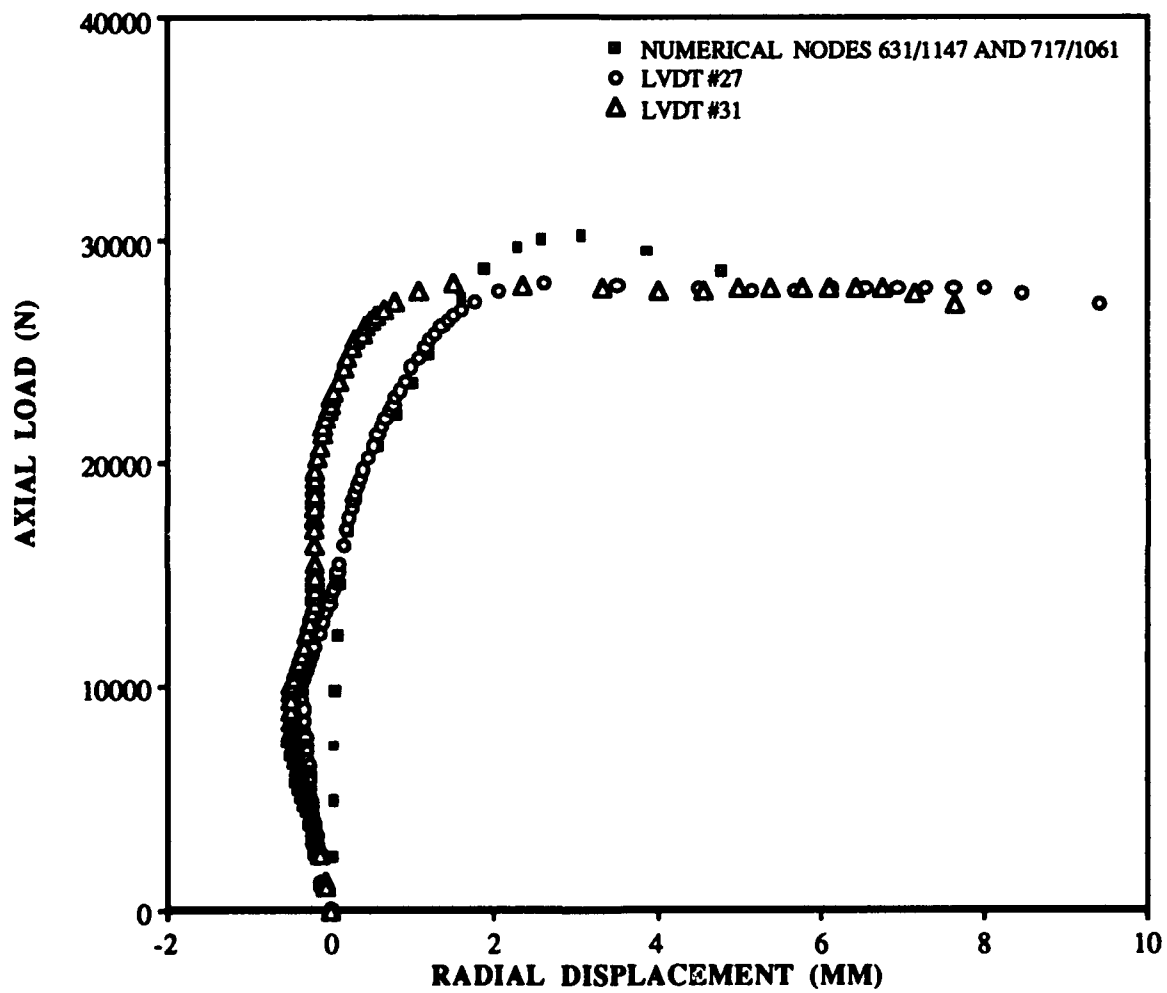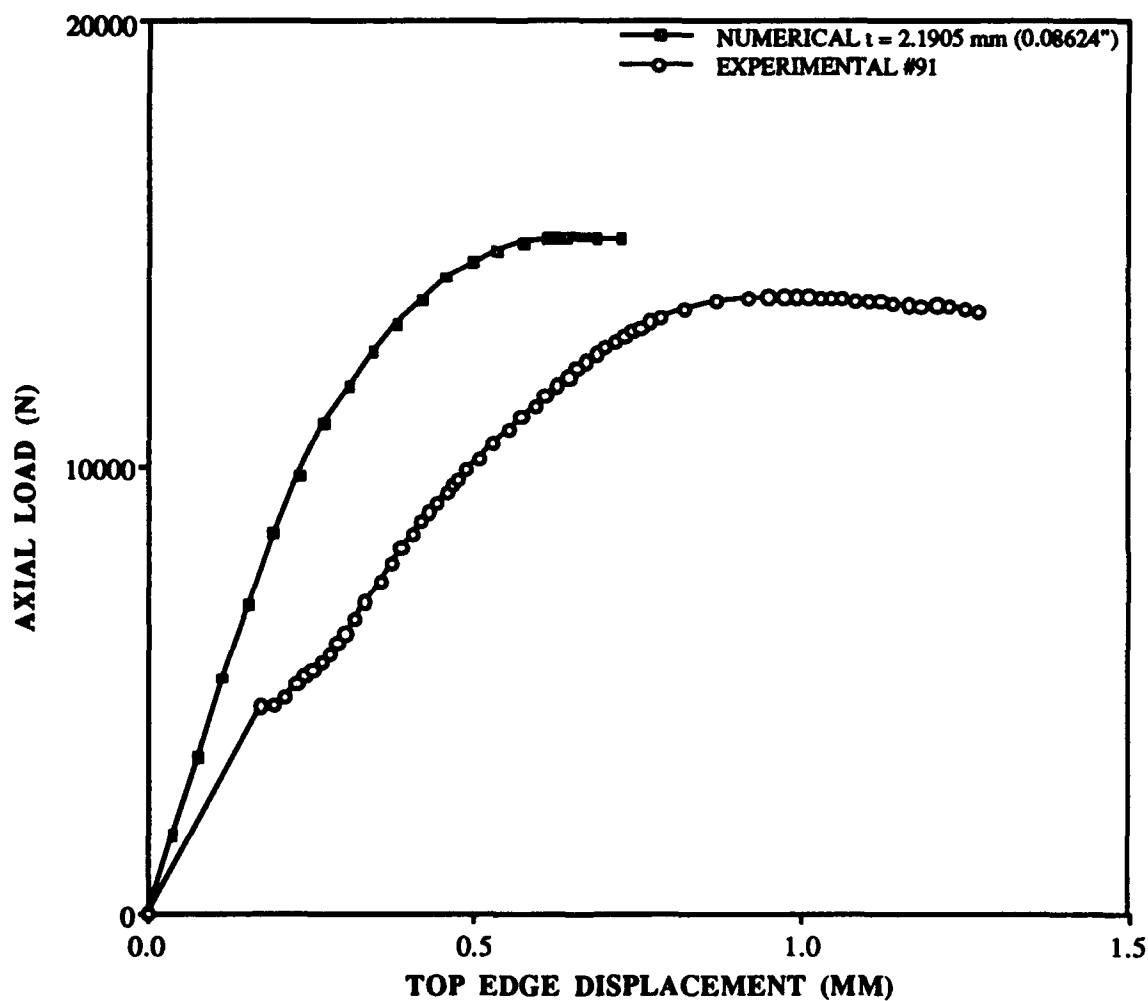
Fig. 71: Load vs. Top Edge Displacement,
Numerical Compared to Experiment #91,
127 mm x 127 mm (5" x 5") Cutout,
304.8 mm x 508 mm (12" x 20") Panel,
[0/45/-45/90]2s
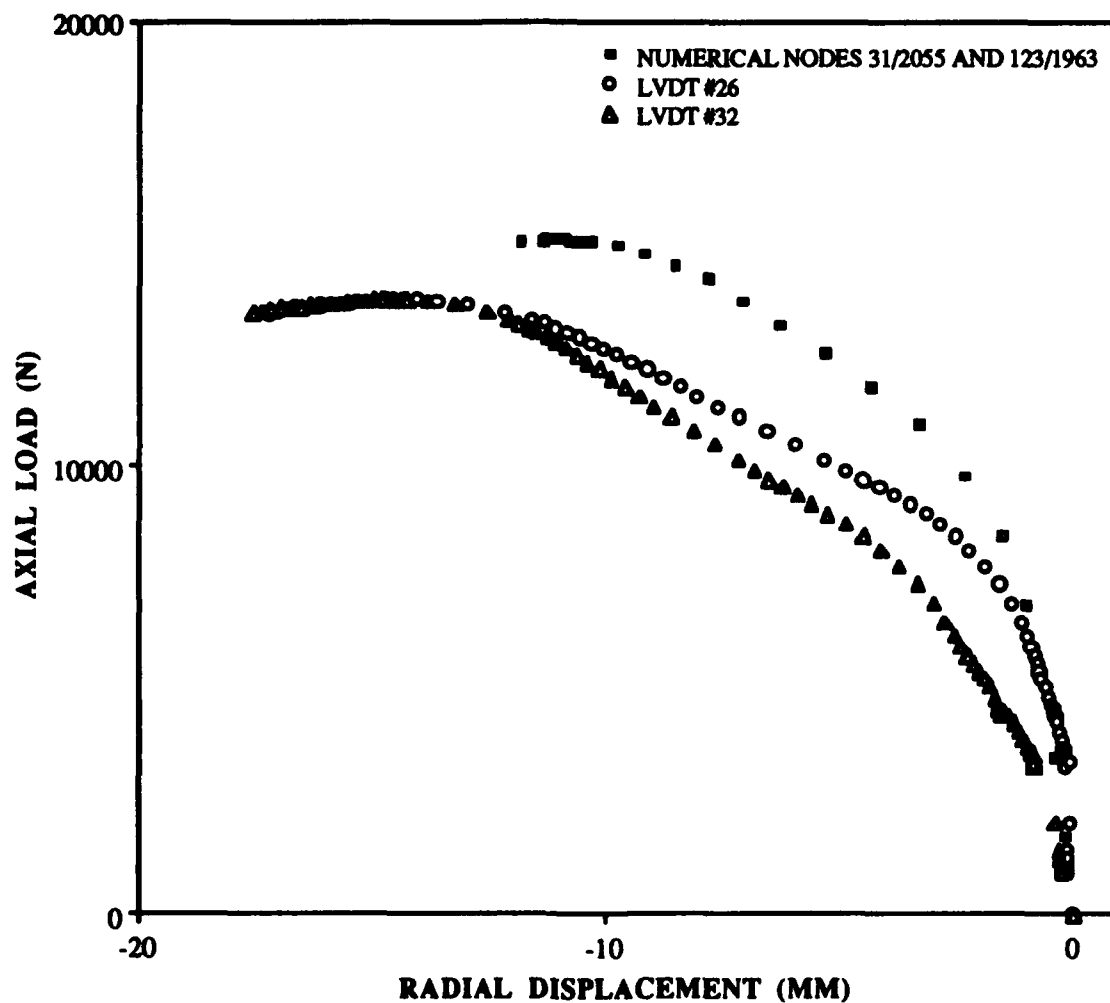
Fig. 72: Load vs. Radial Displacement,
Numerical Compared to Experiment #91,
127 mm x 127 mm (5" x 5") Cutout,
304.8 mm x 508 mm (12" x 20") Panel,
[0/45/-45/90]2s

151
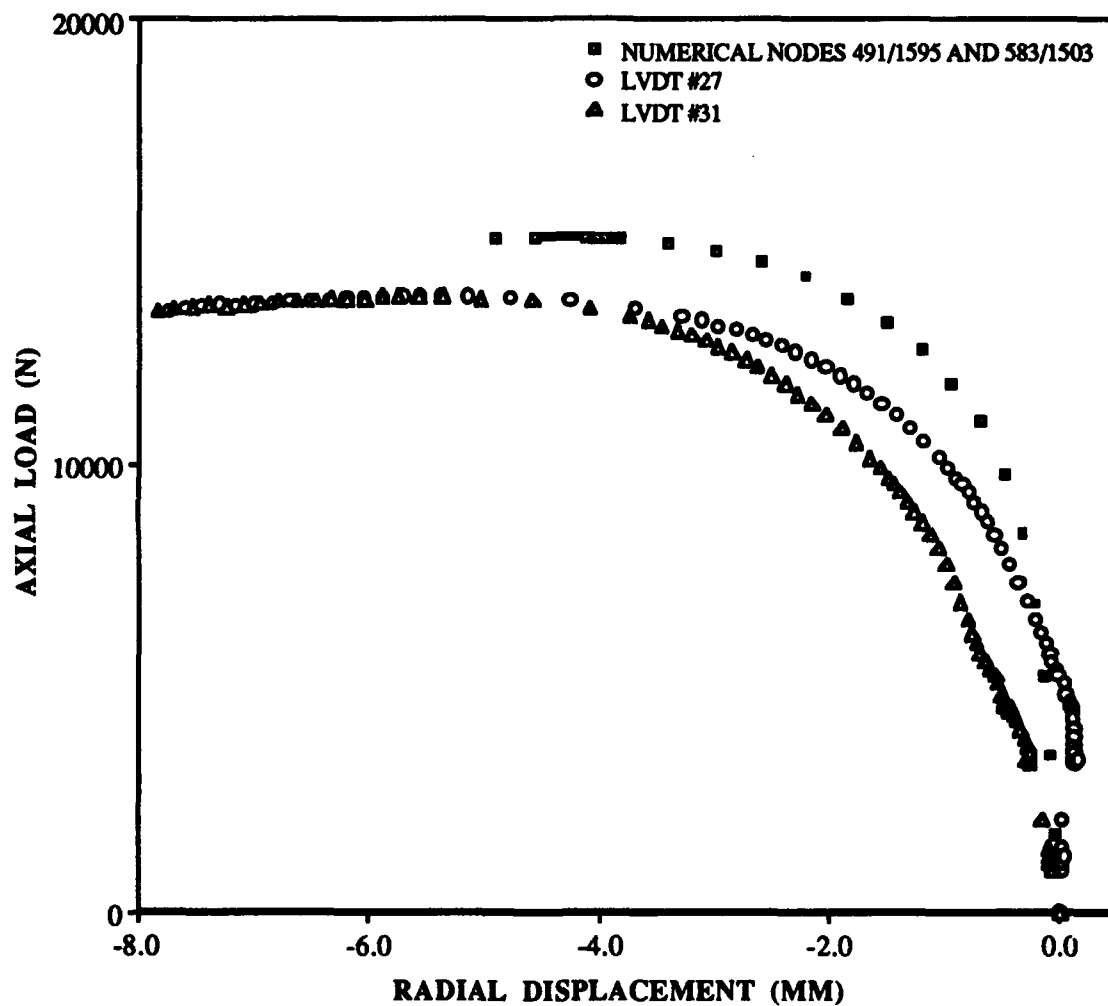
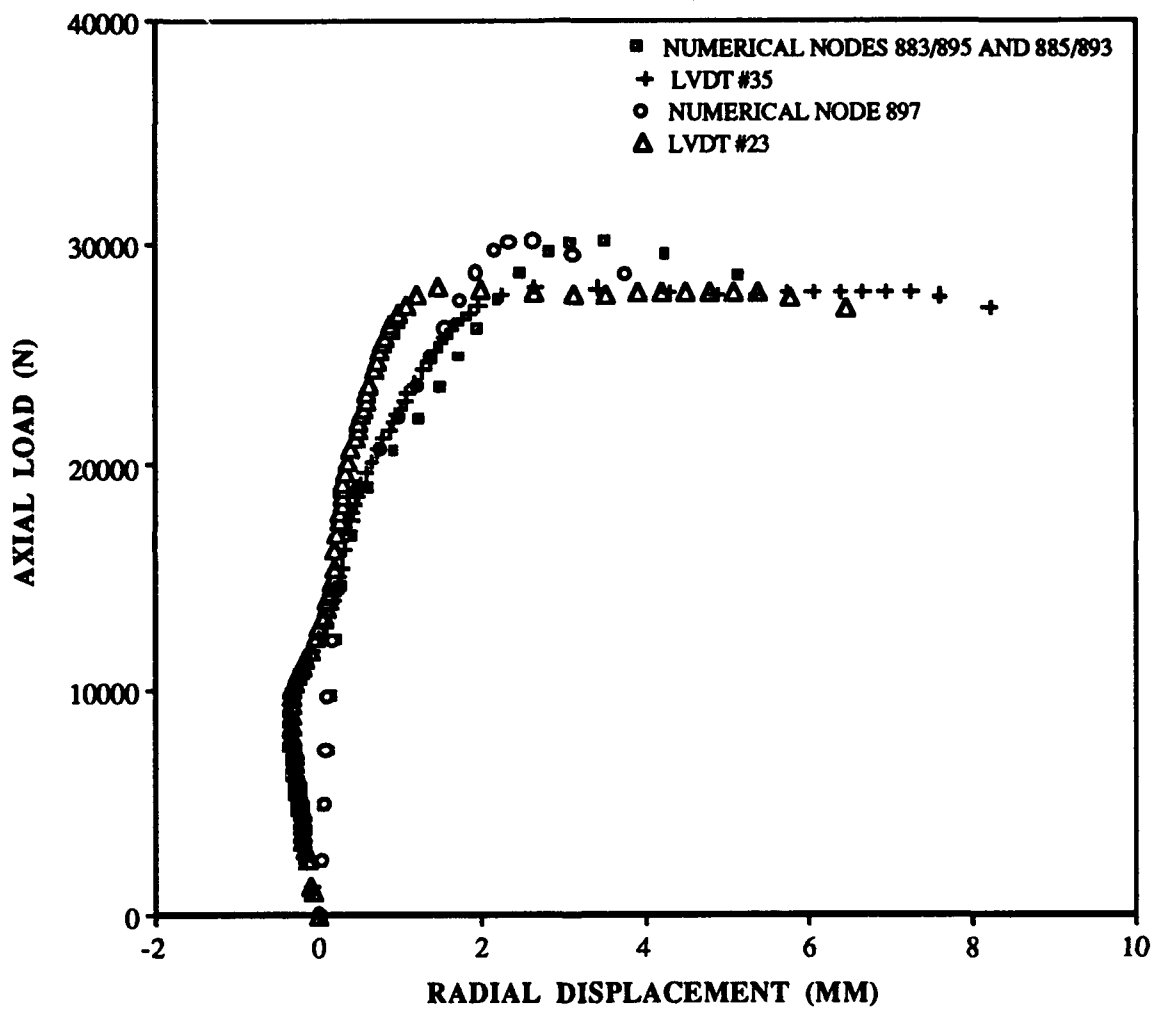Fig. 73: Load vs. Radial Displacement,
Numerical Compared to Experiment #91,
127 mm x 127 mm (5" x 5") Cutout,
304.8 mm x 508 mm (12" x 20") Panel,
[0/45/-45/90]2s

152
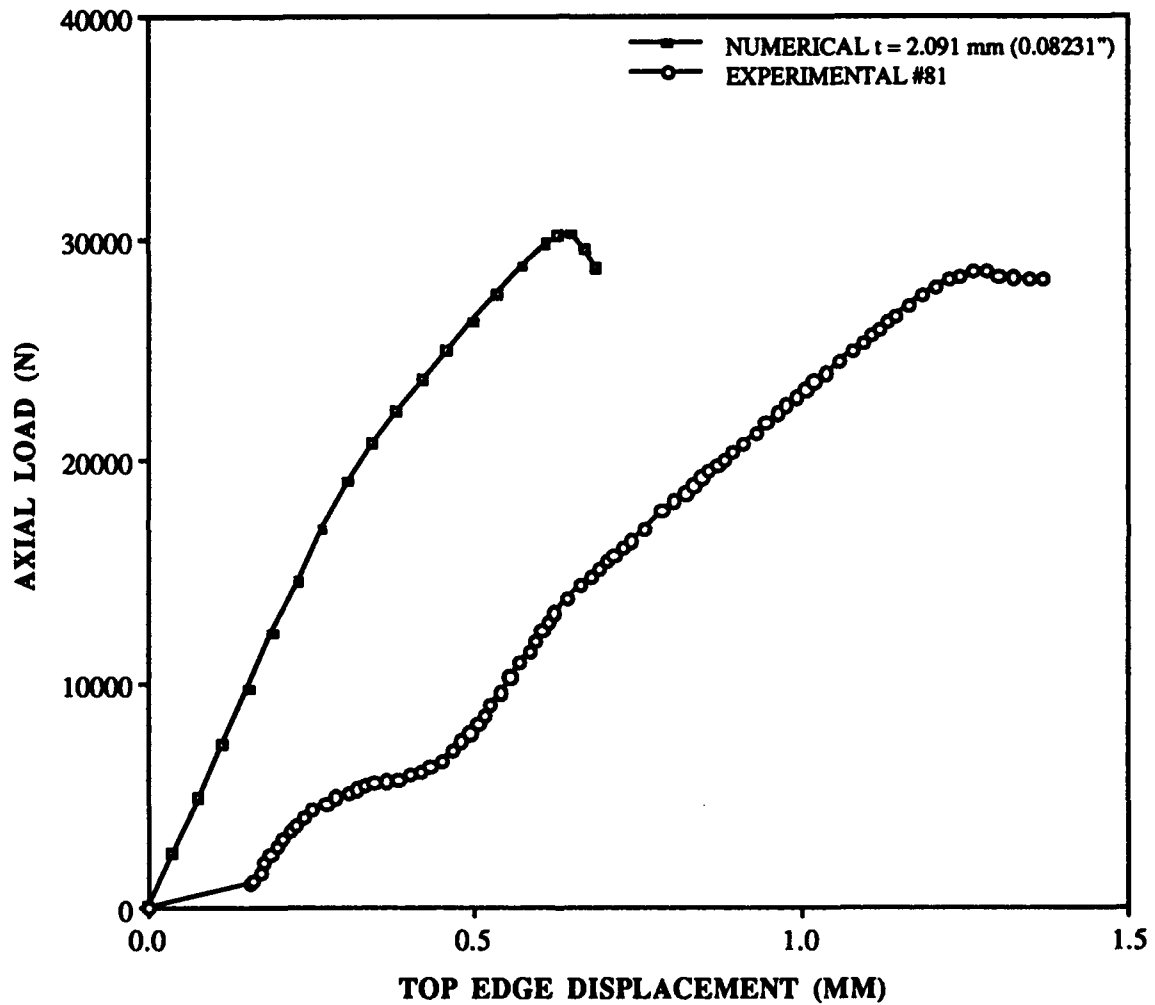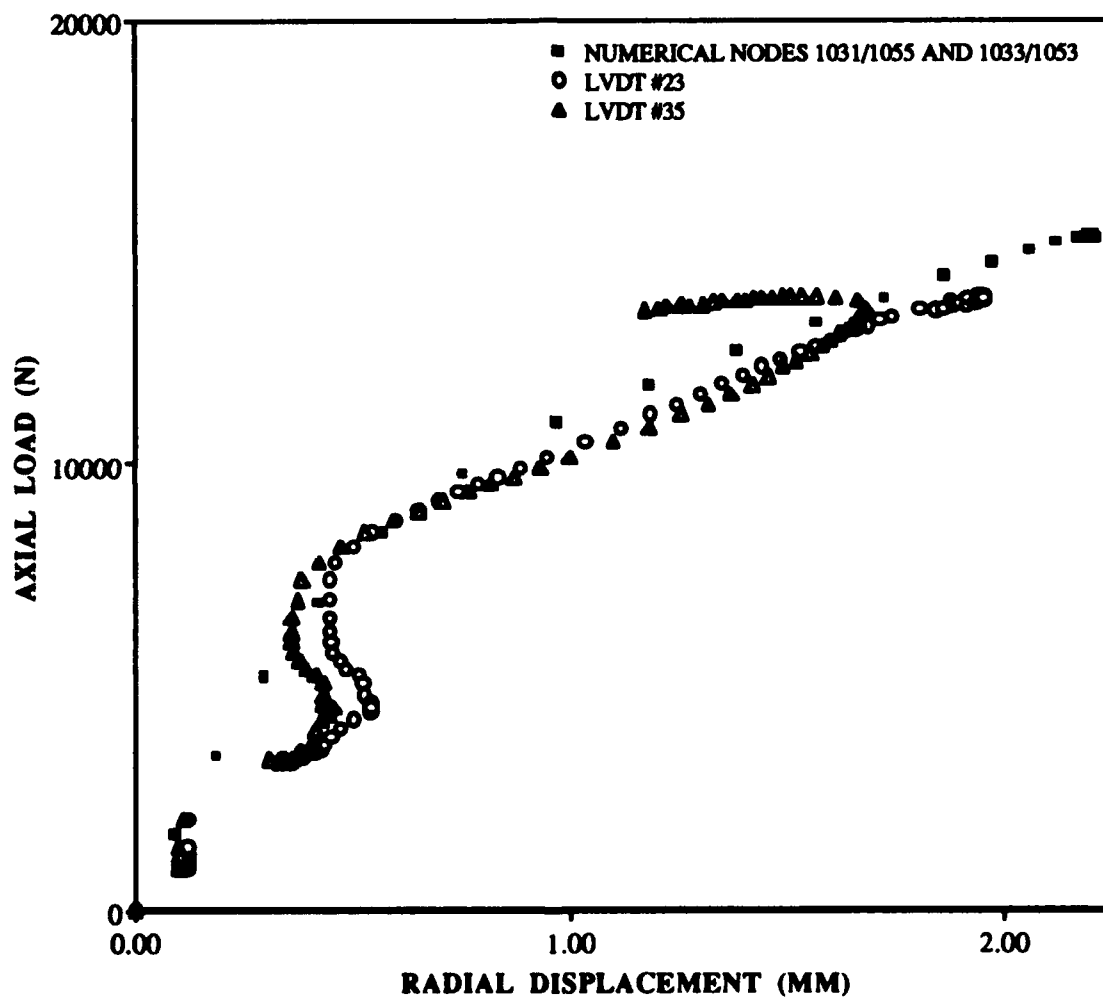
Fig. 74: Load vs. Radial Displacement,
Numerical Compared to Experiment #91,
127 mm x 127 mm (5" x 5") Cutout,
304.8 mm x 508 mm (12" x 20") Panel,
[0/45/-45/90]2s

153
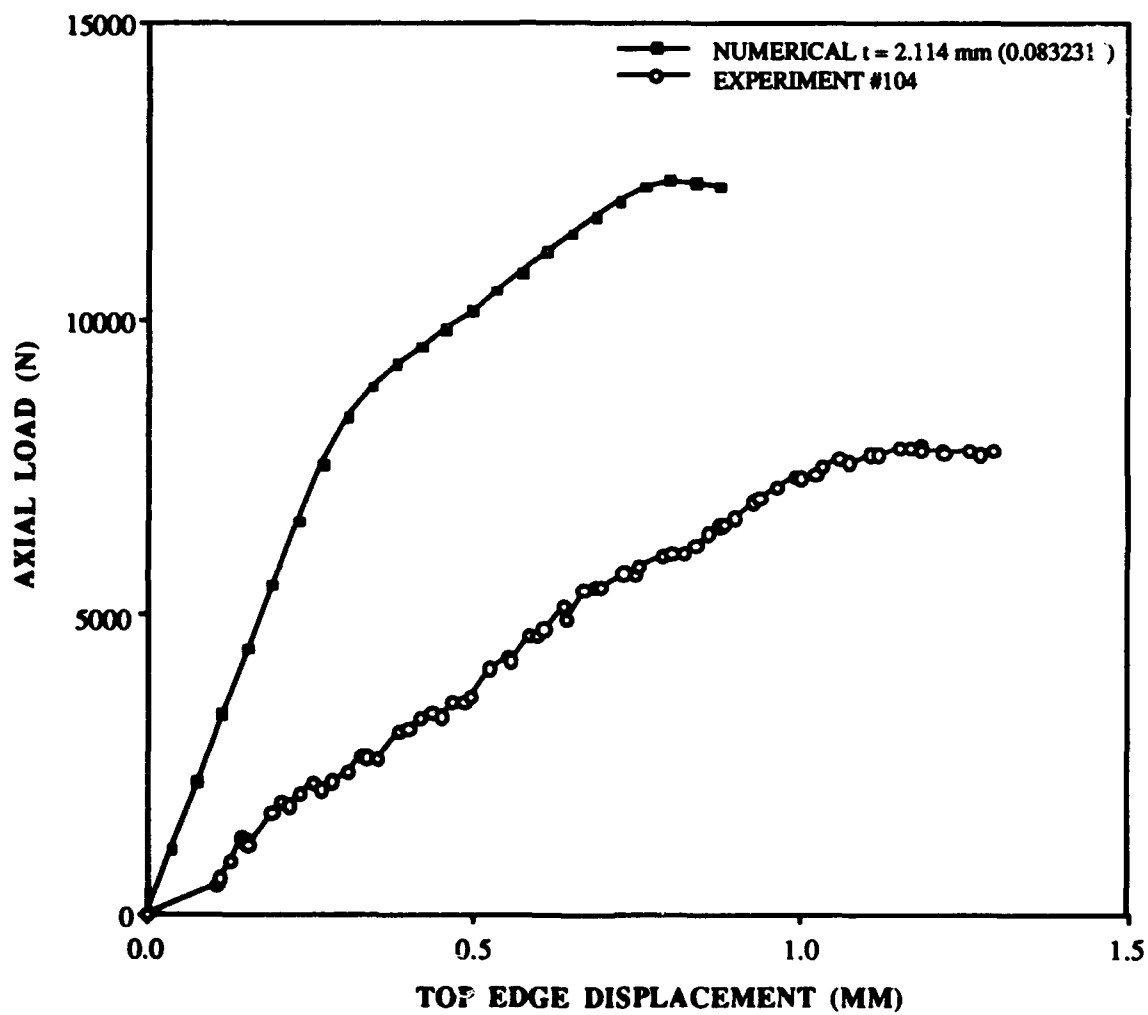
Fig. 75: Load vs. Top Edge Displacement,
Numerical Compared to Experiment #104,
203.2 mm x 50.8 mm (8" x 2") Cutout,
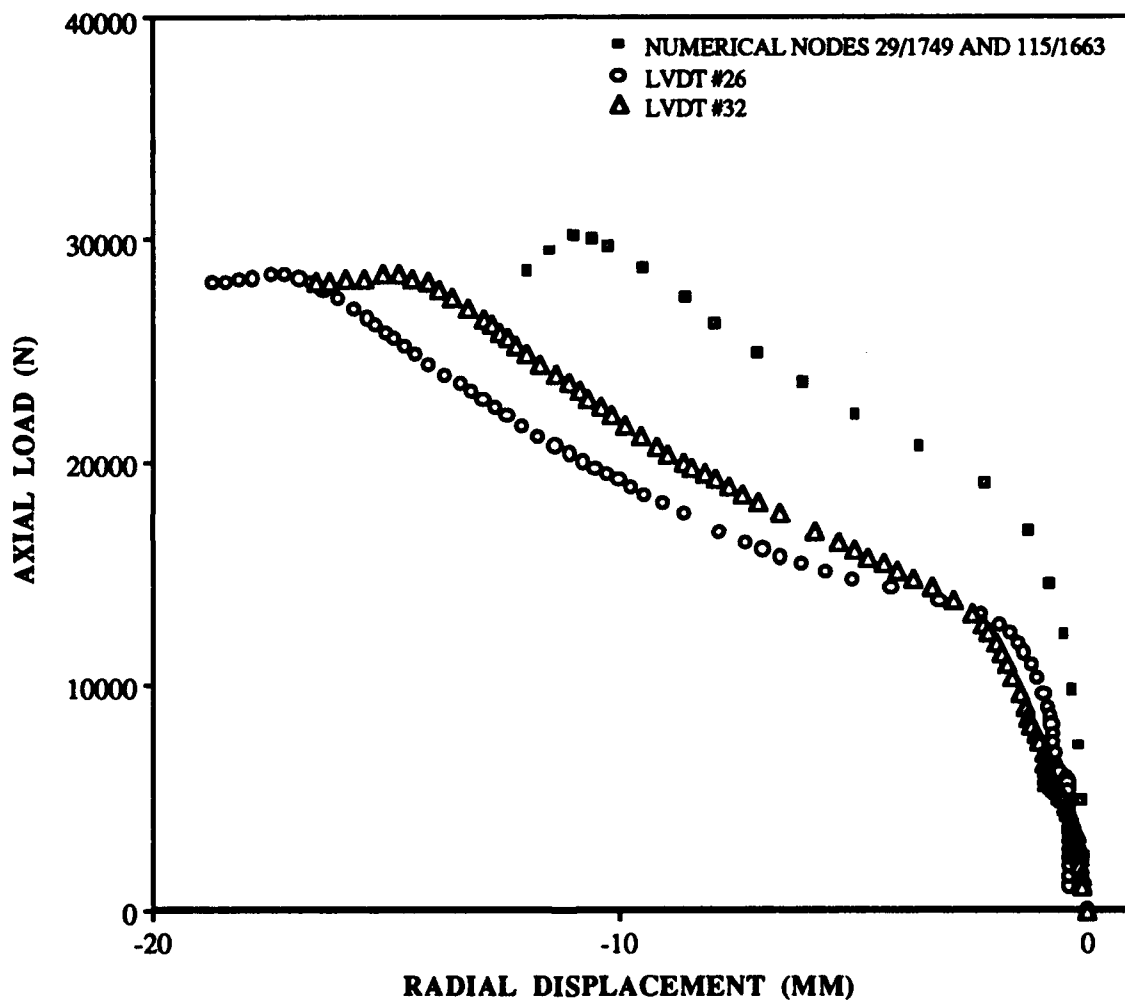304.8 mm x 508 mm (12" x 20") Panel,
[0/45/-45/90]2s
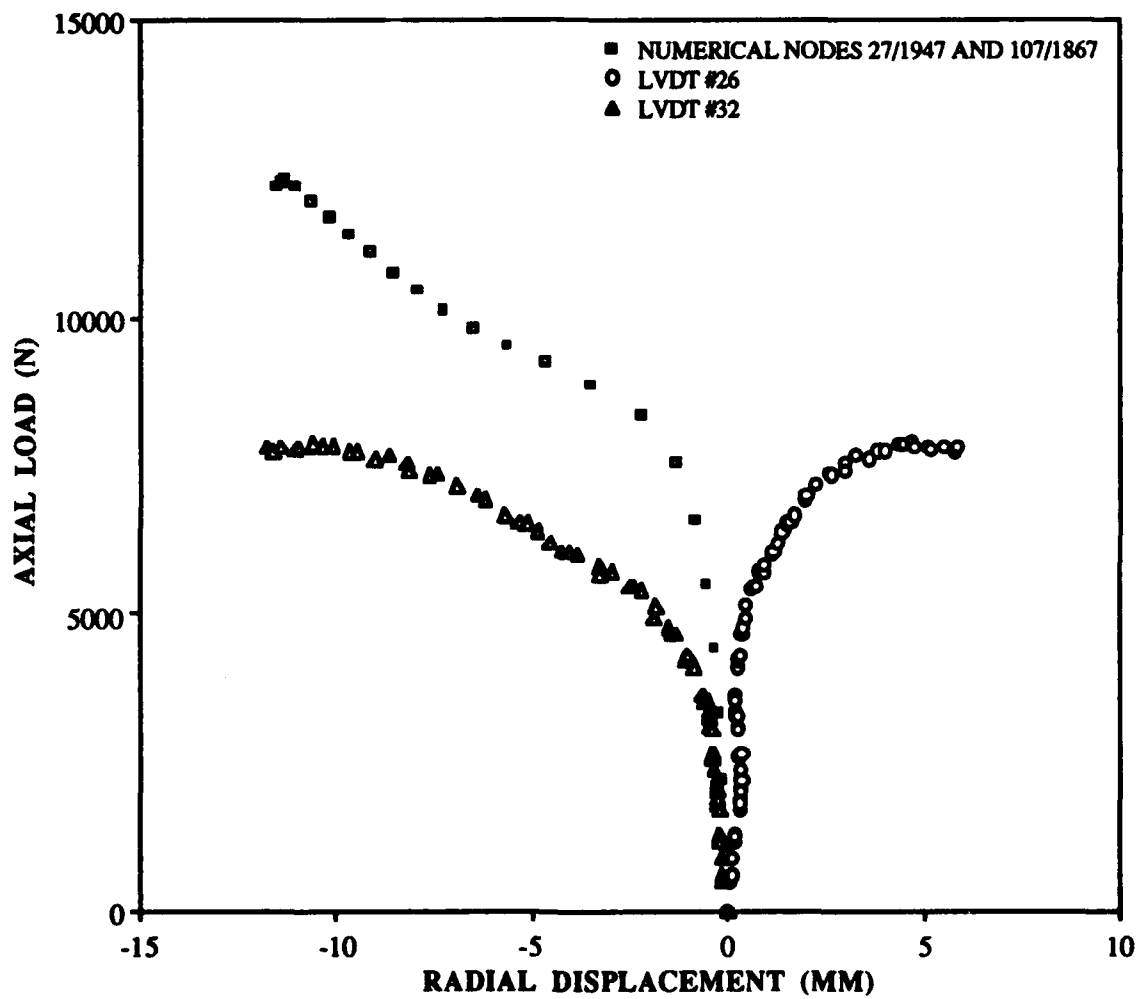
Fig. 76: Load vs. Radial Displacement,
Numerical Compared to Experiment #104,
203.2 mm x 50.8 mm (8" x 2") Cutout,
304.8 mm x 508 mm (12" x 20") Panel,
[0/45/-45/90]2s

155
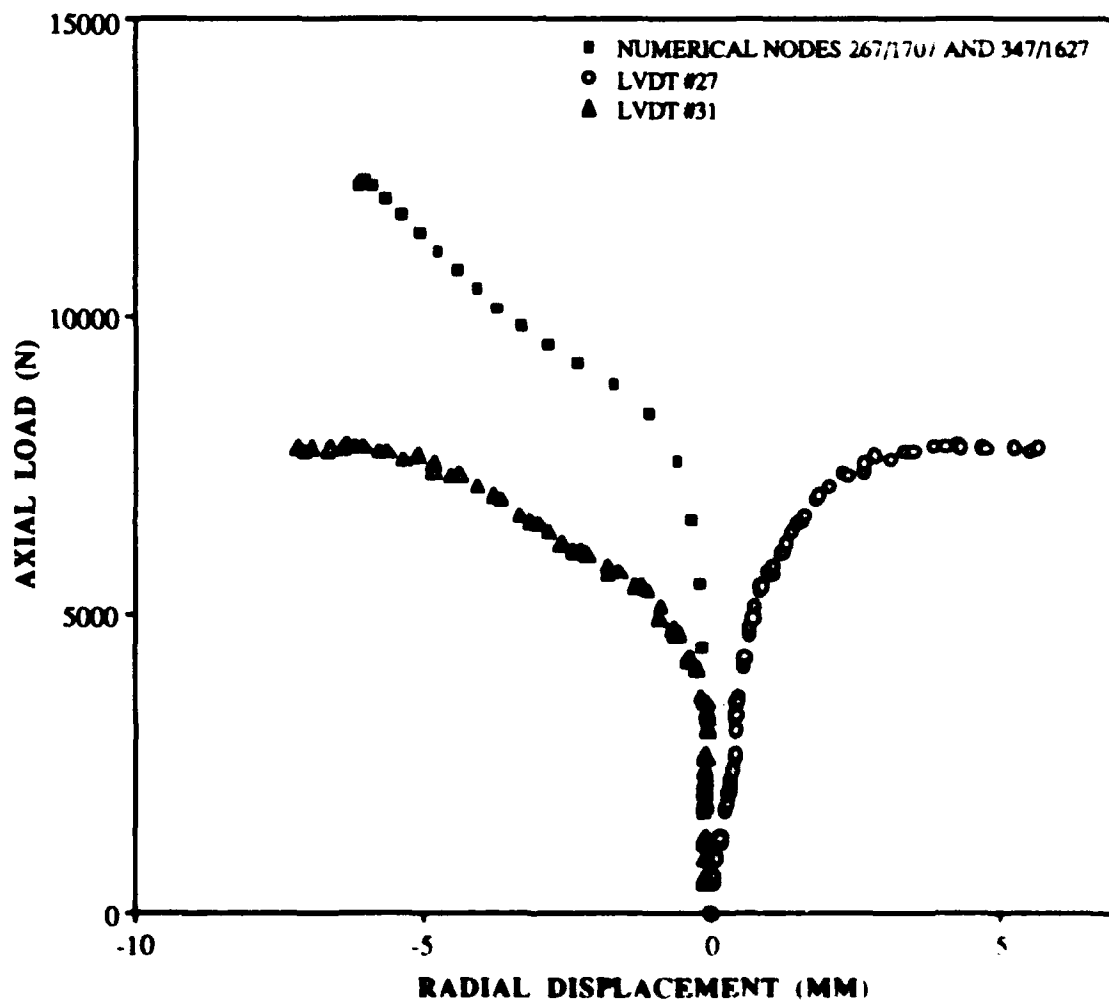
Fig. 77: Load vs. Radial Displacement.
Numerical Compared to Experiment #104.
203.2 mm x 50.8 mm (8" x 2") Cutout.
304.8 mm x 508 mm (12" x 20") Panel.
[0/45/-45/90]2s
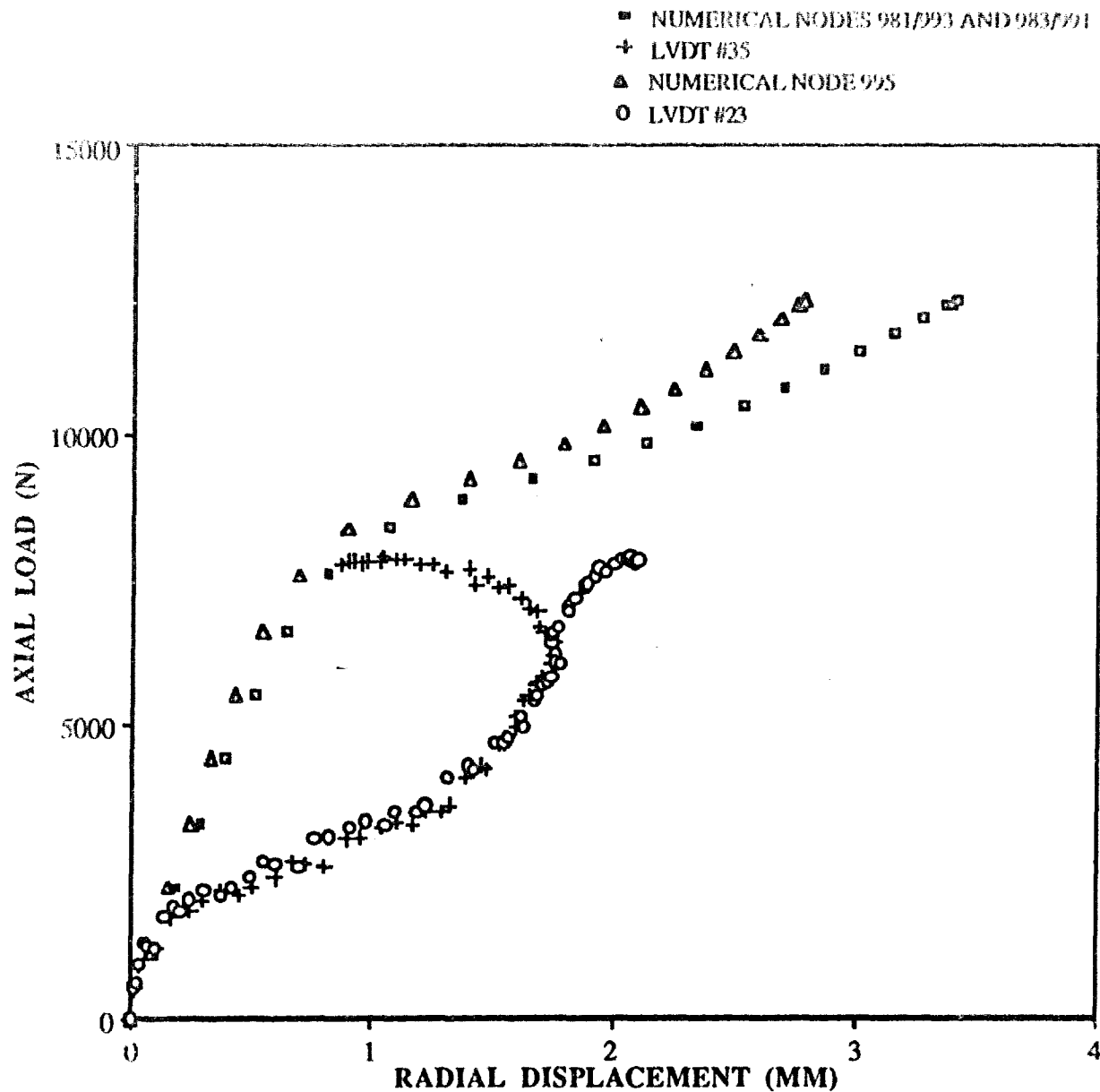
Fig. 78: Load vs. Radial Displacement,
Numerical Compared to Experiment #104,
203.2 mm x 50.8 mm (8" x 2") Cutout,
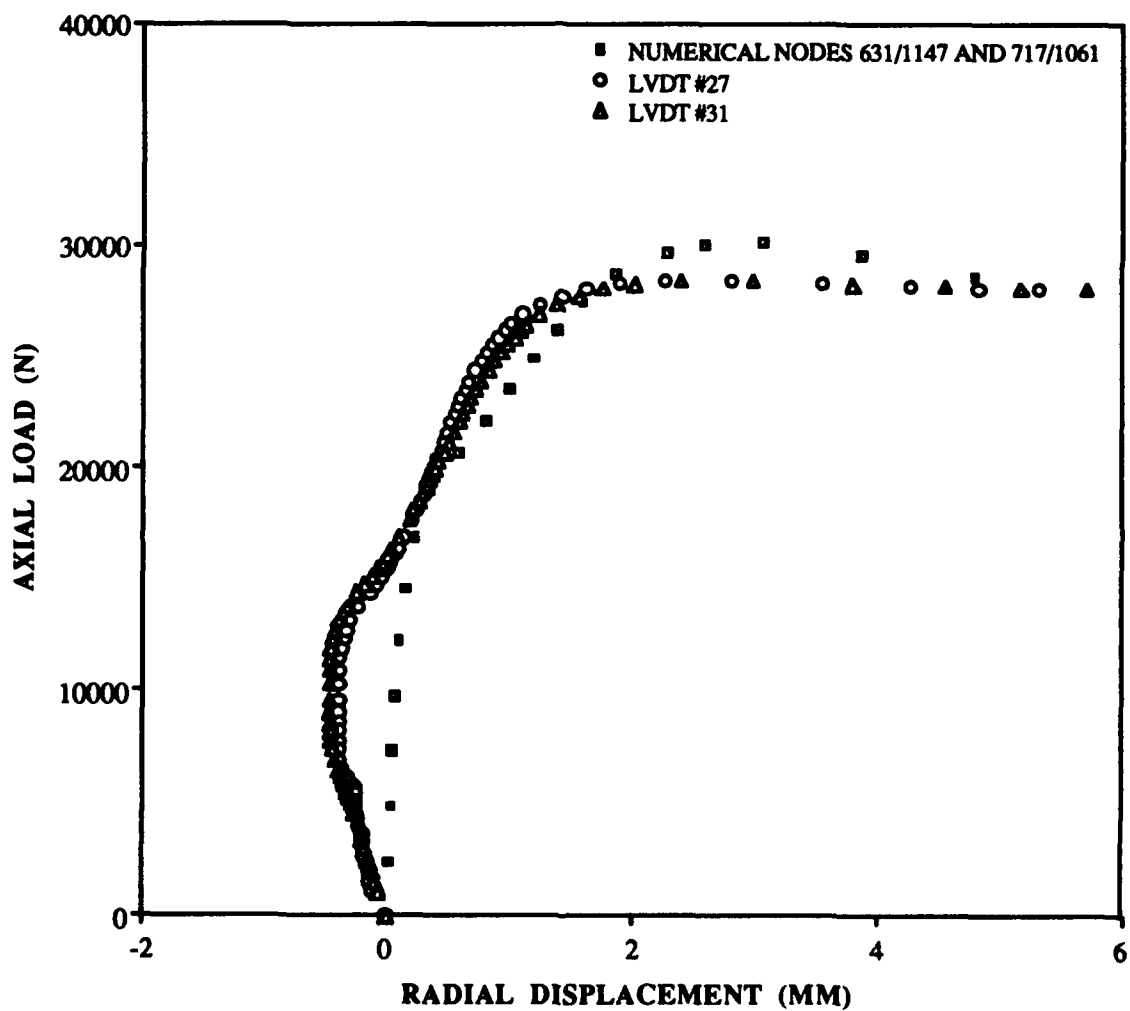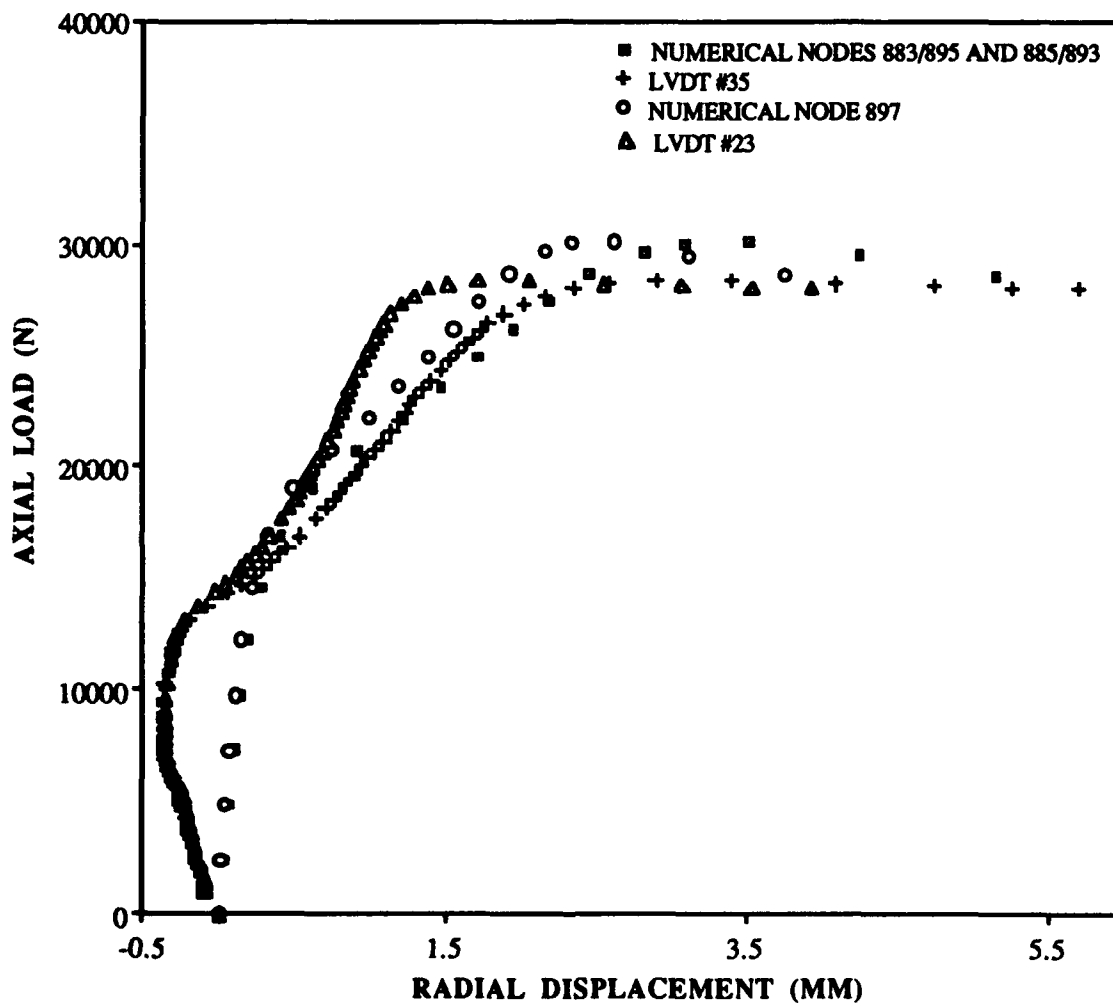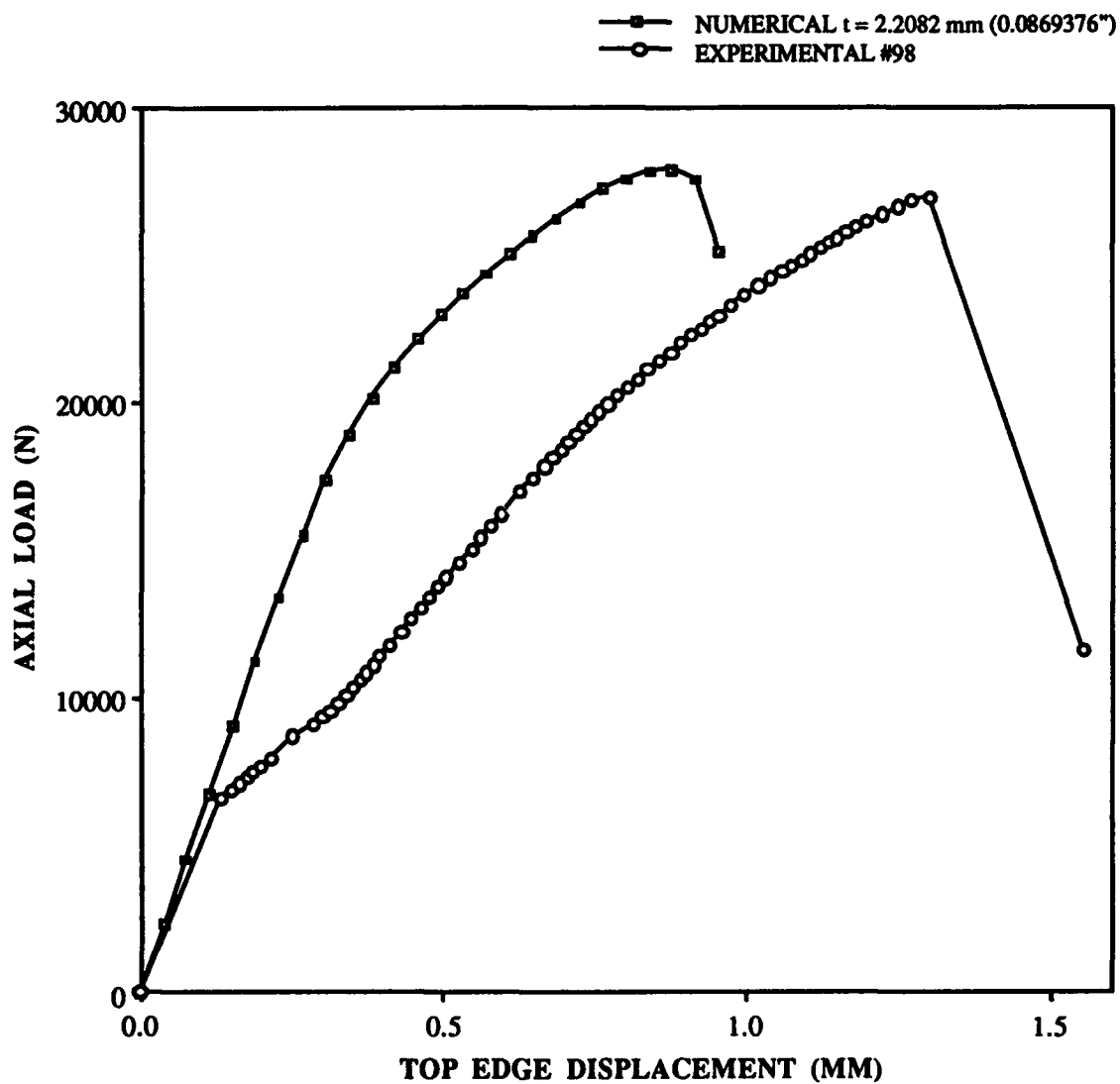304.8 mm x 508 mm (12" x 20") Panel,
[0/45/-45/90]2s
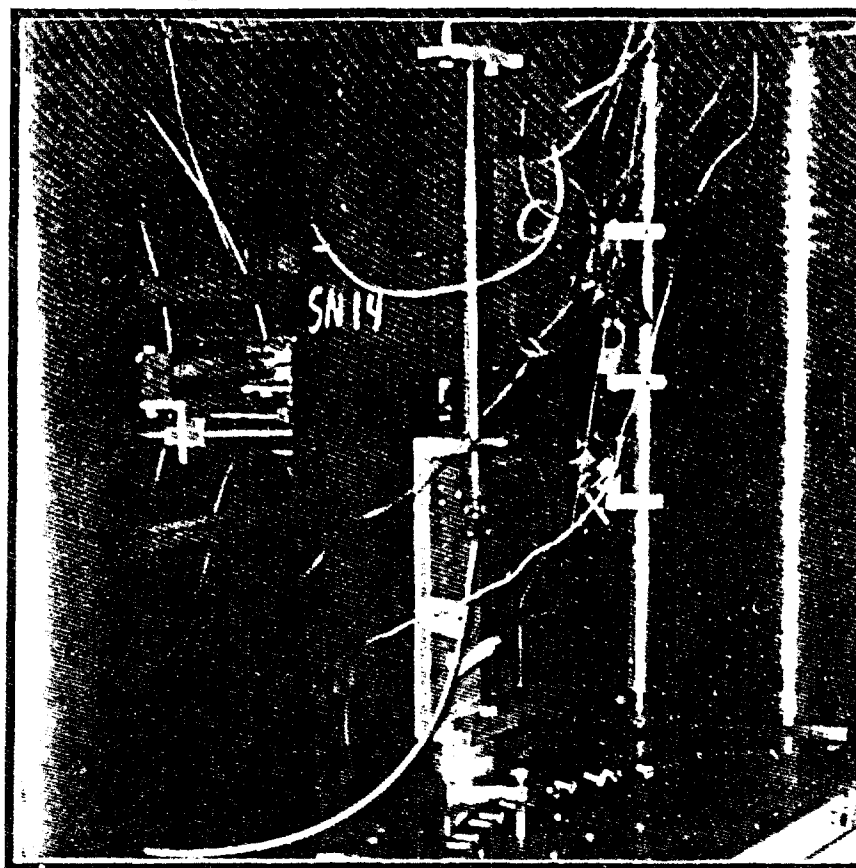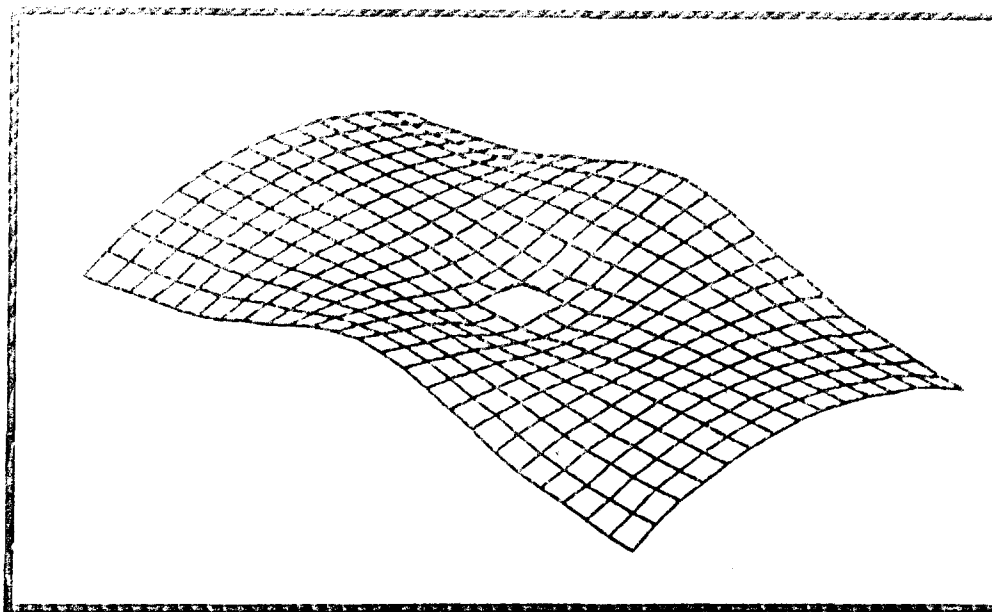
Figure 79. Numerical Orthotropic Plot of Panel Compared to Experimental
Panel at Collapse for a 304.8 mm x 508 mm (12" x 20") Panel
With a 50.8 mm x 50.8 mm (2" x 2") Cutout [0/45/-45/90]2s

158
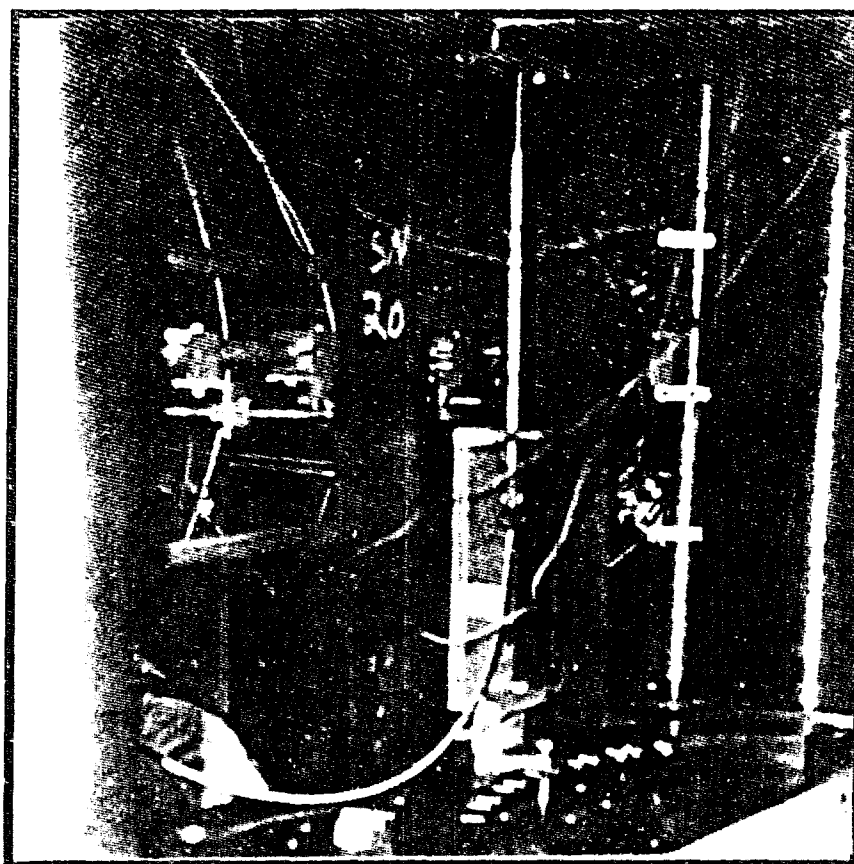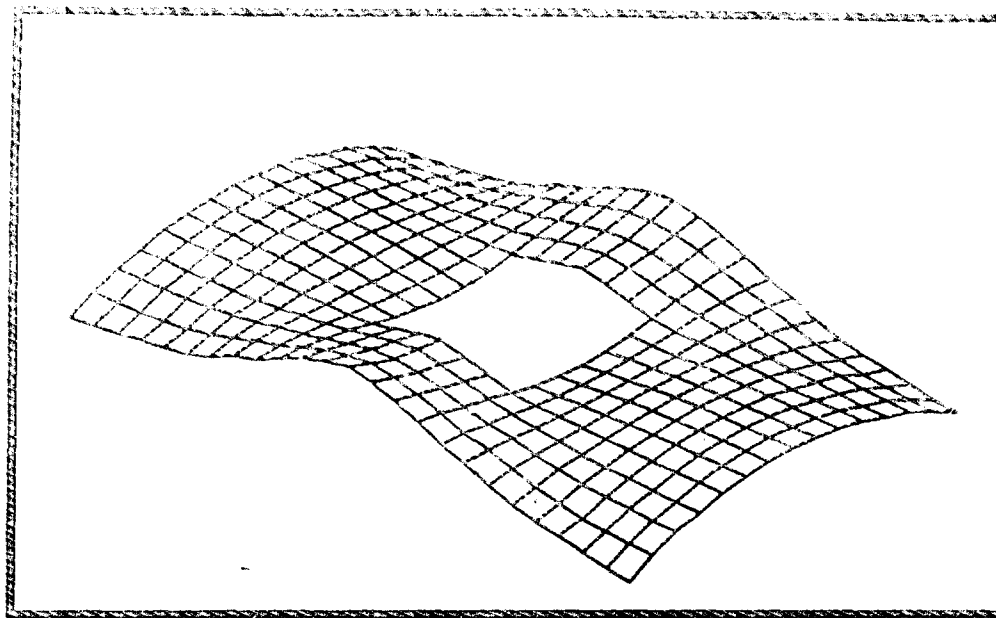
Figure 80. Numerical Orthotropic Plot of Panel Compared to Experimental
Panel at Collapse for a 304.8 mm x 508 mm (12" x 20") Panel
With a 101.6 mm x 101.6 mm (4" x 4") Cutout [0/45/-45/90]2s

159
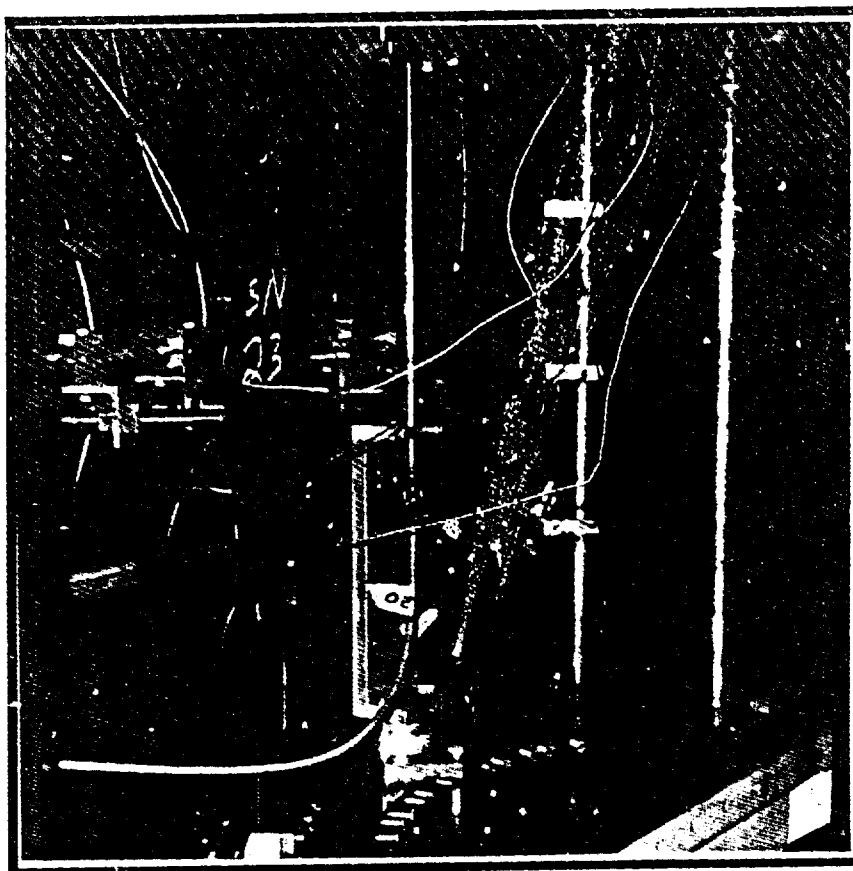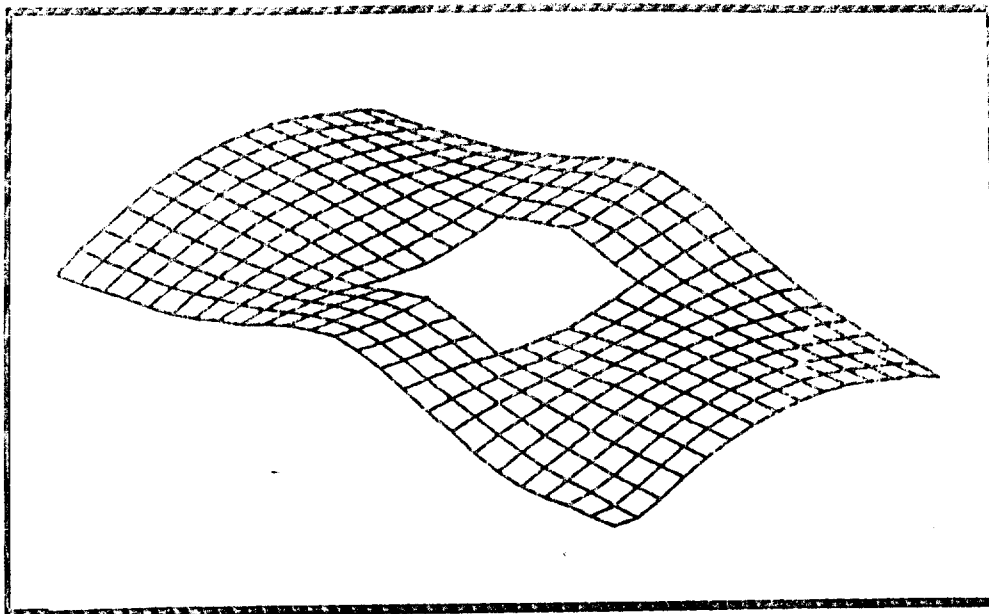
Figure 81. Numerical Orthotropic Plot of Panel Compared to Experimental
Panel at Collapse for a 304.8 mm x 508 mm (12" x 20") Panel
With a 127 mm x 127 mm (5" x 5") Cutout [0/45/-45/90]2s
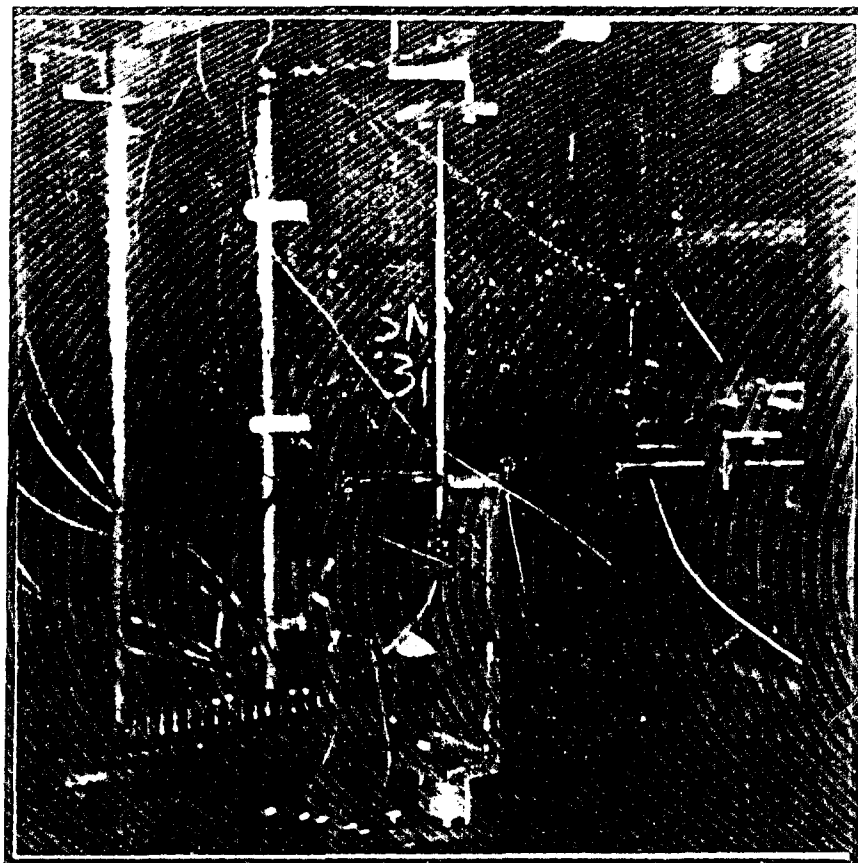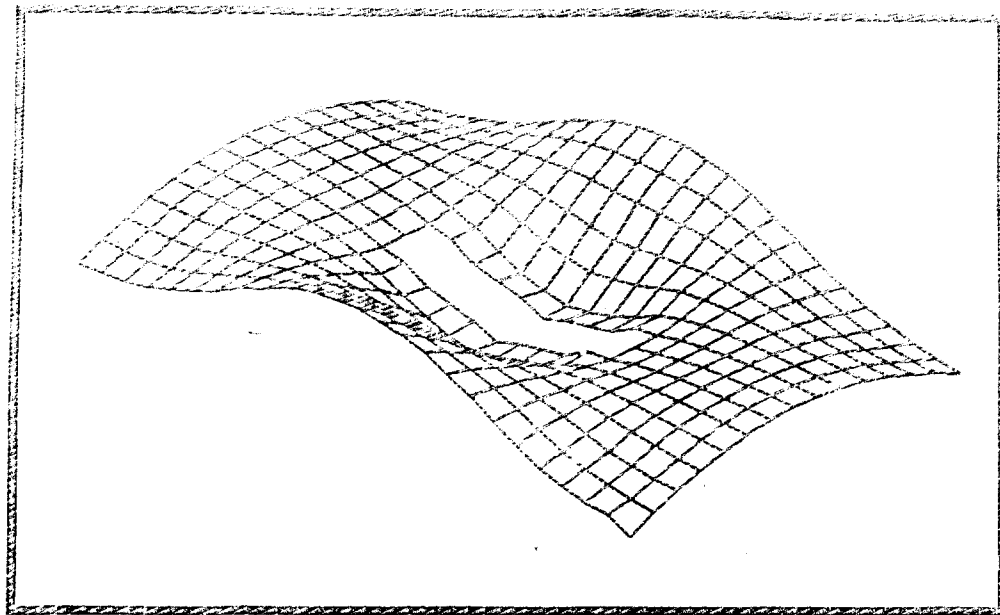
Figure 82. Numerical Orthotropic Plot of Panel Compared to Experimental
Panel at Collapse for a 304.8 mm x 508 mm (12" x 20") Panel
With a 50.8 mm x 203.2 mm (2" x 8") Cutout [0/45/-45/90]2s

161
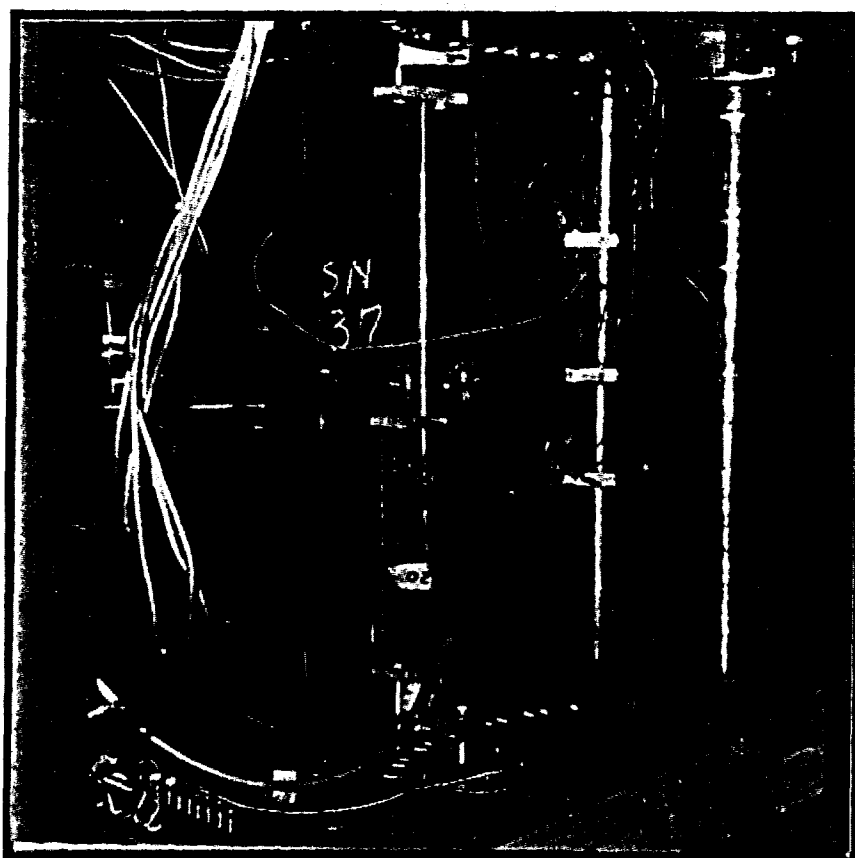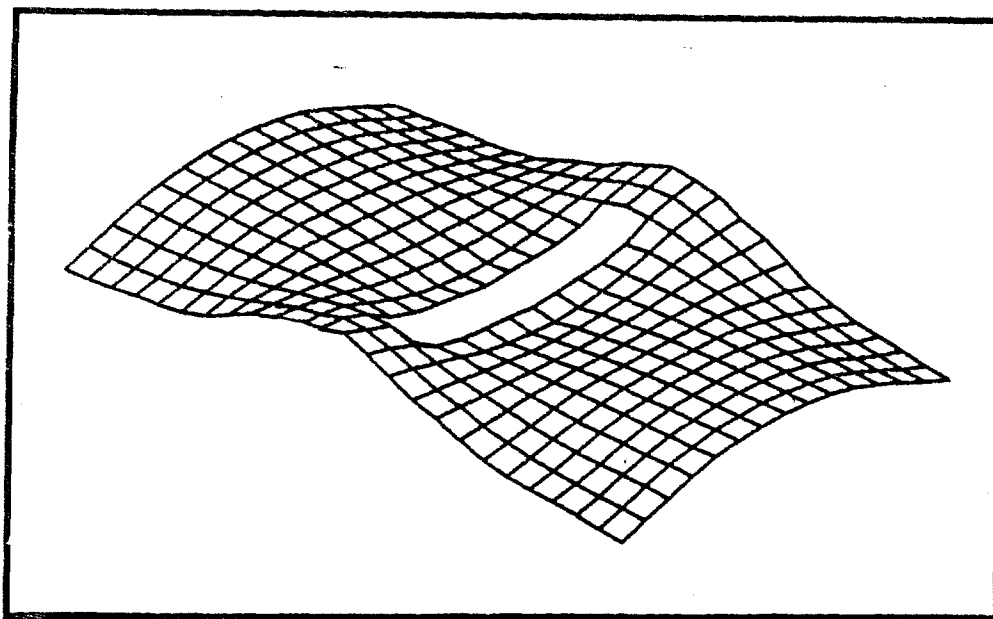
Figure 83. Numerical Orthotropic Plot of Panel Compared to Experimental
Panel at Collapse for a 304.8 mm x 508 mm (12" x 20") Panel
With a 203.2 mm x 50.8 mm (8" x 2") Cutout [0/45/-45/90]2s

6. Conclusions

1. The one-dimensional collapse load estimating technique, based on the Euler buckling model, was found to provide an acceptable estimate for the collapse load when varying average ply thickness for a panel with a centrally located cutout. This technique is most accurate when collapse loads are predicted for panel cutout combinations that experience a large degree of bending.

2. The one-dimensional collapse load estimate for varying panel extensional width for a centrally located cutout was most accurate for panel cutout combinations that approximate the one dimensional Euler buckling model. Specifically, panels with small extensional lengths will provide estimates using this technique that show the closest correlation to the SHELL numerical collapse loads. This technique is beneficial in determining the effect of varying cutout dimensions for panels with equivalent cutout area on the panel collapse load.

3. The one-dimensional collapse load Euler buckling estimate for varying panel axial length was not verified numerically using SHELL. However, this technique was used to determine the effects of the slight variations of axial length on the test panel collapse loads. It was concluded

163

that the small variations in panel axial length did not
significantly affect the panel collapse load. Future studies
should consider verifying this conclusion numerically using
SHELL.

4. The results of the SHELL radius of curvature parametric
study indicate that a small increase (10%) in panel radius of
curvature results in a significant decrease (4.8%) in panel
collapse load. This finding confirmed that the flattening of
the eight ply panel's radius of curvature around a large
cutout that occurred when mounted in the axial compression
fixture was the primary cause of the significant decrease
between the experimental and numerical collapse loads.

5. The results of the ply lay up parametric study indicated
that the panel collapse load and panel response for a panel
with unsupported vertical edges are unaffected by reversing
the +45 and -45 plies in a symmetric quasi-isotropic lay up.

6. The numerical panel response indicated that the maximum
radial displacements occurred at the panel vertical edge at
or near the panel horizontal centerline. Exact symmetry of
the radial displacements about the horizontal and vertical
centerline of the panels did not occur. Rather, equivalent
magnitudes and directions of radial displacements occurred at
diagonals to each other. This behaviour is brought about by

the presence of the +45 and -45 degree plies which affect the bending stiffness terms D_{16} and D_{26}. The stiffness terms in turn affect the in plane twisting moment M_{xy}. The magnitudes of radial displacements ranged from 4-12 times the panel thickness. These large displacements indicate that a nonlinear theory which addresses large rotations, like SHELL, is required.

7. The numerical maximum bending rotations (ψ_s) were inclined to occur at the panel vertical edge at or near the panel horizontal centerline. The bending rotations and radial displacements increased as the horizontal centerline of the panel was approached along the panel free vertical edge. Similarily, equivalent magnitudes of bending rotations occurred at diagonals to each other throughout the panel.

8. The numerical local maximum radial displacements tended to occur at the vertical cutout edge along the panel horizontal centerline. The local maximum bending rotations, occurred at or near the cutout corners when transverse shear effects became significant. The distribution of transverse shear increased with increased panel thickness.

9. The maximum numerical panel transverse shear strains (ϵ_4 and ϵ_5) occurred at or near the cutout corners. The magnitudes of ϵ_4 transverse shear strains were significant

along the horizontal edge of the cutout while the magnitudes of the ε_5 transverse shear strain were significant along the vertical edges of the cutout and panel. The ε_4 shear strains, significant in magnitude, primarily collected along the cutout horizontal edges and near the panel corners. However, magnitudes of transverse shear ε_4 at the panel corners were two to ten times less than the magnitudes experienced along the cutout horizontal edges. In comparison, equivalent magnitudes of ε_5 transverse shear strain occurred at the vertical cutout edges and along the panel vertical edges. Again, similar to radial displacements and bending rotations, equivalent magnitudes of transverse shear strains occurred at diagonals to each other.

10. The collapse of panels with equivalent cutout areas are determined by how the axial compressive energy is absorbed by the panel. A panel with a cutout that absorbs the majority of axial compressive energy through bending will see a reduction in flexural rigidity and collapse at a lower load. In comparison, a panel with an equivalent cutout area that absorbs the majority of axial compressive energy through transverse shear will see a increase in flexural rigidity and collapse at a higher load. This was confirmed numerically by comparing the collapse load of panels with equivalent cutout area but varying cutout dimensions. It was found that the panel that experienced the largest distribution of ε_5

transverse shear strain (in terms of magnitude and axial length of the cutout) along the vertical cutout edge, exhibited a flexible response and collapsed at a higher collapse load than panels with equivalent cutout areas.

11. The collapse load and stiffness of a panel was verified numerically to decrease with an increase in cutout area. In the case of panels with equivalent cutout areas the collapse load and stiffness tended to decrease with a reduction in panel extensional width. However, as the presence of transverse shear increases, the cutout which absorbs the majority of axial compressive energy through shear, will collapse at a higher load than its equivalent cutout area counterparts. In addition, the load versus displacement curves become more non-linear as the cutout area increases and the extensional width decreases.

12. The collapse load and stiffness of a panel increased with increased panel thickness when comparing panels of equivalent axial lengths. The effect of increasing axial length from 304.8 mm to 508 mm numerically for panels with equivalent number of plies resulted in a collapse load decrease for all panel configurations. The effects of increasing panel axial length on the panel collapse load significantly effected panels with large cutout areas. In comparison, collapse loads for panels with small extensional widths (50.8 mm) were mildly affected by an increase of panel axial length from 304.8 mm to 508 mm.

small panel extensional lengths could have resulted in these
panels exhibiting asymmetrical panel responses
experimentally.

15.   The panel restraint modification corrected the anomaly
experienced in previous experimentation for quasi-isotropic
panels. This is concluded since panel responses were
symmetrical for panels that exceeded the recommended
horizontal edge tolerance for even loading to occur. It is
recommended that this modification be confirmed for use with
cross-ply panel lay ups. Although, this problem was
exhibited in previous research using both quasi-isotropic and
cross-ply panels, the effects of circumferential shift of the
panel was most prevalent for the cross ply panels.
Therefore, additional tests should be run using cross-ply
panels to qualify this modification for these panel
configurations.

Bibliography

1. Dennis, Scott T. _Large Displacement and Rotational Formulation for Laminated Cylindrical Shells Including Parabolic Transverse Shear_. PhD dissertation. School of Engineering, Air Force Institute of Technology (AETC), Wright-Patterson AFB OH, May 1988 (AD-A194871).

2. Lee, Catherine E. and Anthony N. Palazotto. "Nonlinear Collapse Analysis of Composite Cylindrical Panels with Small Cutouts or Notches," _Composite Structures, 4_: 217-229 (1985).

3. Bushnell, David. _Computerized Buckling Analysis of Shells_. The Netherlands: Martinus Nijhoff Publishers, 1985.

4. Dennis, Scott T. and Anthony N. Palazotto, "Static Response of a Cylindrical Composite Panel with Cutouts Using a Geometrically Nonlinear Theory," _AIAA Journal, 28_: No.6, 1082-1088 (June, 1990).

5. Cook, Robert D. and others. _Concepts and Applications of Finite Element Analysis_. New York: John Wiley and Sons, 1989.

6. Becker, Marvin L., Anthony N. Palazotto, and Narendra S. Khot, "Experimental Investigation of the Instability of Composite Cylindrical Panels," _Experimental Mechanics, 22_: 372-376 (October, 1982).

7. Harper, James G. _Buckling Analysis of Laminated Composite Circular Cylindrical Shells_. MS thesis, AFIT/GAE/AA/78D-8. School of Engineering, Air Force Institute of Technology (AETC), Wright-Patterson AFB OH, December 1978 (AD-A081905).

8. Hebert, John S. _Analytical/Experimental Linear Bifurcation of Curved Cylindrical Composite Panels_. MS thesis, AFIT/GAE/AA/82D-14. School of Engineering, Air Force Institute of Technology (AETC), Wright-Patterson AFB OH, December 1982 (AD-124664).

9. Almroth, B. O., F. A. Brogan, and M. B. Marlowe, "Stability of Cylinders with Circular Cutouts," _AIAA Journal, 11_: No. 11, 1582-1584 (November 1973).

10. Almroth, B. O., and F. A. Brogan, "Bifurcation Buckling as an Approximation of the Collapse Load for General Shells," *AIAA Journal, 10*: No. 4, 463-467 (April 1972).

11. Sobel, L. H., T. Weller, and B. L. Agarwal, Buckling of Cylindrical Panels Under Axial Compression," *Computers and Structures, 6*: 29-35 (February, 1976).

12. Almroth, Bo O., "Influence of Edge Conditions on the Stability of Axially Compressed Cylindrical Shells," *AIAA Journal, 4*: 134-140 (1966).

13. Rehfield, L. W., and W. L. Hallauer, "Edge Restraint Effect on Buckling of Compressed Curved Panels," *AIAA Journal 6*: 187-189 (January 1968).

14. Tisler, Thomas W. *Collapse Analysis of Cylindrical Composite Panels with Large Cutouts Under Axial Load*. MS thesis, AFIT/GAE/AA/86D-18. School of Engineering, Air Force Institute of Technology (AETC), Wright-Patterson AFB OH, December 1986 (AD-A179112).

15. Janisse, Thomas C. *A Parametric Study of Surface Imperfections and Small Cutouts in a Composite Panel*. MS thesis, AFIT/GAE/AA/82D-15. School of Engineering, Air Force Institute of Technology (AETC), Wright-Patterson AFB OH, December 1982 (AD-A124739).

16. Knight, N. F., Jr., and J. H. Starnes Jr., "Postbuckling Behavior of Axially Compressed Graphite-Epoxy Cylindrical Panels With Circular Holes," *Proceedings of the 1984 Pressure Vessel and Piping Conference and Exhibition*. 153-167. New York: The American Society of Mechanical Engineers, 1984.

17. Schimmels, Scott A. *Investigation of Collapse Characteristics of Cylindrical Composite Panels With Large Cutouts*. MS thesis, AFIT/GAE/ENY/89D-33. School of Engineering, Air Force Institute of Technology (AETC), Wright-Patterson AFB OH, December 1989 (AD-A216378).

18. Hatfield, James C. *Effect of Thickness and Ply Layup on the Collapse Characteristics of Cylindrical Composite Shells with Large Cutouts*. MS thesis, AFIT/GAE/ENY/92D-20. School of Engineering, Air Force Institute of Technology (AETC), Wright-Patterson AFB OH, December 1992 (AD-A258909).

19. Palazotto, Anthony N. and Scott T. Dennis. _Nonlinear Analysis of Shell Structures_. Washington DC: American Institute of Aeronautics and Astronautics, Inc., 1992.

20. Agarwal, Bhagwan D. and Lawrence J. Broutman. _Analysis and Performance of Fiber Composites_. New York: John Wiley and Sons, Inc., 1990.

21. Jones, Robert M. _Mechanics of Composite Materials_. New York: Hemisphere Publishing Corporation, 1975.

22. Saada, Adel S. _Elasticity Theory and Applications_. Malabar, FL: Krieger Publishing Company, Inc., 1989.

23. Sandhu, R. S., G. P. Sendeckyj, G. A. Shoeppner, and J. E. Pappas, "Initiation and Prevention of Edge Delamination With and Without Residual Stresses," Presented at the 74th Meeting of Structure and Materials Panel of AGARD, Patras, Greece (May 1992).

24. Schimmels, Scott A. and Anthony N. Palazotto, "Collapse Characteristics of Cylindrical Composite Panels Under Axial Loads," _AIAA Journal 30_: No. 5, 1447-1449 (May 1992).

25. Horban, Blaise A. _The Effects of Through the Thickness Delaminations on Curved Composite Panels_. MS thesis, AFIT/GAE/AA/85D-8. School of Engineering, Air Force Institute of Technology (AETC), Wright-Patterson AFB OH, December 1985 (AD-A164110).

26. Wilder, Brendan L. _A Study of Damage Tolerance in Curved Composite Panels_. MS thesis, AFIT/GAE/AA/88M-3. School of Engineering, Air Force Institute of Technology (AETC), Wright-Patterson AFB OH, March 1988 . (AD-A190617).

27. Palazotto, Anthony N. and Thomas W. Tisler, "Experimental Collapse Determination of Cylindrical Composite Panels with Large Cutouts Under Axial Load," _Computer Structures 12_: No. 1, 61-78 (1989).

28. Gere, James M. and Stephen P. Timoshenko. _Mechanics of Materials_ (Second Edition). Boston: PWS Engineering, 1984.

APPENDIX A

EXPERIMENTAL TEST PLAN

TEST PLAN

Geometric Instability Studies

1. Program Information

a.	Organization	WL/FIBCA
b.	Project Number	24010366
c.	Security Classification	Unclassified
d.	Project Engineer	Capt John C. Del Barga, AFIT/ENY
e.	Project Advisor	Dr. Anthony Palazotto, AFIT/ENY
f.	Project Sponsor	Dr. R.S. Sandhu, WL/FIBCA
g.	Fabrication Engineer	Mr. D.J. Dolvin, WL/FIBCA
h.	Instrumentation Engineer	Assigned by FIBT
i.	Test Engineer	Assigned by FIBE
j.	Test Location	WL/FIBEC, Bldg 65, Area B

2. Program Objective

The objective of this project is to study the geometric instability (buckling load/displacement) of composite panels with varying panel cutout planform areas under axial compressive load. The test specimens of cylindrical cross-section will be fabricated.

3. Fabrication

The following paragraphs provide technical details to fabricate specimens required to conduct the buckling studies.

3.1 Material

The specimens required for this research will be fabricated using a graphite/epoxy (AS4/3501-6) material system.

3.2 Stacking Sequence and Thickness of Panels

Curved specimens (sizes specified in paragraph 3.3) will be fabricated using the material system of paragraph 3.1 and will conform to the following sequences:

Table 1. Panel Layup

Panel Configuration	Stacking Sequence	Total Number of Plies
A	[0/+45/-45/90]s	8
B	[0/+45/-45/90]2s	16
C	[0/+45/-45/90]3s	24

The panels will be uniform in thickness, having an average ply thickness after cure of 0.00525" ±0.0003"

3.3 Specimens

3.3.1 Size

For the material system specified in paragraph 3.1, the size and the number of specimens will be in accordance with Table 2. All panels have a radius of curvature of 12". In addition the specimens will have centrally located square and rectangular cutouts.

Table 2. Specimen Designation

Specimen Designator*	Reference Figure **
A8-13-44-1	A1
A8-13-44-2	A1
A8-21-44-1	A2
A8-21-44-2	A2
B16-21-44-1	A2
B16-21-44-2	A2
C24-21-44-1	A2
C24-21-44-2	A2
A8-13-82-1	A3
A8-13-82-2	A3
A8-21-82-1	A4
A8-21-82-2	A4
B16-21-82-1	A4
B16-21-82-2	A4
C24-21-82-1	A4
C24-21-82-2	A4
A8-13-28-1	A5
A8-13-28-2	A5
A8-21-28-1	A6
A8-21-28-2	A6

Table 2.   (Continued)

Specimen Designator*	Reference Figure **
B16-21-28-1	A6
B16-21-28-2	A6
C24-21-28-1	A6
C24-21-28-2	A6
A8-13-22-1	A7
A8-13-22-2	A7
A8-21-22-1	A8
A8-21-22-2	A8
B16-21-22-1	A8
B16-21-22-2	A8
C24-21-22-1	A8
C24-21-22-2	A8
A8-13-55-1	A9
A8-13-55-2	A9
A8-21-55-1	A10
A8-21-55-2	A10
B16-21-55-1	A10
B16-21-55-2	A10
C24-21-55-1	A10
C24-21-55-2	A10

* Specimens are designated as:

```
XX - YY - ZZ - N
 |    |    |    |__ __ __  Specimen number
 |    |    |
 |    |    |__ __ __ __    Size of cutout
 |    |                    (4"x4", 8"x2", 2"x8", 2"x2", 5"x5")
 |    |
 |    |__ __ __ __ __ __   Height of panel 13" or 21"
 |
 |__ __ __ __ __ __ __ _   Panel Designator A,B, and C
                           (see table 1), followed by the
                           number of plies in the panel
```

** Cut holes of dimensions as specified above, using a router with the method developed for cutting curved panels.

3.3.2 Curing Cycle

The curing cycle recommended by manufacturer will be used.

3.3.3 Void Content

The void content will not be in excess of one percent, with variations of thickness specified in paragraph 3.2.

3.3.4 Determination of Flaws

All panels will be subjected to a C-scan to determine flaws before being cut. The final acceptance or rejection of panels will be made by the project engineer.

3.3.5 Resin Content

Samples will be taken at suitable locations to determine resin content, fiber volume, and void fractions for the panels being used.

3.4 Basic Material Properties

The elastic properties required will be extracted from "Initiation and Prevention of Edge Delamination with and without Residual Stresses," Table 2 (May 1992).

4. Testing

4.1 Test Procedure

4.1.1 Specimens will be instrumented with back-to-back strain gages and linear variable differential transducers (LVDTs). The purpose of the strain gages is to insure uniform loading across the top of the panels. The LVDTs will be measuring axial displacements (u) and radial displacements (w) during the compressive static loading.

4.1.2 The testing will be performed on the 30,000 lb hydraulic machine, which will require some modification so that all circumferential movement will be restricted. For these studies the vertical-edge supports will be removed. The compressive loads will be applied using a uniform displacement of 0.05" per minute. The panels will be compressed up to the buckling load and the load will be released. A total of two tests will be performed on each different specimen configuration. The following data will be collected:

a. Applied Load versus Radial Displacement

b. Applied Load versus Axial Displacement

5. Report

The results of this study will be compared to a finite element model. The final results and analysis will be incorporated into a master's degree thesis for the project engineer.

RADIUS OF CURVATURE

12.0

THICKNESS (SEE TABLE 1)

13.0

4.0

4.0

Note: All dimensions in inches
Future studies should use tolerances of 0.001

ARC LENGTH = 12.0
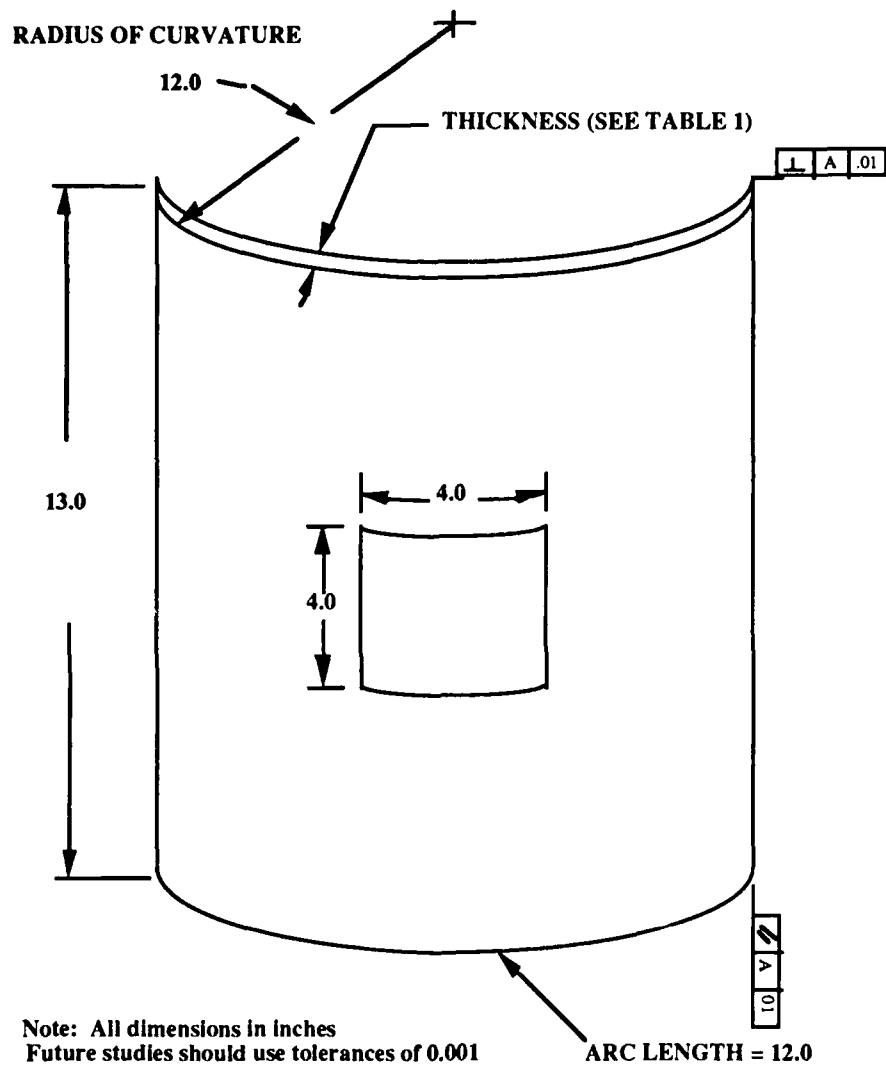
Figure A1. Panel Size 12 x 13 with 4 x 4 Central Cutout
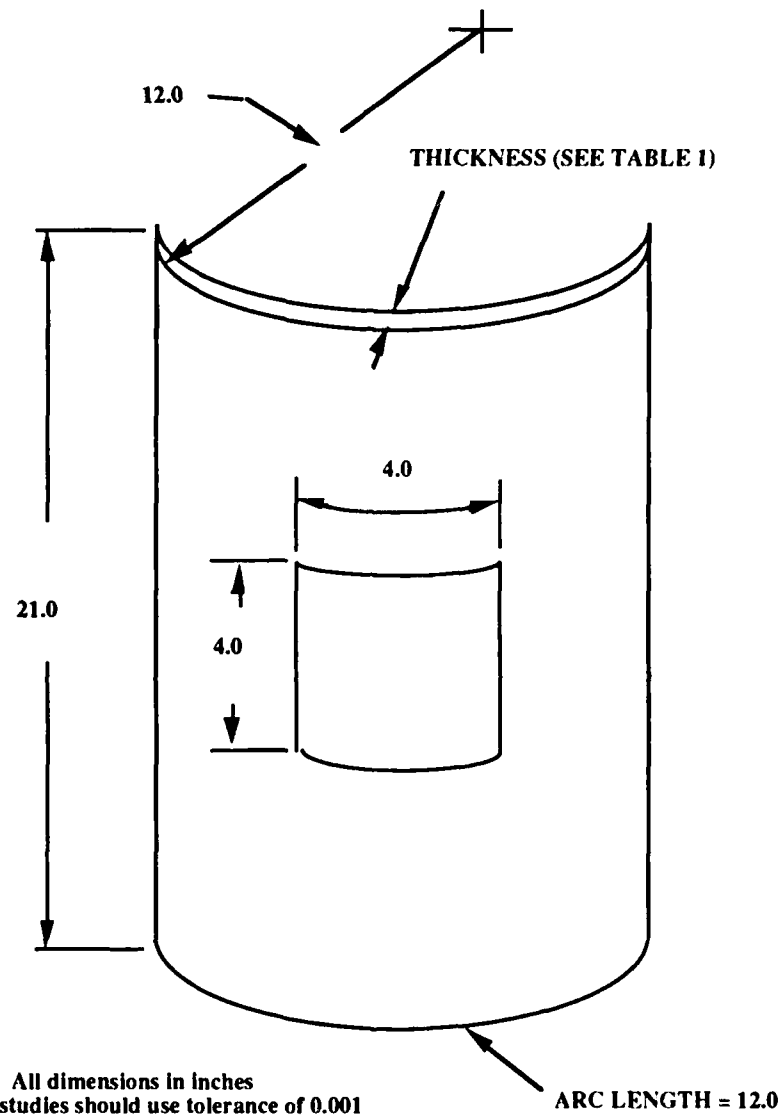
Figure A2. Panel Size 12 x 21 with 4 x 4 Central Cutout

RADIUS OF CURVATURE

12.0

THICKNESS (SEE TABLE 1)

⊥ | A | .01

13.0

8.0

2.0

⊘ | A | .01

Note: All dimensions in inches
uture studies should use 0.001 tolerance

ARC LENGTH = 12.0
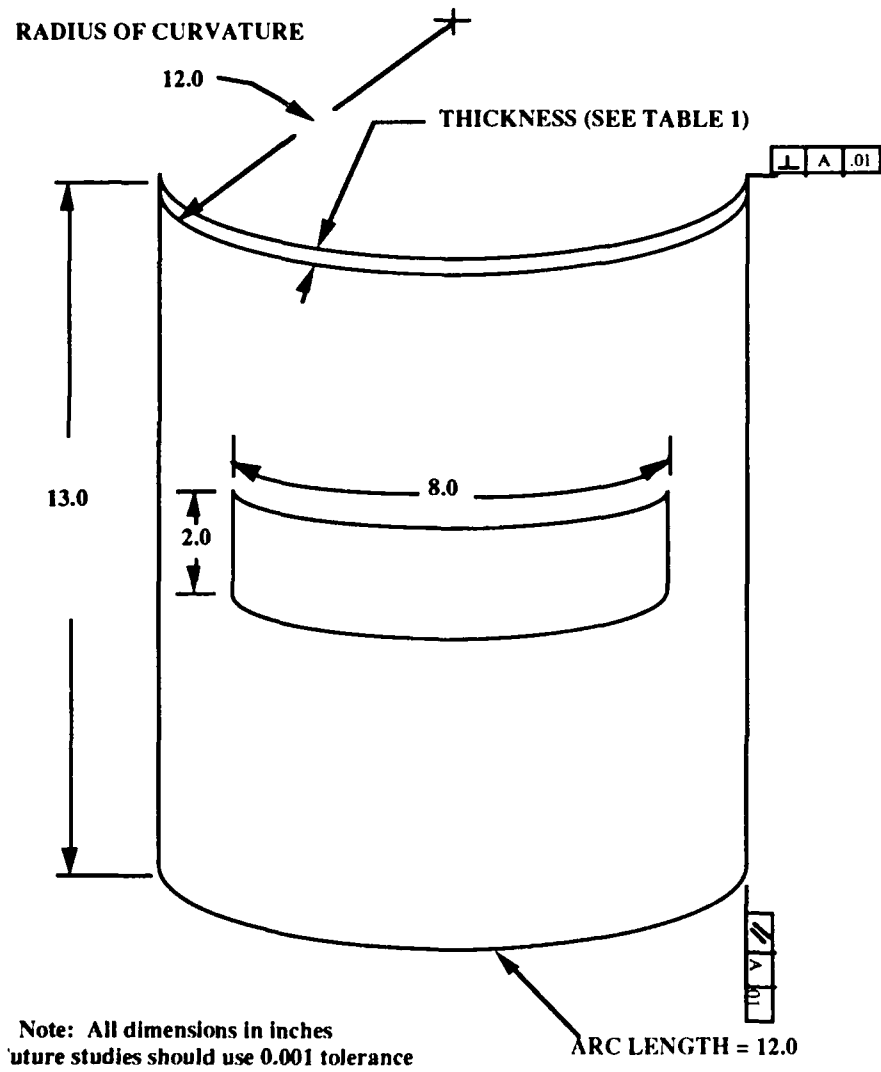
Figure A3. Panel Size 12 x 13 with 8 x 2 Central Cutout

181

12.0

THICKNESS (SEE TABLE 1)

21.0

8.0

2.0

Note: All dimensions in inches
ature studies should use tolerance of 0.001

ARC LENGTH = 12.0
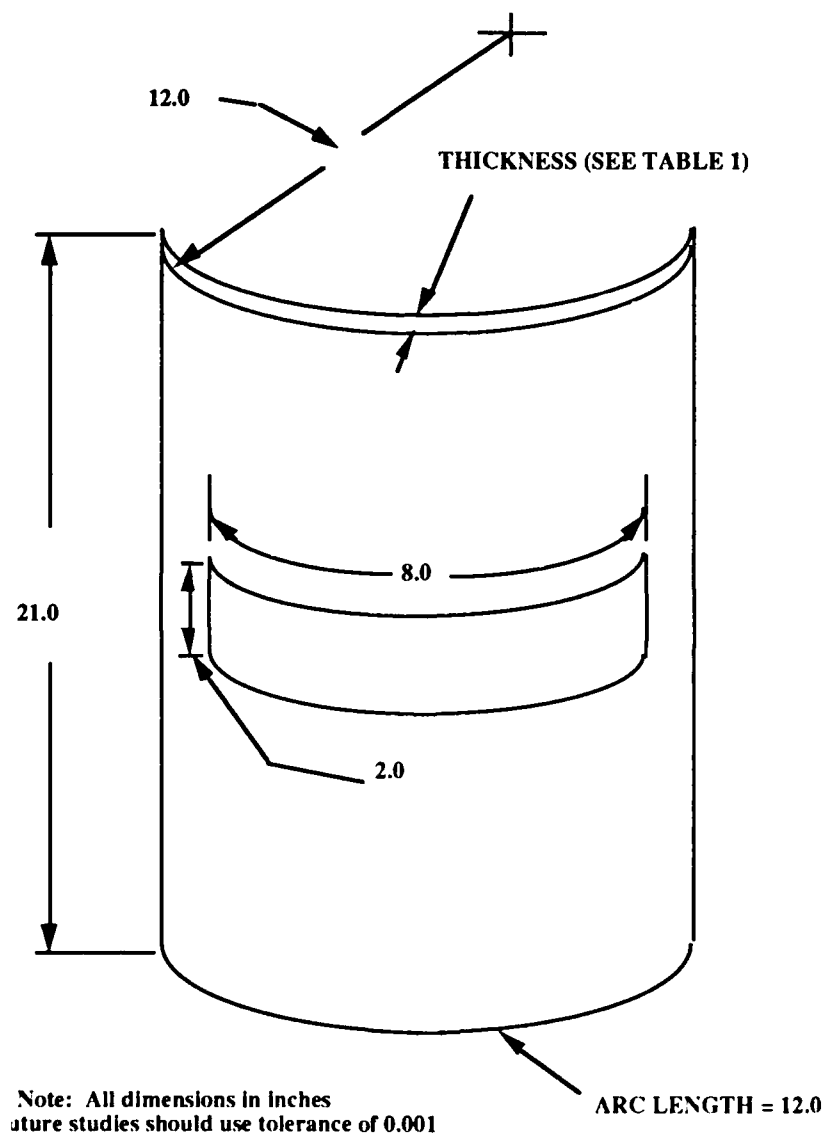
Figure A4. Panel Size 12 x 21 with 8 x 2 Central Cutout

RADIUS OF CURVATURE

12.0

THICKNESS (SEE TABLE 1)

⊥ | A | .01

2.0

13.0

8.0

∠ | A | .01

Note: All dimensions in inches
iture studies should use tolerance of 0.001

ARC LENGTH = 12.0
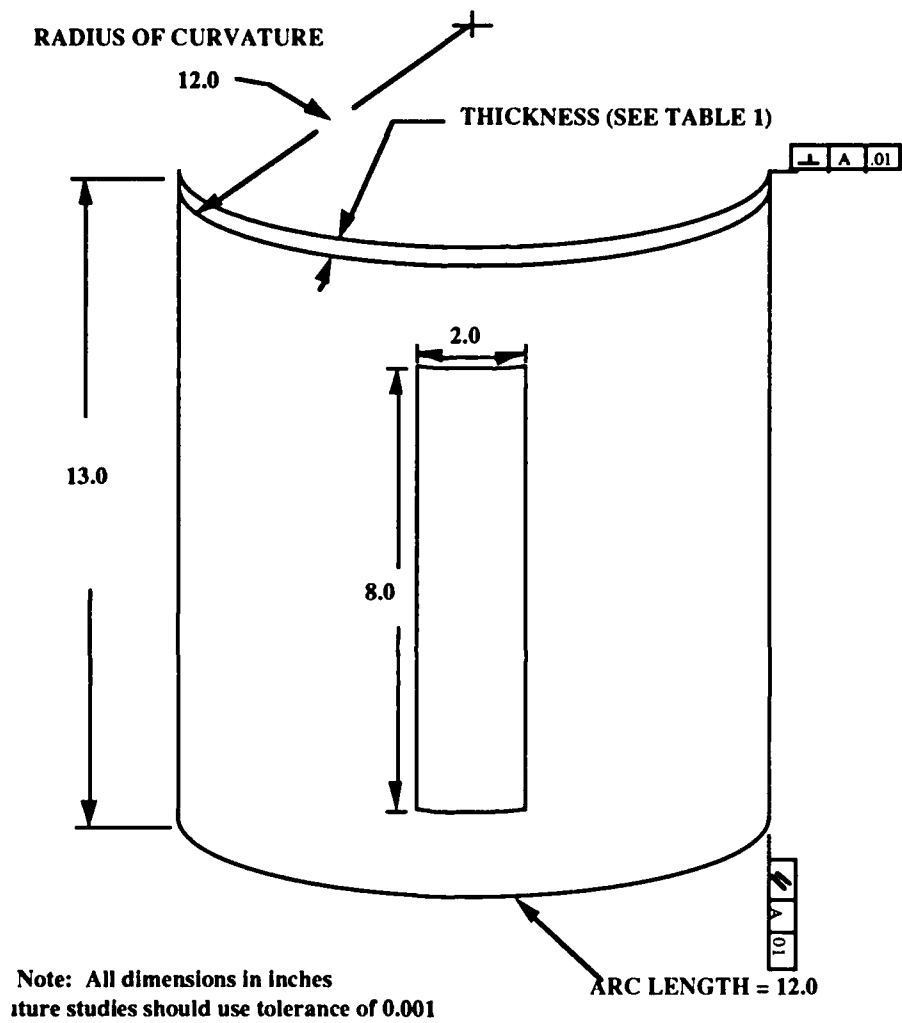
Figure A5. Panel Size 12 x 13 with 2 x 8 Central Cutout

12.0

THICKNESS (SEE TABLE 1)

2.0

21.0

8.0

Note: All dimensions in inches
uture studies should use tolerance of 0.001

ARC LENGTH = 12.0
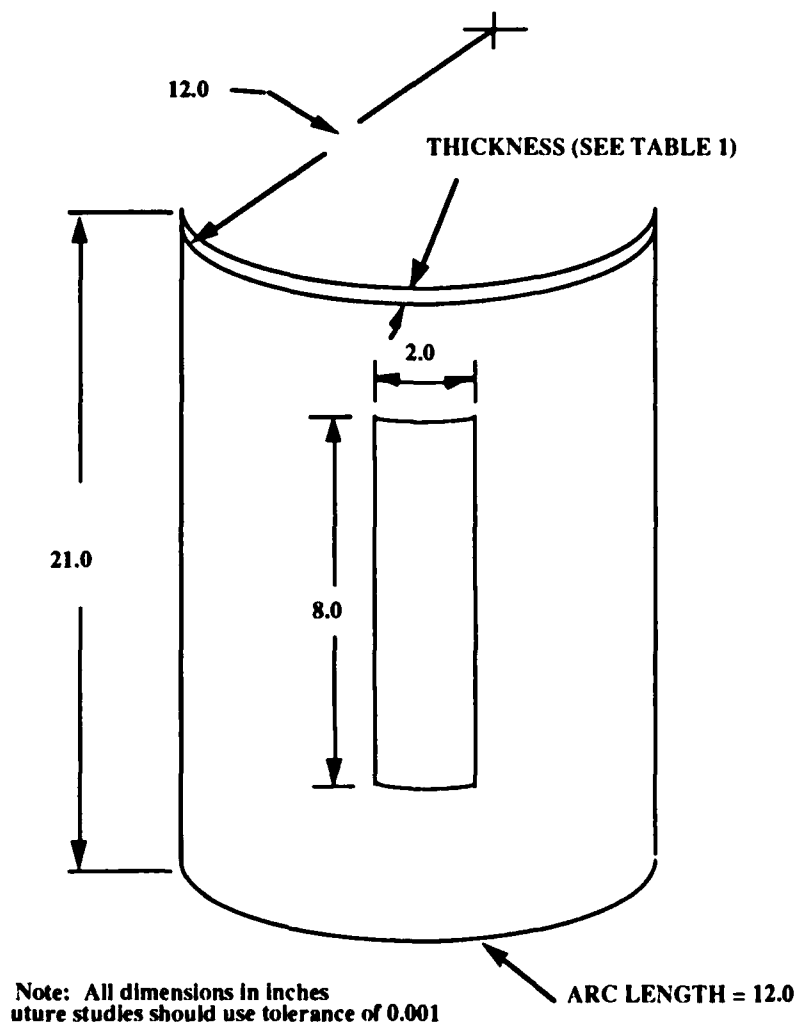
Figure A6. Panel Size 12 x 21 with 2 x 8 Central Cutout

RADIUS OF CURVATURE

12.0

THICKNESS (SEE TABLE 1)

⊥ A .01

13.0

2.0

2.0

Note: All dimensions in inches
uture studies should use tolerance of 0.001

ARC LENGTH = 12.0
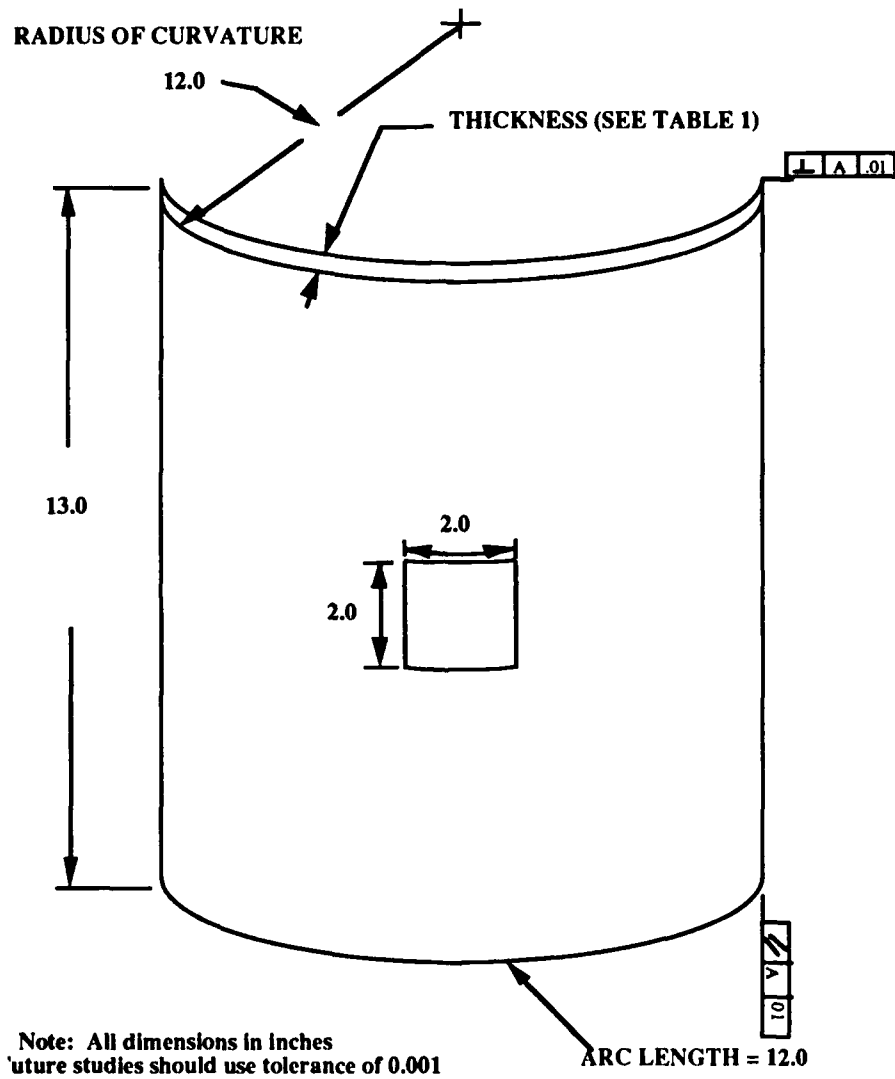
Figure A7. Panel Size 12 x 13 with 2 x 2 Central Cutout

12.0

THICKNESS (SEE TABLE 1)

21.0

2.0

2.0

Note: All dimensions in inches
uture studies should use tolerance of 0.001

ARC LENGTH = 12.0
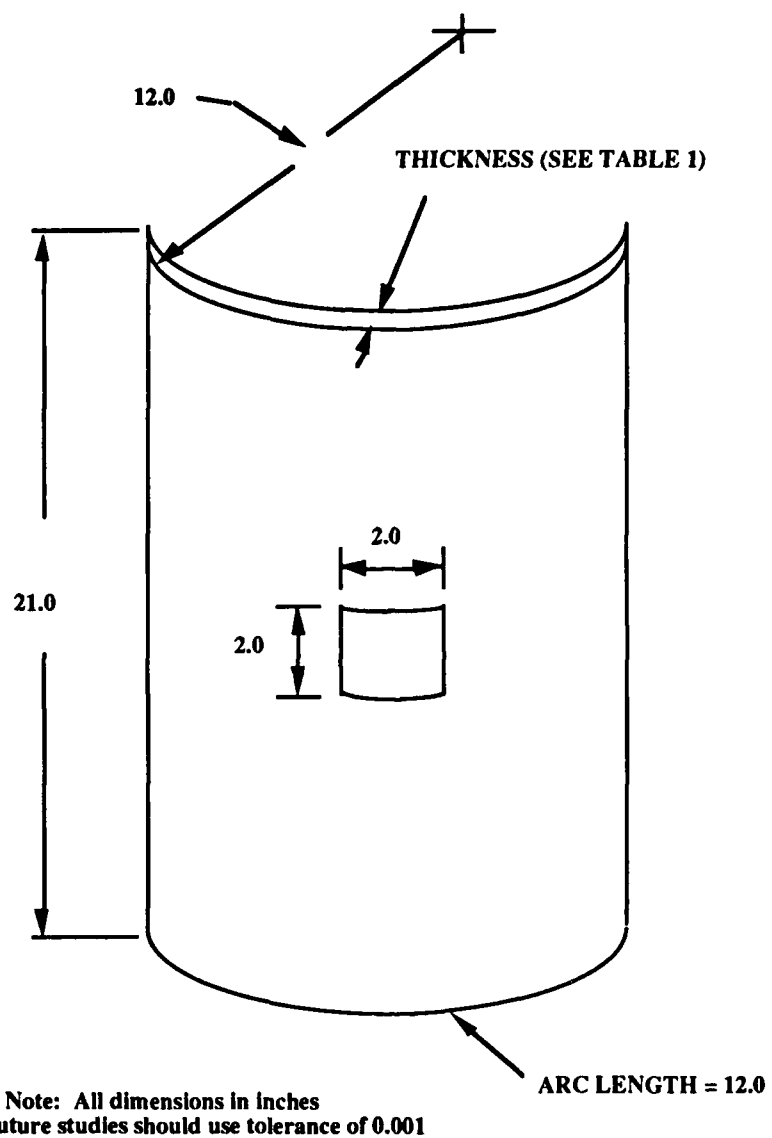
Figure A8. Panel Size 12 x 21 with 2 x 2 Central Cutout

186

RADIUS OF CURVATURE

12.0

THICKNESS (SEE TABLE 1)

⊥ | A | .01

13.0

5.0

5.0

Note: All dimensions in inches
ıture studies should use tolerance of 0.001

ARC LENGTH = 12.0
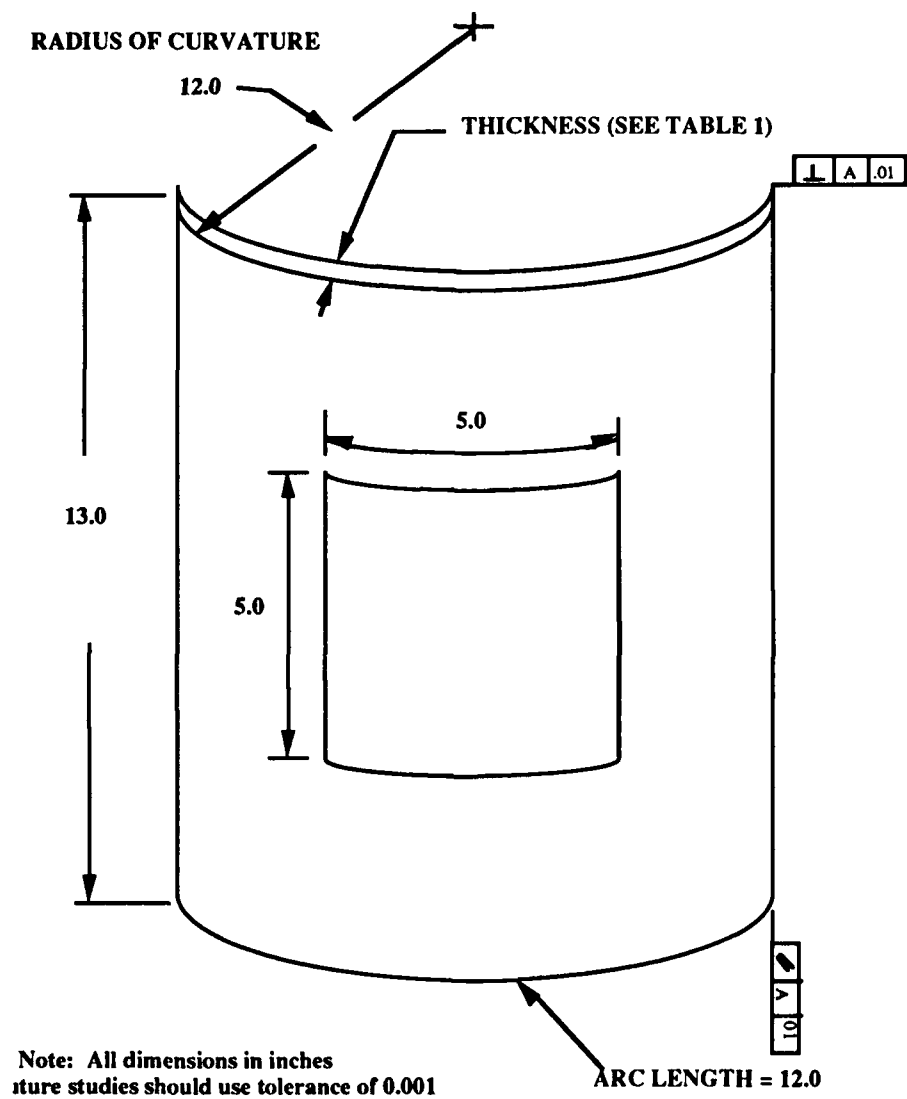
Figure A9. Panel Size 12 x 13 with 5 x 5 Central Cutout

187

12.0

THICKNESS (SEE TABLE 1)

5.0

21.0

5.0

Note: All dimensions in inches
uture studies should use tolerance of 0.001

ARC LENGTH = 12.0
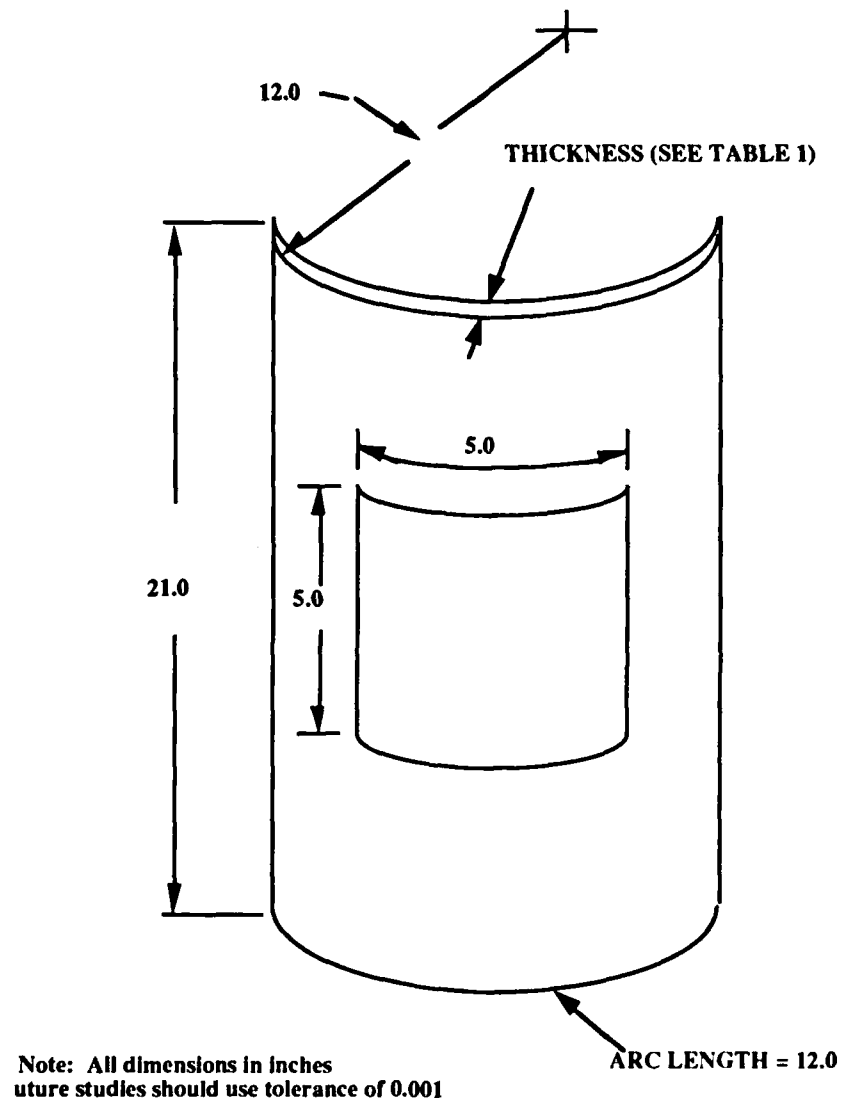
Figure A10. Panel Size 12 x 21 with 5 x 5 Central Cutout

188
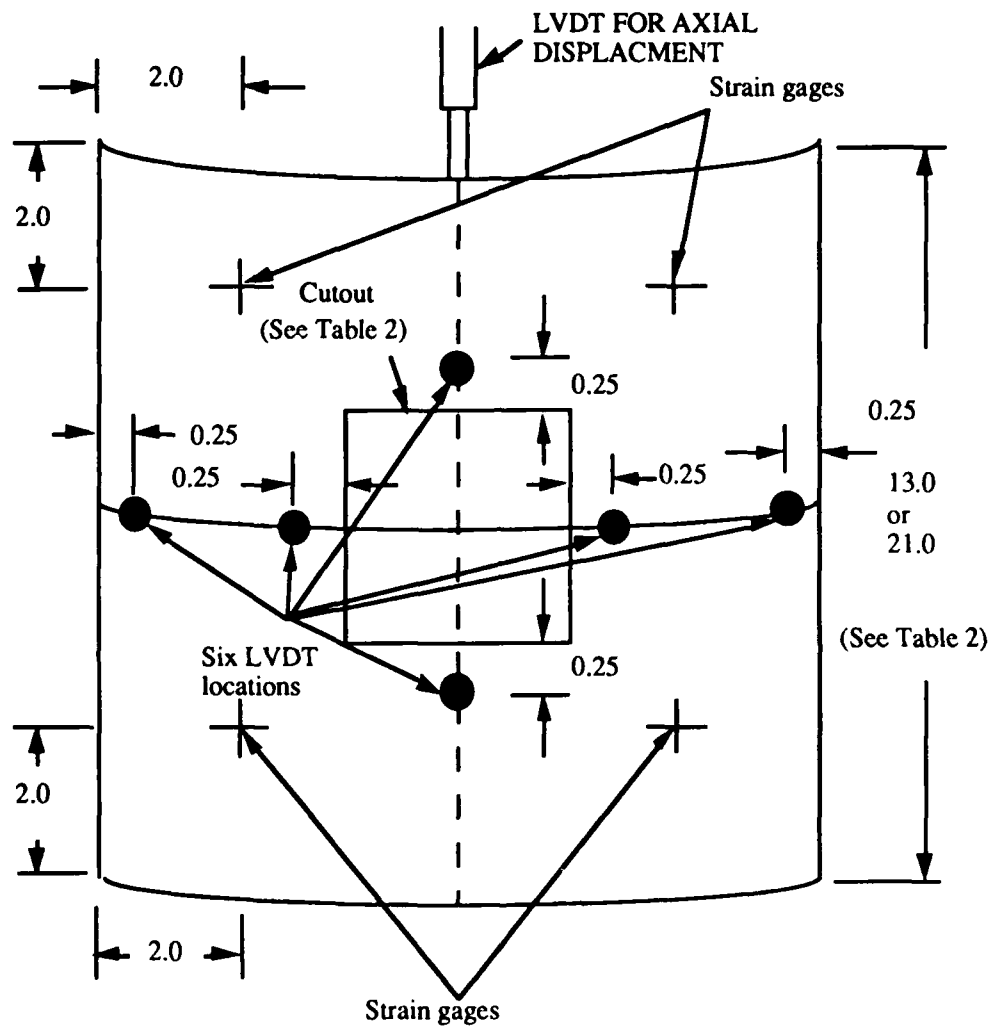
Figure A11. LVDT and Strain Gage Locations

189

Appendix B: Panel Length Tolerance Data

Panel Designator (Experiment #)	Average L	ΔL_{max}
A8-13-22-1 (64, 74)	330.10 mm (12.996")	0.000 mm (0.000")
A8-13-22-2 (65)	330.07 mm (12.995")	0.000 mm (0.000")
A8-13-44-1 (66)	330.07 mm (12.995")	0.000 mm (0.000")
A8-13-44-2 (67)	330.27 mm (13.00267")	0.051 mm (0.002")
A8-13-55-1 (68)	330.05 mm (12.994")	0.051 mm (0.002")
A8-13-55-2 (69)	330.07 mm (12.995")	0.000 mm (0.000")
A8-13-28-1 (70)	330.07 mm (12.995")	0.000 mm (0.000")
A8-13-28-2 (71, 75)	330.12 mm (12.997")	0.000 mm (0.000")
A8-13-82-1 (72, 76)	330.07 mm (12.995")	0.000 mm (0.000")
A8-13-82-2 (73)	330.07 mm (12.995")	0.000 mm (0.000")
A8-21-22-1 (82)	533.48 mm (21.003")	0.000 mm (0.000")
A8-21-22-2 (83)	533.37 mm (20.999")	0.203 mm (0.008")*
A8-21-44-1 (89)	533.43 mm (21.001")	0.076 mm (0.003")
A8-21-44-2 (88)	533.40 mm (21.000")	0.000 mm (0.000")
A8-21-55-1 (94)	533.50 mm (21.004")	0.000 mm (0.000")
A8-21-55-2 (95)	533.39 mm (20.9996")	0.127 mm (0.005")*

Panel Designator (Experiment #)	Average L	ΔL_{max}
A8-21-28-1 (100, 108)	533.53 mm (21.005")	0.000 mm (0.000")
A8-21-28-2 (101)	533.53 mm (21.005")	0.000 mm (0.000")
A8-21-82-1 (107)	533.53 mm (21.005")	0.000 mm (0.000")
A8-21-82-2 (106)	533.45 mm (21.002")	0.051 mm (0.002")
B16-21-22-1 (80)	533.27 mm (20.995")	0.000 mm (0.000")
B16-21-22-2 (81)	533.44 mm (21.0015")	0.076 mm (0.003")
B16-21-44-1 (86)	533.49 mm (21.0035")	0.025 mm (0.001")
B16-21-44-2 (87)	533.30 mm (20.996")	0.000 mm (0.000")
B16-21-55-1 (90)	533.40 mm (21.000")	0.000 mm (0.000")
B16-21-55-2 (91)	533.46 mm (21.0025")	0.025 mm (0.001")
B16-21-28-1 (98)	533.30 mm (20.996")	0.076 mm (0.003")
B16-21-28-2 (99)	533.31 mm (20.9965")	0.025 mm (0.001")
B16-21-82-1 (105)	533.46 mm (21.0025")	0.076 mm (0.003")
B16-21-82-2 (104)	533.43 mm (21.001")	0.051 mm (0.002")
C24-21-22-1 (77, 78)	533.40 mm (21.000")	0.000 mm (0.000")
C24-21-22-2 (79)	533.43 mm (21.001")	0.178 mm (0.007")*

Appendix B. (Continued)

Panel Designator (Experiment #)	Average L	ΔL_{max}
C24-21-44-1 (85)	533.44 mm (21.0017")	0.076 mm (0.003")
C24-21-44-2 (84)	533.48 mm (21.0033")	0.025 mm (0.001")
C24-21-55-1 (92)	533.43 mm (21.001")	0.178 mm (0.007")*
C24-21-55-2 (93)	533.42 mm (21.0007")	0.051 mm (0.002")
C24-21-28-1 (96, 109)	533.48 mm (21.003")	0.152 mm (0.006")*
C24-21-28-2 (97)	533.45 mm (21.002")	0.000 mm (0.000")
C24-21-82-1 (103)	533.45 mm (21.002")	0.000 mm (0.000")
C24-21-82-2 (102)	533.45 mm (21.002")	0.203 mm (0.008")*

* Tolerance of 0.0762 mm (0.003") exceeded.

192

Appendix C. Correlation Table

Panel Designator	Panel Serial Number (S/N)	Experiment Number
A8-13-22-1	1	64
A8-13-22-2	2	65
A8-13-22-1*	1	74
A8-13-44-1	3	66
A8-13-44-2	4	67
A8-13-55-1	5	68
A8-13-55-2	6	69
A8-13-28-1	7	70
A8-13-28-2	8	71
A8-13-28-2*	8	75
A8-13-82-1	9	72
A8-13-82-2	10	73
A8-13-82-1*	9	76
A8-21-22-1	15	82
A8-21-22-2	16	83
A8-21-44-1	22	89
A8-21-44-2	21	88
A8-21-55-1	27	94
A8-21-55-2	28	95
A8-21-28-1	33	100
A8-21-28-2	34	101
A8-21-28-1*	33	108
A8-21-82-1	40	107

Panel Designator	Panel Serial Number (S/N)	Experiment Number
A8-21-82-2	39	106
B16-21-22-1	13	80
B16-21-22-2	14	81
B16-21-44-1	19	86
B16-21-44-2	20	87
B16-21-55-1	23	90
B16-21-55-2	24	91
B16-21-28-1	31	98
B16-21-28-2	32	99
B16-21-82-1	38	105
B16-21-82-2	37	104
C24-21-22-1	11	77
C24-21-22-2	12	79
C24-21-22-1*	11	78
C24-21-44-1	18	85
C24-21-44-2	17	84
C24-21-55-1	25	92
C24-21-55-2	26	93
C24-21-28-1	29	96
C24-21-28-2	30	97
C24-21-28-1*	29	109
C24-21-82-1	36	103
C24-21-82-2	35	102

* Denotes a retest of a panel

APPENDIX D

SAMPLE INPUT DECK USED IN
THE SHELL FINITE ELEMENT PROGRAM

SHELL Input Deck Sequence

* Line 1   Title

* Line 2

   IEL   Element type

                                 IEL = 2 cylindrical shell

   NPE   Nodes per element

                                 NPE = 8

   NANAL(1)   Nonlinear analysis

                                 NANAL(1) = 0

   NANAL(2)   Symmetric laminate

                                 NANAL(2) = 2

   NANAL(3)   Large rotation

                                 NANAL(3) = 0

   IMESH   Automatic mesh generation

                                 IMESH = 1

   NPRNT   Do not print elasticity matrices

                                 NPRNT = 0

   NPRINT   Do not print elemental stiffness
                                            matrices

                                 NPRINT = 0

   NCUT   Number of elements to cutout

* Line 3

   INTYP   Displacement increment type

                                 INTYP = 1

* Line 3 (continued)

NINC   Number of increments

IMAX   Maximum number of iterations

IRES   Do not update stiffness every
                              iteration

                                  IRES = 0

TOL   Percent convergence tolerance

* Lines 4-5

TABLE(NINC)   Real number multiplicative
                              factors of prescribed
                              displacements

* Line 6

NX   Number of elemental subdivisions
                              in the x direction

NY   Number of elemental subdivisions
                              in the y direction

* Lines 7-14

DX(I)   Distance between nodes along
                              the x direction

* Lines 15-20

DY(I)   Distance between nodes along
                              the y direction

* Lines 21-30   Assigned element numbers
                              of cutout to be deleted

* Line 31

LD   Load type parameter

                                  LD = 0

PO   Distributed load intensity

                                  PO = 0.0

* Line 32

    NBDY

Number of nodes with specified primary degrees of freedom (e.g. for this study specified the degrees of freedom at the top and bottom horizontal edge of panel and inside the cutout region)

* Lines 33-77

Specified degrees of freedom for top panel nodes (1 = prescribed and 0 = free)

* Lines 78-122

Specified degrees of freedom for bottom panel nodes

* Lines 123-383

Specified degrees of freedom for nodes which fall within the cutout area (excludes those nodes that fall on the cutout boundary)

* Lines 384-404

Values for the top panel nodes degrees of freedom (either zero or the prescribed displacement increment in inches)

* Lines 404-425

Values for the bottom panel nodes degrees of freedom

* Lines 425-517

Values for the cutout nodes degrees of freedom

* Line 518

    NBSF

Number of point loads (zero)

NBSF = 0

* Line 519

    E1

Young's modulus along fibers

    E2

Young's modulus transverse to fibers

    G12

Shear modulus

    NU12

Major Poisson's ratio

* Line 520

    G13   1-3 Shear modulus

    G23   2-3 Shear modulus

* Line 521

    NP   Number of plies

    PT   Ply thickness

* Lines 522-523   Ply orientation angle

* Line 524   Radius of curvature

* Line 525   Number of nodal forces
to be calculated along the
top edge of the panel

* Lines 526-530   Degree of freedom number
associated with loading
direction (u), for each
panel top edge node

* Line 531   Number of elements stresses
to be calculated for this
study zero

```
1    12X20 [0/45/-45/90}2s 5" Cutout
2    2,8,0,2,0,1,0,0,100
3    1,18,80,0,.001
4    1.,2.,3.,4.,5.,6.,7.,8.,9.,10.,
5    11.,12.,13.,14.,15.,16.,17.,18.
6    30,22
7    0.50,0.50,0.50,0.50,0.50,0.50,0.50,0.50,
8    0.50,0.50,0.25,0.25,0.25,0.25,0.25,0.25,
9    0.25,0.25,0.25,0.25,0.25,0.25,0.25,0.25,
10   0.25,0.25,0.25,0.25,0.25,0.25,0.25,0.25,
11   0.25,0.25,0.25,0.25,0.25,0.25,0.25,0.25,
12   0.25,0.25,0.25,0.25,0.25,0.25,0.25,0.25,
13   0.25,0.25,0.50,0.50,0.50,0.50,0.50,0.50,
14   0.50,0.50,0.50,0.50
15   0.50,0.50,0.25,0.25,0.25,0.25,0.25,0.25,
16   0.25,0.25,0.25,0.25,0.25,0.25,0.25,0.25,
17   0.25,0.25,0.25,0.25,0.25,0.25,0.25,0.25,
18   0.25,0.25,0.25,0.25,0.25,0.25,0.25,0.25,
19   0.25,0.25,0.25,0.25,0.25,0.25,0.25,0.25,
20   0.25,0.25,0.50,0.50
21   191,192,193,194,195,196,197,198,199,200,
22   221,222,223,224,225,226,227,228,229,230,
23   251,252,253,254,255,256,257,258,259,260,
24   281,282,283,284,285,286,287,288,289,290,
25   311,312,313,314,315,316,317,318,319,320,
26   341,342,343,344,345,346,347,348,349,350,
27   371,372,373,374,375,376,377,378,379,380,
28   401,402,403,404,405,406,407,408,409,410,
29   431,432,433,434,435,436,437,438,439,440,
30   461,462,463,464,465,466,467,468,469,470
31   0,0.0
32   351
33   61,1,1,1,1,1,1,1
34   92,1,1,0,0,0,0,0
35   153,1,1,1,1,1,1,1
36   184,1,1,0,0,0,0,0
37   245,1,1,1,1,1,1,1
38   276,1,1,0,0,0,0,0
39   337,1,1,1,1,1,1,1
40   368,1,1,0,0,0,0,0
41   429,1,1,1,1,1,1,1
42   460,1,1,0,0,0,0,0
43   521,1,1,1,1,1,1,1
44   552,1,1,0,0,0,0,0
45   613,1,1,1,1,1,1,1
46   644,1,1,0,0,0,0,0
47   705,1,1,1,1,1,1,1
48   736,1,1,0,0,0,0,0
49   797,1,1,1,1,1,1,1
50   828,1,1,0,0,0,0,0
51   889,1,1,1,1,1,1,1
52   920,1,1,0,0,0,0,0
```

```
53    981,1,1,1,1,1,1,1
54    1012,1,1,0,0,0,0,0
55    1073,1,1,1,1,1,1,1
56    1104,1,1,0,0,0,0,0
57    1165,1,1,1,1,1,1,1
58    1196,1,1,0,0,0,0,0
59    1257,1,1,1,1,1,1,1
60    1288,1,1,0,0,0,0,0
61    1349,1,1,1,1,1,1,1
62    1380,1,1,0,0,0,0,0
63    1441,1,1,1,1,1,1,1
64    1472,1,1,0,0,0,0,0
65    1533,1,1,1,1,1,1,1
66    1564,1,1,0,0,0,0,0
67    1625,1,1,1,1,1,1,1
68    1656,1,1,0,0,0,0,0
69    1717,1,1,1,1,1,1,1
70    1748,1,1,0,0,0,0,0
71    1809,1,1,1,1,1,1,1
72    1840,1,1,0,0,0,0,0
73    1901,1,1,1,1,1,1,1
74    1932,1,1,0,0,0,0,0
75    1993,1,1,1,1,1,1,1
76    2024,1,1,0,0,0,0,0
77    2085,1,1,1,1,1,1,1
78    1,1,1,1,1,1,1,1
79    62,1,1,0,0,0,0,0
80    93,1,1,1,1,1,1,1
81    154,1,1,0,0,0,0,0
82    185,1,1,1,1,1,1,1
83    246,1,1,0,0,0,0,0
84    277,1,1,1,1,1,1,1
85    338,1,1,0,0,0,0,0
86    369,1,1,1,1,1,1,1
87    430,1,1,0,0,0,0,0
88    461,1,1,1,1,1,1,1
89    522,1,1,0,0,0,0,0
90    553,1,1,1,1,1,1,1
91    614,1,1,0,0,0,0,0
92    645,1,1,1,1,1,1,1
93    706,1,1,0,0,0,0,0
94    737,1,1,1,1,1,1,1
95    798,1,1,0,0,0,0,0
96    829,1,1,1,1,1,1,1
97    890,1,1,0,0,0,0,0
98    921,1,1,1,1,1,1,1
99    982,1,1,0,0,0,0,0
100   1013,1,1,1,1,1,1,1
101   1074,1,1,0,0,0,0,0
102   1105,1,1,1,1,1,1,1
103   1166,1,1,0,0,0,0,0
104   1197,1,1,1,1,1,1,1
```

```
105    1258,1,1,0,0,0,0,0
106    1289,1,1,1,1,1,1,1
107    1350,1,1,0,0,0,0,0
108    1381,1,1,1,1,1,1,1
109    1442,1,1,0,0,0,0,0
110    1473,1,1,1,1,1,1,1
111    1534,1,1,0,0,0,0,0
112    1565,1,1,1,1,1,1,1
113    1626,1,1,0,0,0,0,0
114    1657,1,1,1,1,1,1,1
115    1718,1,1,0,0,0,0,0
116    1749,1,1,1,1,1,1,1
117    1810,1,1,0,0,0,0,0
118    1841,1,1,1,1,1,1,1
119    1902,1,1,0,0,0,0,0
120    1933,1,1,1,1,1,1,1
121    1994,1,1,0,0,0,0,0
122    2025,1,1,1,1,1,1,1
123     625,1,1,0,0,0,0,0
124     626,1,1,0,0,0,0,0
125     627,1,1,0,0,0,0,0
126     628,1,1,0,0,0,0,0
127     629,1,1,0,0,0,0,0
128     630,1,1,0,0,0,0,0
129     631,1,1,0,0,0,0,0
130     632,1,1,0,0,0,0,0
131     633,1,1,0,0,0,0,0
132     666,1,1,0,0,0,0,0
133     667,1,1,1,1,1,1,1
134     668,1,1,0,0,0,0,0
135     669,1,1,1,1,1,1,1
136     670,1,1,0,0,0,0,0
137     671,1,1,1,1,1,1,1
138     672,1,1,0,0,0,0,0
139     673,1,1,1,1,1,1,1
140     674,1,1,0,0,0,0,0
141     675,1,1,1,1,1,1,1
142     676,1,1,0,0,0,0,0
143     677,1,1,1,1,1,1,1
144     678,1,1,0,0,0,0,0
145     679,1,1,1,1,1,1,1
146     680,1,1,0,0,0,0,0
147     681,1,1,1,1,1,1,1
148     682,1,1,0,0,0,0,0
149     683,1,1,1,1,1,1,1
150     684,1,1,0,0,0,0,0
151     717,1,1,0,0,0,0,0
152     718,1,1,0,0,0,0,0
153     719,1,1,0,0,0,0,0
154     720,1,1,0,0,0,0,0
155     721,1,1,0,0,0,0,0
156     722,1,1,0,0,0,0,0
```

```
157    723,1,1,0,0,0,0,0
158    724,1,1,0,0,0,0,0
159    725,1,1,0,0,0,0,0
160    758,1,1,0,0,0,0,0
161    759,1,1,1,1,1,1,1
162    760,1,1,0,0,0,0,0
163    761,1,1,1,1,1,1,1
164    762,1,1,0,0,0,0,0
165    763,1,1,1,1,1,1,1
166    764,1,1,0,0,0,0,0
167    765,1,1,1,1,1,1,1
168    766,1,1,0,0,0,0,0
169    767,1,1,1,1,1,1,1
170    768,1,1,0,0,0,0,0
171    769,1,1,1,1,1,1,1
172    770,1,1,0,0,0,0,0
173    771,1,1,1,1,1,1,1
174    772,1,1,0,0,0,0,0
175    773,1,1,1,1,1,1,1
176    774,1,1,0,0,0,0,0
177    775,1,1,1,1,1,1,1
178    776,1,1,0,0,0,0,0
179    809,1,1,0,0,0,0,0
180    810,1,1,0,0,0,0,0
181    811,1,1,0,0,0,0,0
182    812,1,1,0,0,0,0,0
183    813,1,1,0,0,0,0,0
184    814,1,1,0,0,0,0,0
185    815,1,1,0,0,0,0,0
186    816,1,1,0,0,0,0,0
187    817,1,1,0,0,0,0,0
188    850,1,1,0,0,0,0,0
189    851,1,1,1,1,1,1,1
190    852,1,1,0,0,0,0,0
191    853,1,1,1,1,1,1,1
192    854,1,1,0,0,0,0,0
193    855,1,1,1,1,1,1,1
194    856,1,1,0,0,0,0,0
195    857,1,1,1,1,1,1,1
196    858,1,1,0,0,0,0,0
197    859,1,1,1,1,1,1,1
198    860,1,1,0,0,0,0,0
199    861,1,1,1,1,1,1,1
200    862,1,1,0,0,0,0,0
201    863,1,1,1,1,1,1,1
202    864,1,1,0,0,0,0,0
203    865,1,1,1,1,1,1,1
204    866,1,1,0,0,0,0,0
205    867,1,1,1,1,1,1,1
206    868,1,1,0,0,0,0,0
207    901,1,1,0,0,0,0,0
208    902,1,1,0,0,0,0,0
```

```
209    903,1,1,0,0,0,0,0
210    904,1,1,0,0,0,0,0
211    905,1,1,0,0,0,0,0
212    906,1,1,0,0,0,0,0
213    907,1,1,0,0,0,0,0
214    908,1,1,0,0,0,0,0
215    909,1,1,0,0,0,0,0
216    942,1,1,0,0,0,0,0
217    943,1,1,1,1,1,1,1
218    944,1,1,0,0,0,0,0
219    945,1,1,1,1,1,1,1
220    946,1,1,0,0,0,0,0
221    947,1,1,1,1,1,1,1
222    948,1,1,0,0,0,0,0
223    949,1,1,1,1,1,1,1
224    950,1,1,0,0,0,0,0
225    951,1,1,1,1,1,1,1
226    952,1,1,0,0,0,0,0
227    953,1,1,1,1,1,1,1
228    954,1,1,0,0,0,0,0
229    955,1,1,1,1,1,1,1
230    956,1,1,0,0,0,0,0
231    957,1,1,1,1,1,1,1
232    958,1,1,0,0,0,0,0
233    959,1,1,1,1,1,1,1
234    960,1,1,0,0,0,0,0
235    993,1,1,0,0,0,0,0
236    994,1,1,0,0,0,0,0
237    995,1,1,0,0,0,0,0
238    996,1,1,0,0,0,0,0
239    997,1,1,0,0,0,0,0
240    998,1,1,0,0,0,0,0
241    999,1,1,0,0,0,0,0
242    1000,1,1,0,0,0,0,0
243    1001,1,1,0,0,0,0,0
244    1034,1,1,0,0,0,0,0
245    1035,1,1,1,1,1,1,1
246    1036,1,1,0,0,0,0,0
247    1037,1,1,1,1,1,1,1
248    1038,1,1,0,0,0,0,0
249    1039,1,1,1,1,1,1,1
250    1040,1,1,0,0,0,0,0
251    1041,1,1,1,1,1,1,1
252    1042,1,1,0,0,0,0,0
253    1043,1,1,1,1,1,1,1
254    1044,1,1,0,0,0,0,0
255    1045,1,1,1,1,1,1,1
256    1046,1,1,0,0,0,0,0
257    1047,1,1,1,1,1,1,1
258    1048,1,1,0,0,0,0,0
259    1049,1,1,1,1,1,1,1
260    1050,1,1,0,0,0,0,0
```

```
261    1051,1,1,1,1,1,1,1
262    1052,1,1,0,0,0,0,0
263    1085,1,1,0,0,0,0,0
264    1086,1,1,0,0,0,0,0
265    1087,1,1,0,0,0,0,0
266    1088,1,1,0,0,0,0,0
267    1089,1,1,0,0,0,0,0
268    1090,1,1,0,0,0,0,0
269    1091,1,1,0,0,0,0,0
270    1092,1,1,0,0,0,0,0
271    1093,1,1,0,0,0,0,0
272    1126,1,1,0,0,0,0,0
273    1127,1,1,1,1,1,1,1
274    1128,1,1,0,0,0,0,0
275    1129,1,1,1,1,1,1,1
276    1130,1,1,0,0,0,0,0
277    1131,1,1,1,1,1,1,1
278    1132,1,1,0,0,0,0,0
279    1133,1,1,1,1,1,1,1
280    1134,1,1,0,0,0,0,0
281    1135,1,1,1,1,1,1,1
282    1136,1,1,0,0,0,0,0
283    1137,1,1,1,1,1,1,1
284    1138,1,1,0,0,0,0,0
285    1139,1,1,1,1,1,1,1
286    1140,1,1,0,0,0,0,0
287    1141,1,1,1,1,1,1,1
288    1142,1,1,0,0,0,0,0
289    1143,1,1,1,1,1,1,1
290    1144,1,1,0,0,0,0,0
291    1177,1,1,0,0,0,0,0
292    1178,1,1,0,0,0,0,0
293    1179,1,1,0,0,0,0,0
294    1180,1,1,0,0,0,0,0
295    1181,1,1,0,0,0,0,0
296    1182,1,1,0,0,0,0,0
297    1183,1,1,0,0,0,0,0
298    1184,1,1,0,0,0,0,0
299    1185,1,1,0,0,0,0,0
300    1218,1,1,0,0,0,0,0
301    1219,1,1,1,1,1,1,1
302    1220,1,1,0,0,0,0,0
303    1221,1,1,1,1,1,1,1
304    1222,1,1,0,0,0,0,0
305    1223,1,1,1,1,1,1,1
306    1224,1,1,0,0,0,0,0
307    1225,1,1,1,1,1,1,1
308    1226,1,1,0,0,0,0,0
309    1227,1,1,1,1,1,1,1
310    1228,1,1,0,0,0,0,0
311    1229,1,1,1,1,1,1,1
312    1230,1,1,0,0,0,0,0
```

```
313    1231,1,1,1,1,1,1,1
314    1232,1,1,0,0,0,0,0
315    1233,1,1,1,1,1,1,1
316    1234,1,1,0,0,0,0,0
3?7    1235,1,1,1,1,1,1,1
318    1236,1,1,0,0,0,0,0
319    1269,1,1,0,0,0,0,0
320    1270,1,1,0,0,0,0,0
321    1271,1,1,0,0,0,0,0
322    1272,1,1,0,0,0,0,0
323    1273,1,1,0,0,0,0,0
324    1274,1,1,0,0,0,0,0
325    1275,1,1,0,0,0,0,0
326    1276,1,1,0,0,0,0,0
327    1277,1,1,0,0,0,0,0
328    1310,1,1,0,0,0,0,0
329    1311,1,1,1,1,1,1,1
330    1312,1,1,0,0,0,0,0
331    1313,1,1,1,1,1,1,1
332    1314,1,1,0,0,0,0,0
333    1315,1,1,1,1,1,1,1
334    1316,1,1,0,0,0,0,0
335    1317,1,1,1,1,1,1,1
336    1318,1,1,0,0,0,0,0
337    1319,1,1,1,1,1,1,1
338    1320,1,1,0,0,0,0,0
339    1321,1,1,1,1,1,1,1
340    1322,1,1,0,0,0,0,0
341    1323,1,1,1,1,1,1,1
342    1324,1,1,0,0,0,0,0
343    1325,1,1,1,1,1,1,1
344    1326,1,1,0,0,0,0,0
345    1327,1,1,1,1,1,1,1
346    1328,1,1,0,0,0,0,0
347    1361,1,1,0,0,0,0,0
348    1362,1,1,0,0,0,0,0
349    1363,1,1,0,0,0,0,0
350    1634,1,1,0,0,0,0,0
351    1365,1,1,0,0,0,0,0
352    1366,1,1,0,0,0,0,0
353    1367,1,1,0,0,0,0,0
354    1368,1,1,0,0,0,0,0
355    1369,1,1,0,0,0,0,0
356    1402,1,1,0,0,0,0,0
357    1403,1,1,1,1,1,1,1
358    1404,1,1,0,0,0,0,0
359    1405,1,1,1,1,1,1,1
360    1406,1,1,0,0,0,0,0
361    1407,1,1,1,1,1,1,1
362    1408,1,1,0,0,0,0,0
363    1409,1,1,1,1,1,1,1
364    1410,1,1,0,0,0,0,0
```

```
365    1411,1,1,1,1,1,1,1
366    1412,1,1,0,0,0,0,0
367    1413,1,1,1,1,1,1,1
368    1414,1,1,0,0,0,0,0
369    1415,1,1,1,1,1,1,1
370    1416,1,1,0,0,0,0,0
371    1417,1,1,1,1,1,1,1
372    1418,1,1,0,0,0,0,0
373    1419,1,1,1,1,1,1,1
374    1420,1,1,0,0,0,0,0
375    1453,1,1,0,0,0,0,0
376    1454,1,1,0,0,0,0,0
377    1455,1,1,0,0,0,0,0
378    1456,1,1,0,0,0,0,0
379    1457,1,1,0,0,0,0,0
380    1458,1,1,0,0,0,0,0
381    1459,1,1,0,0,0,0,0
382    1460,1,1,0,0,0,0,0
383    1461,1,1,0,0,0,0,0
384    -.001,0.,0.,0.,0.,0.,0.,-.001,0.,-.001,
385    0.,0.,0.,0.,0.,0.,-.001,0.,-.001,0.,
386    0.,0.,0.,0.,0.,-.001,0.,-.001,0.,0.,
387    0.,0.,0.,0.,-.001,0.,-.001,0.,0.,0.,
388    0.,0.,0.,-.001,0.,-.001,0.,0.,0.,0.,
389    0.,0.,-.001,0.,-.001,0.,0.,0.,0.,0.,
390    0.,-.001,0.,-.001,0.,0.,0.,0.,0.,0.,
391    -.001,0.,-.001,0.,0.,0.,0.,0.,0.,-.001,
392    0.,-.001,0.,0.,0.,0.,0.,0.,-.001,0.,
393    -.001,0.,0.,0.,0.,0.,0.,-.001,0.,-.001,
394    0.,0.,0.,0.,0.,0.,-.001,0.,-.001,0.,
395    0.,0.,0.,0.,0.,-.001,0.,-.001,0.,0.,
396    0.,0.,0.,0.,-.001,0.,-.001,0.,0.,0.,
397    0.,0.,0.,-.001,0.,-.001,0.,0.,0.,0.,
398    0.,0.,-.001,0.,-.001,0.,0.,0.,0.,0.,
399    0.,-.001,0.,-.001,0.,0.,0.,0.,0.,0.,
400    -.001,0.,-.001,0.,0.,0.,0.,0.,0.,-.001,
401    0.,-.001,0.,0.,0.,0.,0.,0.,-.001,0.,
402    -.001,0.,0.,0.,0.,0.,0.,-.001,0.,-.001,
403    0.,0.,0.,0.,0.,0.,-.001,0.,-.001,0.,
404    0.,0.,0.,0.,0.,0.,0.,0.,0.,0.,
405    0.,0.,0.,0.,0.,0.,0.,0.,0.,0.,
406    0.,0.,0.,0.,0.,0.,0.,0.,0.,0.,
407    0.,0.,0.,0.,0.,0.,0.,0.,0.,0.,
408    0.,0.,0.,0.,0.,0.,0.,0.,0.,0.,
409    0.,0.,0.,0.,0.,0.,0.,0.,0.,0.,
410    0.,0.,0.,0.,0.,0.,0.,0.,0.,0.,
411    0.,0.,0.,0.,0.,0.,0.,0.,0.,0.,
412    0.,0.,0.,0.,0.,0.,0.,0.,0.,0.,
413    0.,0.,0.,0.,0.,0.,0.,0.,0.,0.,
414    0.,0.,0.,0.,0.,0.,0.,0.,0.,0.,
415    0.,0.,0.,0.,0.,0.,0.,0.,0.,0.,
416    0.,0.,0.,0.,0.,0.,0.,0.,0.,0.,
```

```
417    0.,0.,0.,0.,0.,0.,0.,0.,0.,0.,
418    0.,0.,0.,0.,0.,0.,0.,0.,0.,0.,
419    0.,0.,0.,0.,0.,0.,0.,0.,0.,0.,
420    0.,0.,0.,0.,0.,0.,0.,0.,0.,0.,
421    0.,0.,0.,0.,0.,0.,0.,0.,0.,0.,
422    0.,0.,0.,0.,0.,0.,0.,0.,0.,0.,
423    0.,0.,0.,0.,0.,0.,0.,0.,0.,0.,
424    0.,0.,0.,0.,0.,0.,0.,0.,0.,0.,
425    0.,0.,0.,0.,0.,0.,0.,0.,0.,0.,
426    0.,0.,0.,0.,0.,0.,0.,0.,0.,0.,
427    0.,0.,0.,0.,0.,0.,0.,0.,0.,0.,
428    0.,0.,0.,0.,0.,0.,0.,0.,0.,0.,
429    0.,0.,0.,0.,0.,0.,0.,0.,0.,0.,
430    0.,0.,0.,0.,0.,0.,0.,0.,0.,0.,
431    0.,0.,0.,0.,0.,0.,0.,0.,0.,0.,
432    0.,0.,0.,0.,0.,0.,0.,0.,0.,0.,
433    0.,0.,0.,0.,0.,0.,0.,0.,0.,0.,
434    0.,0.,0.,0.,0.,0.,0.,0.,0.,0.,
435    0.,0.,0.,0.,0.,0.,0.,0.,0.,0.,
436    0.,0.,0.,0.,0.,0.,0.,0.,0.,0.,
437    0.,0.,0.,0.,0.,0.,0.,0.,0.,0.
438    0.,0.,0.,0.,0.,0.,0.,0.,0.,0.,
439    0.,0.,0.,0.,0.,0.,0.,0.,0.,0.,
440    0.,0.,0.,0.,0.,0.,0.,0.,0.,0.,
441    0.,0.,0.,0.,0.,0.,0.,0.,0.,0.,
442    0.,0.,0.,0.,0.,0.,0.,0.,0.,0.,
443    0.,0.,0.,0.,0.,0.,0.,0.,0.,0.,
444    0.,0.,0.,0.,0.,0.,0.,0.,0.,0.
445    0.,0.,0.,0.,0.,0.,0.,0.,0.,0.,
446    0.,0.,0.,0.,0.,0.,0.,0.,0.,0.,
447    0.,0.,0.,0.,0.,0.,0.,0.,0.,0.,
448    0.,0.,0.,0.,0.,0.,0.,0.,0.,0.,
449    0.,0.,0.,0.,0.,0.,0.,0.,0.,0.,
450    0.,0.,0.,0.,0.,0.,0.,0.,0.,0.,
451    0.,0.,0.,0.,0.,0.,0.,0.,0.,0.,
452    0.,0.,0.,0.,0.,0.,0.,0.,0.,0.
453    0.,0.,0.,0.,0.,0.,0.,0.,0.,0.,
454    0.,0.,0.,0.,0.,0.,0.,0.,0.,0.,
455    0.,0.,0.,0.,0.,0.,0.,0.,0.,0.,
456    0.,0.,0.,0.,0.,0.,0.,0.,0.,0.,
457    0.,0.,0.,0.,0.,0.,0.,0.,0.,0.,
458    0.,0.,0.,0.,0.,0.,0.,0.,0.,0.,
459    0.,0.,0.,0.,0.,0.,0.,0.,0.,0.,
460    0.,0.,0.,0.,0.,0.,0.,0.,0.,0.,
461    0.,0.,0.,0.,0.,0.,0.,0.,0.,0.,
462    0.,0.,0.,0.,0.,0.,0.,0.,0.,0.,
463    0.,0.,0.,0.,0.,0.,0.,0.,0.,0.,
464    0.,0.,0.,0.,0.,0.,0.,0.,0.,0.,
465    0.,0.,0.,0.,0.,0.,0.,0.,0.,0.,
466    0.,0.,0.,0.,0.,0.,0.,0.,0.,0.,
467    0.,0.,0.,0.,0.,0.,0.,0.,0.,0.,
468    0.,0.,0.,0.,0.,0.,0.,0.,0.,0.,
```

```
469  0.,0.,0.,0.,0.,0.,0.,0.,0.,0.,
470  0.,0.,0.,0.,0.,0.,0.,0.,0.,0.,
471  0.,0.,0.,0.,0.,0.,0.,0.,0.,0.,
472  0.,0.,0.,0.,0.,0.,0.,0.,0.,0.,
473  0.,0.,0.,0.,0.,0.,0.,0.,0.,0.,
474  0.,0.,0.,0.,0.,0.,0.,0.,0.,0.,
475  0.,0.,0.,0.,0.,0.,0.,0.,0.,0.,
476  0.,0.,0.,0.,0.,0.,0.,0.,0.,0.,
477  0.,0.,0.,0.,0.,0.,0.,0.,0.,0.,
478  0.,0.,0.,0.,0.,0.,0.,0.,0.,0.,
479  0.,0.,0.,0.,0.,0.,0.,0.,0.,0.,
480  0.,0.,0.,0.,0.,0.,0.,0.,0.,0.,
481  0.,0.,0.,0.,0.,0.,0.,0.,0.,0.,
482  0.,0.,0.,0.,0.,0.,0.,0.,0.,0.,
483  0.,0.,0.,0.,0.,0.,0.,0.,0.,0.,
484  0.,0.,0.,0.,0.,0.,0.,0.,0.,0.,
485  0.,0.,0.,0.,0.,0.,0.,0.,0.,0.,
486  0.,0.,0.,0.,0.,0.,0.,0.,0.,0.,
487  0.,0.,0.,0.,0.,0.,0.,0.,0.,0.,
488  0.,0.,0.,0.,0.,0.,0.,0.,0.,0.,
489  0.,0.,0.,0.,0.,0.,0.,0.,0.,0.,
490  0.,0.,0.,0.,0.,0.,0.,0.,0.,0.,
491  0.,0.,0.,0.,0.,0.,0.,0.,0.,0.,
492  0.,0.,0.,0.,0.,0.,0.,0.,0.,0.,
493  0.,0.,0.,0.,0.,0.,0.,0.,0.,0.,
494  0.,0.,0.,0.,0.,0.,0.,0.,0.,0.,
495  0.,0.,0.,0.,0.,0.,0.,0.,0.,0.,
496  0.,0.,0.,0.,0.,0.,0.,0.,0.,0.,
497  0.,0.,0.,0.,0.,0.,0.,0.,0.,0.,
498  0.,0.,0.,0.,0.,0.,0.,0.,0.,0.,
499  0.,0.,0.,0.,0.,0.,0.,0.,0.,0.,
500  0.,0.,0.,0.,0.,0.,0.,0.,0.,0.,
501  0.,0.,0.,0.,0.,0.,0.,0.,0.,0.,
502  0.,0.,0.,0.,0.,0.,0.,0.,0.,0.,
503  0.,0.,0.,0.,0.,0.,0.,0.,0.,0.,
504  0.,0.,0.,0.,0.,0.,0.,0.,0.,0.,
505  0.,0.,0.,0.,0.,0.,0.,0.,0.,0.,
506  0.,0.,0.,0.,0.,0.,0.,0.,0.,0.,
507  0.,0.,0.,0.,0.,0.,0.,0.,0.,0.,
508  0.,0.,0.,0.,0.,0.,0.,0.,0.,0.,
509  0.,0.,0.,0.,0.,0.,0.,0.,0.,0.,
510  0.,0.,0.,0.,0.,0.,0.,0.,0.,0.,
511  0.,0.,0.,0.,0.,0.,0.,0.,0.,0.,
512  0.,0.,0.,0.,0.,0.,0.,0.,0.,0.,
513  0.,0.,0.,0.,0.,0.,0.,0.,0.,0.,
514  0.,0.,0.,0.,0.,0.,0.,0.,0.,0.,
515  0.,0.,0.,0.,0.,0.,0.,0.,0.,0.,
516  0.,0.,0.,0.,0.,0.,0.,0.,0.,0.,
517  0.,0.,0.,0.,0.,0.,0.
518  0
519  19.7e6,1.579e6,0.925e6,0.276,
520  0.925e6,0.462e6
```

```
521    16,0.00539
522    0.,45.,-45.,90.,0.,45.,-45.,90.,90.,-45.,
523    45.,0.,90.,-45.,45.,0.
524    12.0
525    45
526    271,338,610,677,949,1016,1288,1355,1627,1694,
527    1966,2033,2305,2372,2644,2711,2983,3050,3322,
528    3389,3661,3728,4000,4067,4339,4406,4678,4775,
529    5017,5084,5356,5423,5695,5762,6034,6101,6373,
530    6440,6712,6779,7051,7118,7390,7457,7729
531    0
```

APPENDIX E

ADDITIONAL NUMERICAL/EXPERIMENTAL
AXIAL LOAD VERSUS DISPLACEMENT CURVES
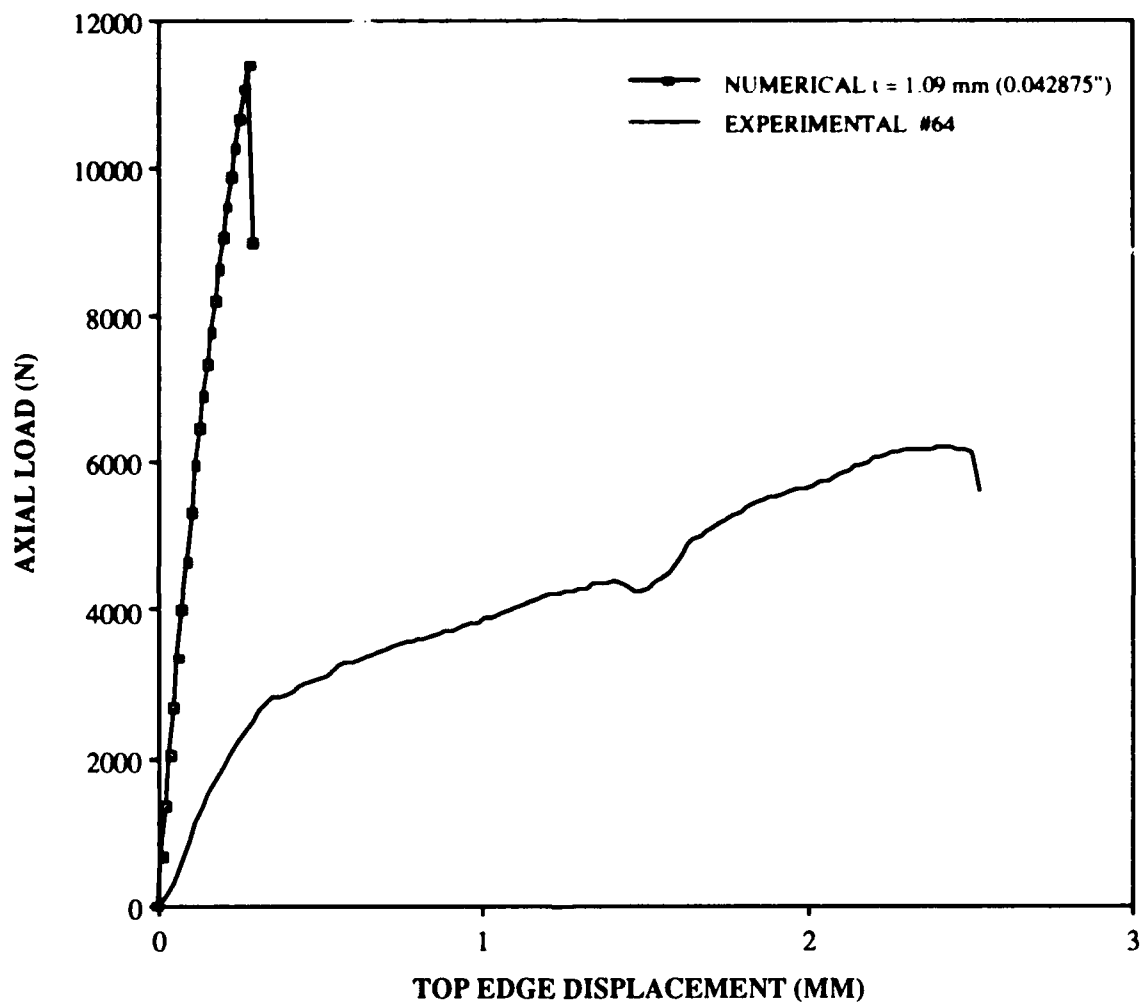
Fig. 84: Load vs. Top Edge Displacement,
Numerical Compared to Experiment #64,
50.8 mm x 50.8 mm (2" x 2") Cutout
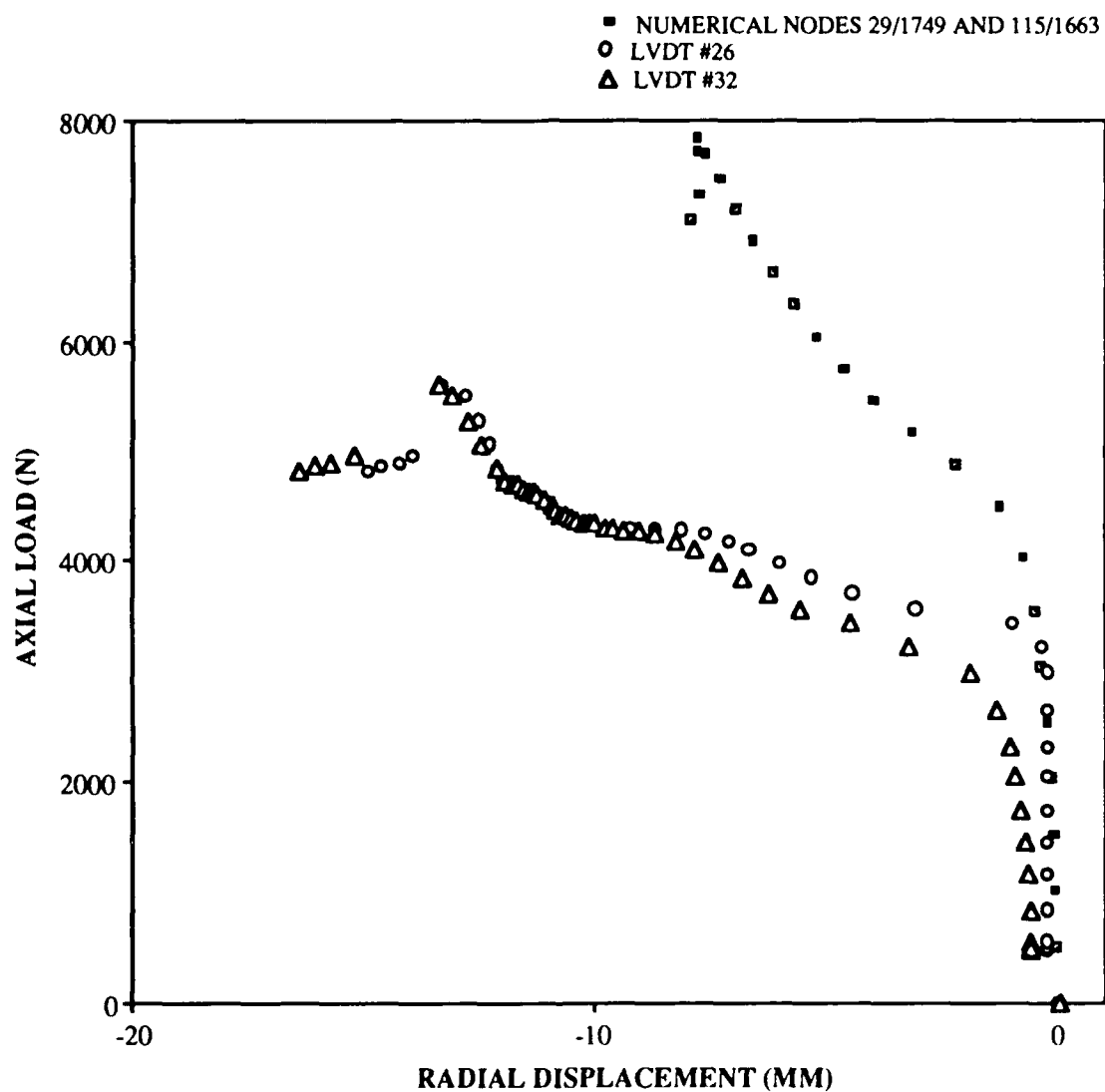304.8 mm x 304.8 mm (12" X 12") Panel
[0/45/-45/90]s
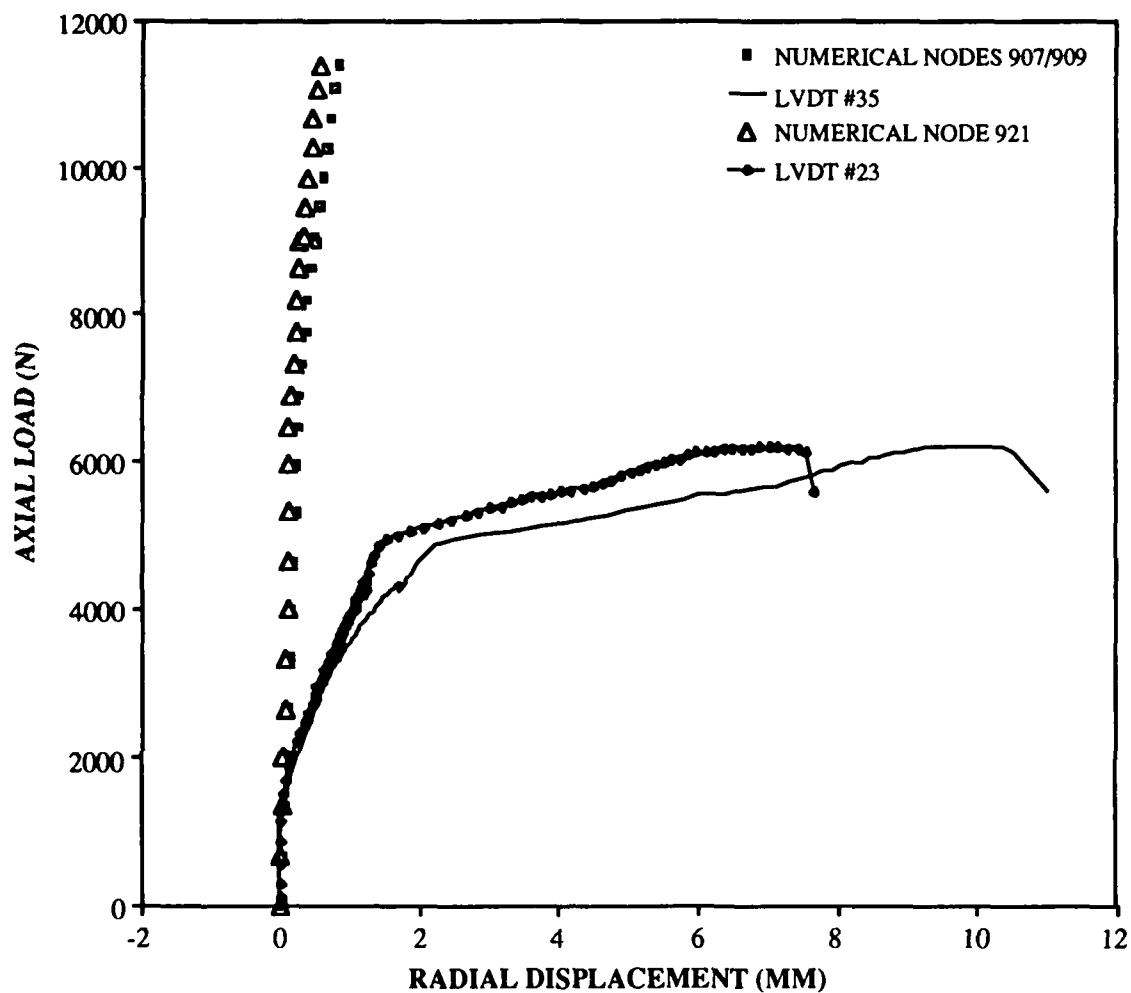
Fig. 85: Load vs. Radial Displacement,
Numerical Compared to Experiment #64,
50.8 mm x 50.8 mm (2" x 2") Cutout,
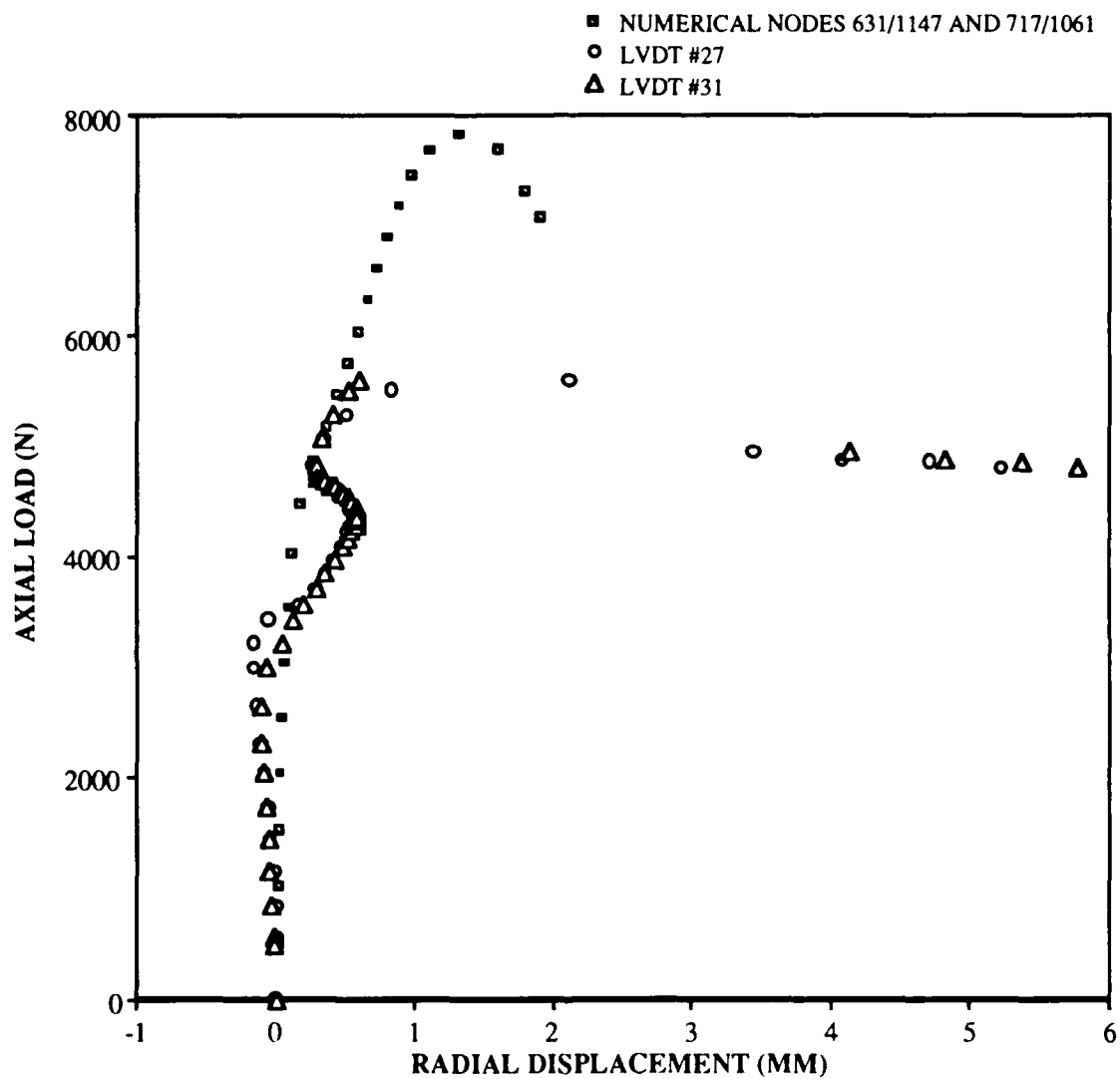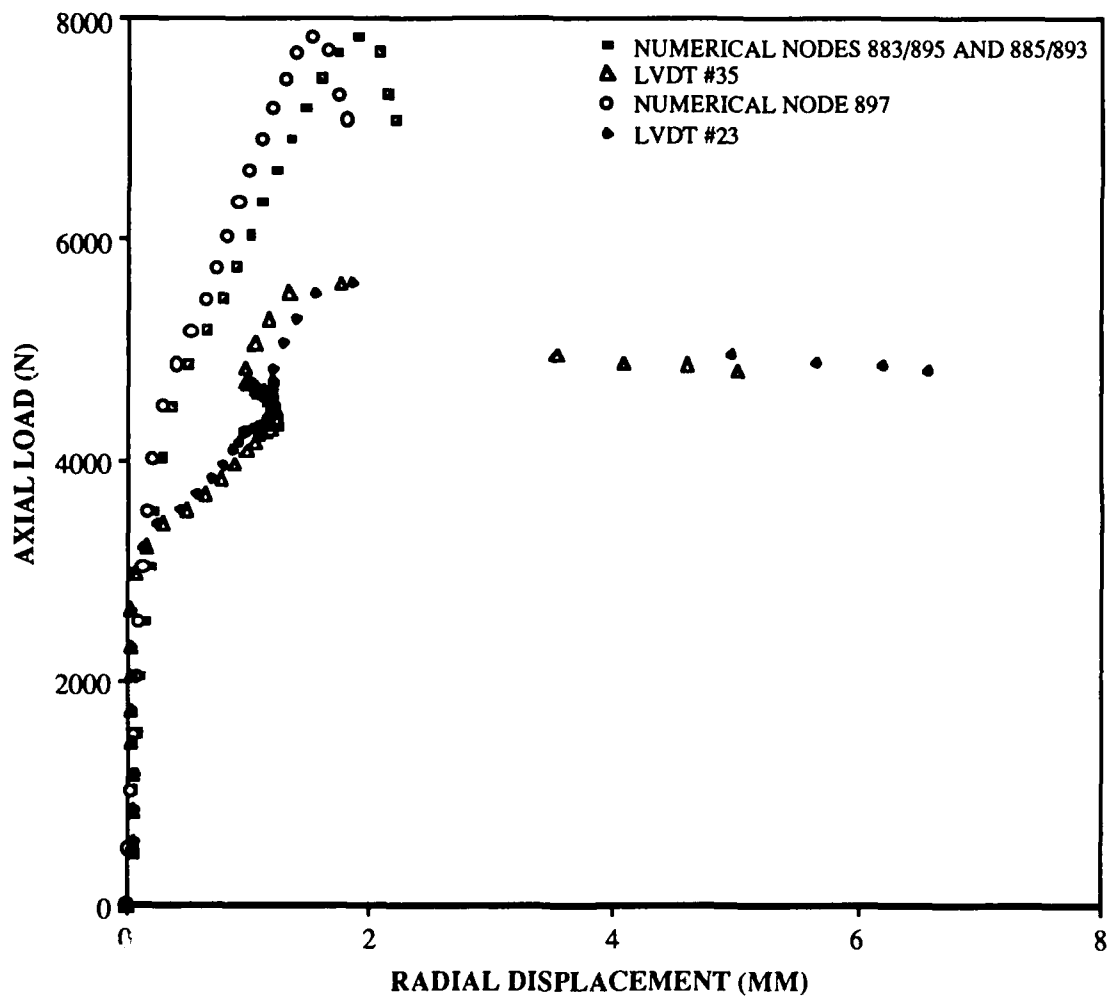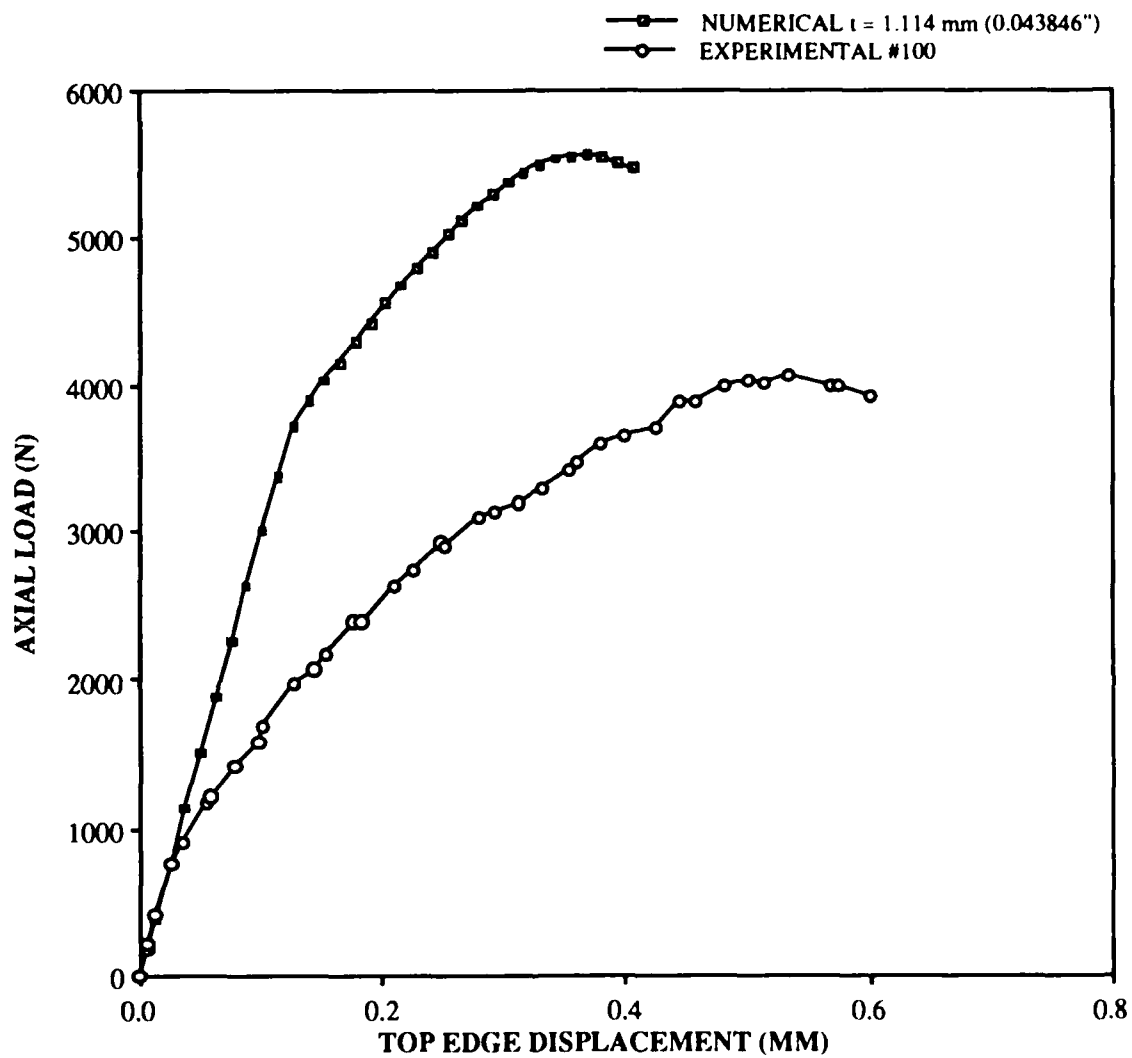304.8 mm x 304.8 mm (12" x 12") Panel,
[0/45/-45/90]s
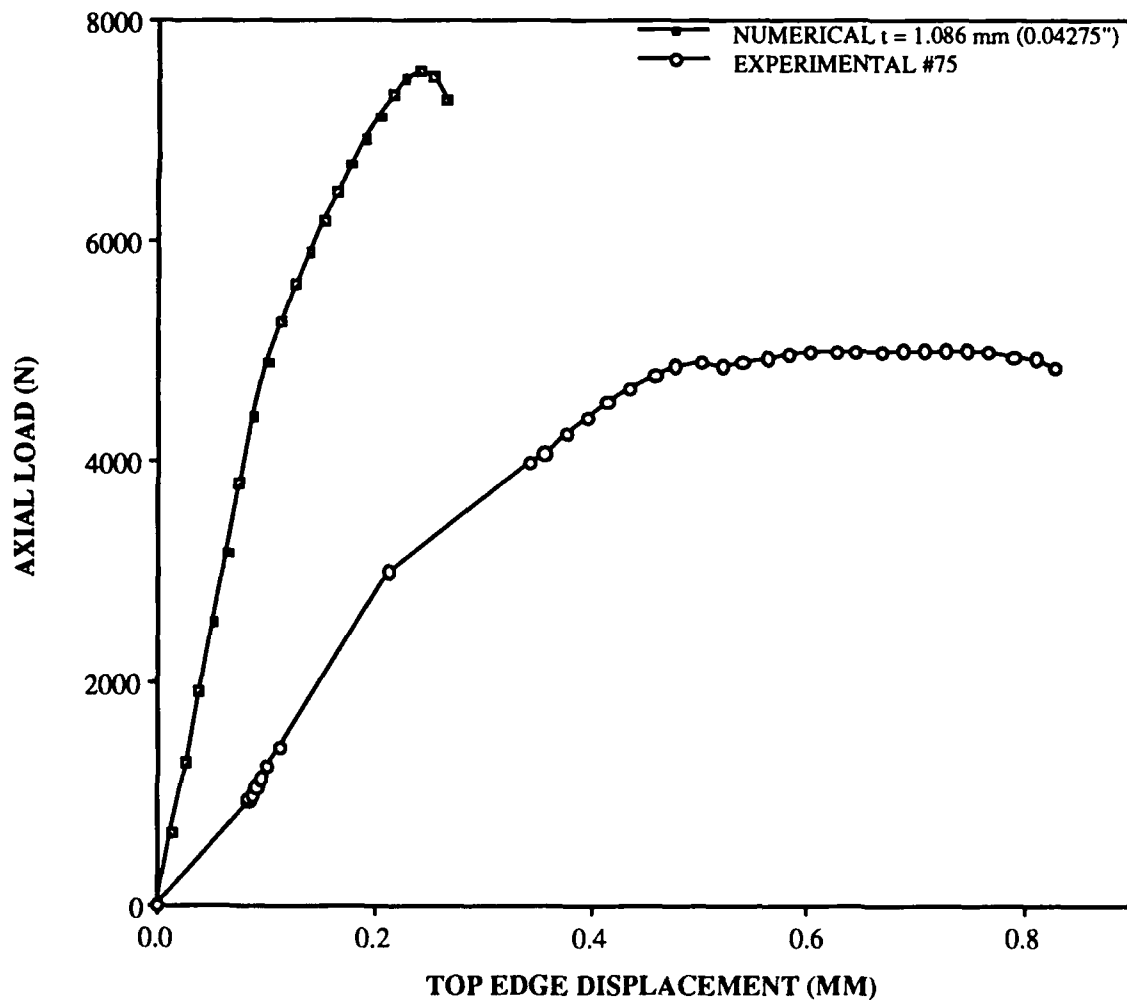
Fig. 86: Load vs. Top Edge Displacement,
Numerical Compared to Experiment #75,
50.8 mm x 203.2 mm (2" x 8") Cutout,
304.8 mm x 304.8 mm (12" x 12") Panel,
[0/45/-45/90]s
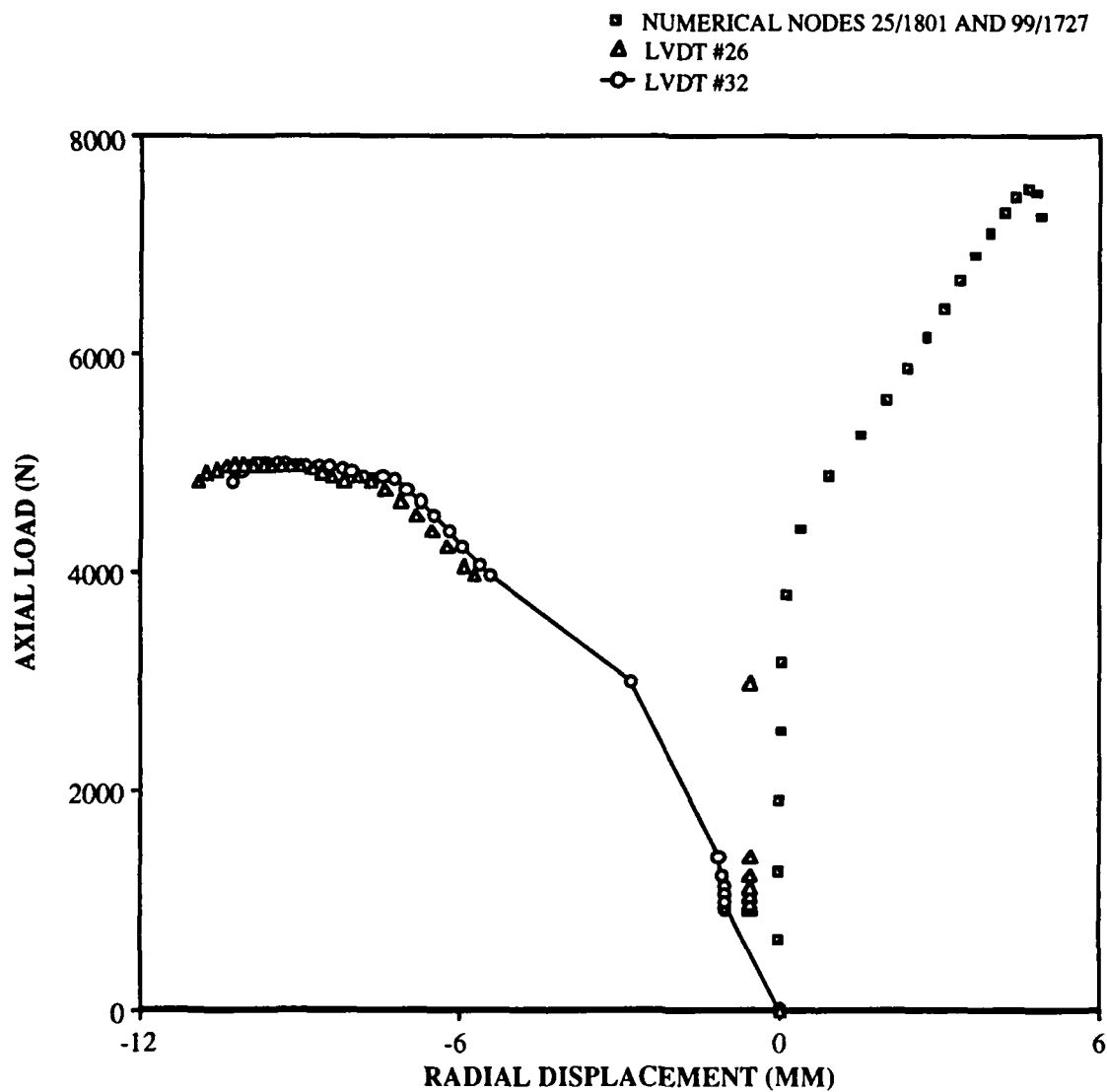
Fig. 87: Load vs. Radial Displacement,
Numerical Compared to Experiment #75,
50.8 mm x 203.2 mm (2" x 8") Cutout,
304.8 mm x 304.8 mm (12" x 12") Panel,
[0/45/-45/90]s

215
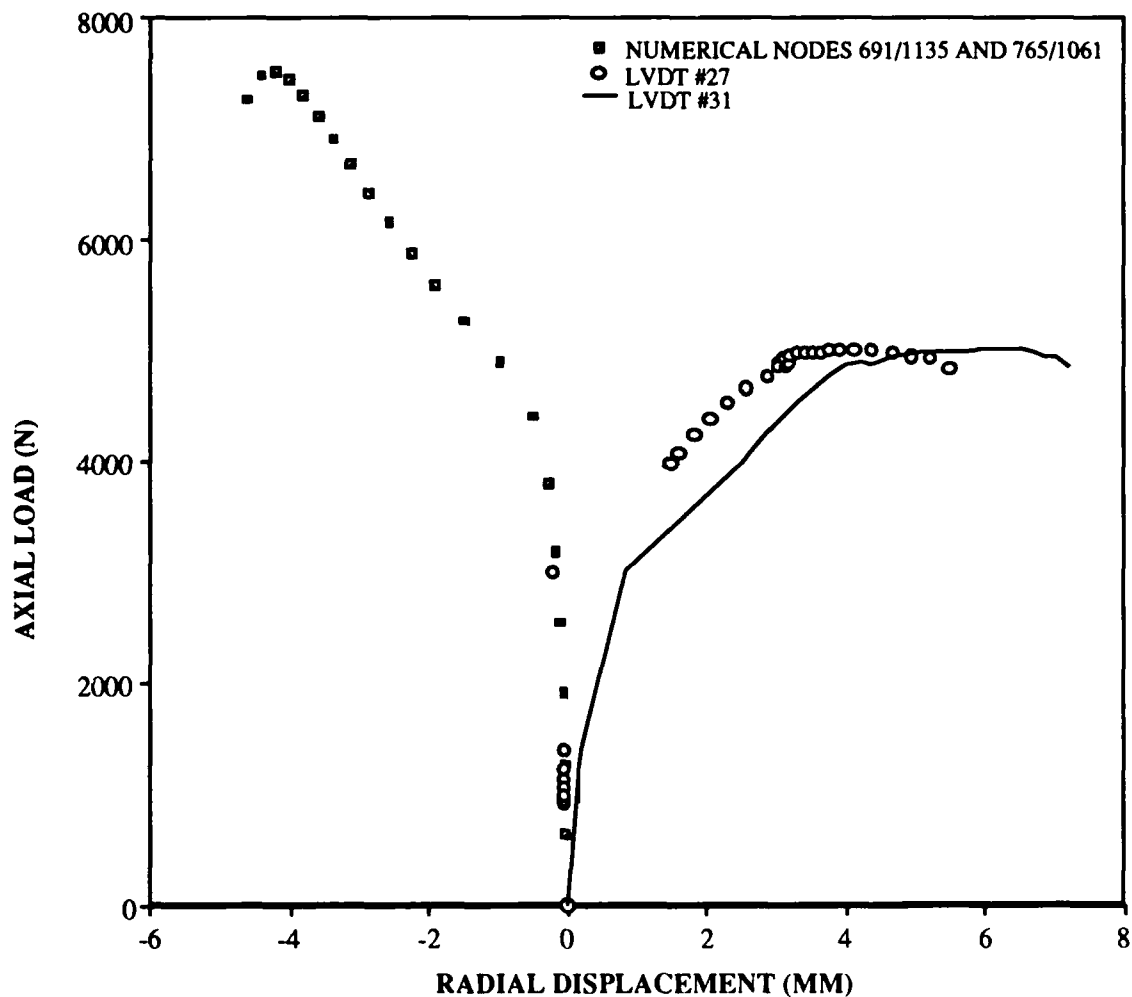
Fig. 88: Load vs. Radial Displacement,
Numerical Compared to Experiment #75,
50.8 mm x 203.2 mm (2" x 8") Cutout,
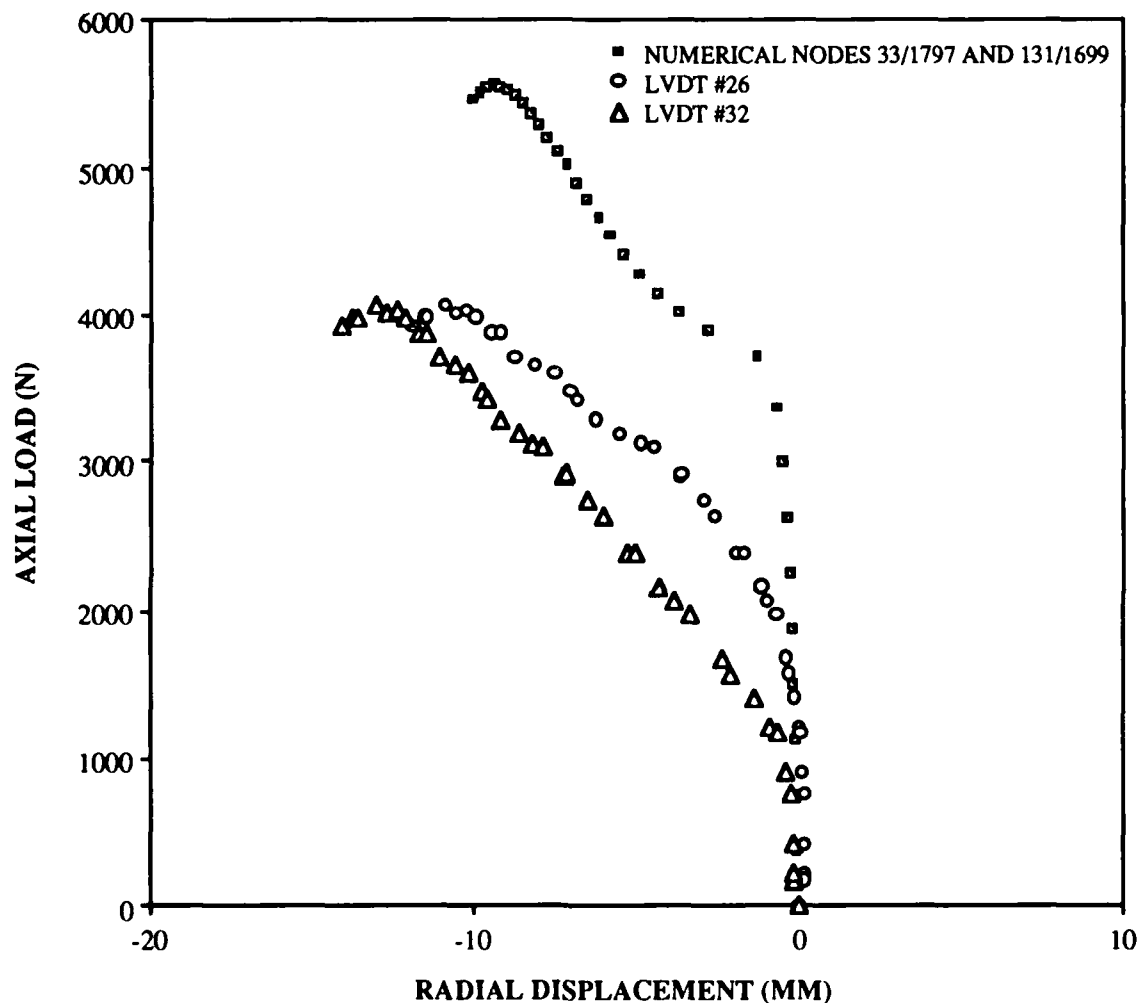304.8 mm x 304.8 mm (12" x 12") Panel,
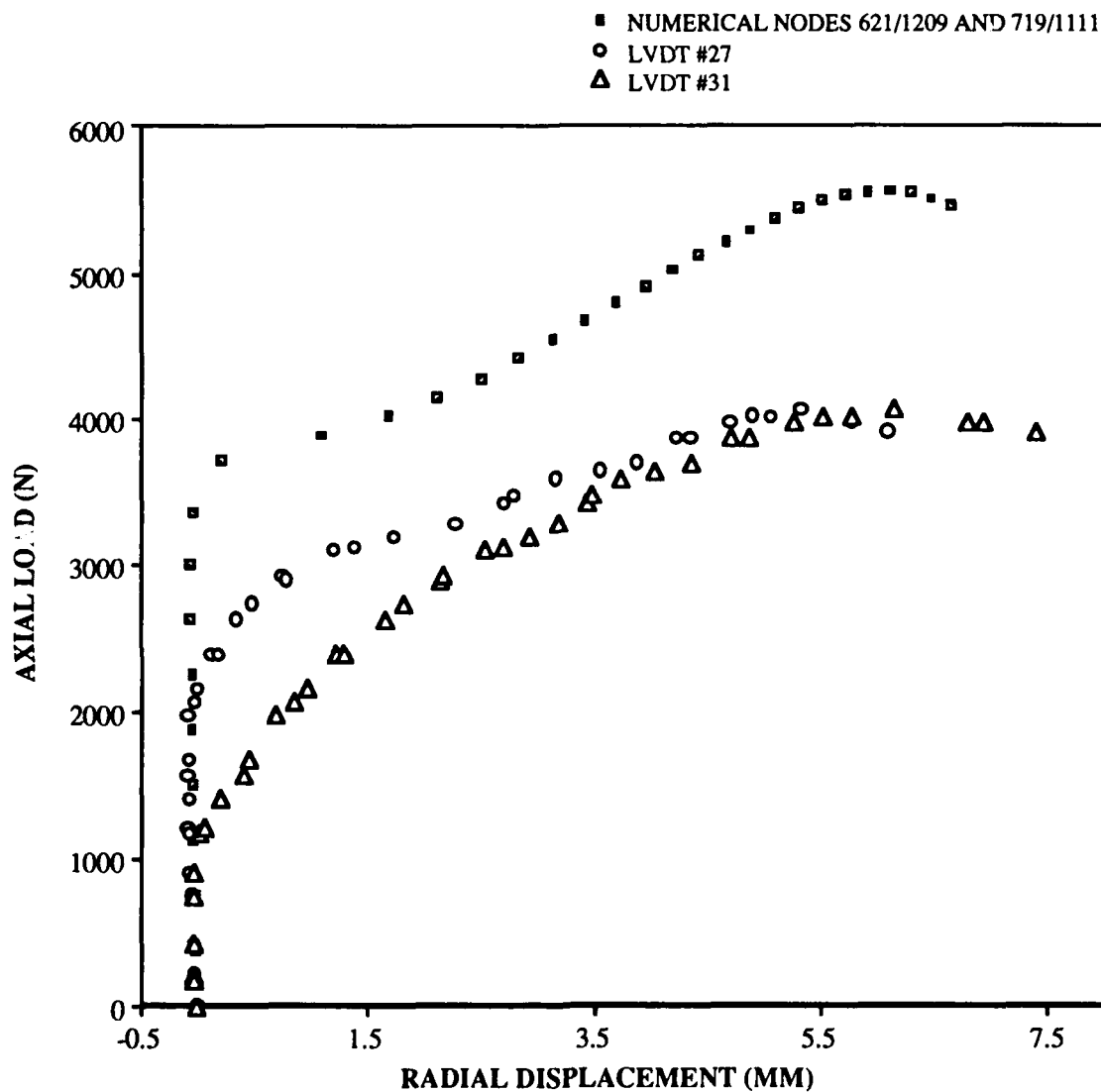[0/45/-45/90]s
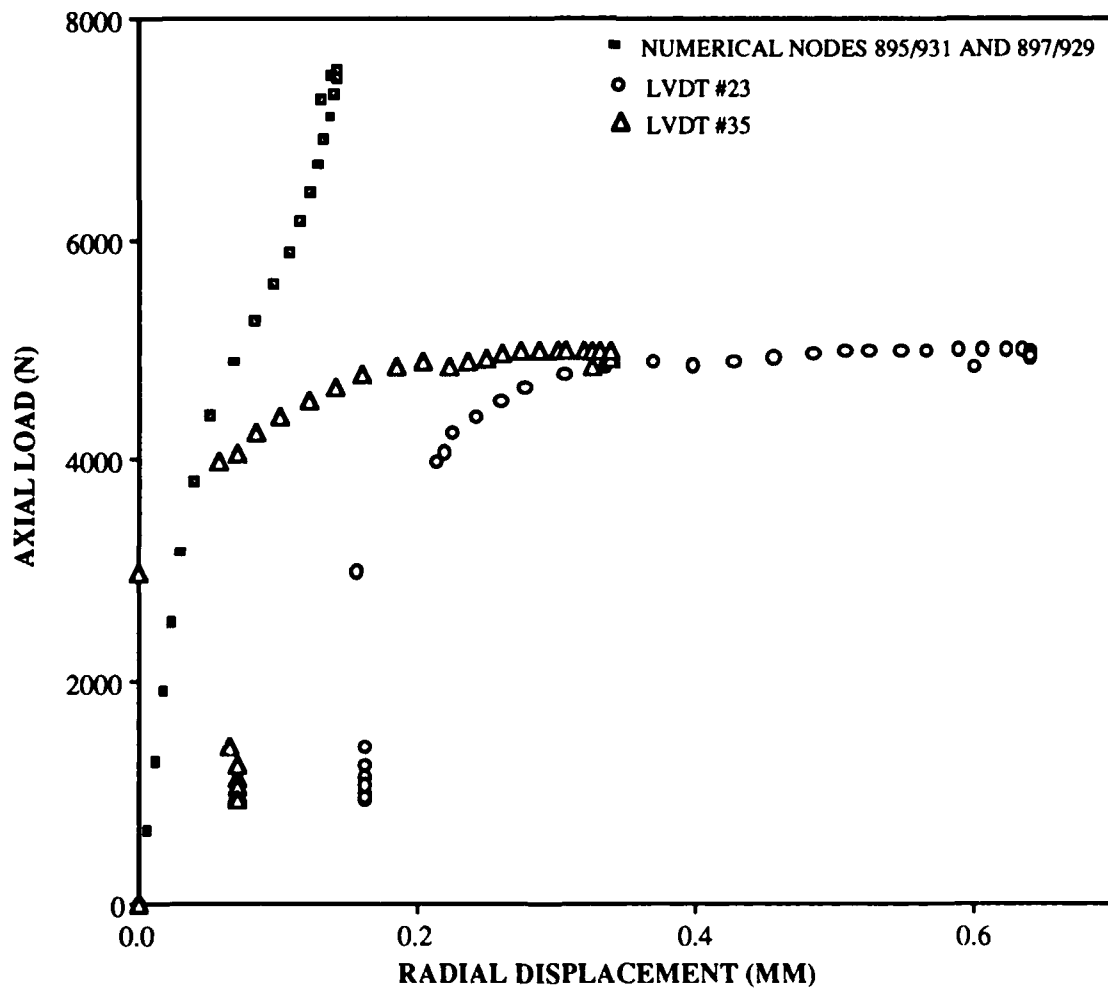
Fig. 89: Load vs. Radial Displacement,
Numerical Compared to Experiment #75,
50.8 mm x 203.2 mm (2" x 8") Cutout,
304.8 mm x 304.8 mm (12" x 12") Panel,
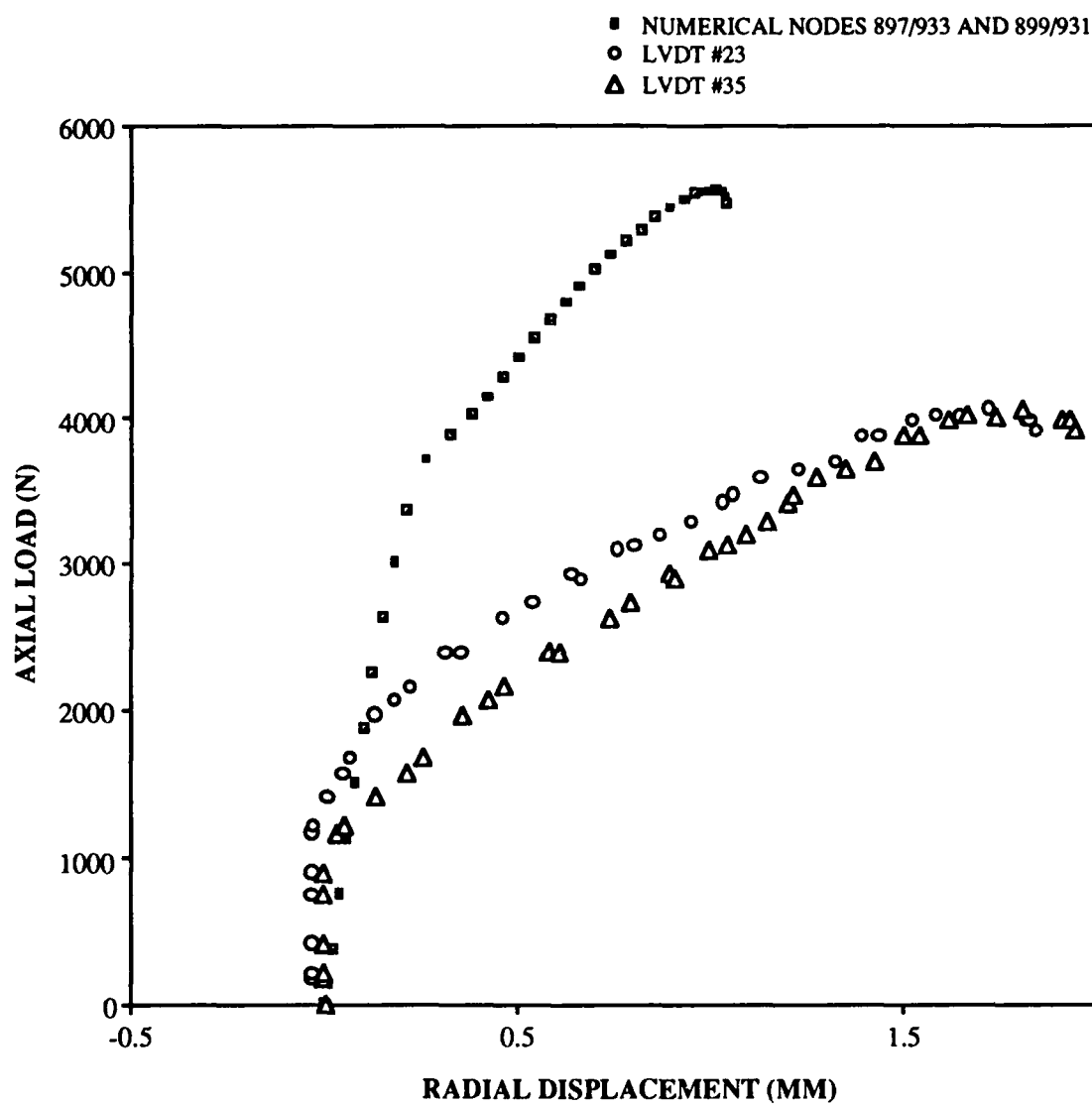[0/45/-45/90]s
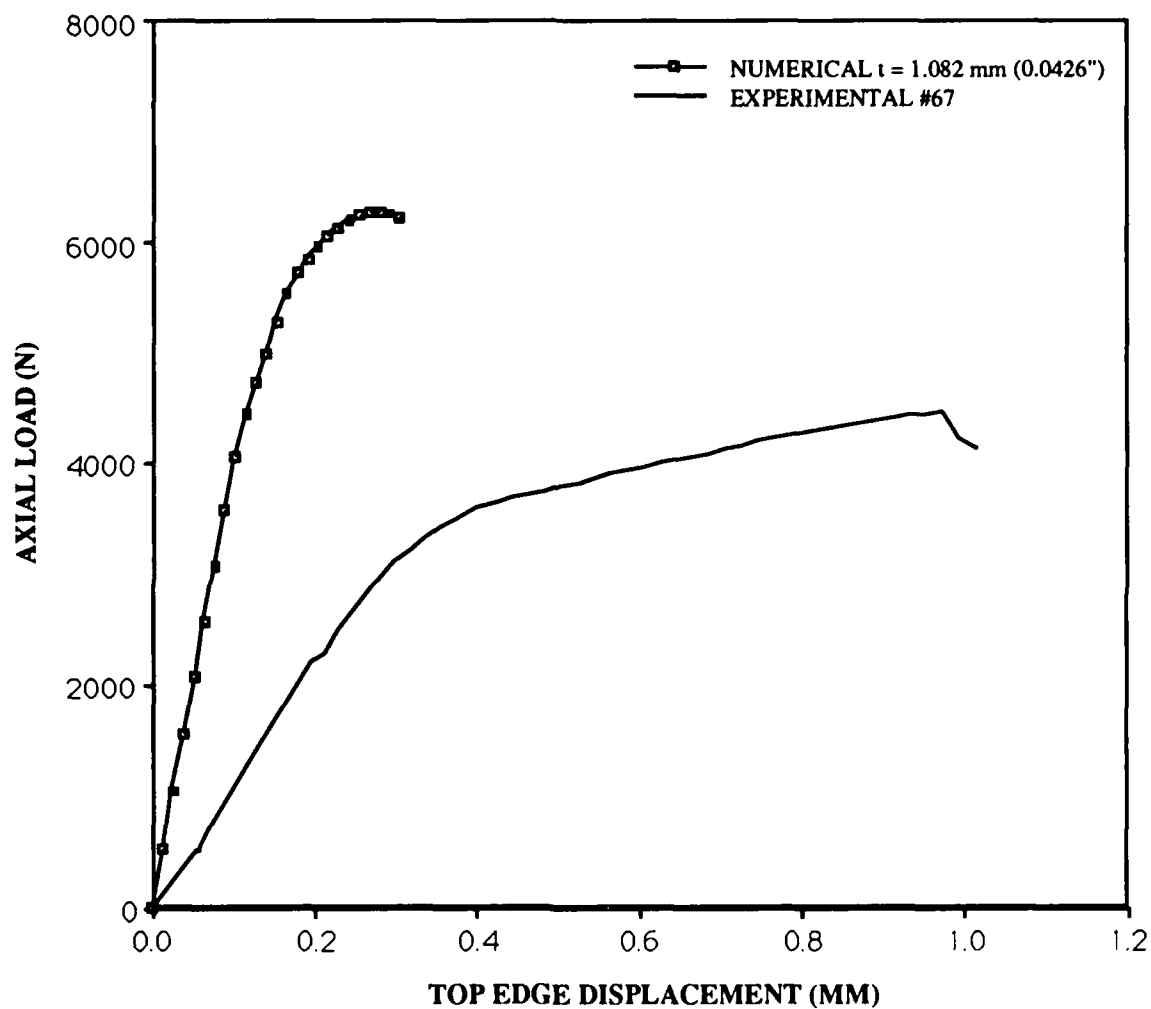
Fig 90: Load vs. Top Edge Displacement,
Numerical Compared to Experiment #67,
101.6 mm x 101.6 mm (4" x 4") Cutout,
304.8 mm x 304.8 mm (12" x 12") Panel,
[0/45/-45/90]s
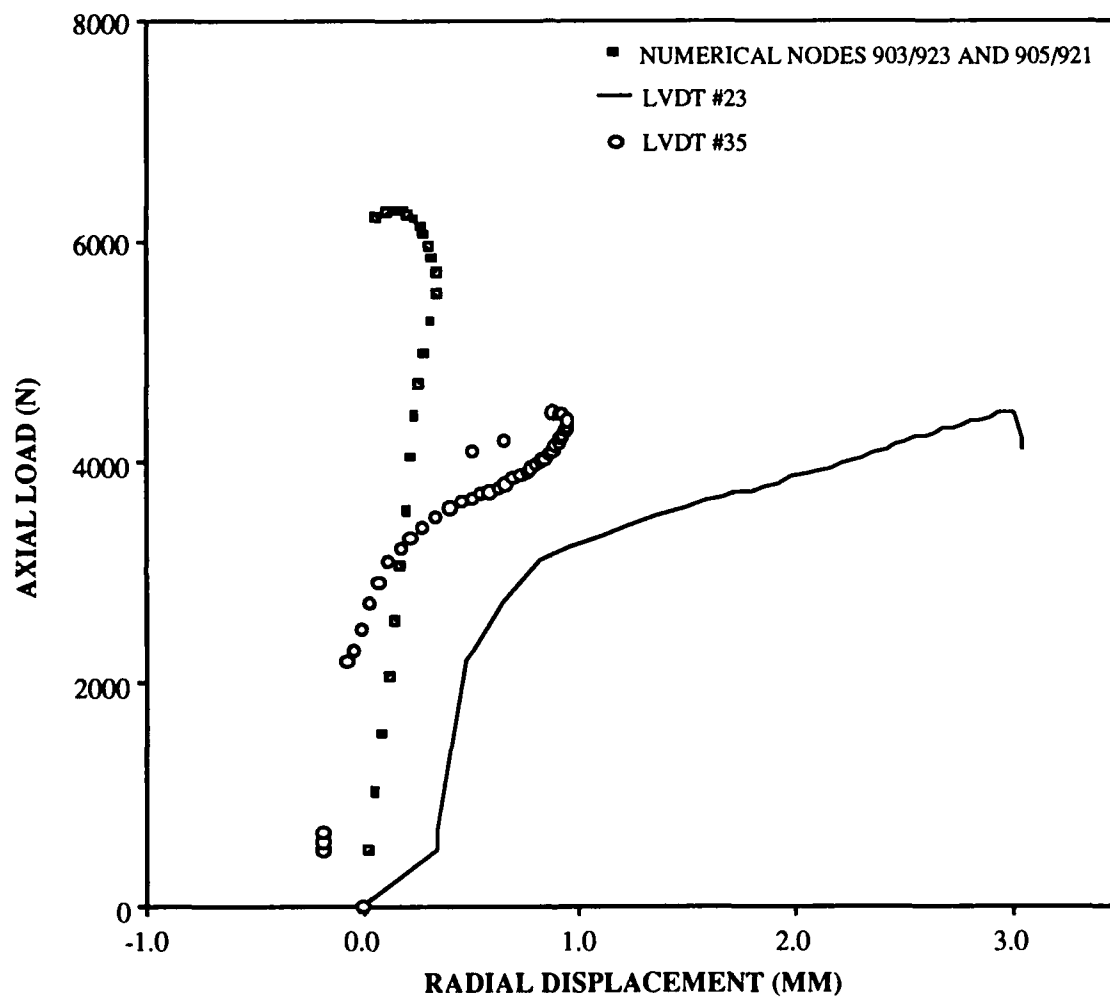
Fig. 91: Load vs. Radial Displacement,
Numerical Compared to Experiment #67,
101.6 mm x 101.6 mm (4" x 4") Cutout,
304.8 mm x 304.8 mm (12" x 12") Panel,
[0/45/-45/90]s
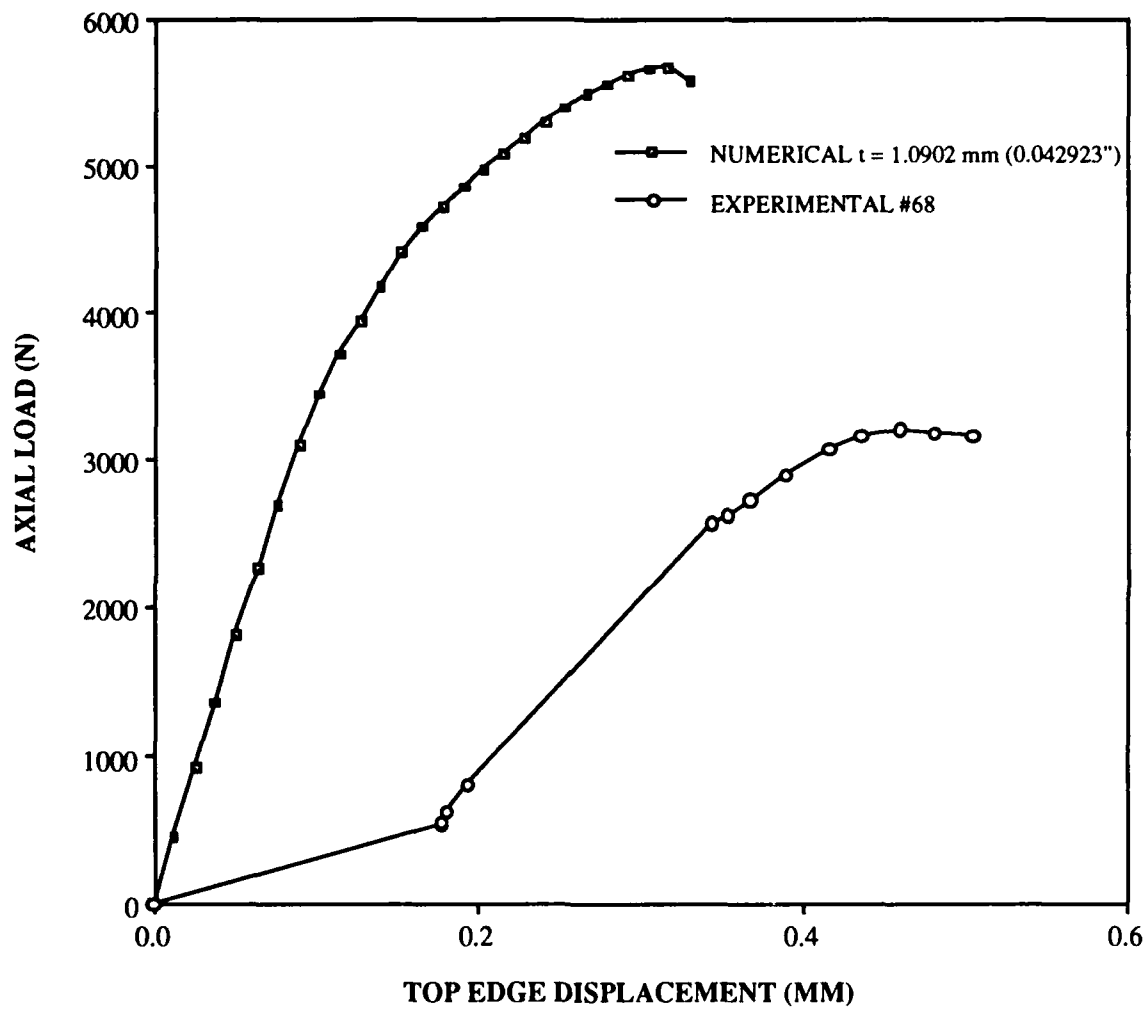
Fig. 92: Load vs. Top Edge Displacement,
Numerical Compared to Experiment #68,
127 mm x 127 mm (5" x 5") Cutout,
304.8 mm x 304.8 mm (12" x 12") Panel,
[0/45/-45/90]s
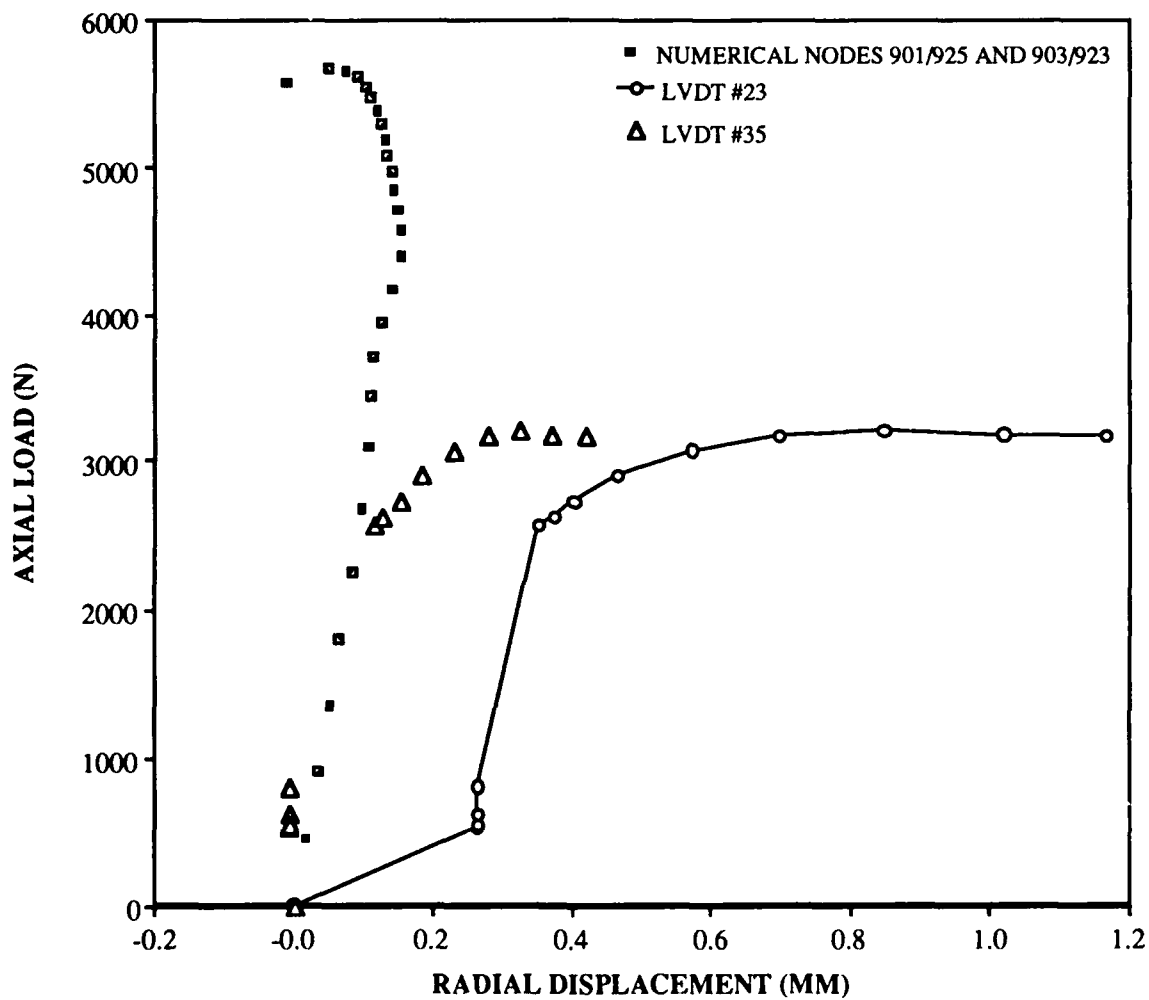
Fig. 93: Load vs. Radial Displacement,
Numerical Compared to Experiment #68,
127 mm x 127 mm (5" x 5") Cutout,
304.8 mm x 304.8 mm (12" x 12") Panel,
[0/45/-45/90]s
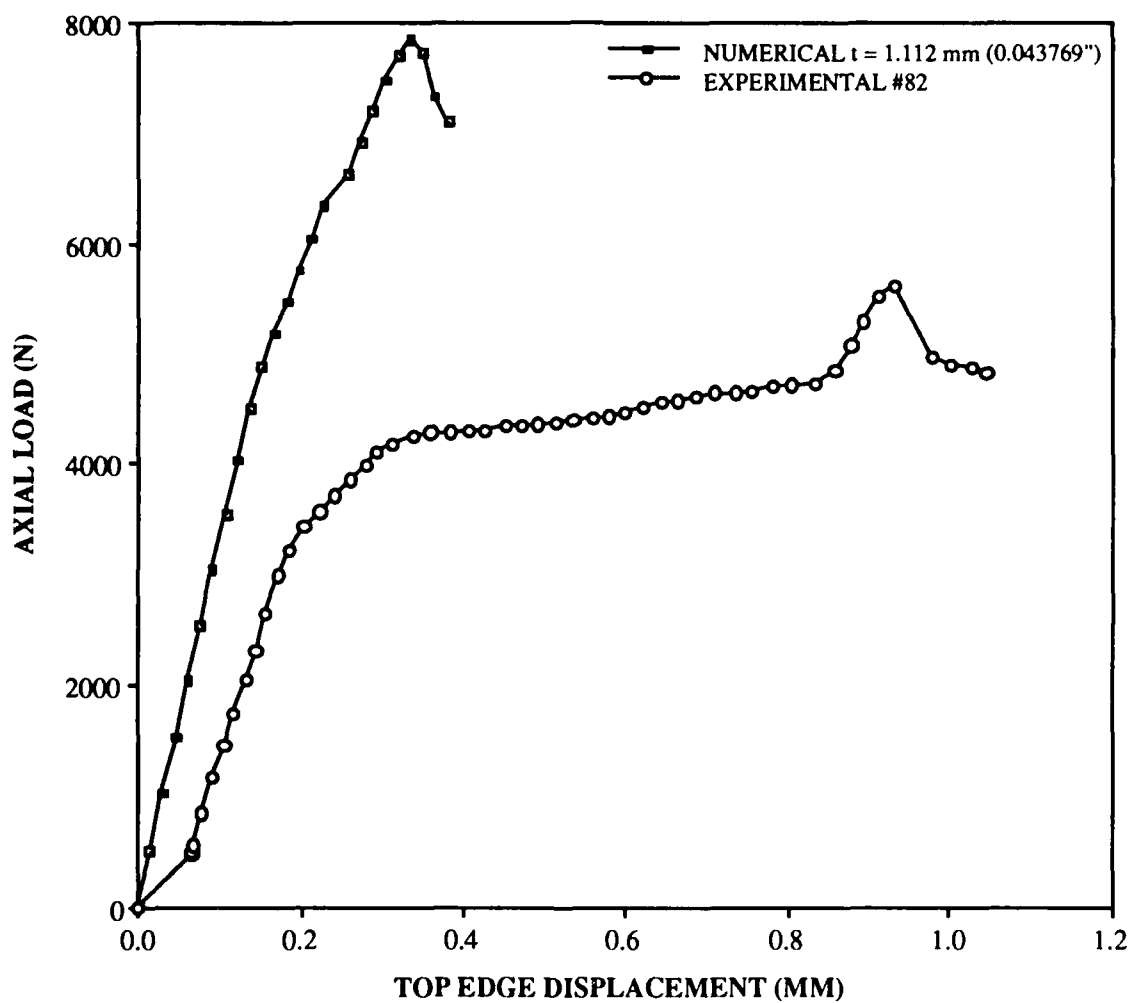
Fig. 94: Load vs. Top Edge Displacement,
Numerical Compared to Experiment #82,
50.8 mm x 50.8 mm (2" x 2") Cutout,
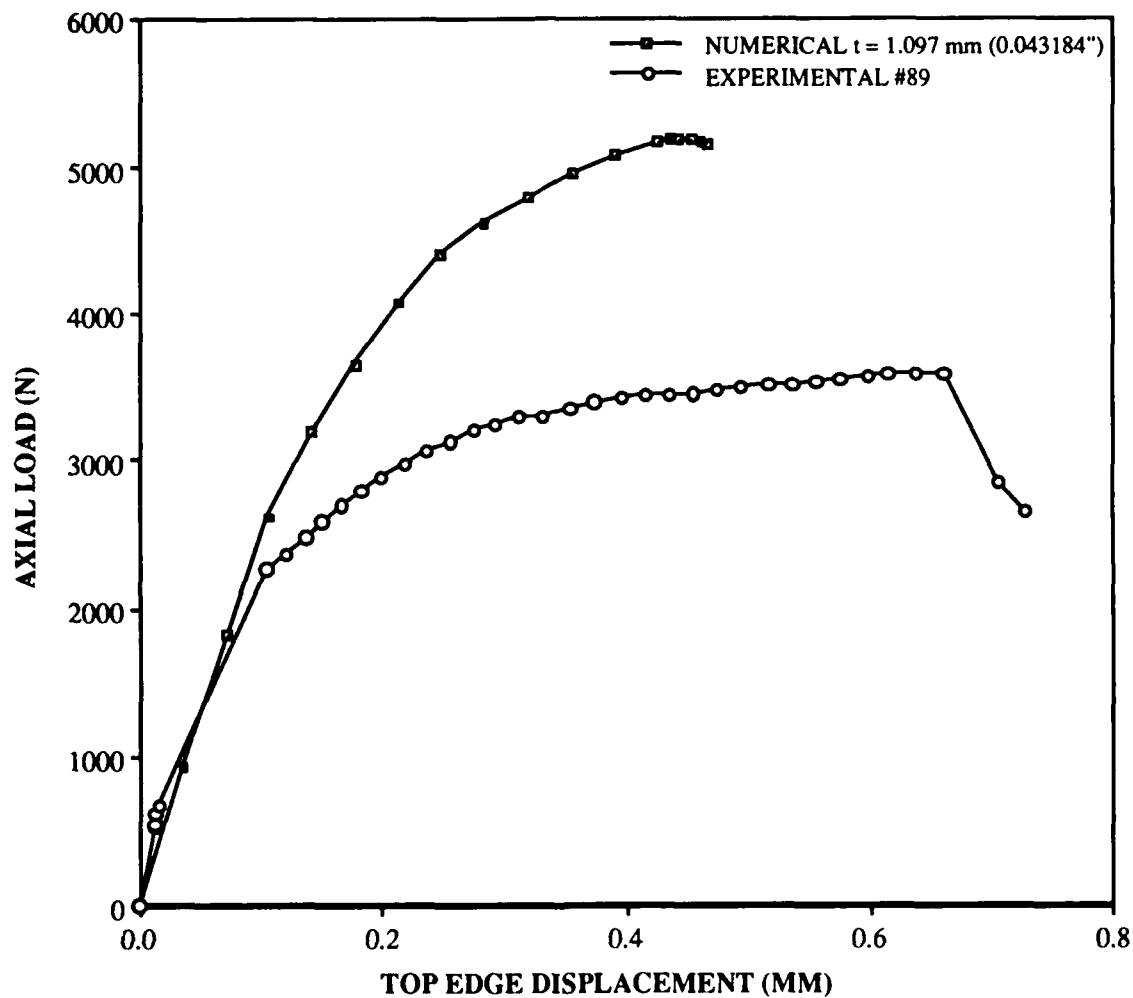304.8 mm x 508 mm (12" x 20") Panel,
[0/45/-45/90]s

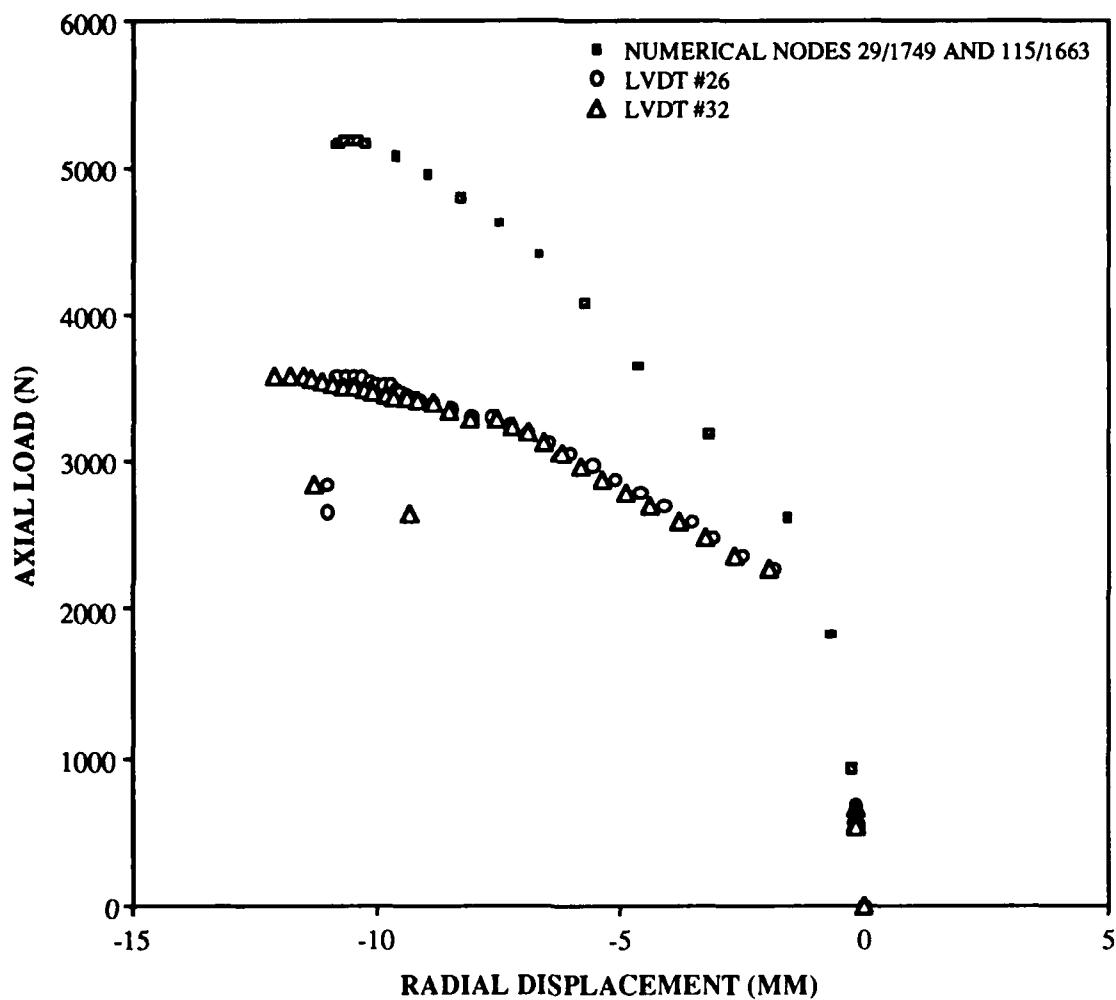Fig. 95: Load vs. Radial Displacement,
Numerical Compared to Experiment #82,
50.8 mm x 50.8 mm (2" x 2") Cutout,
304.8 mm x 508 mm (12" x 20") Panel,
[0/45/-45/90]s

223

Fig. 96: Load vs. Radial Displacement,
Numerical Compared to Experiment #82,
50.8 mm x 50.8 mm (2" x 2") Cutout,
304.8 mm x 508 mm (12" x 20") Panel,
[0/45/-45/90]s

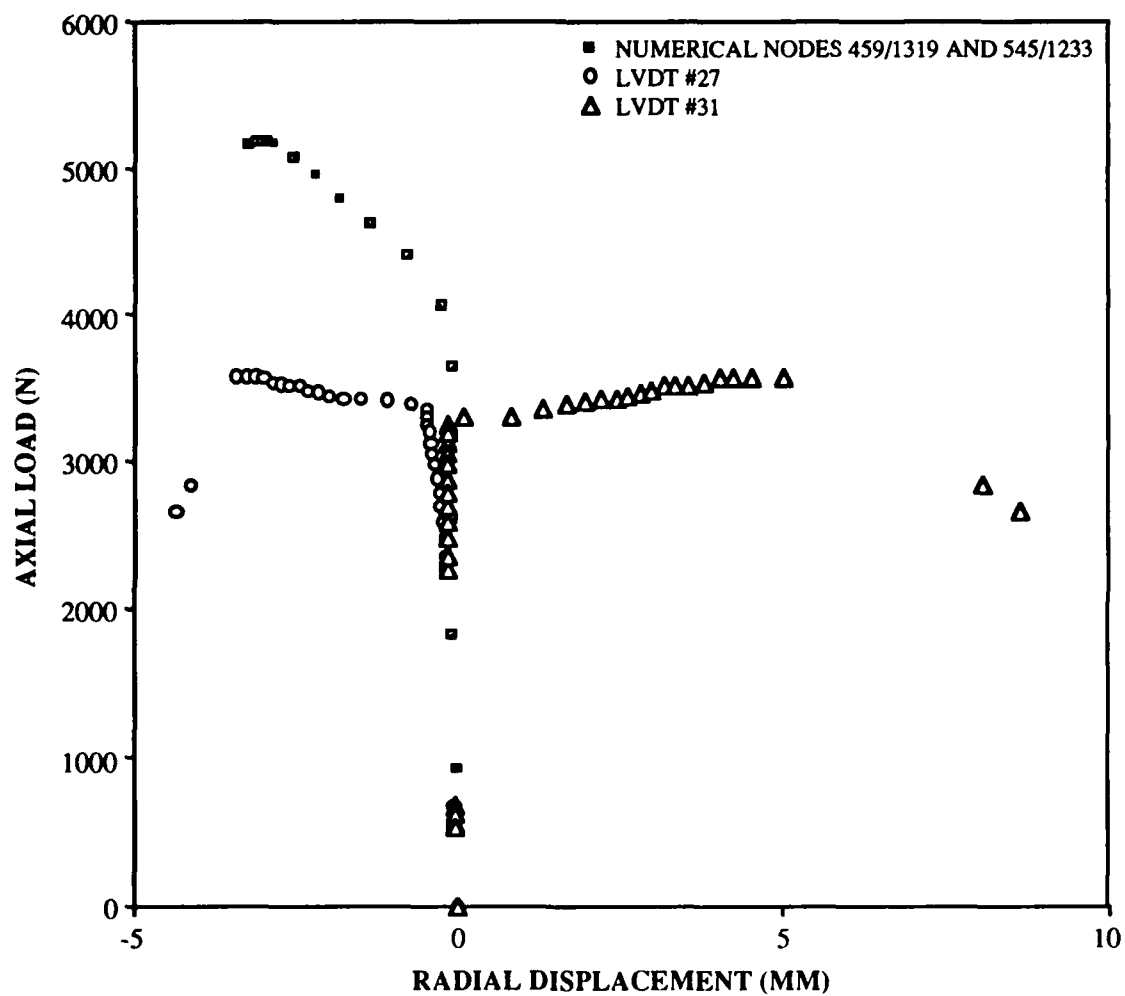Fig. 97: Load vs. Radial Displacement,
Numerical Compared to Experiment #82,
50.8 mm x 50.8 mm (2" x 2") Cutout,
304.8 mm x 508 mm (12" x 20") Panel,
[0/45/-45/90]s

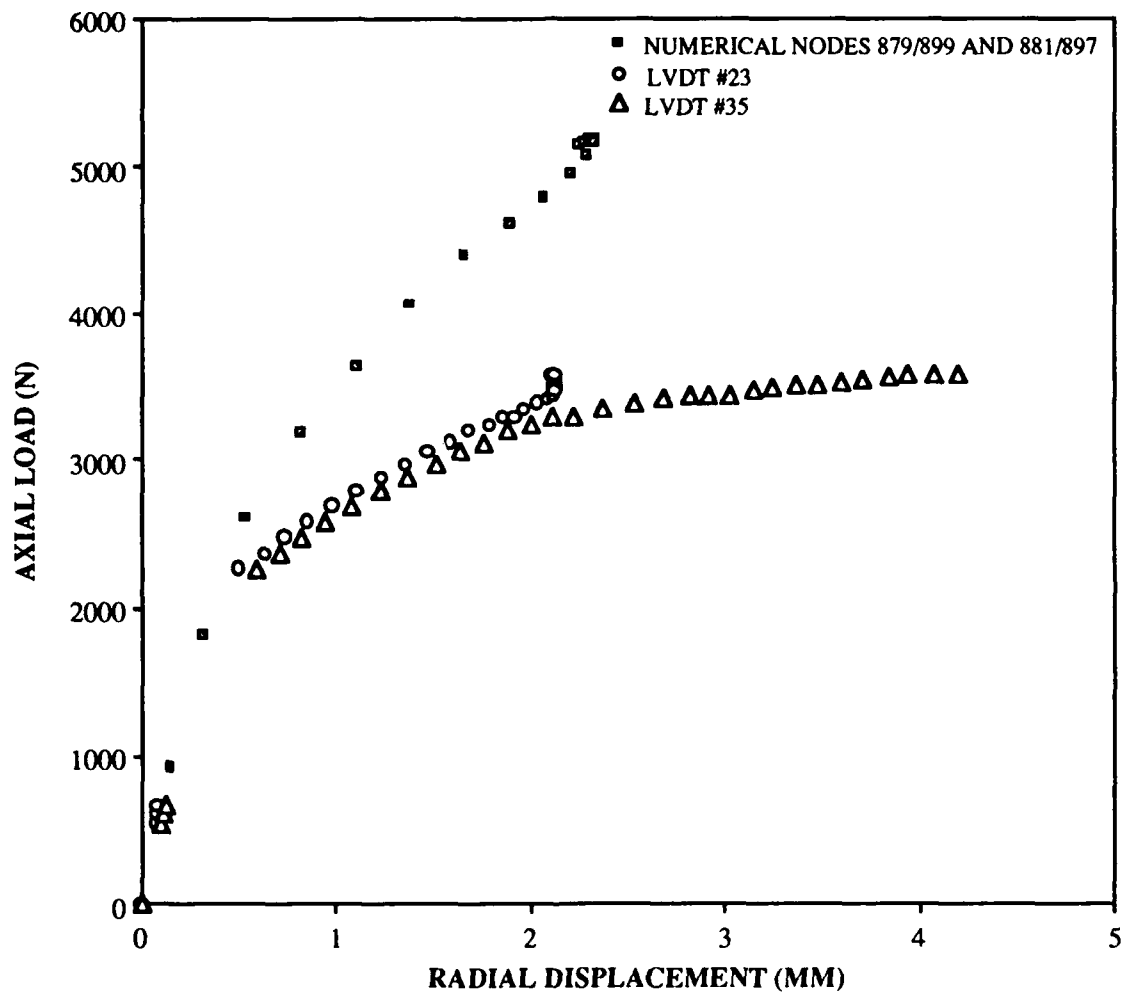Fig. 98: Load vs. Top Edge Displacement,
Numerical Compared to Experiment #100,
50.8 mm x 203.2 mm (2" x 8") Cutout,
304.8 mm x 508 mm (12" x 20") Panel,
[0/45/-45/90]s

Fig. 99: Load vs. Radial Displacement,
Numerical Compared to Experiment #100,
50.8 mm x 203.2 mm (2" x 8") Cutout,
304.8 mm x 508 mm (12" x 20") Panel,
[0/45/-45/90]s

Fig. 100: Load vs. Radial Displacement,
Numerical Compared to Experiment #100,
50.8 mm x 203.2 mm (2" x 8") Cutout,
304.8 mm x 508 mm (12" x 20") Panel,
[0/45/-45/90]s

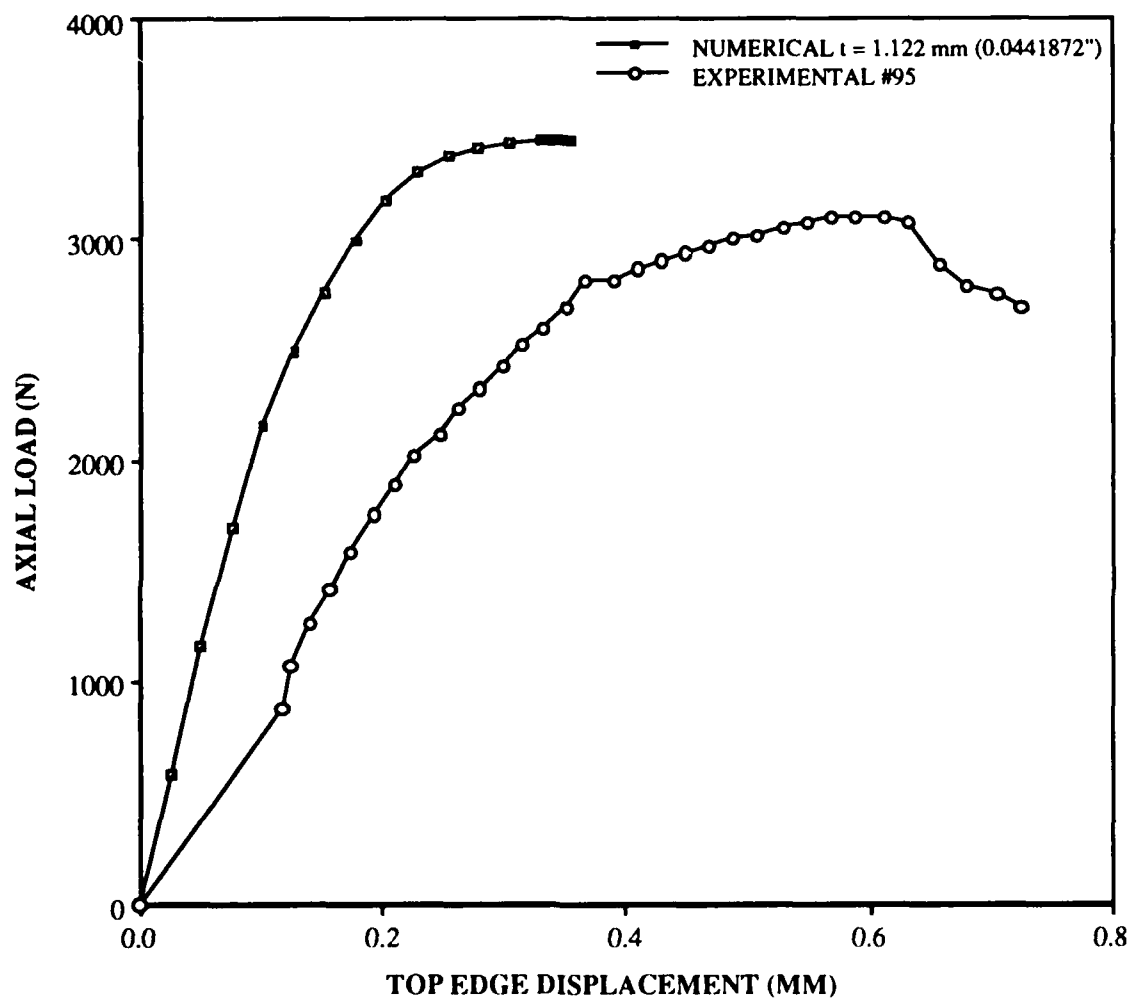Fig. 101: Load vs. Radial Displacement,
Numerical Compared to Experiment #100,
50.8 mm x 203.2 mm (2" x 8") Cutout,
304.8 mm x 508 mm (12" x 20") Panel,
[0/45/-45/90]s

Fig. 102: Load vs. Top Edge Displacement,
Numerical Compared to Experiment #89,
101.6 mm x 101.6 mm (4" x 4") Cutout,
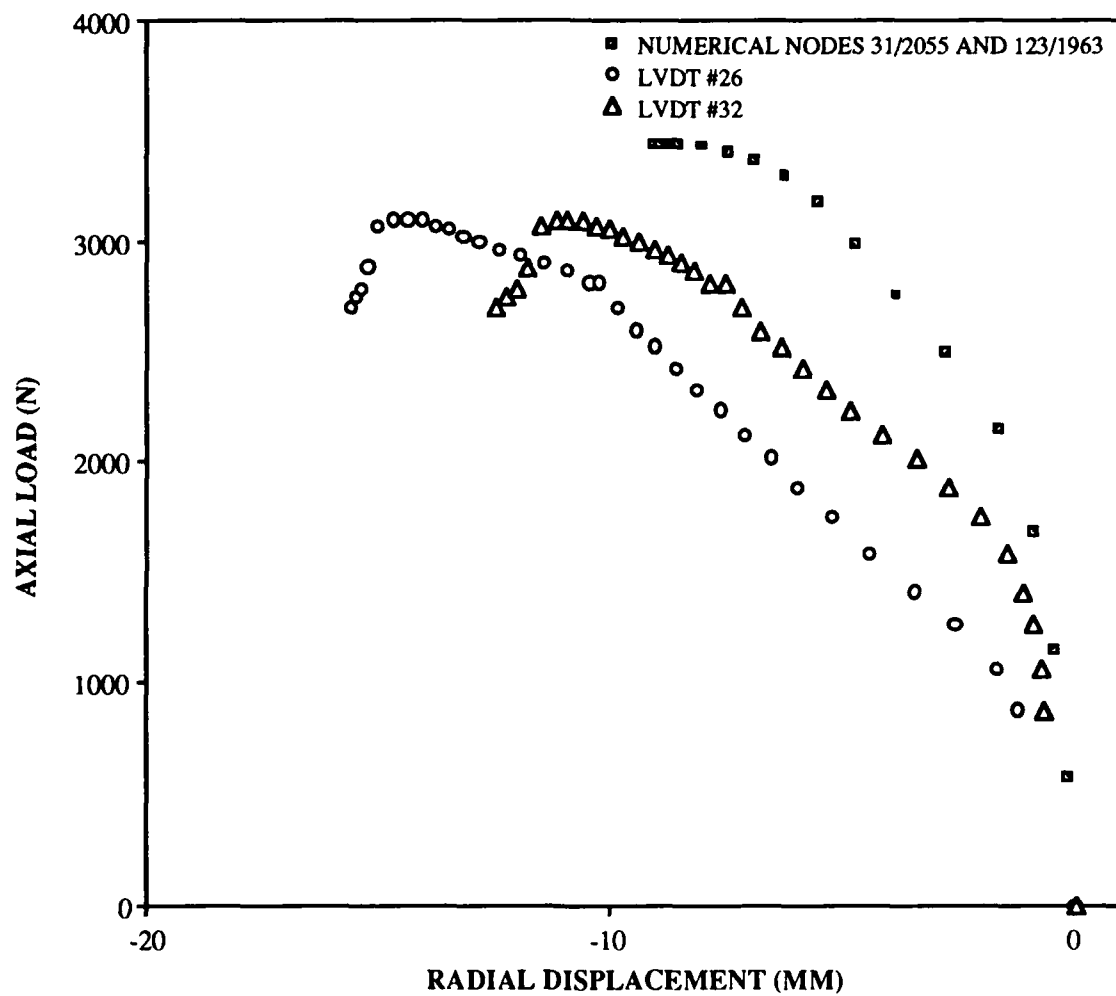304.8 mm x 508 mm (12" x 20") Panel,
[0/45/-45/90]s

Fig. 103: Load vs. Radial Displacement,
Numerical Compared to Experiment #89,
101.6 mm x 101.6 mm (4" x 4") Cutout,
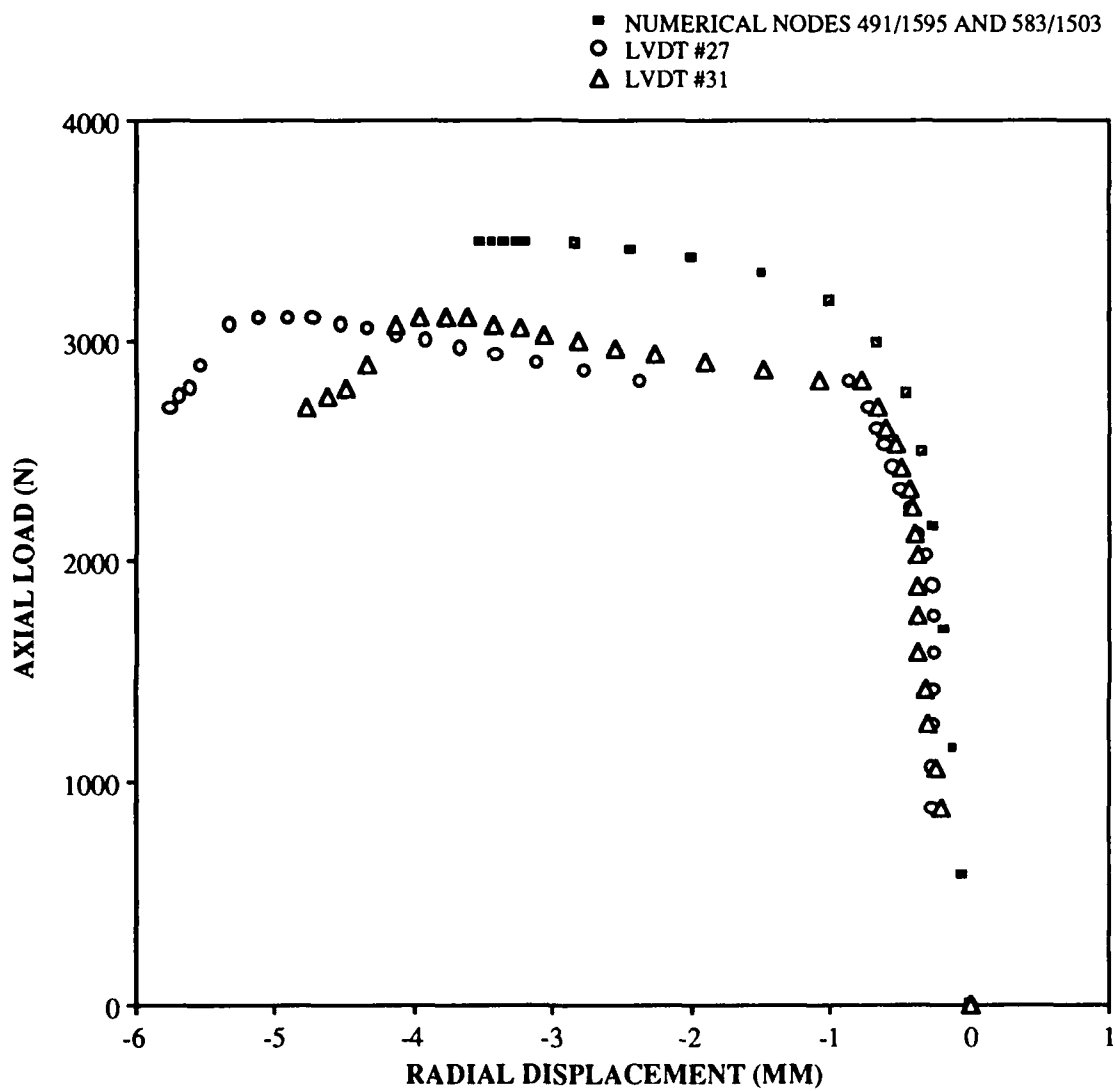304.8 mm x 508 mm (12" x 20") Panel,
[0/45/-45/90]s

Fig. 104: Load vs. Radial Displacement,
Numerical Compared to Experiment #89,
101.6 mm x 101.6 mm (4" x 4") Cutout,
304.8 mm x 508 mm (12" x 20") Panel,
[0/45/-45/90]s

Fig. 105: Load vs. Radial Displacement,
Numerical Compared to Experiment #89,
101.6 mm x 101.6 mm (4" x 4") Cutout,
304.8 mm x 508 mm (12" x 20") Panel,
[0/45/-45/90]s

Fig. 106: Load vs. Top Edge Displacement,
Numerical Compared to Experiment #95,
127 mm x 127 mm (5" x 5") Cutout,
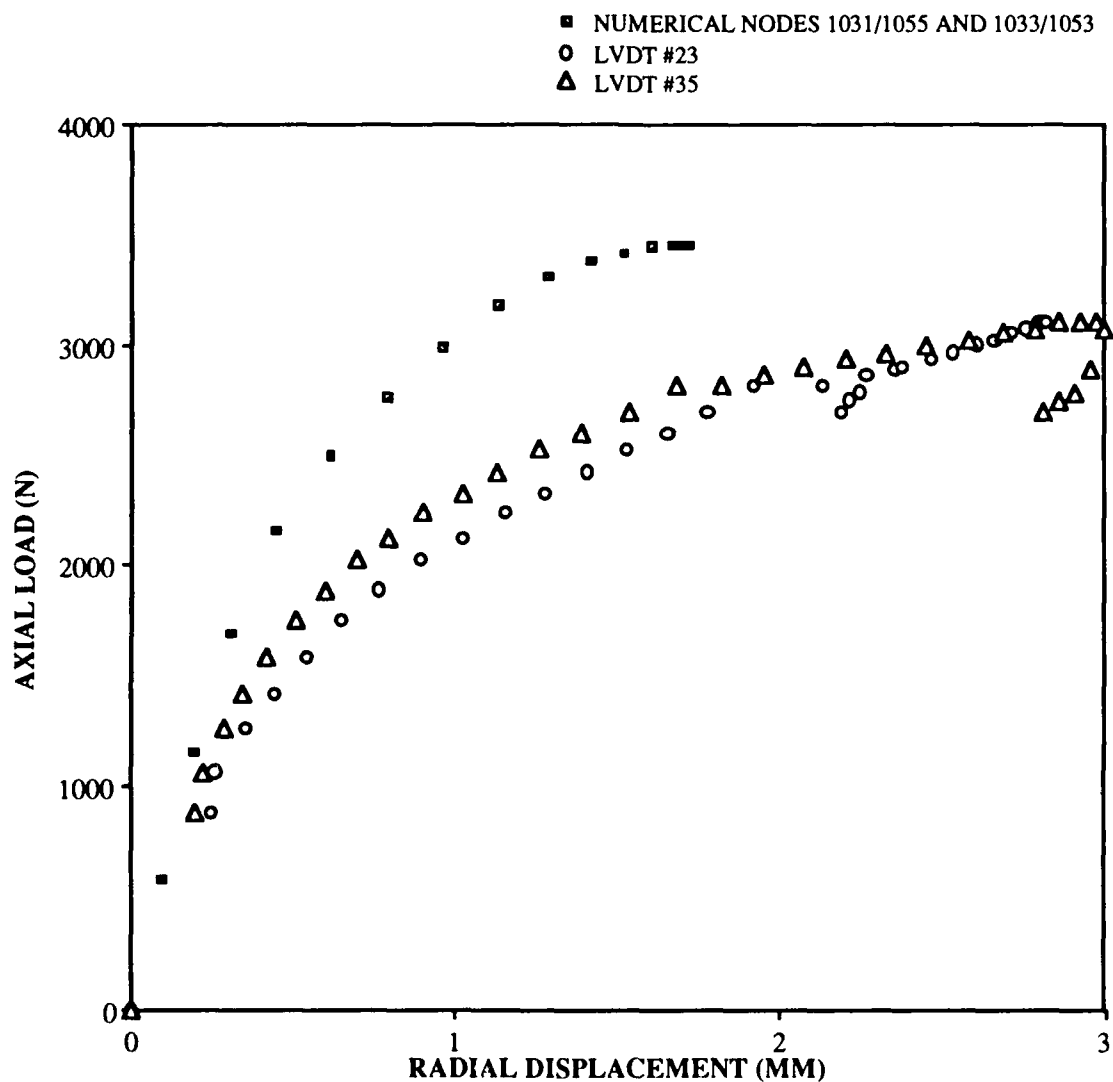304.8 mm x 508 mm (12" x 20") Panel,
[0/45/-45/90]s

Fig. 107: Load vs. Radial Displacement,
Numerical Compared to Experiment #95,
127 mm x 127 mm (5" x 5") Cutout,
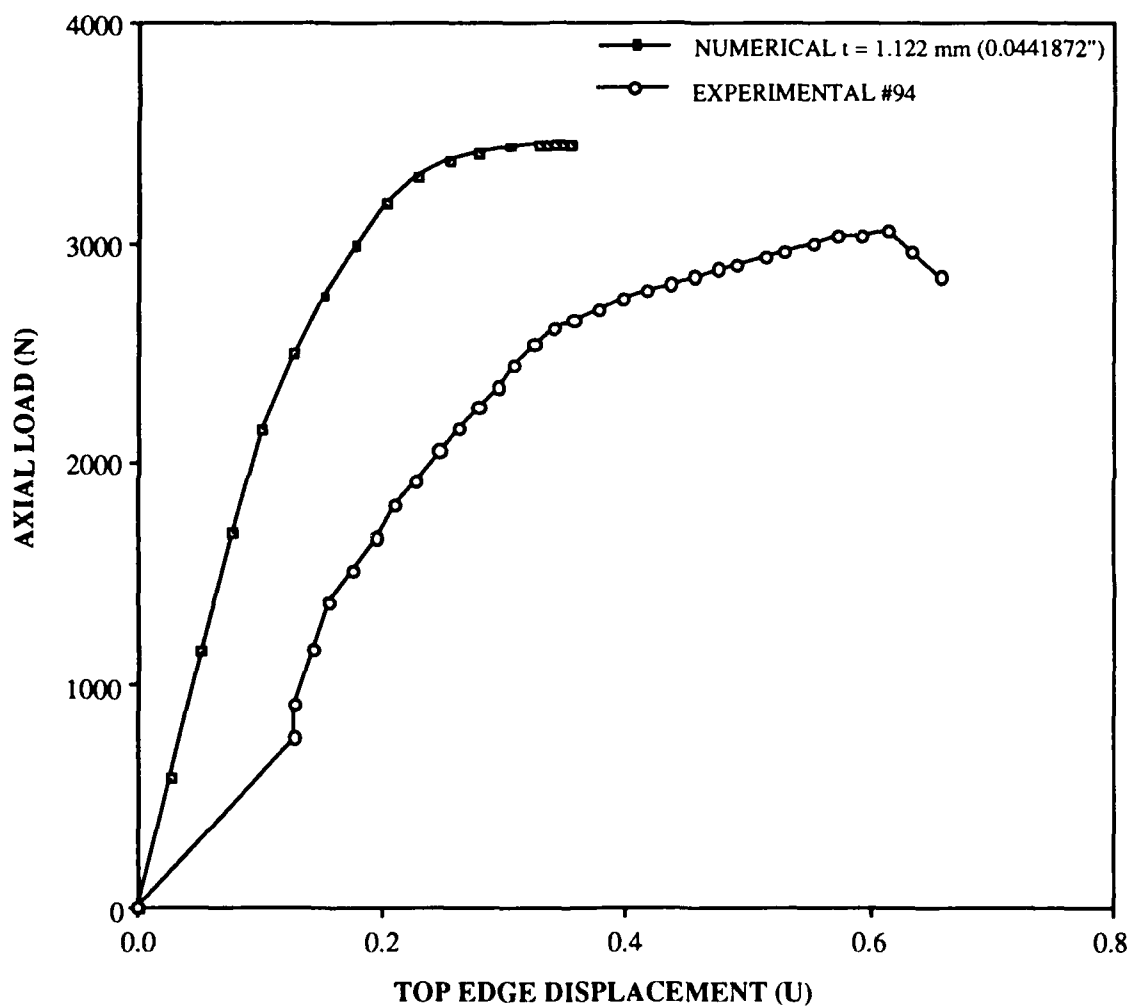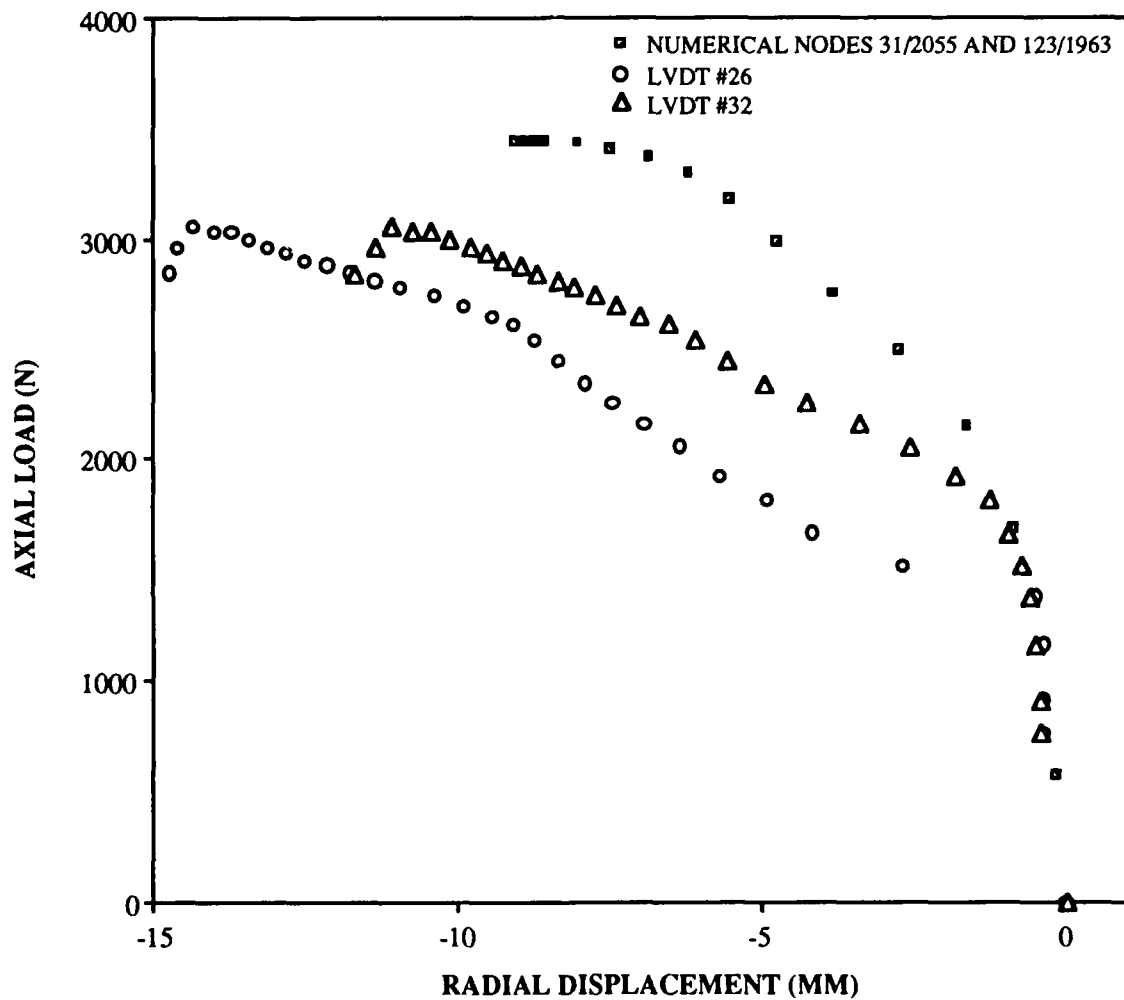304.8 mm x 508 mm (12" x 20") Panel,
[0/45/-45/90]s

Fig. 108: Load vs. Radial Displacement,
Numerical Compared to Experiment #95,
127 mm x 127 mm (5" x 5") Cutout,
304.8 mm x 508 mm (12" x 20") Panel,
[0/45/-45/90]s

Fig. 109: Load vs. Radial Displacement,
Numerical Compared to Experiment #95,
127 mm x 127 mm (5" x 5") Cutout,
304.8 mm x 508 mm (12" x 20") Panel,
[0/45/-45/90]s

Fig. 110: Load vs. Top Edge Displacement,
Numerical Compared to Experiment #94,
127 mm x 127 mm (5" x 5") Cutout,
304.8 mm x 508 mm (12" x 20") Panel,
[0/45/-45/90]s

Fig. 111: Load vs. Radial Displacement,
Numerical Compared to Experiment #94,
127 mm x 127 mm (5" x 5") Cutout,
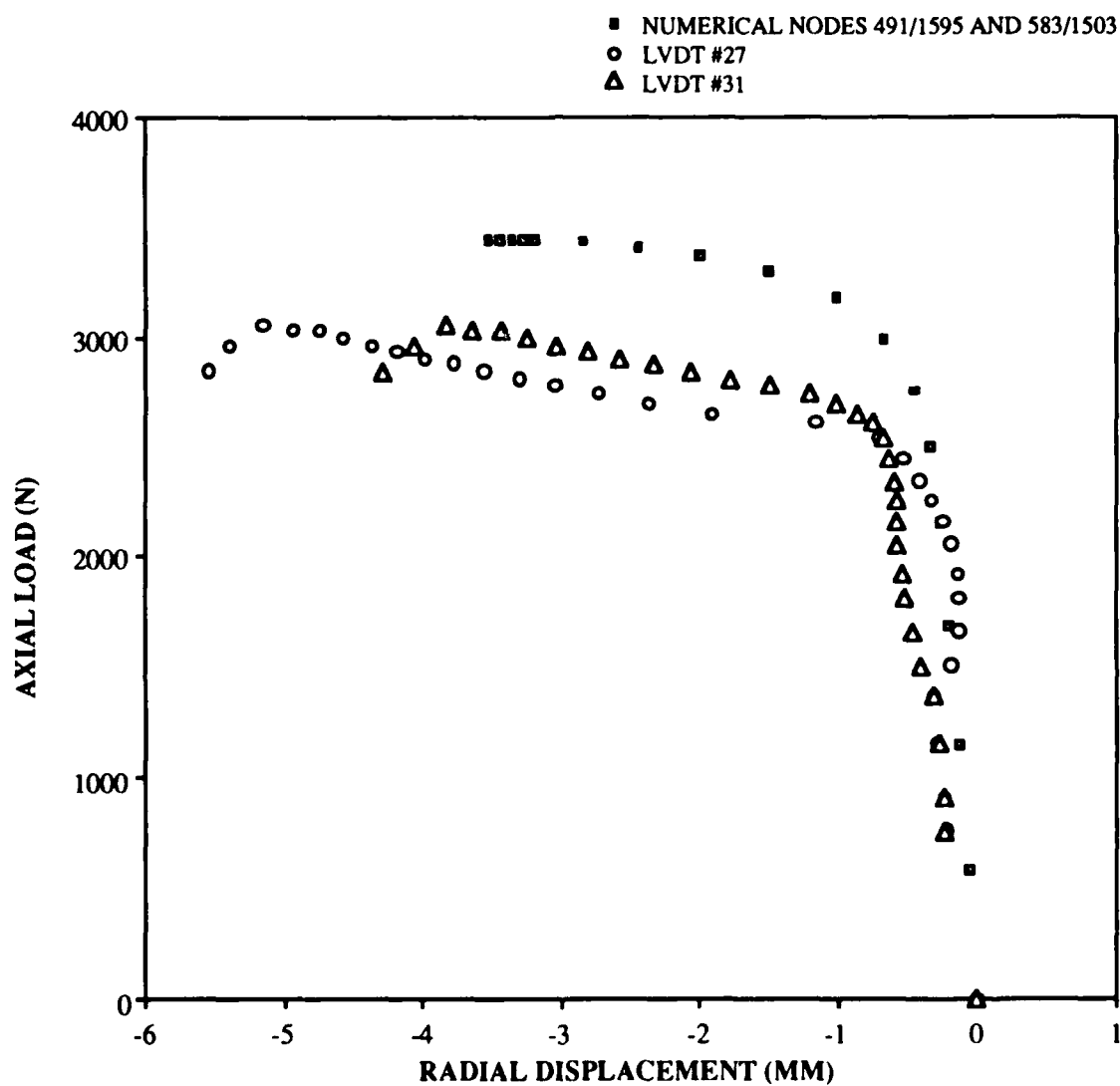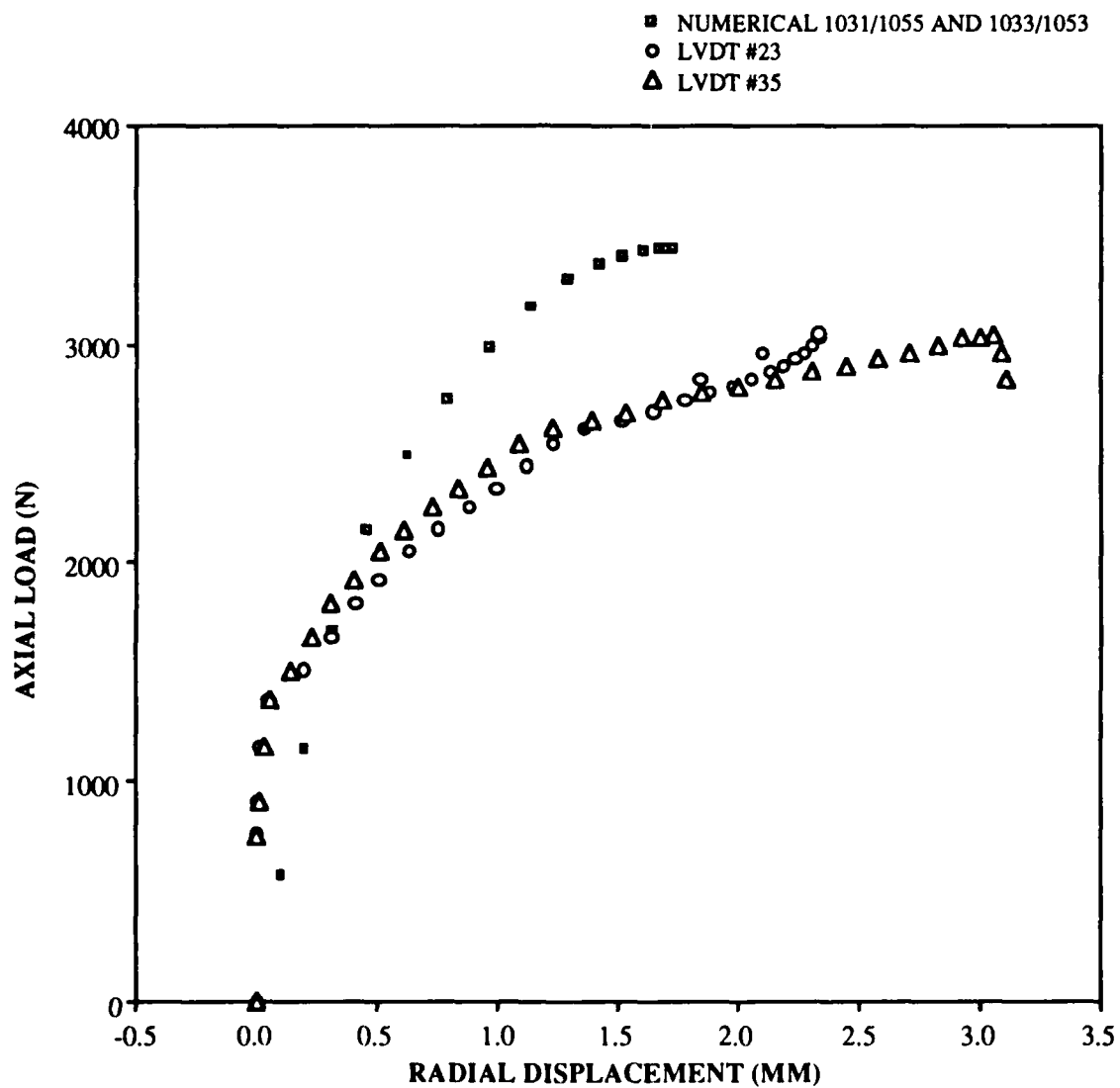304.8 mm x 508 mm (12" x 20") Panel,
[0/45/-45/90]s

Fig. 112: Load vs. Radial Displacement,
Numerical Compared to Experiment #94,
127 mm x 127 mm (5" x 5") Cutout,
304.8 mm x 508 mm (12" x 20") Panel,
[0/45/-45/90]s

240

Fig. 113: Load vs. Radial Displacement,
Numerical Compared to Experiment #94,
127 mm x 127 mm (5" x 5") Cutout,
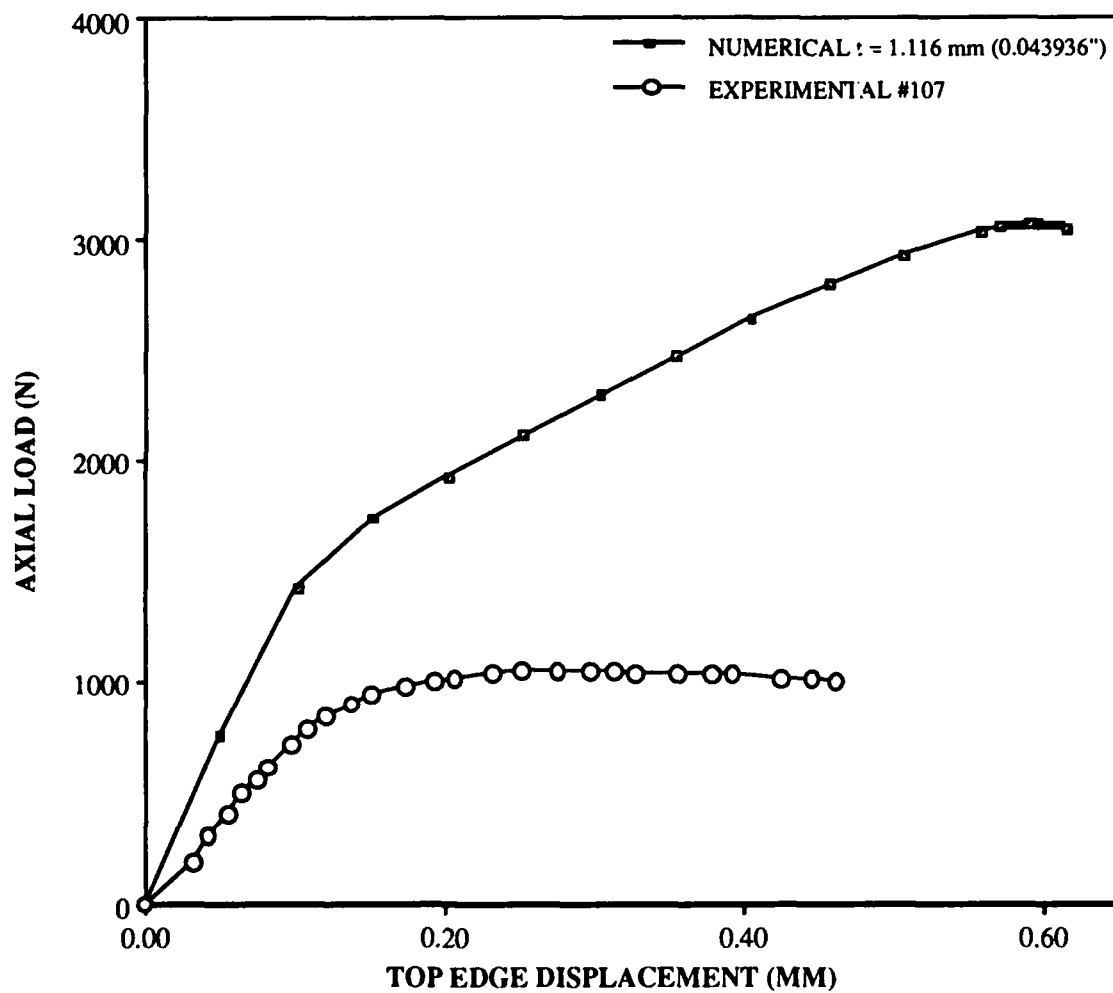304.8 mm x 508 mm (12" x 20") Panel,
[0/45/-45/90]s

Fig. 114: Load vs. Top Edge Displacement,
Numerical Compared to Experiment #107,
203.2 mm x 50.8 mm (8" x 2") Cutout,
304.8 mm x 508 mm (12" x 20") Panel,
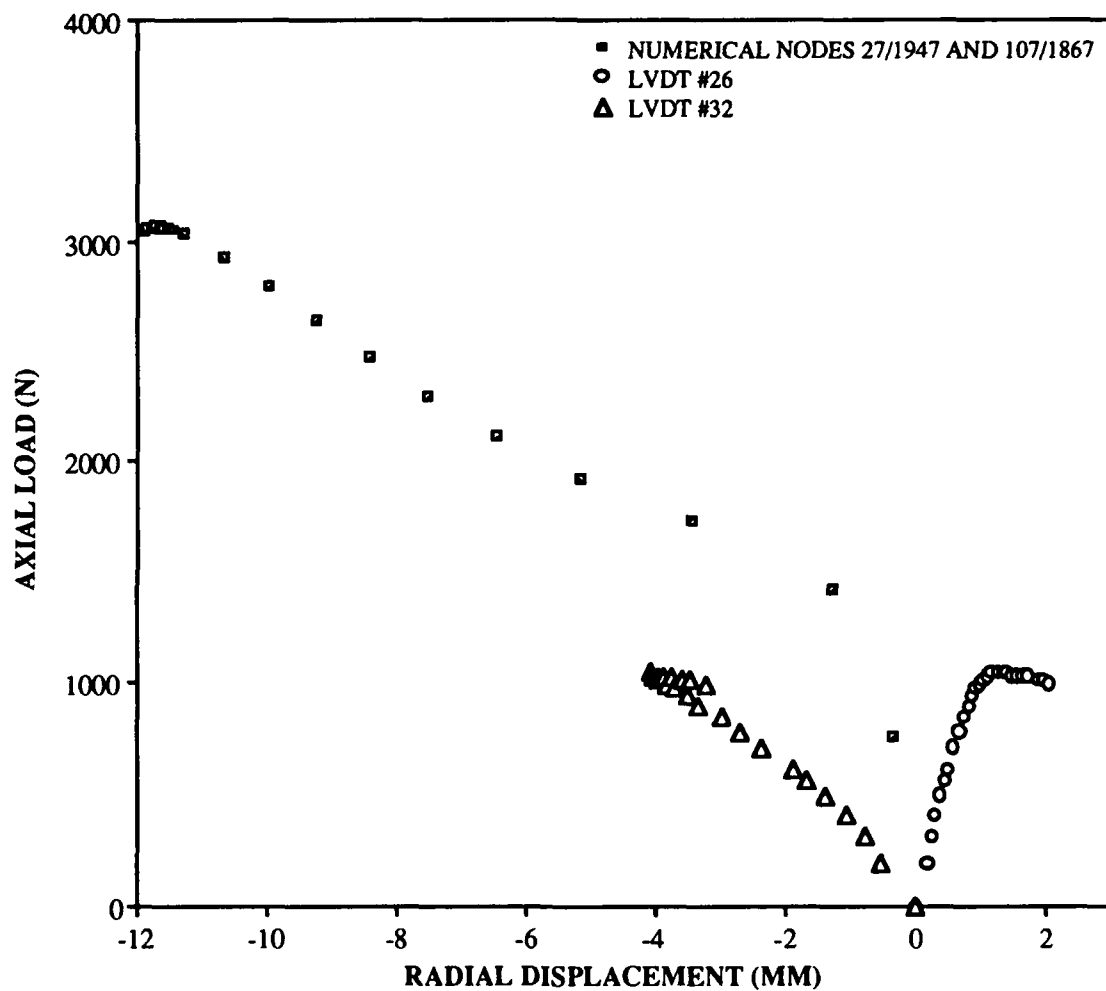[0/45/-45/90]s

Fig. 115: Load vs. Radial Displacement,
Numerical Compared to Experiment #107,
203.2 mm x 50.8 mm (8" x 2") Cutout,
304.8 mm x 508 mm (12" x 20") Panel,
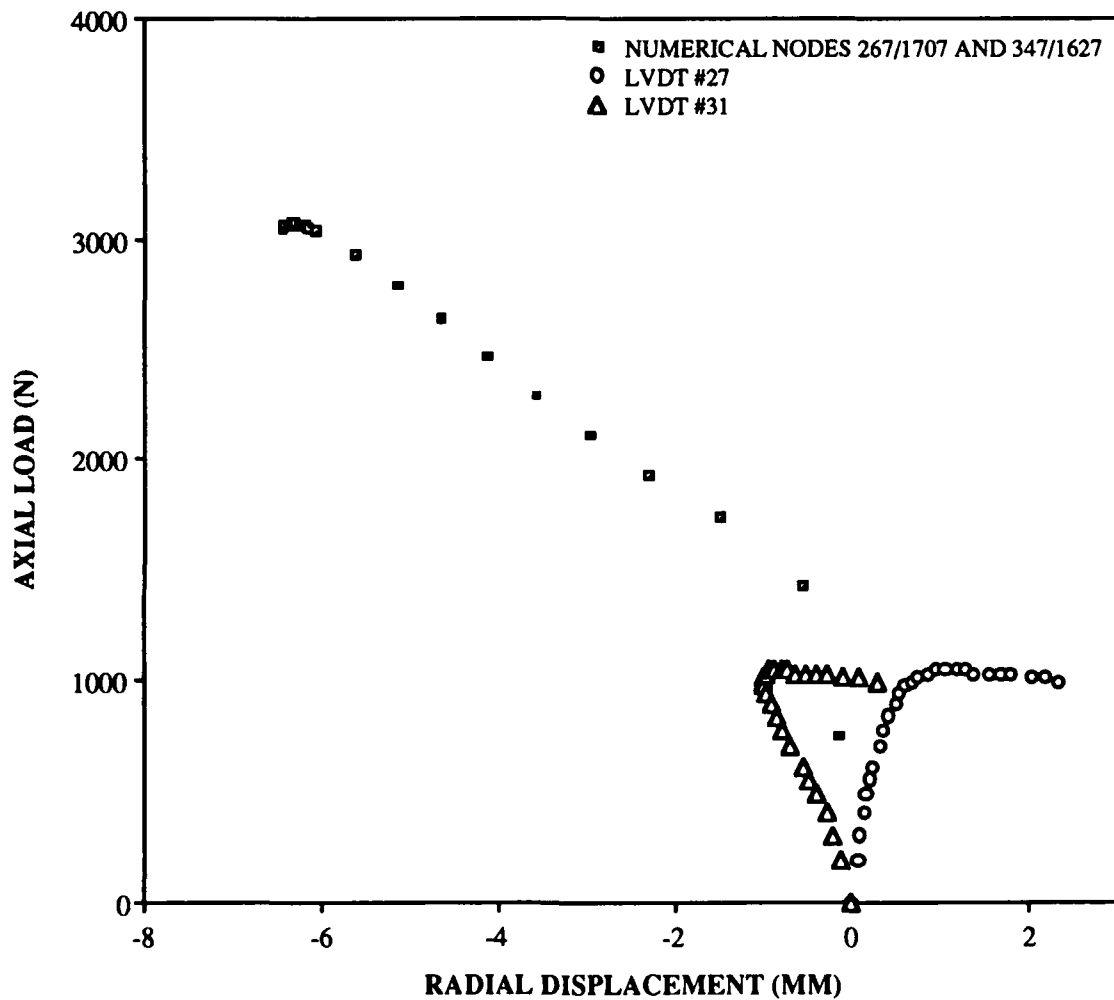[0/45/-45/90]s

243

Fig. 116: Load vs. Radial Displacement,
Numerical Compared to Experiment #107,
203.2 mm x 50.8 mm (8" x 2") Cutout,
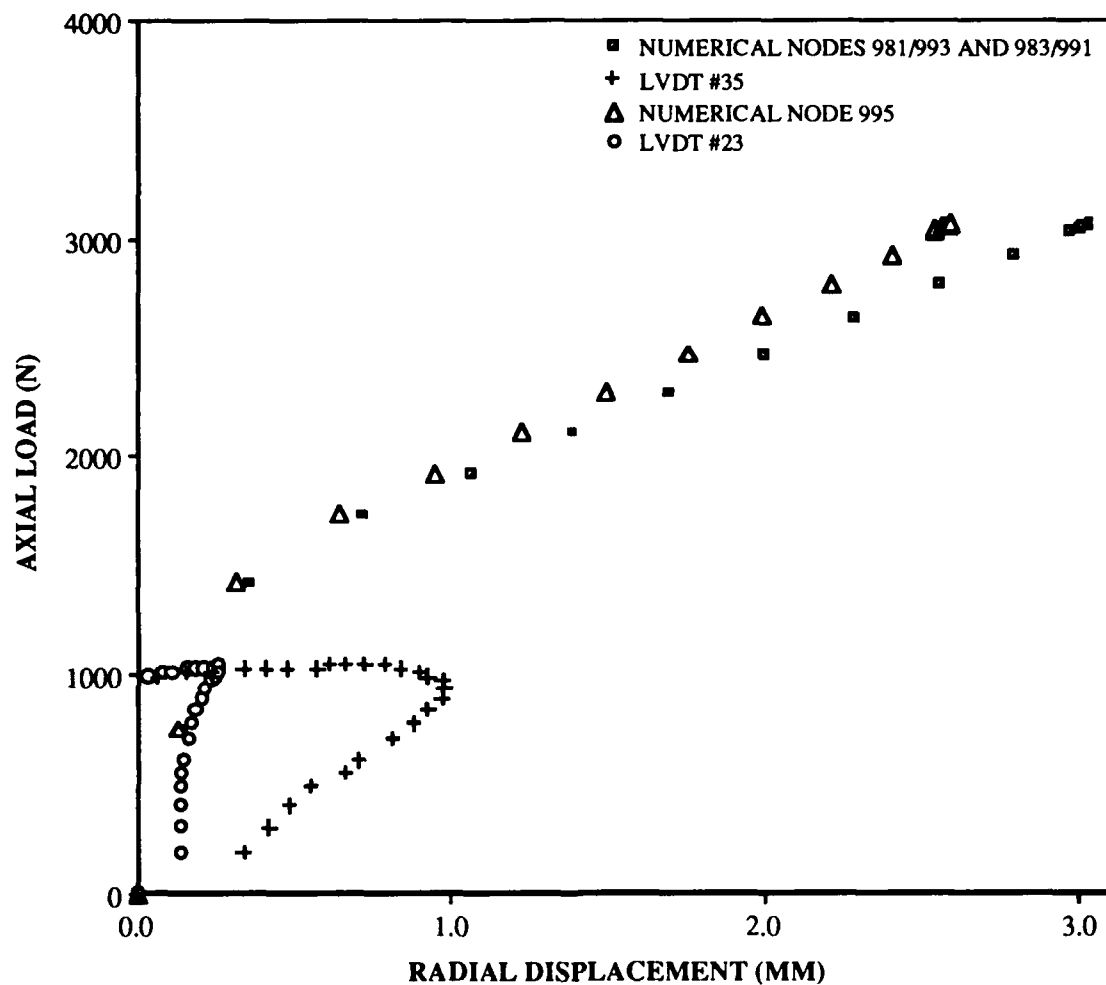304.8 mm x 508 mm (12" x 20") Panel,
[0/45/-45/90]s

Fig. 117: Load vs. Radial Displacement,
Numerical Compared to Experiment #107,
203.2 mm x 50.8 mm (8" x 2") Cutout,
304.8 mm x 508 mm (12" x 20") Panel,
[0/45/-45/90]s

Fig. 118. Load vs. Radial Displacement,
Numerical Compared to Experiment #78,
50.8 mm x 50.8 mm (2" x 2") Cutout,
304.8 mm x 508 mm (12" x 20") Panel,
[0/45/-45/90]3s
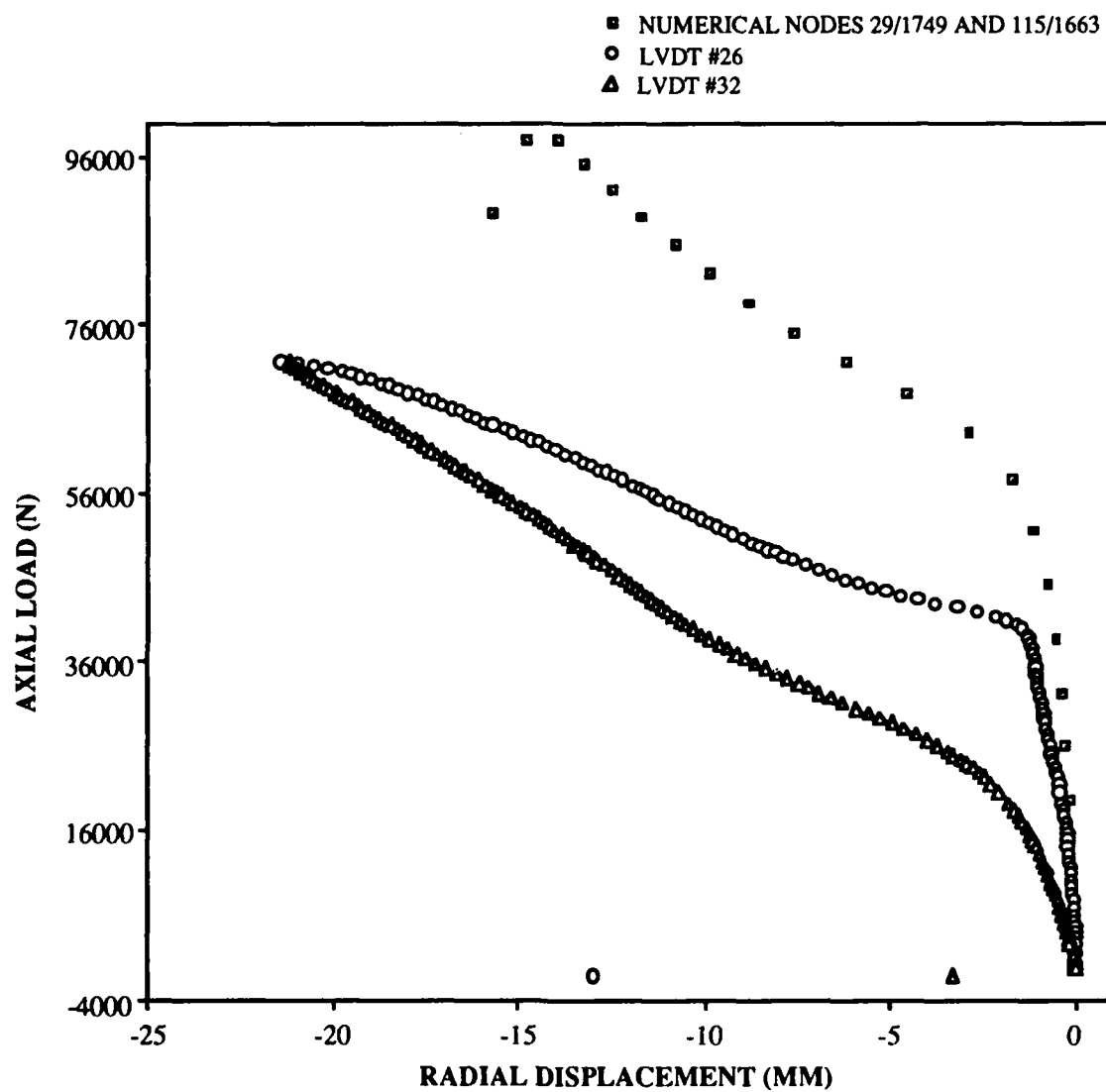
Fig. 119: Load vs. Radial Displacement,
Numerical Compared to Experiment #78,
50.8 mm x 50.8 mm (2" x 2") Cutout,
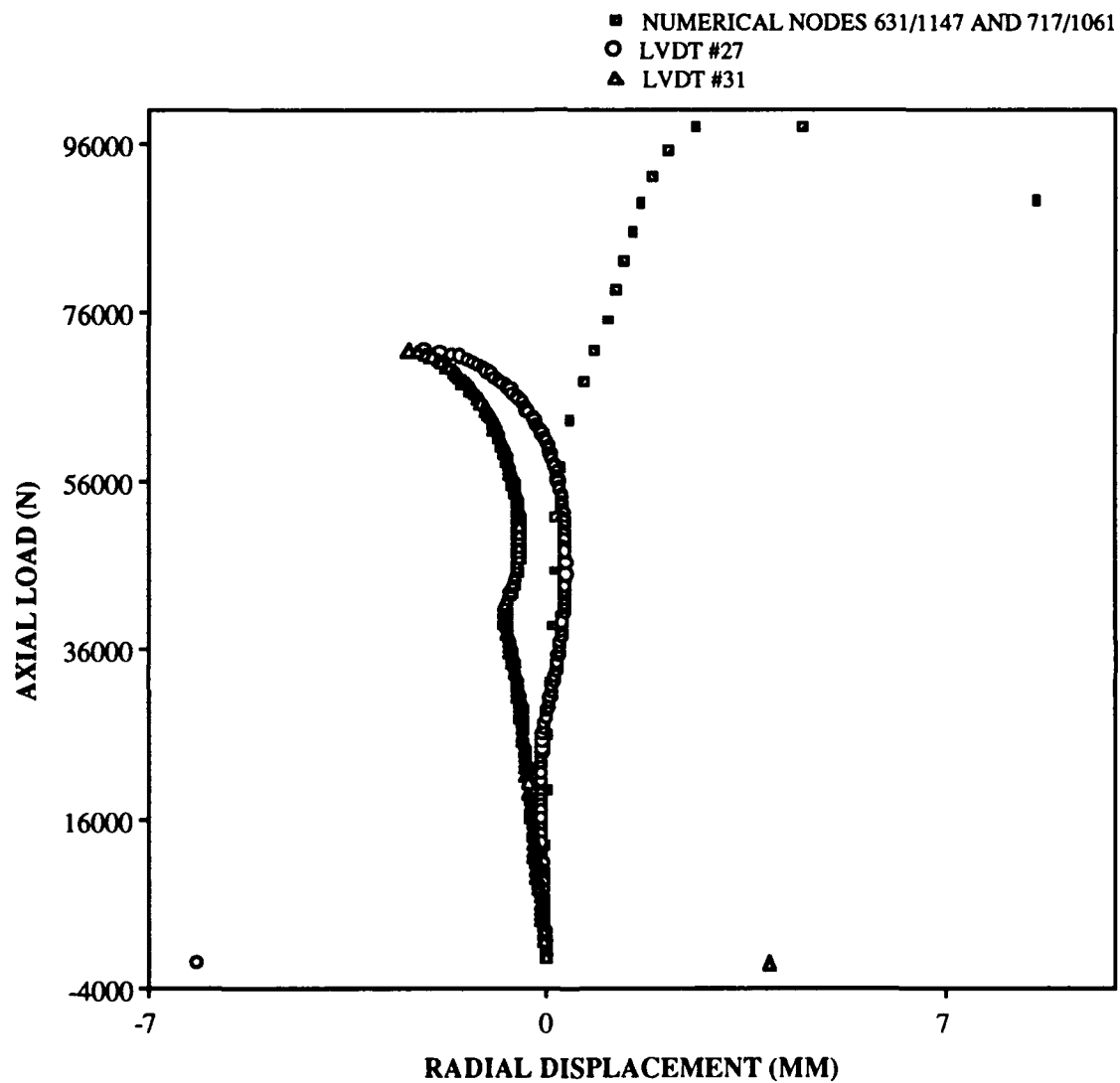304.8 mm x 508 mm (12" x 20") Panel,
[0/45/-45/90]3s

Fig. 120: Load vs. Radial Displacement,
Numerical Compared to Experiment #78,
50.8 mm x 50.8 mm (2" x 2") Cutout,
304.8 mm x 508 mm (12" x 20") Panel,
[0/45/-45/90]3s

Fig. 121: Load vs. Top Edge Displacement,
Numerical Compared to Experiment #97,
50.8 mm x 203.2 mm (2" x 8") Cutout,
304.8 mm x 508 mm (12" x 20") Panel,
[0/45/-45/90]3s

249

Fig. 122: Load vs. Radial Displacement,
Numerical Compared to Experiment #97,
50.8 mm 203.2 mm (2" x 8") Cutout,
304.8 mm x 508 mm (12" x 20") Panel,
[0/45/-45/90]3s

Fig. 123: Load vs. Radial Displacement,
Numerical Compared to Experiment #97,
50.8 mm x 203.2 mm (2" x 8") Cutout,
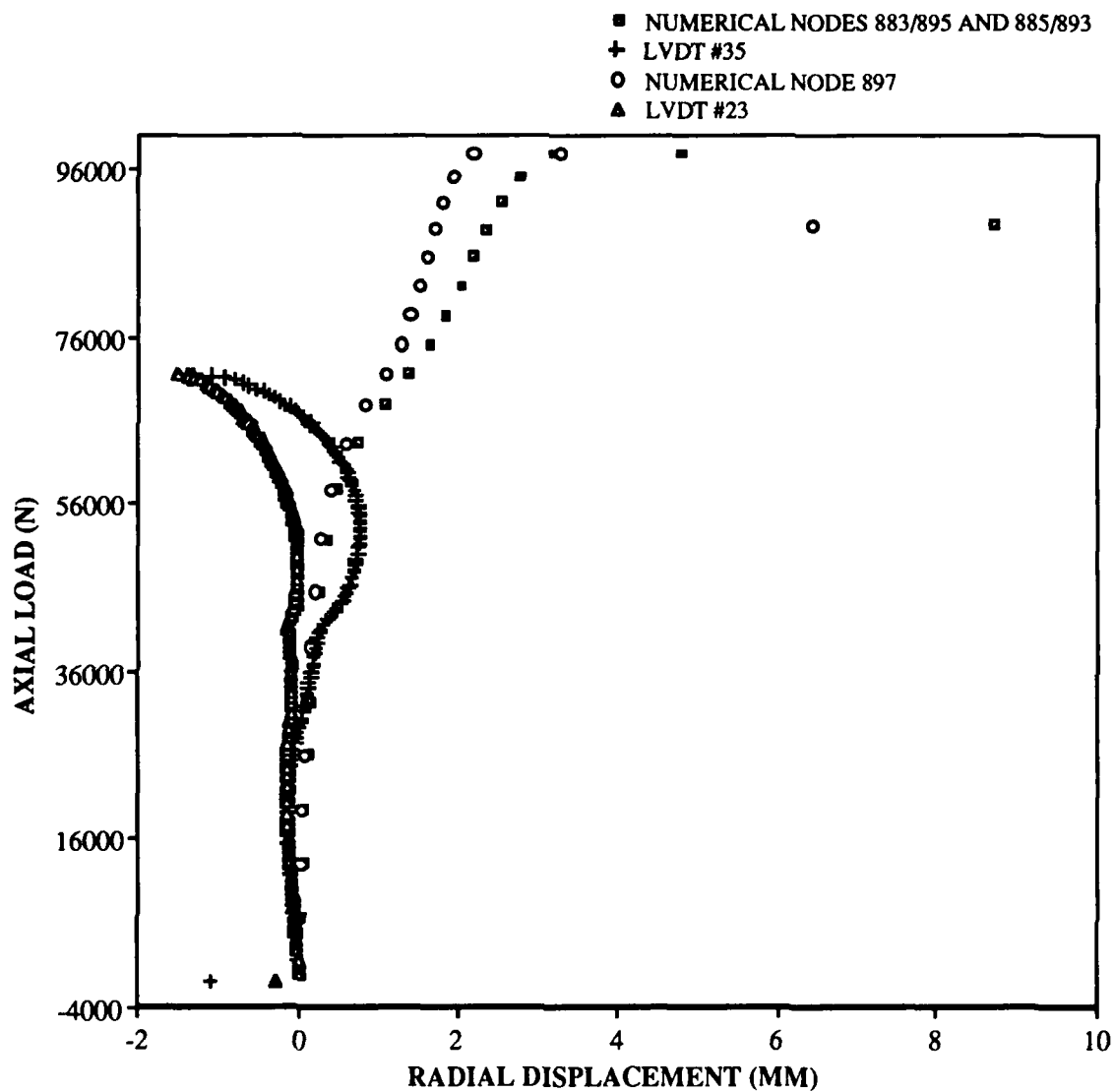304.8 mm x 508 mm (12" x 20") Panel,
[0/45/-45/90]3s

Fig. 124: Load vs. Radial Displacement,
Numerical Compared to Experiment #97,
50.8 mm x 203.2 mm (2" x 8") Cutout,
304.8 mm x 508 mm (12" x 20") Panel,
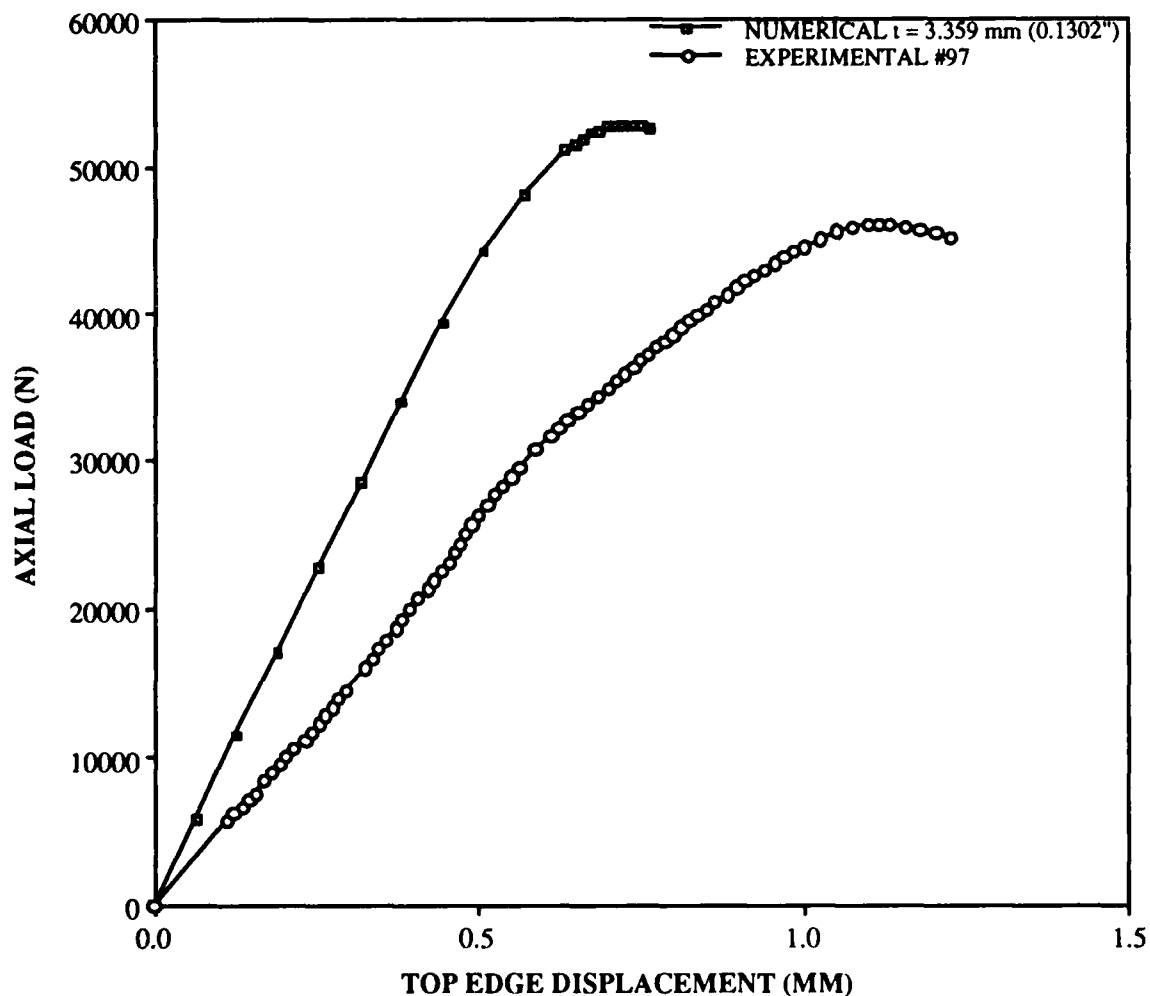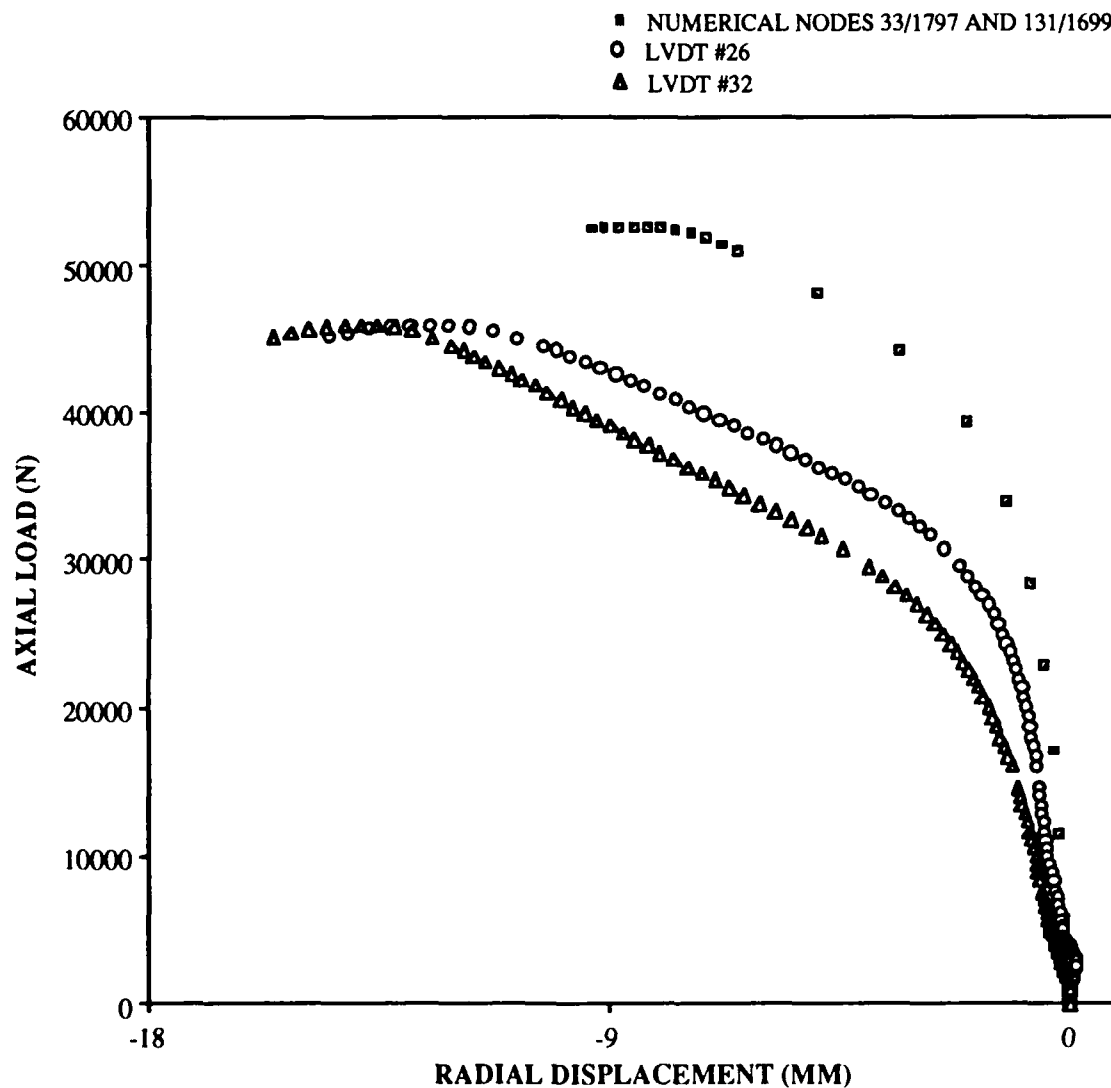[0/45/-45/90]3s

252

Fig 128 Load vs Top Edge Displacement,
Numerical Compared to Experiment #84,
101 6 mm x 101 6 mm (4" x 4") Cutout,
304 8 mm x 508 mm (12" x 20") Panel,
[0/45/-45/90]3s

Fig. 126: Load vs. Radial Displacement,
Numerical Compared to Experiment #84,
101.6 mm x 101.6 mm (4" x 4") Cutout,
304.8 mm x 508 mm (12" x 20") Panel,
[0/45/-45/90]3s
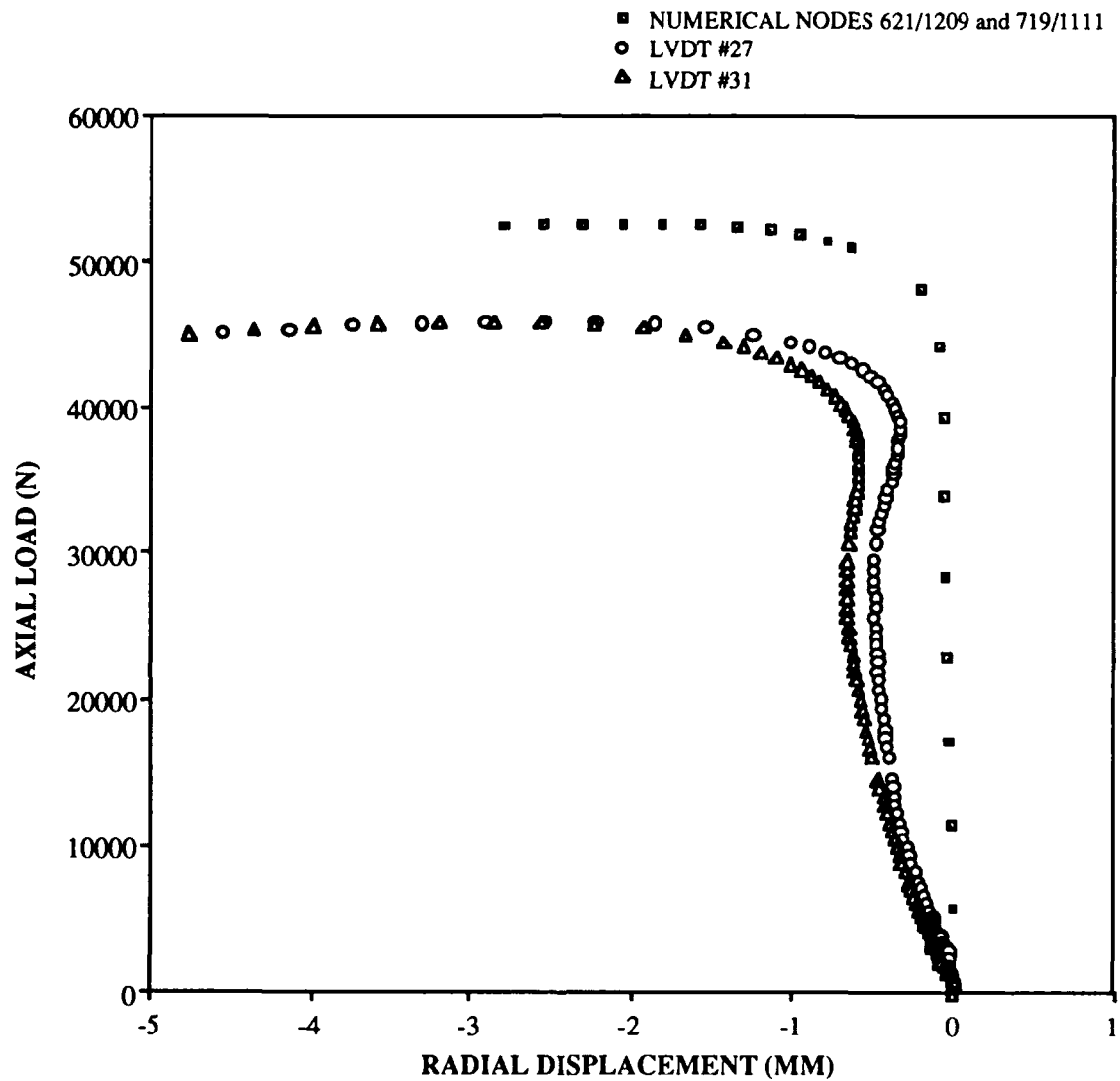
Fig. 127: Load vs. Radial Displacement,
Numerical Compared to Experiment #84,
101.6 mm x 101.6 mm (4" x 4") Cutout,
304.8 mm x 508 mm (12" x 20") Panel,
[0/45/-45/90]3s

Fig. 128: Load vs. Radial Displacement,
Numerical Compared to Experiment #84,
101.6 mm x 101.6 mm (4" x 4") Cutout,
304.8 mm x 508 mm (12" x 20") Panel,
[0/45/-45/90]3s

Fig. 129: Load vs. Top Edge Displacement,
Numerical Compared to Experiment #85,
101.6 mm x 101.6 mm (4" x 4") Cutout,
304.8 mm x 508 mm (12" x 20") Panel,
[0/45/-45/90]3s

Fig. 130: Load vs. Radial Displacement.
Numerical Compared to Experiment #85.
101.6 mm x 101.6 mm (4" x 4") Cutout.
304.8 mm x 508 mm (12" x 20") Panel.
[0/45/-45/90]3s

Fig. 131: Load vs. Radial Displacement,
Numerical Compared to Experiment #85,
101.6 mm x 101.6 mm (4" x 4") Cutout,
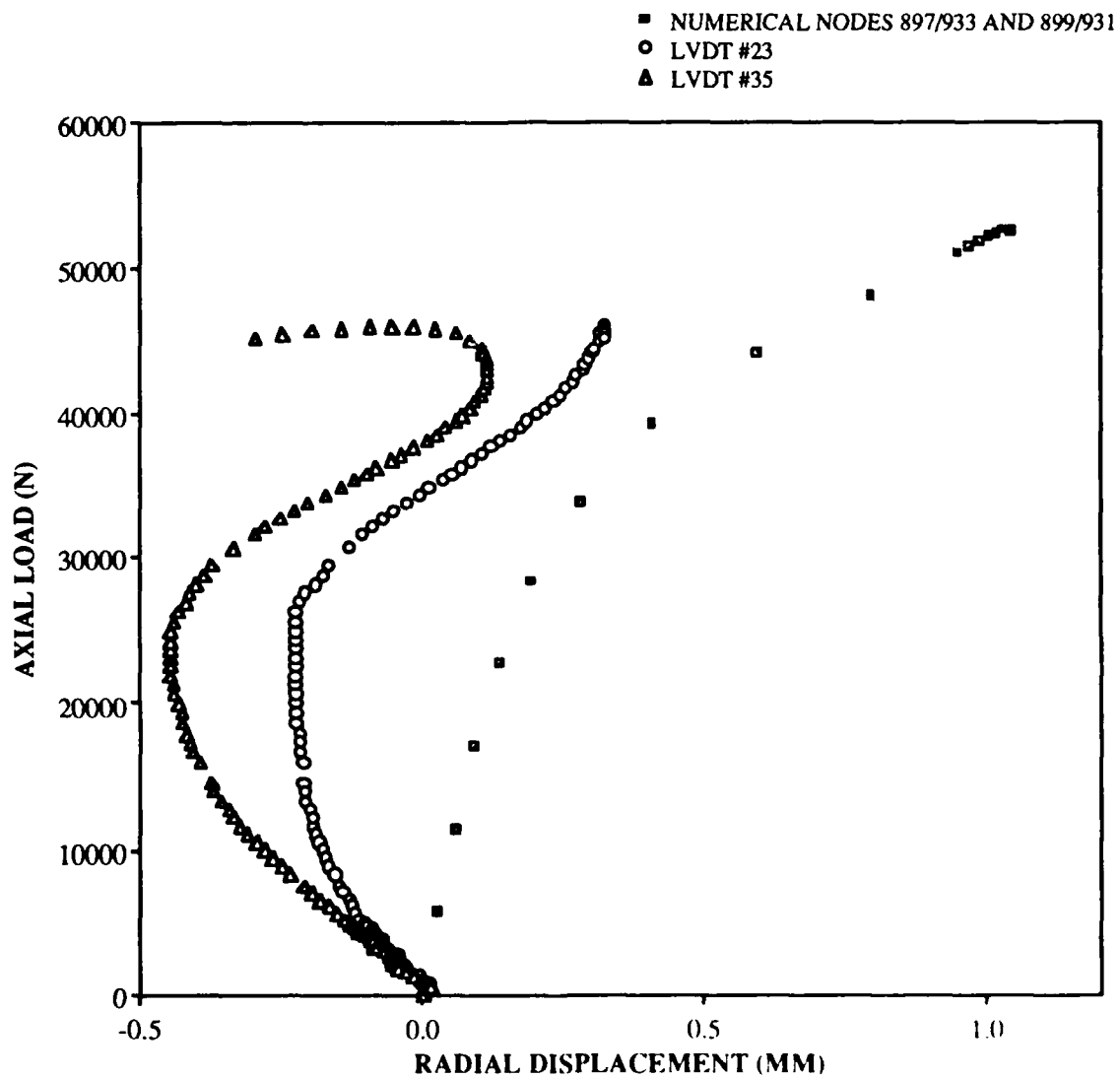304.8 mm x 508 mm (12" x 20") Panel,
[0/45/-45/90]3s
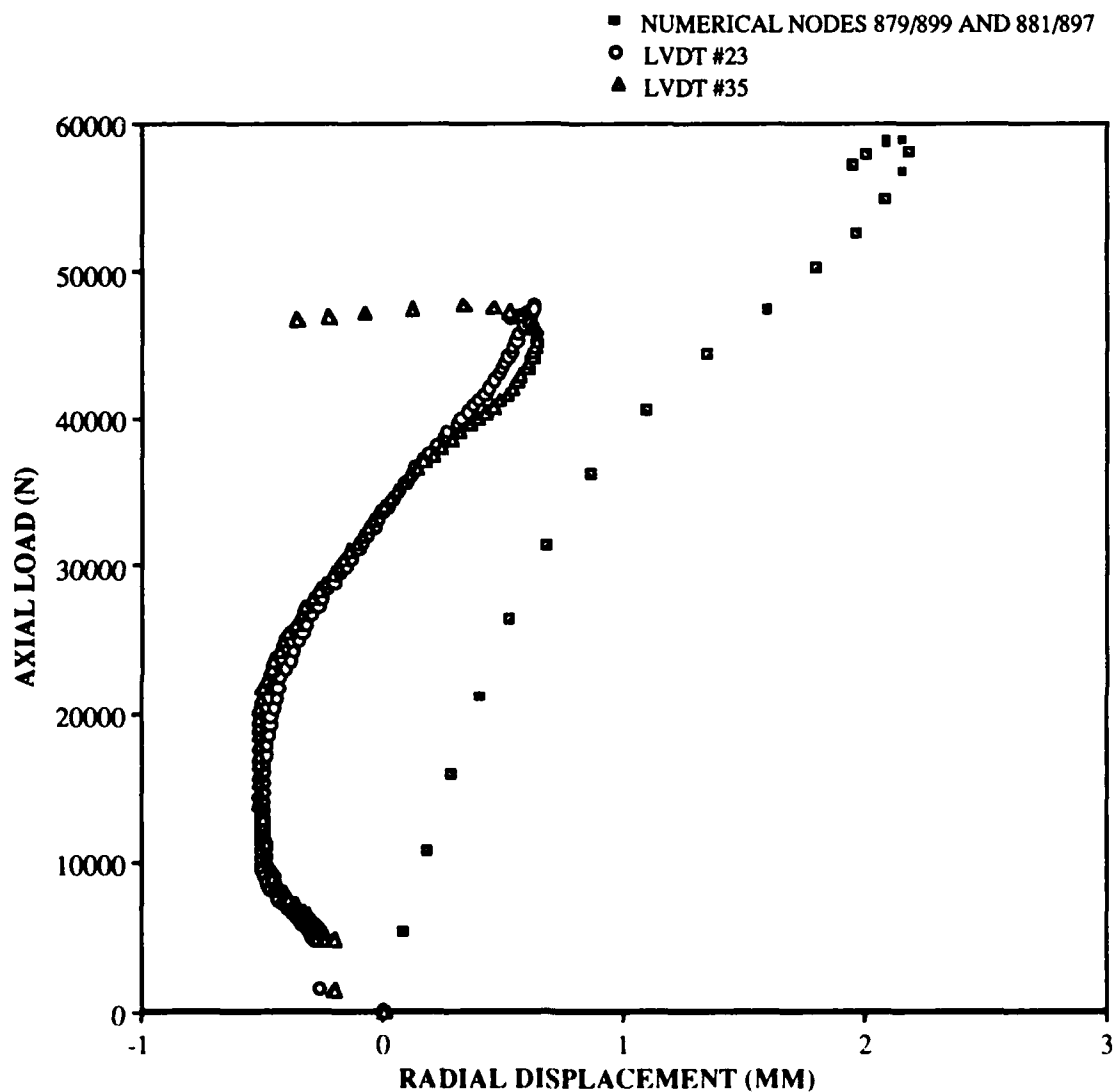
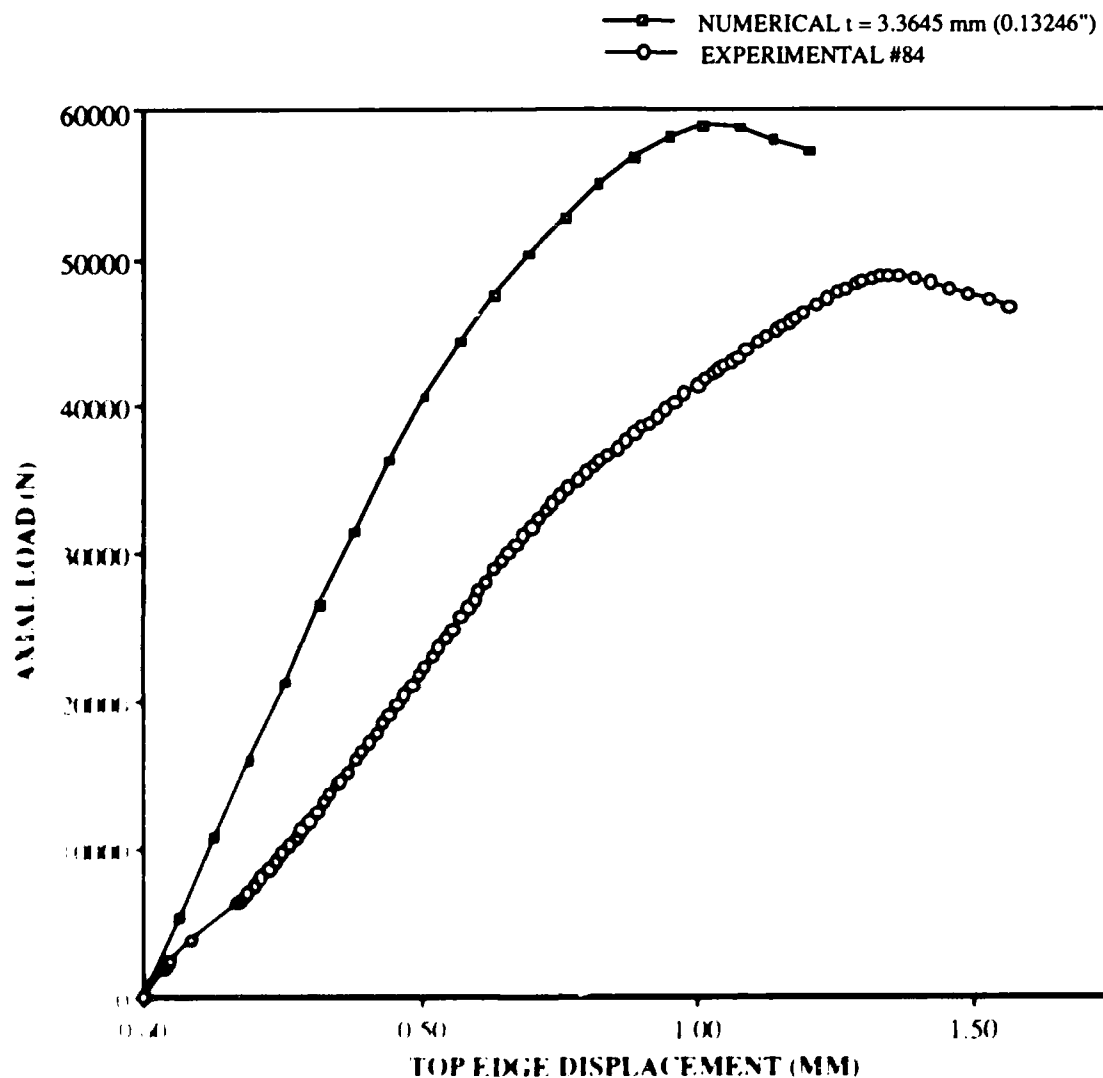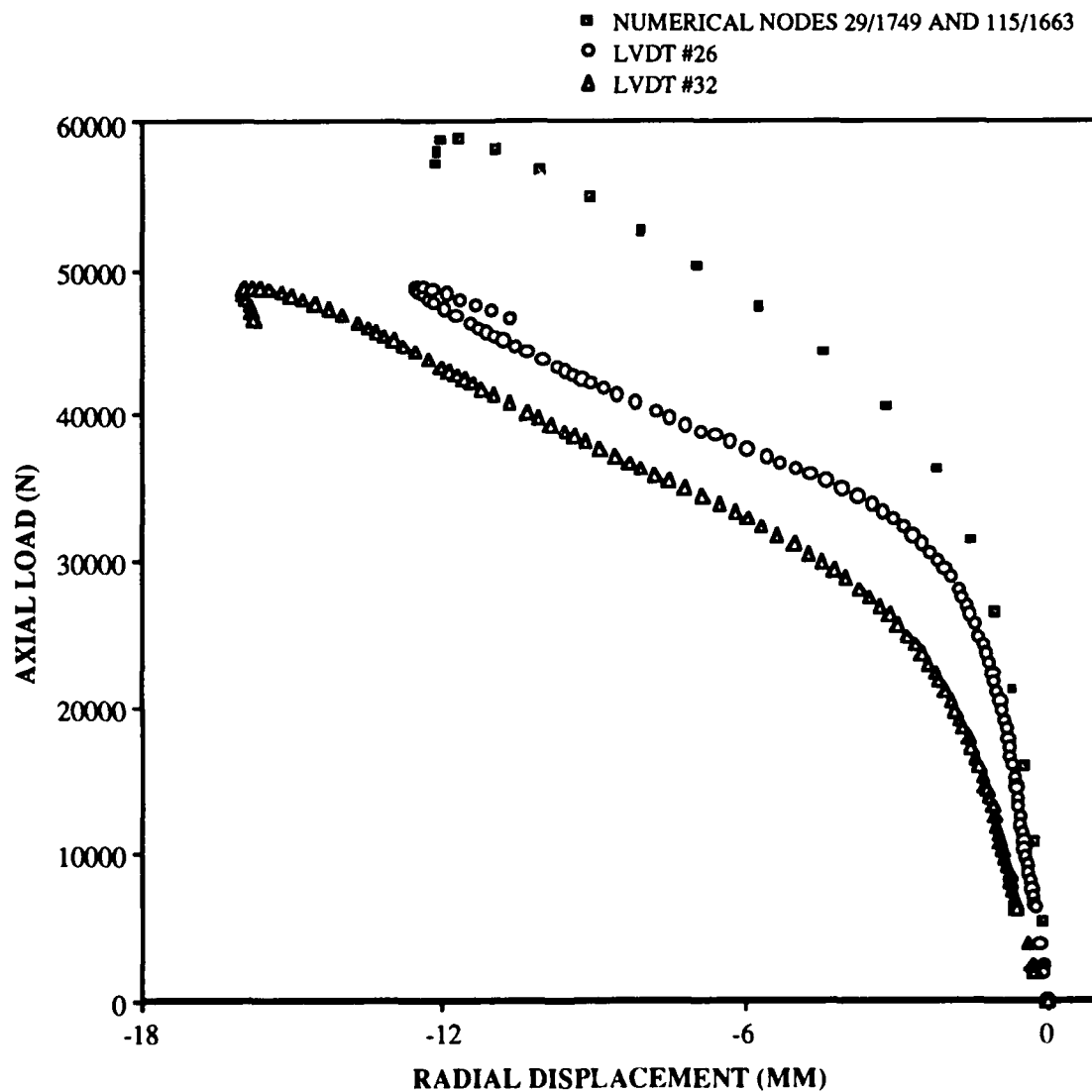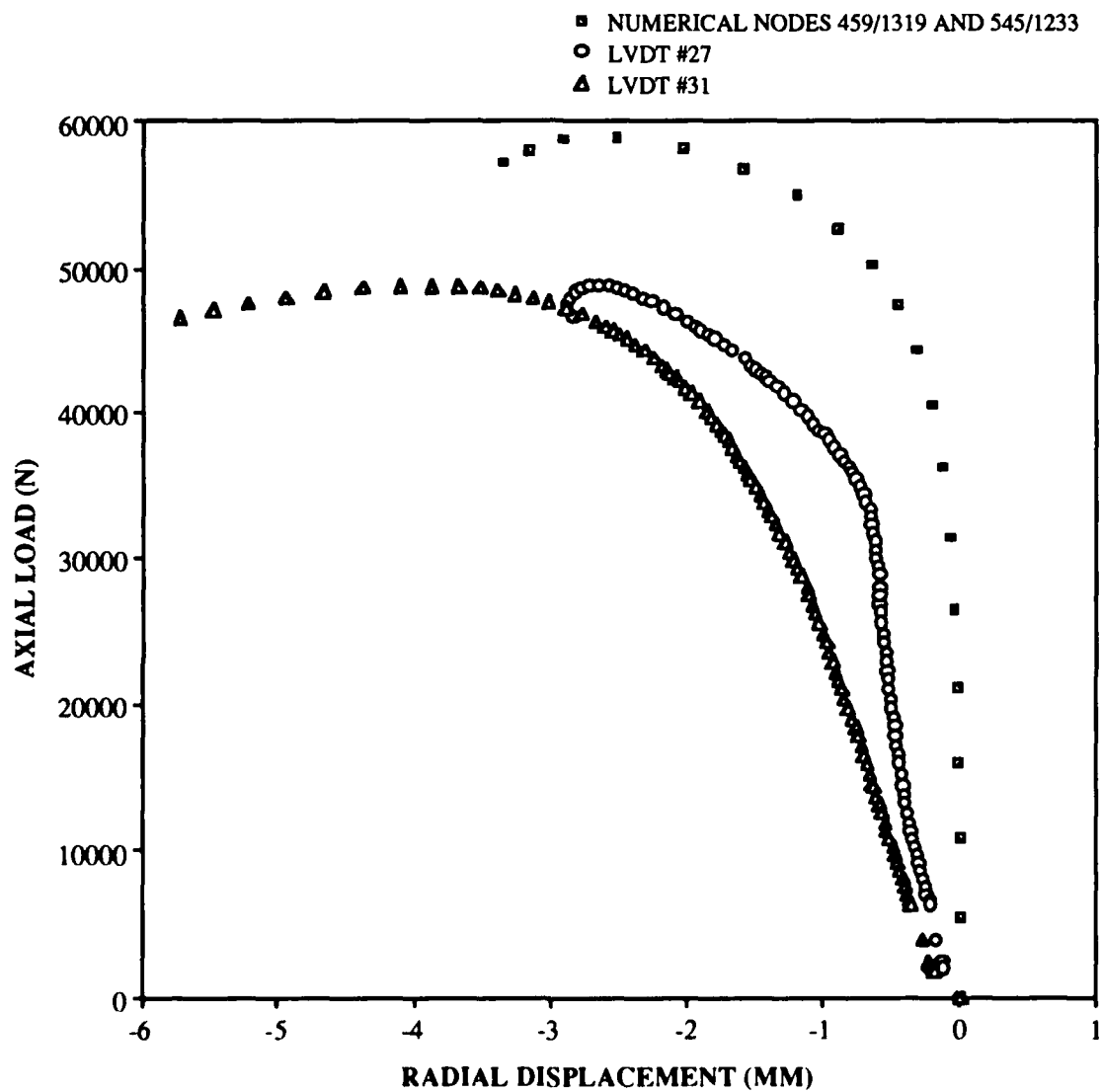Fig. 132: Load vs. Radial Displacement,
Numerical Compared to Experiment #85,
101.6 mm x 101.6 mm (4" x 4") Cutout,
304.8 mm x 508 mm (12" x 20") Panel,
[0/45/-45/90]3s
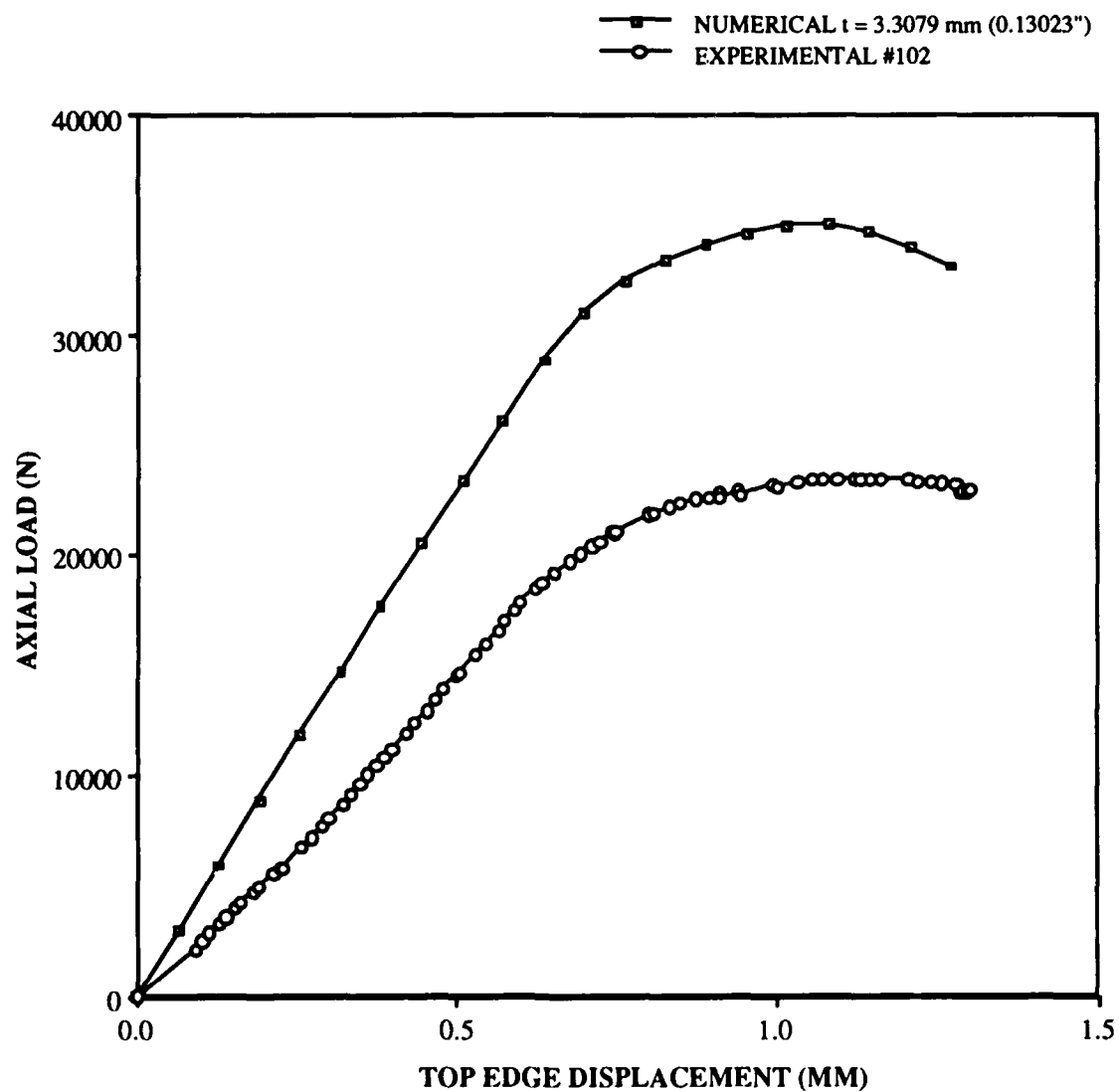
Fig. 133: Load vs. Top Edge Displacement,
Numerical Compared to Experiment #102,
203.2 mm x 50.8 mm (8" x 2") Cutout,
304.8 mm x 508 mm (12" x 20") Panel,
[0/45/-45/90]3s
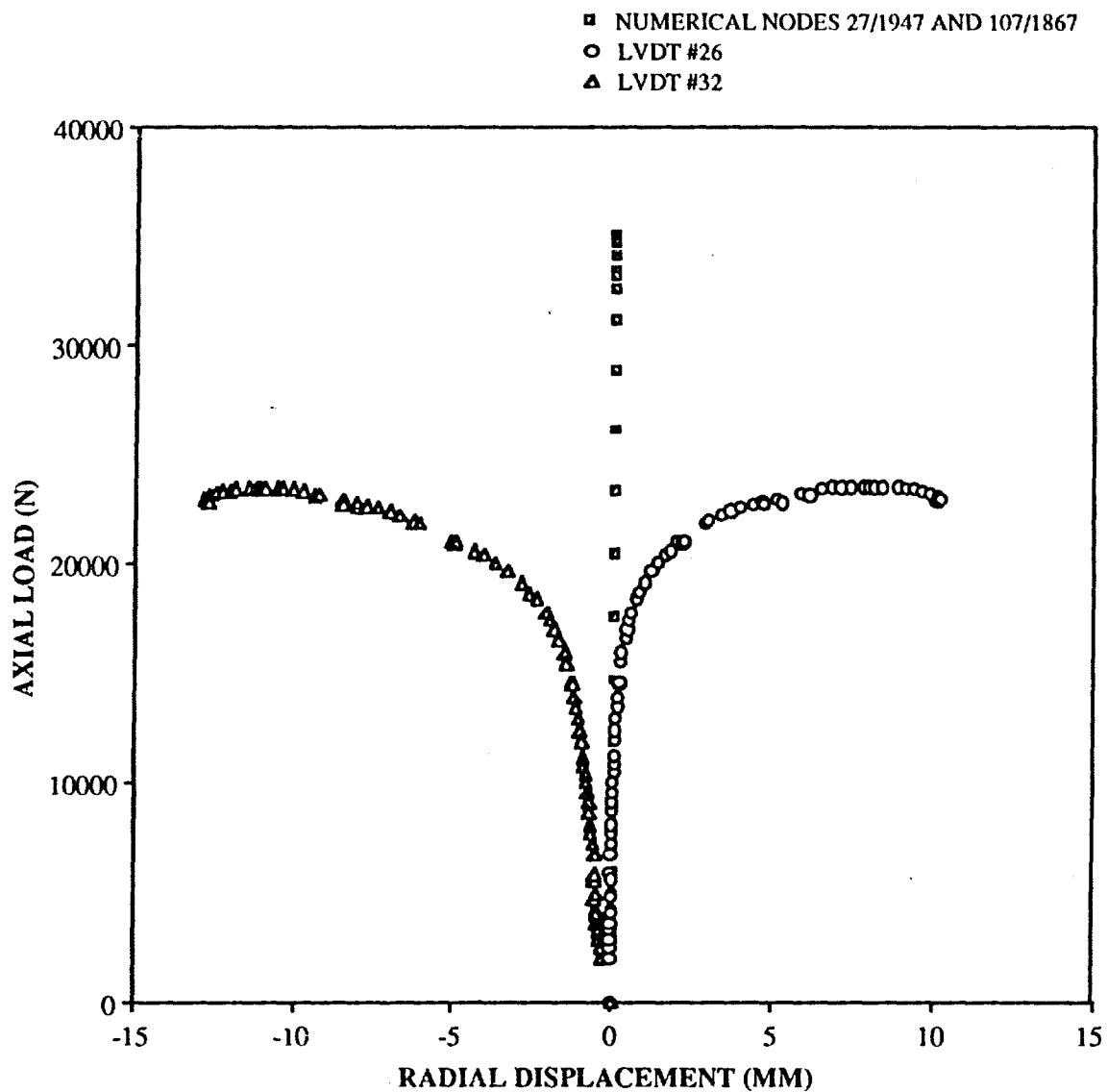
Fig. 134: Load vs. Radial Displacement,
Numerical Compared to Experiment #102,
203.2 mm x 50.8 mm (8" x 2") Cutout,
304.8 mm x 508 mm (12" x 20") Panel,
[0/45/-45/90]3s
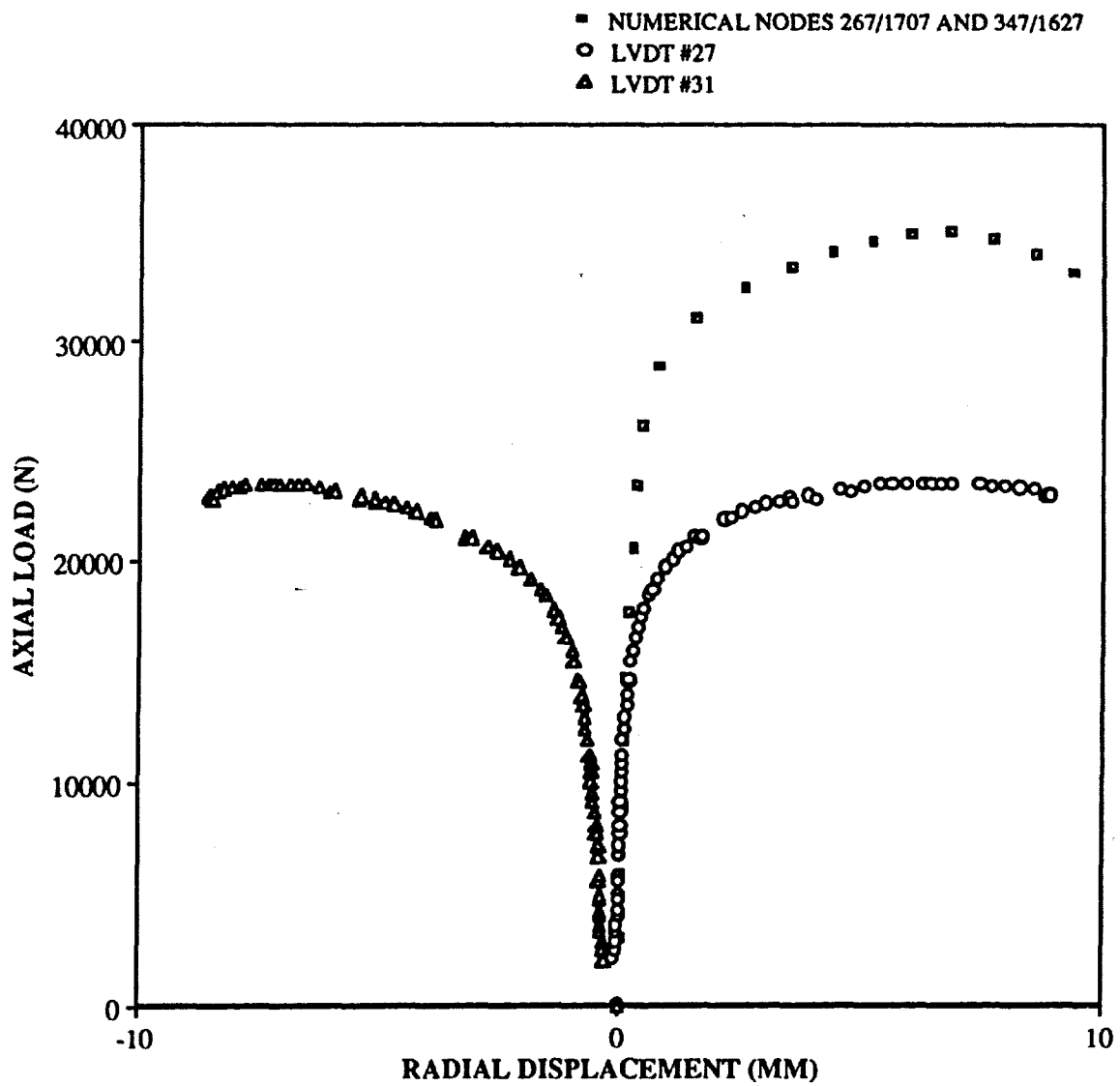
Fig. 135: Load vs. Radial Displacement,
Numerical Compared to Experiment #102,
203.2 mm x 50.8 mm (8" x 2") Cutout,
304.8 mm x 508 mm (12" x 20") Panel,
[0/45/-45/90]3s
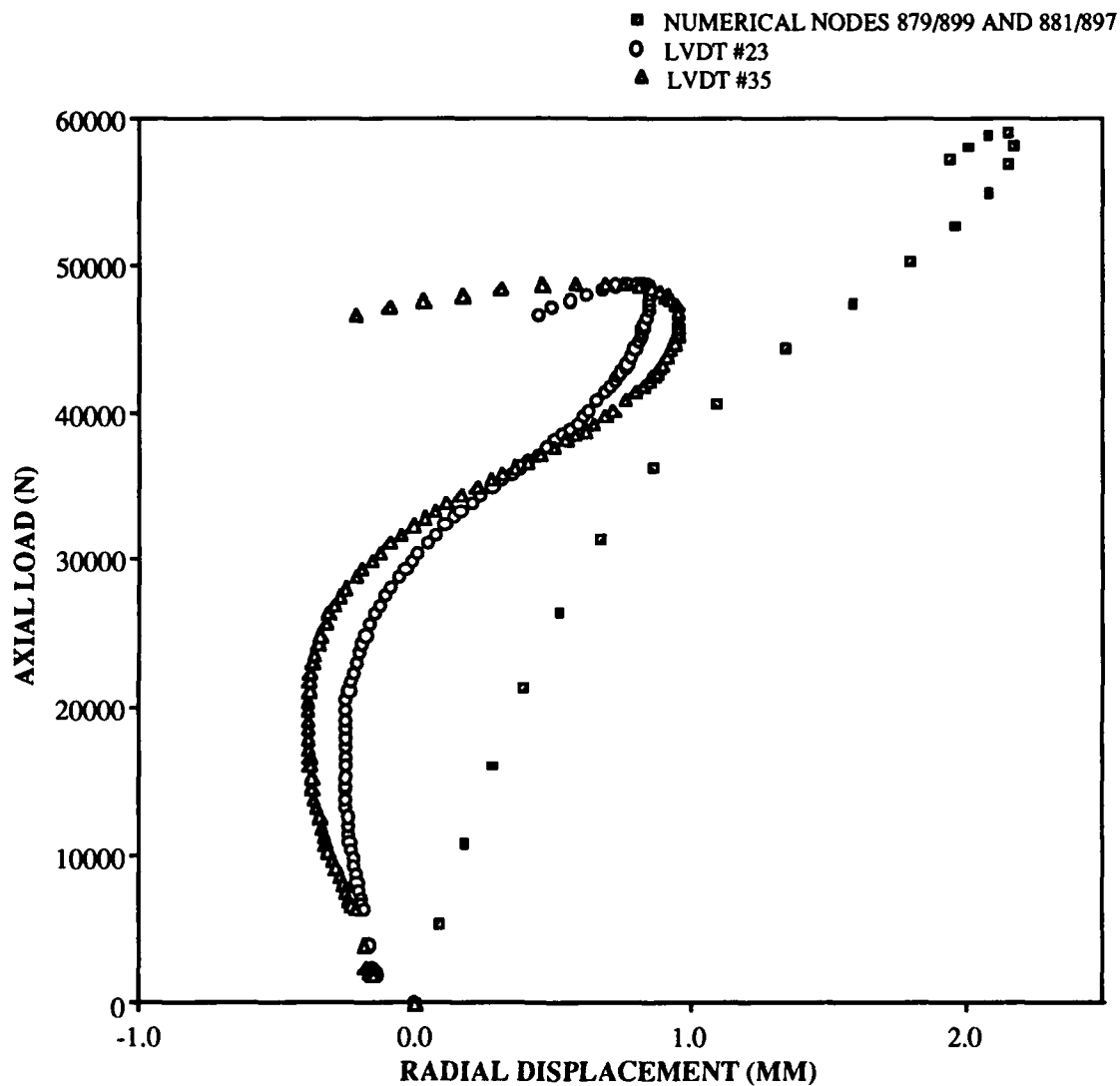
263
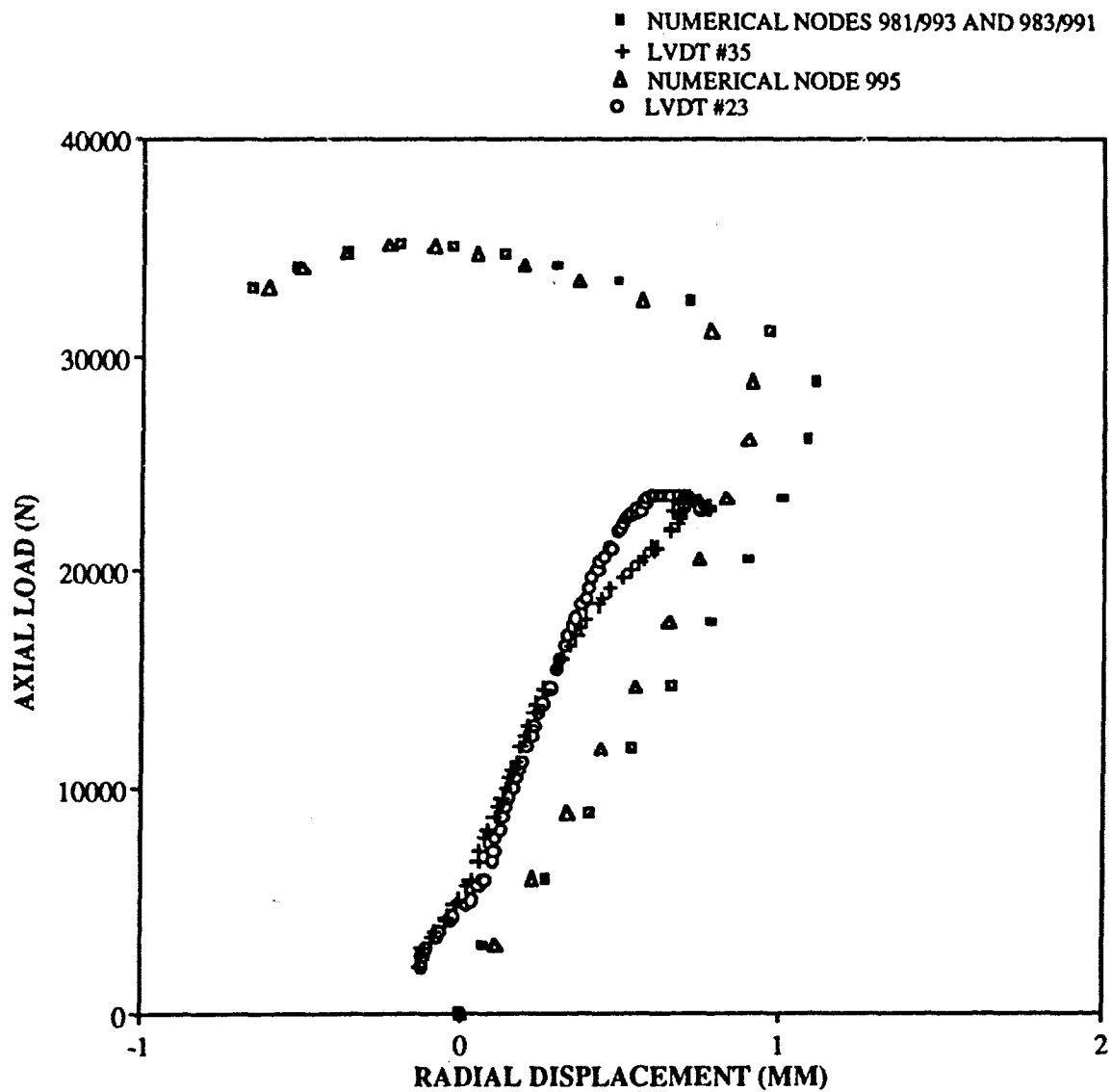
Fig. 136: Load vs. Radial Displacement,
Numerical Compared to Experiment #102,
203.2 mm x 50.8 mm (8" x 2") Cutout,
304.8 mm x 508 mm (12" x 20") Panel,
[0/45/-45/90]3s

NUMERICAL t = 3.3079 mm (0.13023")
EXPERIMENTAL #103
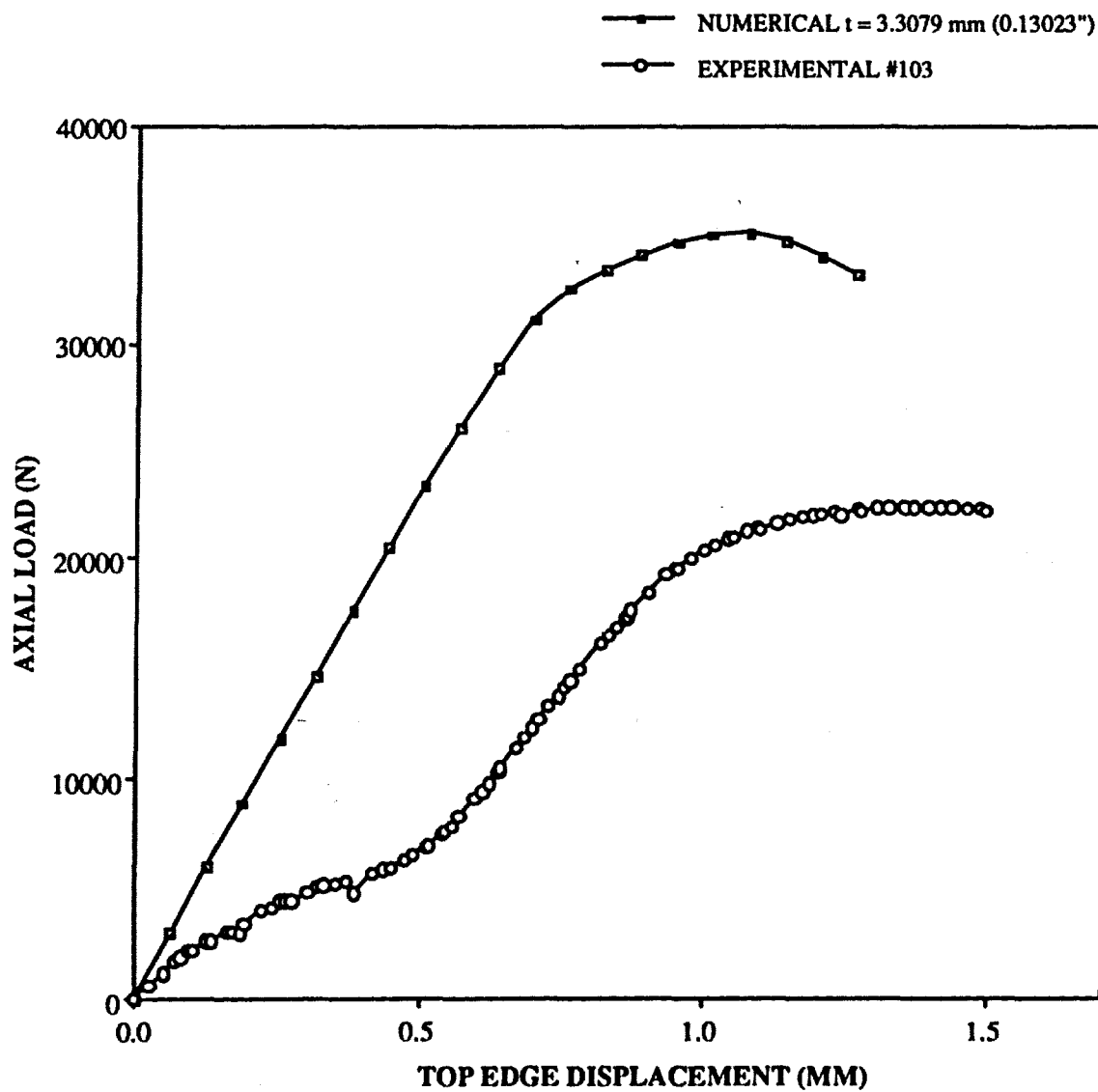
Fig. 137: Load vs. Top Edge Displacement,
Numerical Compared to Experiment #103,
203.2 mm x 50.8 mm (8" x 2") Cutout,
304.8 mm x 508 mm (12" x 20") Panel,
[0/45/-45/90]3s
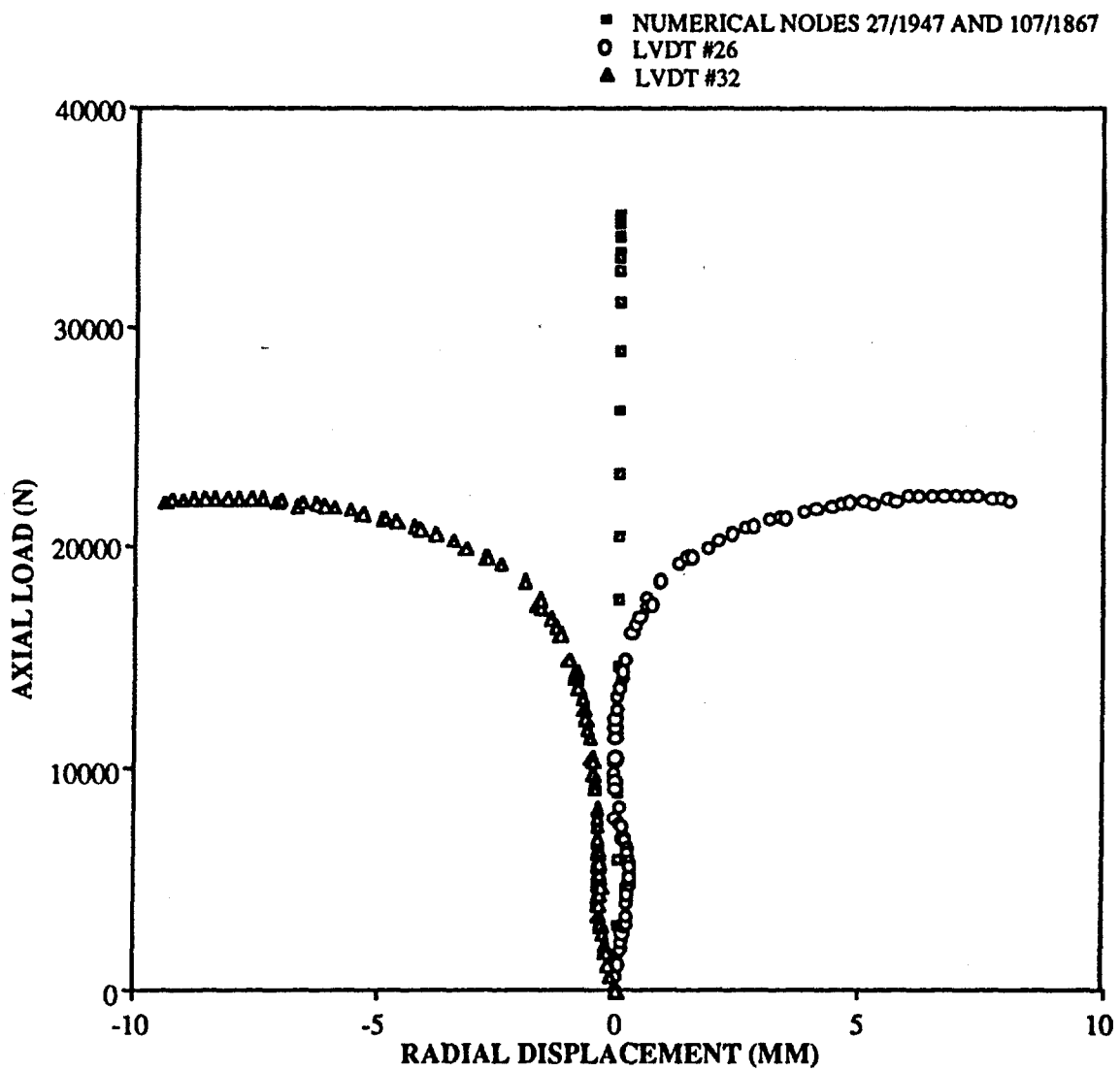
Fig. 138: Load vs. Radial Displacement,
Numerical Compared to Experiment #103,
203.2 mm x 50.8 mm (8" x 2") Cutout,
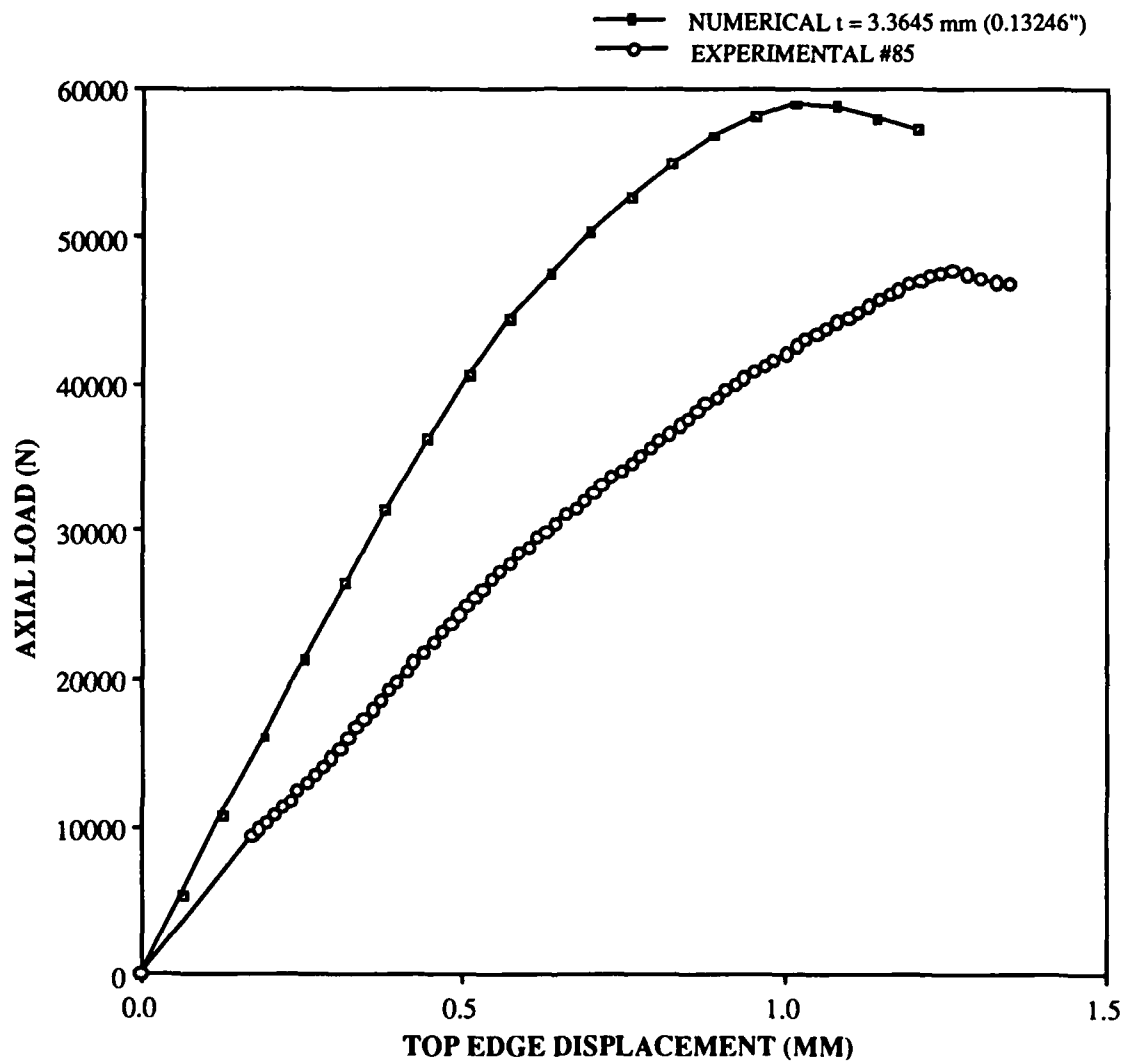304.8 mm x 508 mm (12" x 20") Panel,
[0/45/-45/90]3s
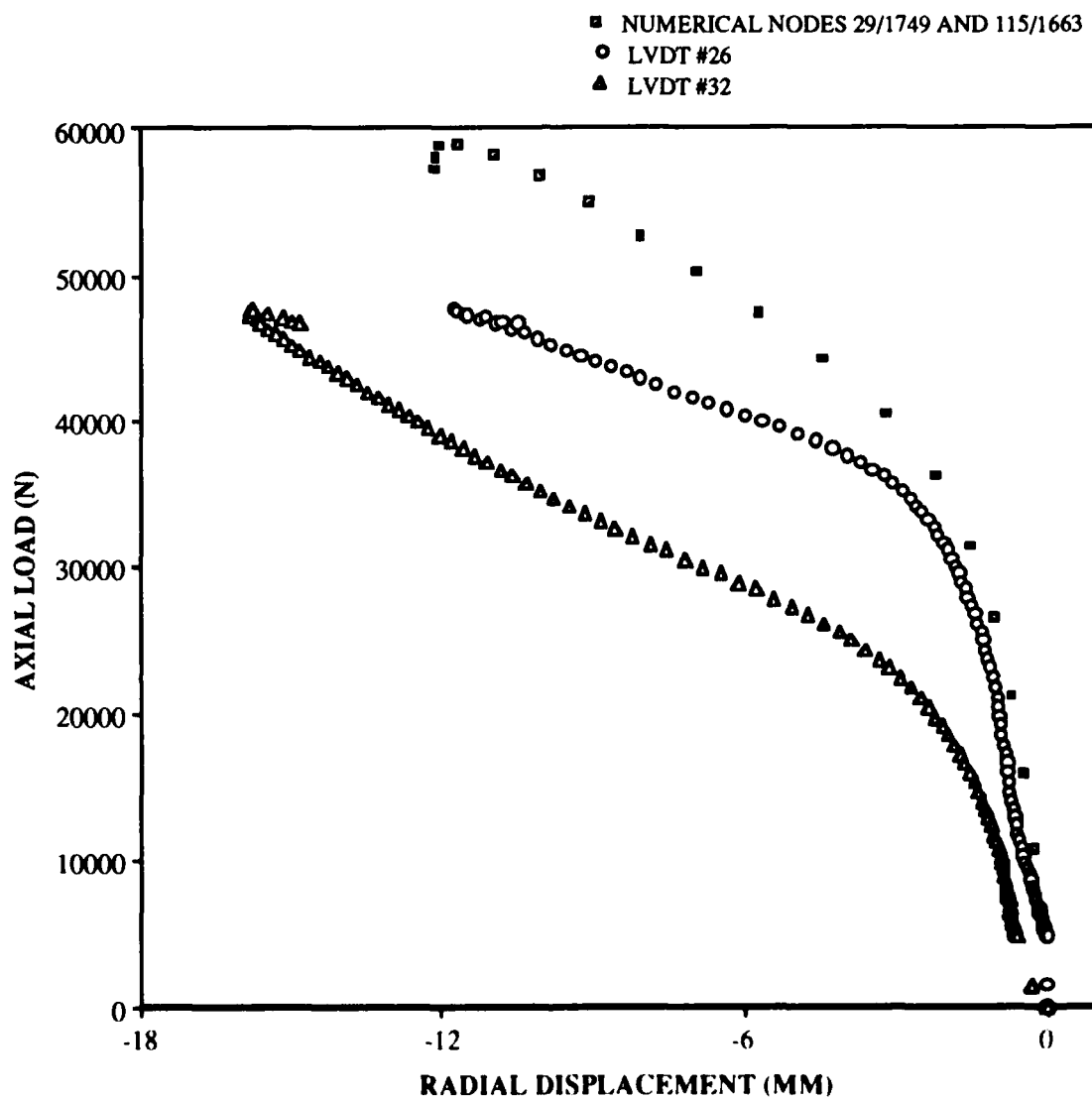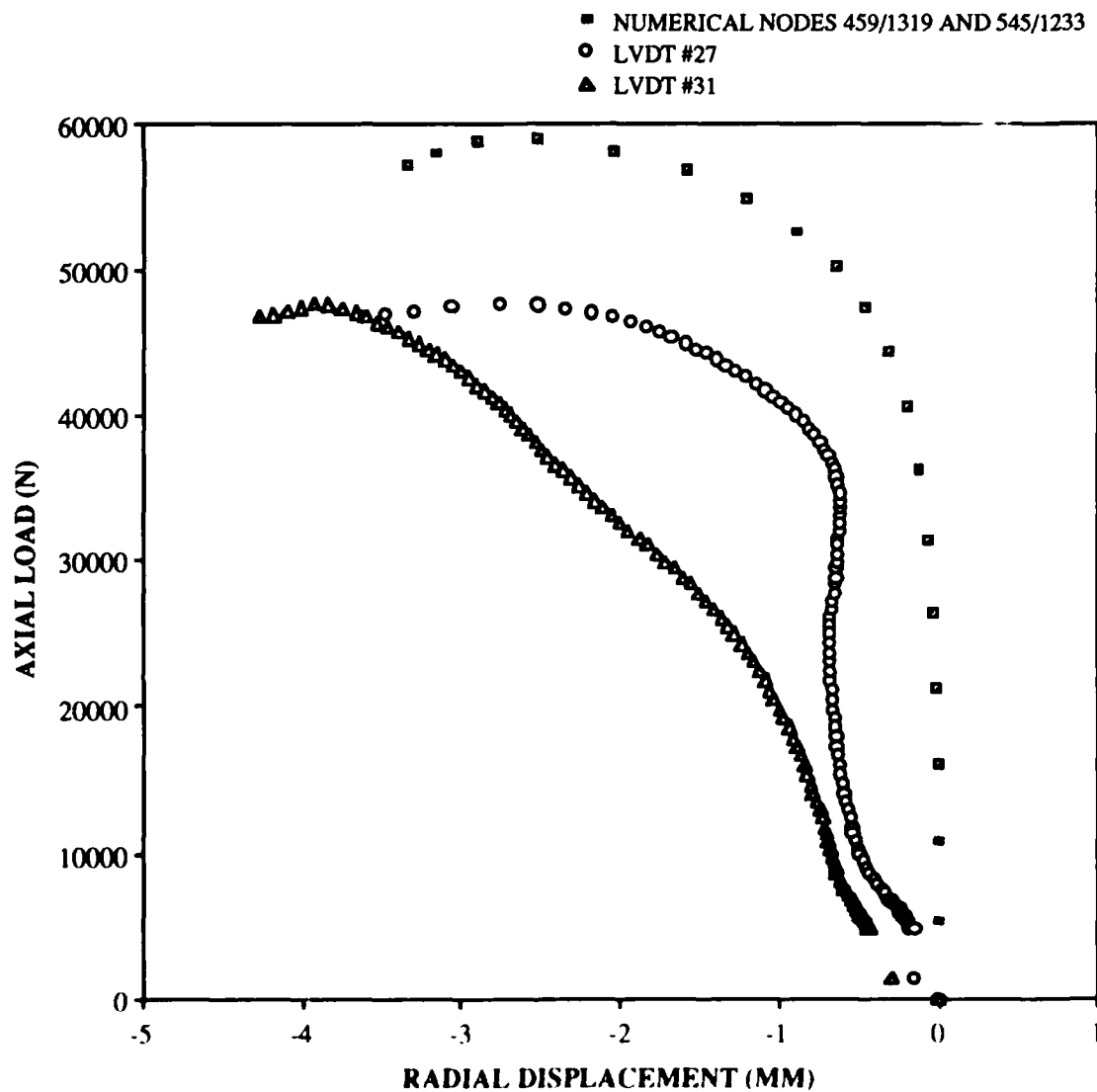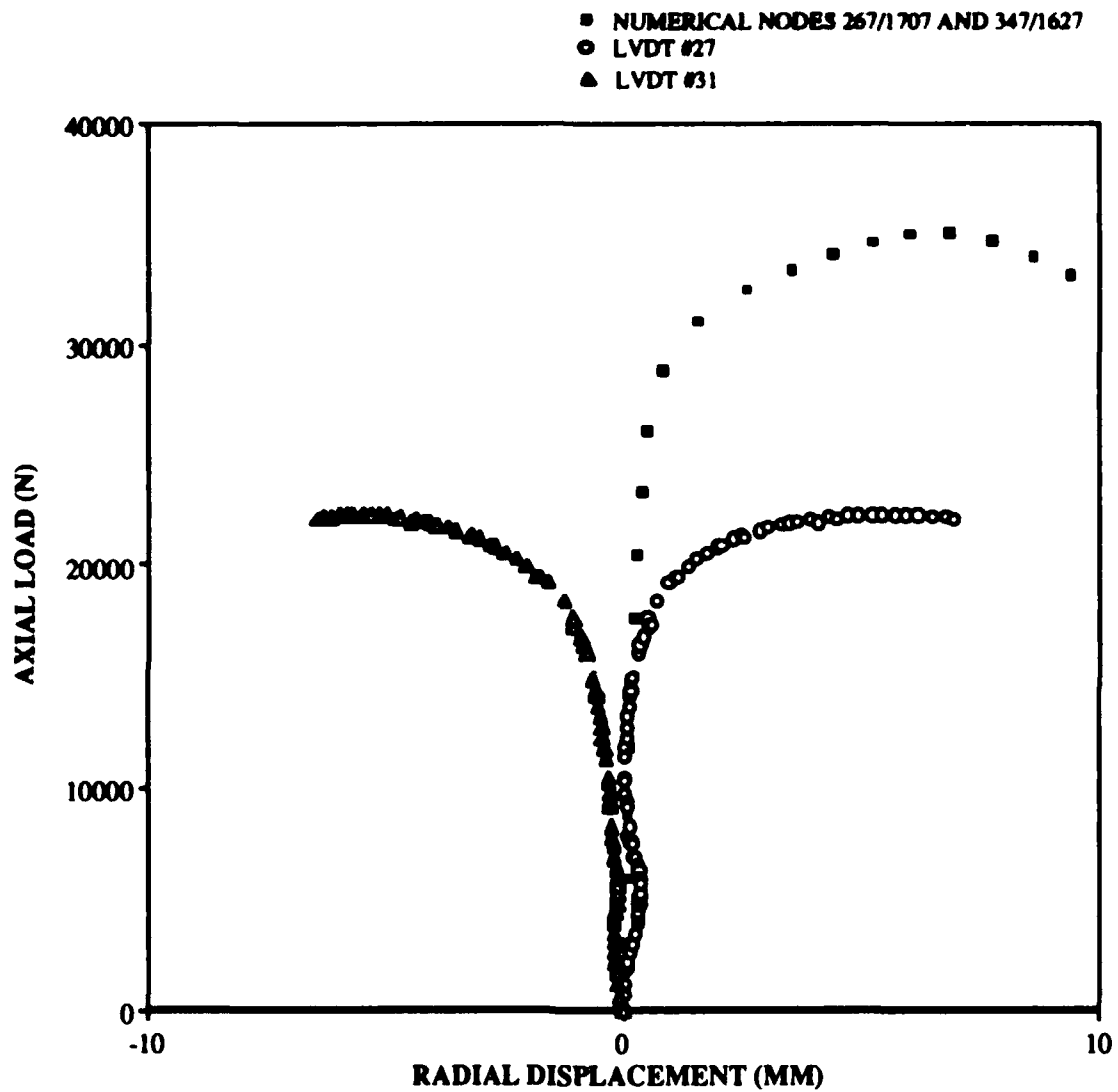
Fig. 139: Load vs. Radial Displacement,
Numerical Compared to Experiment #103,
203.2 mm x 50.8 mm (8" x 2") Cutout,
304.8 mm x 508 mm (12" x 20") Panel,
[0/45/-45/90]3s

267
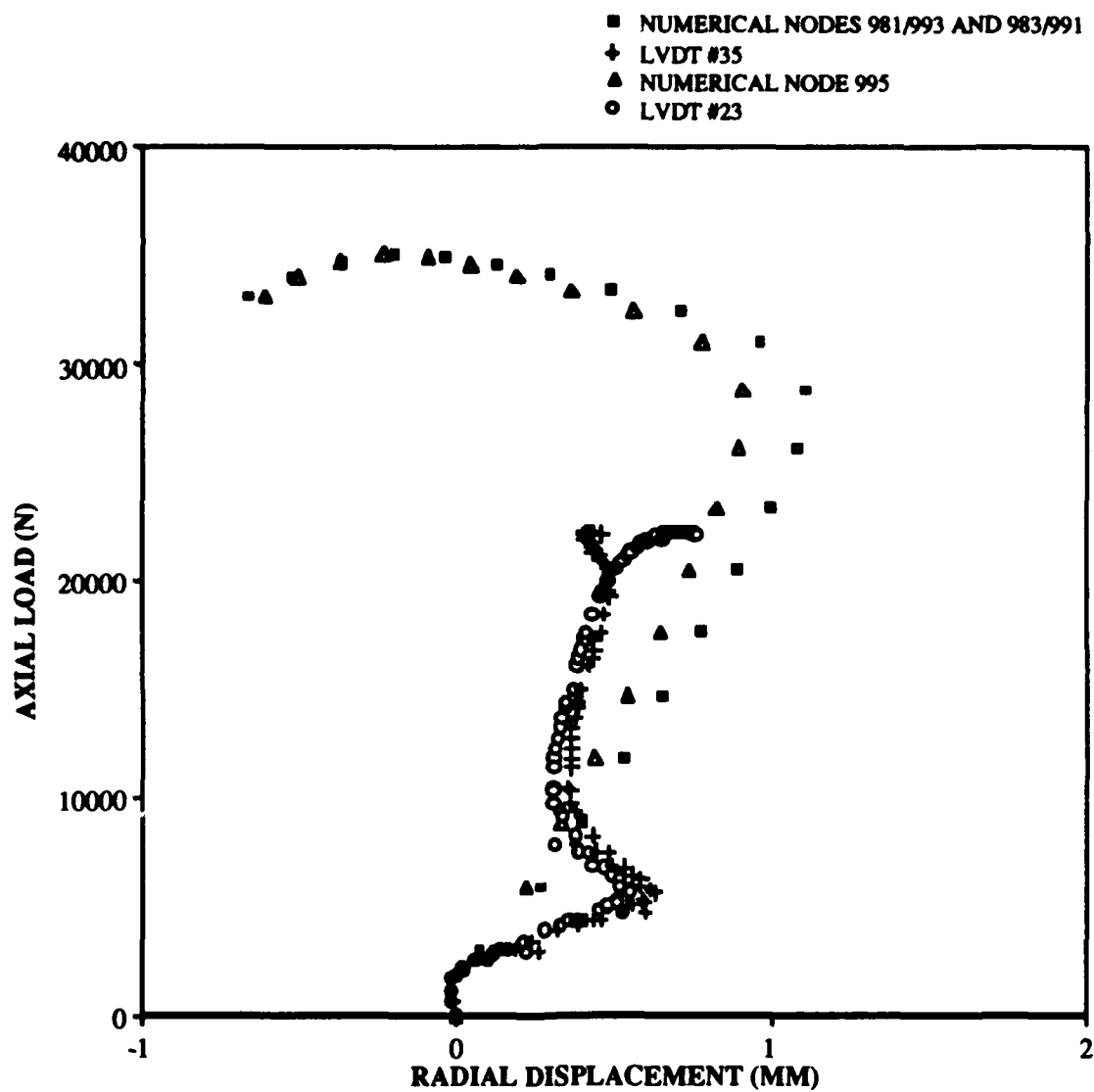
Fig. 140: Load vs. Radial Displacement,
Numerical Compared to Experiment #103,
203.2 mm x 50.8 mm (8" x 2") Cutout,
304.8 mm x 508 mm (12" x 20") Panel,
[0/45/-45/90]3s

<u>Vita</u>

Captain John C. Del Barga was born on 13 February 1964 in San Francisco, California. He graduated from San Carlos High School in San Carlos, California in 1982 and attended the U.S. Air Force Academy, graduating with a Bachelor of Science in Engineering Mechanics in May 1987. Upon graduation, he received a regular commission in the USAF and served his first tour of duty at Norton AFB, California. He began as a System Test Engineer for the Ballistic Missile Organization (BMO) where he directed test planning and test conduct for Peacekeeper Rail Garrison missile processing, assembly, and post launch refurbishment. He served in this role until the Peacekeeper Rail Garrison program was terminated in October, 1991. He then, served as the BMO System Test Branch Chief for the joint Air Force and NASA National Launch System (NLS) program. He was responsible for managing the development of the NLS master test plan until he entered the School of Engineering at the Air Force Institute of Technology in May 1992.

Permanent Address: 1008 Bayswater Avenue
San Mateo, CA 94401

REPORT DOCUMENTATION PAGE

Form Approved
OMB No. 0704-0188

4. TITLE AND SUBTITLE

THE EFFECT OF CUTOUT DIMENSIONALITY ON THE COLLAPSE
CHARACTERISTICS OF CYLINDRICAL COMPOSITE SHELLS OF
VARYING THICKNESS

5. FUNDING NUMBERS

6. AUTHOR(S)

John C. Del Barga, Captain, USAF

7. PERFORMING ORGANIZATION NAME(S) AND ADDRESS(ES)

Air Force Institute of Technology, WPAFB, OH 45433-6583

8. PERFORMING ORGANIZATION REPORT NUMBER

AFIT/GAE/ENY/93D-11

9. SPONSORING/MONITORING AGENCY NAME(S) AND ADDRESS(ES)

Dr. R.S. Sandhu
WL/FIBCA
Bldg 45, Wright-Patterson AFB, OH 45433-6553

10. SPONSORING/MONITORING AGENCY REPORT NUMBER

11. SUPPLEMENTARY NOTES

12a. DISTRIBUTION/AVAILABILITY STATEMENT

Approved for public release; distribution unlimited

12b. DISTRIBUTION CODE

13. ABSTRACT (Maximum 200 words)

This study involved a numerical and experimental investigation of the geometric instability of graphite/epoxy cylindrical panels with free vertical edges undergoing axial compression. Symmetric quasi-isotropic laminates with five different size centralized cutouts, were investigated for two axial lengths of panels and three thicknesses. The study compared experimental data to results from SHELL, a geometrically nonlinear finite-element program which incorporates a parabolic transverse shear strain distribution through the thickness. The research verified that the SHELL program will provide good predictions of the collapse characteristics of a panel with large cutouts of varying dimensions undergoing large displacements and rotations. The best correlation between the numerical and experimental results occurred for 16 ply panels in comparison to 8 and 24 ply panels. The variation between these results is attributed to panel curvature, material, and geometric imperfections. This study verified that cutout dimensionality effects the panel transverse shear strain, which in turn effects the panel collapse load. In addition, this research conducted parametric studies to determine one dimensional models that could be used in lieu of SHELL to estimate collapse loads from a known solution for a panel with geometric variations from the known panel solution.

14. SUBJECT TERMS

Composites, Shells, Cylindrical Panels, Cutouts,
Finite Elements, Nonlinear Analysis, Transverse Shear,
Geometric Instability, Collapse, Graphite/Epoxy

15. NUMBER OF PAGES

291

16. PRICE CODE

17. SECURITY CLASSIFICATION OF REPORT	18. SECURITY CLASSIFICATION OF THIS PAGE	19. SECURITY CLASSIFICATION OF ABSTRACT	20. LIMITATION OF ABSTRACT
Unclassified	Unclassified	Unclassified	UL